

MODELING OF ATOM TRANSFER RADICAL POLYMERIZATION

**MODELING OF SOLUTION AND SURFACE-INITIATED
ATOM TRANSFER RADICAL POLYMERIZATION**

By ERLITA MASTAN, B.Eng, M.A.Sc.

A Thesis Submitted to the School of Graduate Studies
in Partial Fulfilment of the Requirements for
the Degree Doctor of Philosophy

McMaster University © Copyright by Erlita Mastan, October 2015

DOCTOR OF PHILOSOPHY (2015)

McMaster University

(Chemical Engineering)

Hamilton, Ontario

TITLE: Modeling of atom transfer radical polymerization and
surface-initiated atom transfer radical polymerization

AUTHOR: Erlita Mastan
B.Eng. (Ryerson University, Canada)
M.A.Sc (Ryerson University, Canada)

SUPERVISOR: Dr. Shiping Zhu

NUMBER OF PAGES: xxvii, 314

Lay abstract

Polymer materials are used almost everywhere in our daily life from clothing to water bottle. This wide range of applications owes to the nearly infinite possible properties that polymer can possess. Different polymerization processes to synthesize polymers have their own weaknesses and strengths. Herein we investigated the fundamental mechanism of one of the currently most attractive polymerization systems, atom transfer radical polymerization (ATRP). This process allows the synthesis of polymers with precisely tailored chain microstructures, making it possible to create polymer with sophisticated properties. Using modeling approaches, we derived explicit expressions for determining chain properties, allowing detailed investigation of how various factors affect these properties. Through these investigations, we obtained better understanding on the mechanism of ATRP in solution and on surface. This knowledge is crucial in providing insight and guiding experimental designs for better control over the material properties.

Abstract

Controlled radical polymerization (CRP) can be viewed as the middle ground between living anionic polymerization (LAP) and conventional free radical polymerization (FRP). It combines the precise control over polymer structure offered by LAP, under a tolerant reaction condition similar to FRP. One of the most studied CRP is atom transfer radical polymerization (ATRP), with over 10,000 papers published since its introduction in 1995. Despite the numerous studies, knowledge on its fundamental mechanism is still lacking, as evident from the lack of expression for full MWD and polydispersity that account for termination reaction. Since termination is unavoidable in ATRP, the existing expressions give inaccurate predictions as dead chains accumulate. In this study, we derived expressions for full MWD at low conversion and for polydispersity. These expressions allow us to quantify and gain better understanding on the contribution of termination. In addition, the resulting polydispersity expression shows better agreement than the existing equation when correlated with experiment data.

In addition to the aforementioned questions, there are also controversies regarding the kinetics of surface-initiated ATRP, with researchers divided into two schools of theories. We evaluated the validity of these theories by comparing their predictions to experimental trends. Both theories were found to be inadequate in explaining all the experimental observations, thus triggering an investigation of the graft density.

Graft density is an important determining property for polymer brushes, yet little is known about what affects its final value. Through simulations, we investigated the effect of experiment factors on the grafting density. A decrease in the amount of deactivator is found to decrease the grafting density, which could be explained by an increase in the number of monomers added per activation cycle. This knowledge allows us to explain the conflicting experiment observations regarding the growth trends of polymer layers reported in the literatures.

Acknowledgements

I am deeply indebted to my supervisor, Dr. Shiping Zhu, whose endless patience and supports made the completion of this thesis not only possible, but also enjoyable. He treats his students as if we were his own children, letting us choose our own paths while providing tireless supports. He goes above and beyond for our development, gives advices, and opens countless of doors to further our career. His ability to see the big pictures and pinpoint major research challenges are inspiring and a great source of motivation. His direct approach and constructive criticisms are immensely helpful in shaping me to be a better researcher. I appreciate him not micromanaging me, yet staying close enough to ensure I do not stray too far. I can always count on him to put me back on the right track whenever I go in too deep into the realm of unrealistic pursuits. I am truly fortunate to be a part of his research group. Thank you, Dr. Zhu.

I would also like to thank my supervisory committee members, Dr. Robert Pelton and Dr. Igor Zhitomirsky, for their patience, time, and valuable inputs. Their kind support and research expertise help me to better understand my research, to view various problems in different angles, and to broaden my horizons.

I would like to extend my gratitude to Dr. Li Xi for his time in providing research guidance on the surface modeling part of this thesis. Thank you for being approachable and super patient in responding to my endless and often nonsensical

queries. I am also very grateful for the help I received from Mark Hahn from Research and High Performance Computing Support (RHPCS) at McMaster on SHARCNET-related matters. I would like to thank Justyna Derkach, Doug Keller, Paul Gatt, Dan Wright, Lynn Falkiner, Cathie Roberts, Kathy Goodram, Kristina Trollip, Michelle Whalen, and Linda Ellis, who are all incredibly friendly and quick in lending a helping hand. I would also like to thank other faculty members in the Department of Chemical Engineering in McMaster University who have enriched my learning experience and made this department a very welcoming place.

I would like to thank current and former members of PolyMac Zhu research group who provided a positively challenging, lively, and enjoyable research environment. While I cannot list all their names individually here, they all have given me supports that I needed to complete this study. Their dedication and diligence to research never fail to impress and inspire me. I would especially like to thank to Dr. Dapeng Zhou, whom I have had the pleasure collaborating with in the first year of my study. My gratitude also goes to Dr. Wen-Jun Wang and Dr. Shiping Zhu for giving me an invaluable and eye-opening opportunity to visit Zhejiang University in China. Huge thanks to Dr. Wen-Jun Wang and his research group members for their kindness and hospitality in making my stay unforgettable.

To all the friends I have made in McMaster, thank you for all the fun times. I can always find time to complain about not having enough time, especially when it comes with

coffee and great friends! Thank you for lending me your sympathetic ears and for putting up with my iced capps' addiction, even during the harsh winter days. I would also like to thank my friends outside of Mac community for keeping me entertained on the weekend with our pigging-out sessions that have kept me sane.

Last but definitely not least, I owe my deepest gratitude to my parents and siblings who are always there for me through thick and thin, especially during this journey of mine where my self-confidence falters more frequently than I care to admit. You are the reason I am where I am today. Thank you for the confidence you have in me and I am truly sorry for all the worries and anxieties I put you through during the past so many years that I am away from home. Thank you for all the video chats and for updating me on what is happening at home so I am not left out of the inside stories and jokes. Of course, a giant thanks for showing me all the food you are having without me! These things keep me going when I did not think I could go further. Thank you for being the best family one could ever asked for. You are my pillars of support and source of comfort in my times of need.

Table of contents

Lay abstract.....	iii
Abstract.....	iv
Acknowledgements.....	vi
Table of contents.....	ix
List of figures	xiii
List of tables.....	xxiii
List of abbreviations and symbols.....	xxv
Declaration of academic achievement.....	xxvii
1 Introduction	1
§ 1.1 Research background	1
§ 1.2 Research objectives	4
§ 1.3 Thesis organization	5
§ 1.4 Other works.....	10
§ 1.5 References.....	10
2 Literature review on the modeling of CRP systems.....	12
§ 2.1 Abstract.....	13
§ 2.2 Introduction	13
§ 2.3 Modeling techniques	18
2.3.1 Kinetic-based approach.....	18
2.3.2 Stochastic-based approach	23
§ 2.4 Living polymerization.....	25
§ 2.5 Homogeneous controlled radical polymerization (CRP)	29
2.5.1 Nitroxide-mediated polymerization (NMP)	31
2.5.2 Atom transfer radical polymerization (ATRP).....	49

2.5.3	Reversible addition-fragmentation chain transfer (RAFT)	62
§ 2.6	Concluding remarks	74
§ 2.7	References.....	75
3	An explicit expression of molecular weight distribution for ATRP systems.....	89
§ 3.1	Abstract.....	90
§ 3.2	Introduction	91
§ 3.3	Model development.....	97
§ 3.4	Simulation results and discussions	103
3.4.1	Evolution of MWD in ATRP	104
3.4.2	Effect of activation cycles (z) on MWD	106
3.4.3	Effect of dead chain fraction on MWD	111
§ 3.5	Conclusions.....	115
§ 3.6	References.....	117
§ 3.7	Appendix.....	119
4	Molecular weight distribution for ATRP at a moderate to high conversion	132
§ 4.1	Abstract.....	133
§ 4.2	Introduction	133
§ 4.3	Model development.....	138
4.3.1	No termination ($k_t = 0 \rightarrow \phi_t = 0, f_t = 0$).....	140
4.3.2	With termination.....	144
§ 4.4	Simulation results and discussion	151
4.4.1	Without termination.....	152
4.4.2	With termination.....	155
4.4.3	Lack of control versus loss of livingness.....	158
§ 4.5	Conclusion.....	162
§ 4.6	References.....	163
§ 4.7	Appendix.....	165
5	An explicit polydispersity equation for ATRP systems	169

§ 5.1	Abstract.....	170
§ 5.2	Introduction	171
§ 5.3	Mathematical formulations	177
§ 5.4	Results and discussions	183
5.4.1	Analysis of the derived PDI equations.....	184
5.4.2	Comparison with the method of moments	187
5.4.3	Polymerization of HEMA.....	191
5.4.4	Polymerization of MMA.....	193
5.4.5	Polymerization of NIPAM	194
§ 5.5	Conclusion.....	196
§ 5.6	Supporting Information.....	197
5.6.1	Polydispersities of block polymers and blend of polymers	197
5.6.2	Detailed derivation using <i>blend</i> and <i>block</i> strategy.....	201
5.6.3	Differential mass and moments balances.....	209
§ 5.7	References.....	211
6	Literature review on SI-ATRP	213
§ 6.1	Abstract.....	214
§ 6.2	Surface-initiated ATRP (SI-ATRP)	215
§ 6.3	Reactions in SI-ATRP	217
6.3.1	Initiation.....	217
6.3.2	Propagation.....	222
6.3.3	Termination	226
6.3.4	Exchange	237
6.3.5	Transfer	242
6.3.6	Other side reactions.....	243
§ 6.4	Conclusions.....	246
§ 6.5	References.....	247
7	Propagation versus termination in SI-ATRP	252
§ 7.1	Abstract.....	253

§ 7.2	Introduction	254
§ 7.3	Model formulation	257
7.3.1	Living-solution model	260
7.3.2	Propagation model	260
7.3.3	Termination model.....	262
§ 7.4	Results and discussions	264
7.4.1	Kinetics of growth rate	264
7.4.2	Effect of grafting density.....	266
7.4.3	Effect of catalyst concentration (at constant $[C]/[XC]$).....	272
§ 7.5	Conclusion.....	275
§ 7.6	References.....	277
§ 7.7	Appendix.....	279
8	Factors affecting grafting density in SI-ATRP	282
§ 8.1	Abstract.....	283
§ 8.2	Introduction	283
§ 8.3	Simulation details.....	288
§ 8.4	Results and discussions	296
8.4.1	The effect of initiator density.....	297
8.4.2	The effect of catalyst concentration ($[C]$ at a constant $[C]/[XC]$).....	298
8.4.3	The effect of catalyst/deactivator ratio.....	302
8.4.4	The effect of movement per second.....	303
§ 8.5	Conclusion.....	304
§ 8.6	References.....	305
9	Major contributions and recommendations.....	307
§ 9.1	Major contributions.....	307
§ 9.2	Recommendations for future work.....	308
9.2.1	Bulk/solution ATRP studies	308
9.2.2	Surface-initiated ATRP studies.....	311
§ 9.3	References.....	313

List of figures

Figure 2-1. Ideal relation of experimentally obtained data and modeling predictions.....	16
Figure 2-2. Living anionic ring opening polymerization of ethylene oxide.....	26
Figure 2-3. Mechanism of nitroxide-mediated polymerization (NMP). $X \bullet$ is stable nitroxide radical.....	30
Figure 2-4. Mechanism of atom transfer radical polymerization (ATRP). X is halogen group and C is transition metal	30
Figure 2-5. Mechanism of reversible addition-fragmentation chain transfer (RAFT) polymerization. X is RAFT agent without radical leaving group.....	30
Figure 2-6. Reaction scheme of idealized CRP operating under PRE	41
Figure 2-7. Graphical guideline for NMP process with 2% dead chains, 5 h to reach 90% conversion, and dispersity of 1.2 ($\delta = \bar{D} - 1$) ^[115]	47
Figure 2-8. Graphical guideline to determine the limit of control for ATRP of MMA. The blank square indicates the limit of control ^[152]	55
Figure 2-9. Limit of livingness as a function of polymerization rate for bulk ATRP of MMA ^[141]	55
Figure 2-10. Reaction mechanism of ARGET-ATRP and SET-LRP ^[177]	59
Figure 2-11. RAFT as simple degenerative transfer.....	63
Figure 3-1. Various polymerization mechanisms and the resulting full molecular weight distributions	94
Figure 3-2. Understanding the mechanism behind ATRP system by using an analogy to a series of CSTRs	98

Figure 3-3. The analogy of the i^{th} reactor in a series of CSTRs to the i^{th} activation cycles in ATRP reaction system.....	99
Figure 3-4. The possible paths available for a radical chain along with the probabilities.....	100
Figure 3-5. Conceptual graph of variables affecting the degree of control and livingness in ATRP.....	103
Figure 3-6. The evolution of chain length distribution with $\phi_p = 0.3$. Dashed lines: without termination, $f_t = 0$. Solid lines: with termination, $f_t = 0.001$	105
Figure 3-7. Comparison of chain length distribution with various average activation cycles to obtain the same number-average chain length of 100 for the case (a) without and (b) with termination ($f_t = 0.002$)	107
Figure 3-8. The effect of number of activation cycles on polydispersity of system with number-average chain length of 100 and various fractions of terminated chains per activation cycle, f_t	108
Figure 3-9. Comparison of chain distribution with various average activation cycles to obtain the same number-average chain length of 100 for the case with 20% overall dead chain fraction	109
Figure 3-10. Comparison of MWD for cases with number-average chain length of 100 units after 100 activation cycles for various values of dead chain fractions.....	112
Figure 3-11. The effect of dead chain fraction on polydispersity of system with number-average chain length of 100 and various average activation cycles, z	113

Figure 3-12. Comparison of models with and without termination with average activation cycles (z) of 250 and ϕ_p of 0.3 for various dead chain fractions per cycle, f_t	114
Figure 3-13. Simulation results of dormant, dead chains, and overall distributions for polymerization with average activation cycles (z) of 250, ϕ_p of 0.3, and f_t of 0.01 as shown in Figure 3-12.....	114
Figure 4-1. Basic reaction mechanism of ATRP system.....	135
Figure 4-2. Possible reaction pathways of a radical to propagate to add monomeric units, to deactivate with catalyst to form dormant chain, PX , or to terminate with another radical to form dead chain, P	137
Figure 4-3. Discretization of polymerization period to smaller time intervals to obtain CLD.....	139
Figure 4-4. Chain growth history for chains with r monomeric units after 2 intervals in a perfectly living ATRP.....	142
Figure 4-5. Different possible chain growth history for chains with r monomeric units after 2 intervals. Filled circle denotes dead chain-end while hollow circle denotes dormant chain-end.....	147
Figure 4-6. Simulation results of a perfectly living ATRP system. $[M] = 4.7$ M, $[M]:[RX]:[C]:[XC] = 200:1:1:0.1$. (a) Comparison of CLDs obtained by analytical and extended models after 50% and 100% conversion. Solid lines denote extended model with variable probability, dashed lines denote analytical model with probability calculated at $x = 0\%$. (b) Evolution of propagation probability with conversion.....	153
Figure 4-7. (a) Simulation results of CLD for perfectly living ATRP system after 100% conversion ($r_N = 200$). Solid line denotes extended model	

with variable probability, dashed lines denote analytical model with constant probability calculated from various conversions. (b) Evolution of propagation probability with conversion. Polymerization recipe: $[M] = 4.7 \text{ M}$, $[M]:[RX]:[C]:[XC] = 200:1:1:0.1$

.....	154
Figure 4-8. Comparison of CLDs obtained by analytical and extended models after 50% and 75% conversion. Recipe: $[M] = 4.7 \text{ M}$, $[M]:[RX]:[C]:[XC] = 200:1:1:0.1$. Solid lines denote conversion-dependent solution of the extended model, dashed lines denote analytical model with parameters calculated at initial condition.....	156
Figure 4-9. Evolution of simulation parameters with conversion, corresponding to Figure 4-8. (a) Propagation probability. (b) Fraction of dead chains per activation cycle	157
Figure 4-10. Chain length distribution of polymers simulated with the extended model, accounting for conversion dependence, at 50% conversion ($r_N = 100$), with different catalyst and deactivator concentrations. Recipe: $[M] = 4.7 \text{ M}$, $[M]:[RX]:[C]:[XC] = 200 : 1 : a : 0.1a$	159
Figure 4-11. Evolution of simulation parameters with conversion corresponding to Figure 4-10. (a) Propagation probability. (b) Fraction of dead chains per activation cycle	159
Figure 5-1. Initiation and growth steps in a perfectly living anionic polymerization.....	178
Figure 5-2. Initiation, growth, and termination steps in a free radical polymerization.....	178
Figure 5-3. Initiation, growth, and termination steps in an ATRP	178
Figure 5-4. Use of <i>blend</i> and <i>block</i> strategy for an ATRP system with three subpopulations	179

Figure 5-5. Kinetic and dead chain fraction plots for typical ATRP systems under different activation rate constants with $K_{ATRP} = 5 \times 10^{-6}$	189
Figure 5-6. Polydispersity profiles for typical ATRP systems under different activation rate constants with $K_{ATRP} = 5 \times 10^{-6}$	189
Figure 5-7. Polydispersity profiles for typical ATRP systems under different equilibrium constants with $k_a = 5 \text{ M}^{-1}\text{s}^{-1}$	190
Figure 5-8. Estimation of the reaction rate parameters for ATRP of HEMA in DMF at room temperature from the kinetic data. Experiment data were obtained from Beers et al. ^[17]	191
Figure 5-9. Comparison of experimentally obtained polydispersity with the predictions from Equations (6) and (12) for ATRP of HEMA in DMF at room temperature. Experiment data were obtained from Beers et al. ^[17]	192
Figure 5-10. Estimation of the reaction rate parameters for ATRP of MMA in anisole at 90°C from the kinetic data. Experiment data were obtained from Gromada et al. ^[18]	193
Figure 5-11. Comparison of experimentally obtained polydispersity with the predictions from Equations (6) and (12) for ATRP of MMA in anisole at 90°C. Experiment data were obtained from Gromada et al. ^[18]	194
Figure 5-12. Estimation of the reaction rate parameters for ATRP of NIPAM in DMSO at 20°C from the kinetic data. Experiment data were obtained from Bontempo et al. ^[19]	195
Figure 5-13. Comparison of experimentally obtained polydispersity with the predictions from Equations (6) and (12) for ATRP of NIPAM in DMSO at 20°C. Experiment data were obtained from Bontempo et al. ^[19]	196

Figure 6-1. Effect of initiator spacer length on the initiation efficiency of SI-ATRP of styrene and MMA with CuBr. Detailed experimental conditions can be found in the original publications ^[24,25]	220
Figure 6-2. Effect of confinement on grafting efficiency (σ_g/σ_i), as simulated for surface-initiated polymerization within a spherical cavity or channel with various curvatures; R : radius of the cavity. Reprinted with permission from ^[40]	221
Figure 6-3. Model predictions of the chain length of grafted and free polymers in simultaneous surface-initiated polymerization with various grafting densities (σ) and fractions of grafted polymer (η). Reprinted with permission from ^[43]	225
Figure 6-4. <i>Left</i> (a): Possible termination modes involved in SI-ATRP on a flat substrate. The estimated distances shown are calculated based on the assumption of high grafting density (1 chain/nm ²), a typical ratio of radical to dormant chains in ATRP ($[P\cdot]/[PX] = 10^4$ to 10^6), and typical brush thickness of 100 nm. <i>Right</i> (b): Migration of surface radicals through activation/deactivation in SI-ATRP promotes termination between surface radicals. Reprinted with permission from ^[53]	227
Figure 6-5. Growth kinetics of grafted polymer for different catalyst concentrations in SI-ATRP of methyl acrylate (MA) from gold substrate, with $[MA] = 2$ M and $[CuBr_2/Me_6TREN]/[CuCl/Me_6TREN] = 0.3$. Lines show the predicted result from the model. Data points were experimentally obtained: <i>squares</i> 40 mM, <i>circles</i> 2 mM, <i>triangles</i> 0.1 mM ^[53,54]	229
Figure 6-6. Interparticle and intraparticle termination modes between two surface radicals in SI-ATRP on nanoparticles.....	232

Figure 6-7. Interparticle coupling in SI-ATRP on nanoparticles for bulk and miniemulsion systems. The compartmentalization of particles in a miniemulsion prevents macroscopic gelation from occurring. Reprinted with permission from [37].....	234
Figure 6-8. Molecular weight distributions of grafted chains for SI-ATRP of MMA from a concave substrate. Detailed experimental conditions are provided in the original literature. $M_{p,l}$ indicates the molar mass at the peak for the living chains. (1) 50%, $M_{p,l} = 16,320$ g/mol; (2) 62%, $M_{p,l} = 21,880$ g/mol; (3) 91%, $M_{p,l} = 30,020$ g/mol. The lower peak ($M_p = 2500$ g/mol) indicates the presence of dead chains. Reprinted with permission from [39]	236
Figure 6-9. Growth profiles of grafted polystyrene on a silicon wafer with addition of sacrificial initiator (circles) or deactivator (squares). Reprinted with permission from [69].....	239
Figure 6-10. The growing viscous front for SI-ATRP postulated by Behling et al. The local concentration of catalyst in the shaded area is higher than that in the bulk solution, whereas the local concentration of deactivator is lower than that in the bulk. (a) conversion of catalyst (\diamond) to deactivator (\circ) (b) conversion of deactivator to catalyst. Reproduced with permission from [18]	241
Figure 6-11. Generation of a gradient of catalyst-to-deactivator concentration ratio induced by adjusting the distance between the surface and the electrode, resulting in a gradient in the thickness of the grafted polymer layer. Reproduced with permission from [71].....	241
Figure 6-12. Presence of free polymer chains in a grafted nanoparticles system. The free chains act as bridges for the grafted nanoparticles to form a network. Reproduced with permission from [79].....	244

Figure 6-13. SEC results for polystyrene grafted from silica nanoparticles with different polymerization recipes. The concentration axis on the right is only applicable to peaks at 16-17 mL. Reprinted with permission from [29]	244
Figure 6-14. Formation of nanonetwork polymers and carbon materials using SI-ATRP from silica nanoparticles. Reproduced with permission from [81]	246
Figure 7-1. Comparison of growth profiles predicted using living-solution, propagation, and termination models to previously published SI-ATRP experiment data.[25] Simulation parameters are shown in Table 7-2.....	265
Figure 7-2. Growth profiles of the grafted polymer at various graft densities (or initiator densities, τ^*). Solid lines are guides to eyes. (a)–(c) dry thickness profile, (d)–(f) normalized dry thickness profile. (a),(b),(d),(e) SI-ATRP of poly(methyl methacrylate) (PMMA) on gold-coated surfaces.[26,27] (c), (f) SI-ATRP of poly(N-isopropylacrylamide) (PNIPAM) on silicon wafers[29]	267
Figure 7-3. Dry thickness profiles of the grafted polymers grown via SI-ATRP for various grafting densities predicted with $[M]:[C] = 100$ using (a) propagation model (b) termination model. Dashed lines represent simulation results using living-solution model.....	268
Figure 7-4. Normalized thickness profile of the grafted polymers grown via SI-ATRP for various grafting densities predicted with $[M]:[C] = 100$ using (a) propagation model (b) termination model. Dashed lines represent the simulation results obtained using living-solution model	270
Figure 7-5. Dry thickness profiles for SI-ATRP at various catalyst levels with $\tau = 0.5$ chains/nm ² . Solid lines are guides to eyes. (a) $[M] = 2$ mol/L,	

	[XC] = 0.3[C], and [M]/[C] of 50, 1000, and 20,000. ^[16] (b) [M] = 8.7 mol/L, [XC] = 0.1[C], and [M]/[C] of 100, 400, and 1000 ^[24]	272
Figure 7-6.	Dry thickness growth profiles predicted using various models at different catalyst concentrations. Solid lines denote predicted growth profiles using termination model	273
Figure 8-1.	Monte Carlo algorithm used to simulate SI-ATRP process.....	289
Figure 8-2.	The effect of initiator density on the evolution of grafting density ([M] = 3 mol/L, [M]/[C] = 25, and [C]/[XC] = 10).....	297
Figure 8-3.	The effect of catalyst concentration on grafting density, simulated for systems with [M] = 3 mol/L, [C]/[XC] = 10, and (a) $\tau_i/\tau^* = 1$, (b) $\tau_i/\tau^* = 0.25$	298
Figure 8-4.	The number of monomers added per activation cycle with varying catalyst and deactivator concentrations. The value is calculated based on the maximum value exhibited by that system at the beginning of polymerization for [M] = 3 mol/L, [C]/[XC] = 10, and (a) $\tau_i/\tau^* = 1$, (b) $\tau_i/\tau^* = 0.25$	300
Figure 8-5.	The evolution of grafting density and thickness with time for different catalyst and deactivator concentrations ([M] = 3 mol/L, $\tau_i/\tau^* = 1$, and [C]/[XC] = 10)	301
Figure 8-6.	The effect of deactivator concentration on the grafting density ([M] = 3 mol/L, [M]/[C] = 25, and $\tau_i/\tau^* = 1$)	302
Figure 8-7.	The effect of movement attempts per second on the final grafting density, simulated at [M] = 3 mol/L, [M]/[C] = 25, and [C]/[XC] = 10. (a) $\tau_i/\tau^* = 0.25$, (b) $\tau_i/\tau^* = 0.25$ and 1.0	303

Figures in the appendices

Figure A3-1. The activation of initiator molecules followed by deactivation or termination..... 124

Figure A3-2. The analogy of dormant and dead chains that have been activated twice to a series of two reactors 127

Figure A5-1. Diblock polymers 199

Figure A5-2. Blend of two polymer subpopulations 200

Figure A5-3. Polymer subpopulations when the time is divided into two intervals..... 204

List of tables

Table 2-1. Various modeling works on living polymerization.....	28
Table 2-2. Summary of dispersity expressions derived for NMP (and ATRP).....	39
Table 3-1. Reaction mechanisms involved in atom transfer radical polymerization (ATRP).....	97
Table 3-2. Summary of the MWD equations for ATRP system, derived from analogy to a series of CSTRs.....	102
Table 3-3. Simulation results for the evolution of MWD after different activation cycles, corresponding to Figure 3-6.....	105
Table 3-4. Simulation results for the effect of number of activation cycles (z) for cases with and without termination, corresponding to Figure 3-7.....	107
Table 3-5. Simulation results for cases shown in Figure 3-10 with various dead chain fractions to investigate the effect of livingness.....	112
Table 4-1. Reactions involved in atom transfer radical polymerization (ATRP) ...	139
Table 4-2. Reaction rate constants used in simulation of ATRP system.....	151
Table 4-3. Simulation results for perfectly living ATRP corresponding to Figure 4-6 (a).....	153
Table 4-4. Simulation results for ATRP system by model with termination, corresponding to Figure 4-8. Recipe: $[M] = 4.7 \text{ M}$, $[M]:[RX]:[C]:[XC] = 200:1:1:0.1$	156
Table 4-5. Simulation results for ATRP systems corresponding to Figure 4-10	159
Table 5-1. Comparison of the underlying assumptions in the derivation of various polydispersity expressions for ATRP systems.....	185

Table 5-2. Reaction parameters used in the comparison of polydispersity predictions with numerical integration of moments' balances	188
Table 7-1. Underlying assumptions for various models discussed in this study....	259
Table 7-2. Simulation parameter for the model prediction of SI-ATRP experiment data ^[25]	265
Table 7-3. Simulation parameters used for the model prediction in Figure 7-3, Figure 7-4, and Figure 7-6	268
Table 7-4. Comparison of experiment trends to the predicted results from various models	275
Table 8-1. Reaction parameters used in the simulations.....	293

Tables in the appendices

Table A5-1. Differential mass and moments balances for an ATRP system	210
Table A7-1. Relation between wet thickness to grafting density and average chain length for various grafted polymer conformation in good solvent	280

List of abbreviations and symbols

Abbreviations

ATRP	atom transfer radical polymerization
CLD	chain length distribution
CRP	controlled radical polymerization
CSTR	continuous stirred tank reactor
FRP	free radical polymerization (conventional)
LAP	living anionic polymerization
LP	living polymerization
MC	Monte Carlo
MMA	methyl methacrylate
MWD	molecular weight distribution
NMP	nitroxide-mediated radical polymerization
PDI	polydispersity index
PRE	persistent radical effect
QSSA	quasi steady state assumption
RAFT	reversible addition-fragmentation chain transfer
RDRP	reversible deactivation radical polymerization
SI-ATRP	surface-initiated ATRP

Symbols and mathematical variables

$[C]$	concentration of catalyst
$[M]$	concentration of monomer
$[P_r]$	concentration of dead chains with r monomeric units
$[P_rX]$	concentration of dormant chains with r monomeric units
$[P^*]$	concentration of radical chains with r monomeric units

$[Q_i]$	i^{th} moment of polymer chains
$[XC]$	concentration of deactivator
DCF	dead chain fractions
f_t	fraction of chains terminated in one activation cycle
k_a, k_d, k_p, k_t	activation, propagation, deactivation, termination rate constants
k_{tc}	coupling termination rate constant
k_{td}	disproportionation termination rate constant
K and K_{ATRP}	equilibrium constant ($\equiv k_a/k_d$)
L_x, L_y, L_z	lattice size in x, y, and z direction
N_{Av}	Avogadro's number
r_n or r_N	number-average chain length
r_w or r_W	weight-average chain length
PDI or \mathcal{D}	polydispersity index (dispersity)
X or x	conversion
z	average number of activation cycles
$n(r)$	number fraction of polymer chains with r monomeric units
$w(r)$	weight fraction of polymer chains with r monomeric units
ϕ_p	probability of a radical to undergo propagation
ϕ_d	probability of a radical to undergo deactivation
ϕ_t	probability of a radical to undergo termination
τ	graft density

Declaration of academic achievement

This thesis is organized based on a “sandwich” style consisting of 6 journal articles and a prepared manuscript. The contributions from the authors of these articles are summarized below:

- Erlita Mastan is the primary author of the four research papers, a prepared manuscript, and a review paper reproduced in this thesis (Chapter 2-5, 7, & 8).
- Erlita Mastan is one of the co-authors of a review article, whose contribution to the review is included in Chapter 6 of this thesis.
- Dr. Shiping Zhu is the advisor in all the articles, providing continuous guidance, ideas, brainstorming sessions, and revisions to the manuscript drafts.
- Dr. Xiaohui Li is the co-author for a review article reproduced in Chapter 2, giving the necessary revisions to the draft of the review.
- Dr. Dapeng Zhou is the co-author for journal articles reproduced in Chapter 3 and 4, providing the necessary inputs to these manuscript drafts.
- Dr. Amir Khabibullin and Dr. Krzysztof Matyjaszewski are the collaborators from Carnegie Mellon University for a review article that is partly included in Chapter 6.
- Dr. Li Xi is the co-author for a journal article and a prepared manuscript reproduced in Chapter 7 and 8. He lent his expertise and provided the research guidance and discussions needed to complete these works.

1 INTRODUCTION

In this chapter, a brief research background, the main research objectives, and the organization of this thesis are presented.

§ 1.1 Research background

In today's society, polymeric materials can be found from everywhere in our daily life, from commodity products to high-end and specialized products. This wide range of applications owes to their unlimited possibilities in combining properties that different polymers may possess. One of the factors that determine the properties of polymer products is their chain microstructural properties, such as molecular weight distribution, composition distribution, sequence distribution, and chain architectures. These microstructural properties can be tailored during the polymerization processes. Different polymerization techniques offer different

degrees of control over these properties. It is crucial to understand the mechanism behind a polymerization system in order to utilize it to its maximum ability.

Atom transfer radical polymerization (ATRP) is a type of controlled radical polymerization (CRP, or also referred to as reversible deactivation radical polymerization, RDRP^[1]). ATRP is popular due to its ability to precisely synthesize polymer chains with pre-specified properties, tailored by simply altering the polymerization recipes, as well as reactor operation conditions. ATRP is also applicable for the synthesis of densely-grafted and thick polymer brushes through surface-initiated ATRP (SI-ATRP). However, as evident from the reviews of current literatures, there is still a lack of understanding in the mechanisms of ATRP and SI-ATRP.^[2-4] This thesis summarizes our attempts to gain more insights into these mechanisms through modeling approaches. Detailed literature reviews are given in the other chapters of this thesis (Chapter 2 and 6), thus only brief summary of the research background are presented here.

One issue that is often overlooked in the modeling of ATRP or other CRP-based systems is the presence of radical termination reactions. Even though termination in ATRP is suppressed in comparison to the conventional free radical polymerization, this reaction is still unavoidable due to the nature of active radicals. The termination reaction and the resulting dead chains affect the polymerization kinetics and the properties of polymer chains. The effect of termination on the kinetics of various CRP

systems has been investigated in the literature.^[2,5-7] However, the contribution of dead chains on the resulting polymer molecular weight distribution (MWD) and its polydispersity (or also referred to as dispersity^[8]) still could not be quantified. These chain properties have only been investigated under perfectly living conditions.^[3,9] Therefore, the first part of our study is dedicated to investigate how termination affects MWD and polydispersity in bulk/solution ATRP systems. In addition, we aim to obtain most desired explicit expressions for these properties in order to make experimental data correlation easier.

In SI-ATRP systems, multiple literatures reported the growth rates of polymer brushes on flat substrates to decrease with time, even when there is still an abundance of monomer in the solution.^[10,11] This experiment trend can be explained by either a *termination* theory or a *propagation* theory.^[12,13] In the *termination* theory, termination reactions are postulated to occur between surface radicals thus reducing the number of growing chains, which in turns result in the decrease of growth rate (*i.e.*, chemical limitation). On the other hand, the *propagation* theory proposed that the deceleration of growth rate is caused by crowding in the grafted polymer layer, which reduces the number of available monomer for the propagation of polymer chains (*i.e.*, physical limitation). It is important to evaluate the importance of these two theories in order to better understand the SI-ATRP mechanisms. The second part of our study aims to investigate the main factors affecting the kinetics of SI-ATRP. We begin by comparing the reported experiment trends with those predicted by

simplified models developed from the two theories, *termination vs. propagation*. The factors that may affect the resulting grafting density in SI-ATRP are then investigated by means of simulations in attempt to compensate for the difficulty in experimental measurements of grafting density of polymer chains grown on flat substrates.

§ 1.2 Research objectives

The objectives of this study are summarized below, with the detailed contributions of each chapter provided in the following section of thesis organization.

- To derive an explicit expression for polymer molecular weight distribution (MWD) of ATRP that accounts for dead chains under constant concentrations of reactants (Chapter 3)
- To investigate the effect of termination on the MWD of ATRP at varying concentrations of the reactants (Chapter 4)
- To derive an easy-to-use explicit expression for polydispersity of an ATRP system that accounts for the contribution of dead chains (Chapter 5)
- To evaluate the validity of the two existing theories in explaining the growth kinetics of SI-ATRP (Chapter 7)
- To investigate various factors affecting the resulting grafting density of polymer brushes in SI-ATRP (Chapter 8)

§ 1.3 Thesis organization

This thesis follows “sandwich” style, comprising of several published articles in peer-reviewed journals and a prepared manuscript draft. Other than changes in the bibliographic styles and the numbering of figures and tables to ensure consistency throughout this thesis, the text are copied verbatim from the original manuscript, unless otherwise stated. For clarity purposes, this thesis is divided into two main parts, with the first part dealing with bulk/solution ATRP and the second focusing on SI-ATRP. Finally, the main contributions from this thesis along with recommendations for future works are provided in Chapter 9.

Part I – Bulk/solution atom transfer radical polymerization (ATRP)

In the first part of this thesis, the research work on bulk/solution ATRP is first presented, starting with a comprehensive literature review, identifying the key issues in the area, followed by modeling works conducted to fill the gaps found in the literature.

Chapter 2 presents a literature review on the progresses in the modeling work for controlled radical polymerization systems. This review is published in *Progress in Polymer Science* journal, **2015**, 45, p.71-101 (doi:10.1016/j.progpolymsci.2014.12.003). It is evident from this review that there is a lack of information on the effect of termination on the full MWD and on the polydispersity of ATRP systems, despite the

fact that thousands of papers have been published every year for the past two decades in this area. The available expressions were derived under the assumption of a perfectly living condition (*i.e.*, no termination). However, due to the radical nature of propagating chains in ATRP, radical termination is unavoidable. Knowledge of full MWD is desirable and beneficial because it provides information on the whole polymer population. This problem becomes our main research objectives in the subsequent chapters in this first part.

Chapter 3 reports the derivation of an explicit expression of the MWD that accounts for the termination effect. This work is published in *Journal of Polymer Science, Part A: Polymer Chemistry*, **2014**, 52 (5), p.639-651 (doi:10.1002/pola.27046). The expression was derived by analogously relating the activation/deactivation reactions in ATRP to a series of continuous stirred tank reactors (CSTRs) and by assuming constant concentrations of reactants. By borrowing chemical engineering concepts and applying it to the kinetic equations of polymerization, an explicit MWD expression was achieved. This expression allows us to quantify the effect of termination on the broadening of polymer MWD.

Chapter 4 presents the modeling work related to the extension of molecular weight distribution expression derived in Chapter 3 to expand its applicability. The work presented in the previous chapter is limited to the cases in continuous processes or for the polymerization at low monomer conversion due to the constant

concentrations assumed in the derivation. By discretization of polymerization time, this modeling work relaxed the assumption of constant reactants' concentrations. Therefore, this work provided a method to predict the MWD of an ATRP system at a moderate to high conversion. This chapter is a reproduction of an article published in *Macromolecular Theory and Simulations* journal, **2014**, 23 (3), p.227-240 (doi:10.1002/mats.201300166).

Chapter 5 presents a new polydispersity expression for ATRP that accounts for the contribution of dead chains in the distribution broadening. This chapter is a reproduction of a published article in *Macromolecules* journal, **2015**, 48 (18), p.6440-6449 (doi:10.1021/acs.macromol.5b01525). The popular polydispersity expression available in the literature for ATRP can only predict that of the living chains, while ignoring the contribution of dead chains. Using the results from Chapter 3 and 4, an expression for polydispersity was derived by treating the polymer chains as “block” polymers and “blend” of polymer subpopulations. This equation was then used to correlate several experiment data from the literature, showing better agreement than the existing equation. Having an explicit expression for polydispersity allows easier comparison between experiment data with the theoretical prediction, which in turn allows straightforward parameter estimations.

Part II – Surface-initiated ATRP (SI-ATRP)

In the second part of this thesis, the research work on SI-ATRP is presented. The organization is similar to the first part, starting with a comprehensive literature review, identifying the remaining key issues, followed by modeling works conducted in attempts to answer some fundamental questions in this area.

Chapter 6 presents a literature review for SI-ATRP. This review is a result of collaboration with researchers from Carnegie Mellon University, Dr. Amir Khabibullin (primary author) and Dr. Krzysztof Matyjaszewski, and it is published as a chapter in *Controlled Radical Polymerization at and from Solid Surfaces* book, **2015**, p.29-79 (doi:10.1007/12_2015_311), which is volume 270 of the series *Advances in Polymer Science*. This chapter does not include the entire published work, but instead, it only presents the review on various reactions in SI-ATRP, which was contributed by our group at McMaster University. The two theories often used in explaining the kinetics of ATRP as a grafting method, *propagation* and *termination* theories, are summarized in this chapter. The *propagation* theory attributes the decrease in the growth rate of polymer brush to the crowding effect, while assuming perfectly living conditions. On the other hand, the termination theory proposes that the growth of grafted polymer is limited by the termination of surface radicals, thus decreasing the active-end concentration. To date, no conclusion has been reached as to which theory governs the growth kinetics in SI-ATRP.

Chapter 7 reports a comparison of the model predictions based on the *propagation* and *termination* theories. This work is published in *Macromolecular Theory and Simulations* journal, **2015**, 24 (2), p.89-99 (doi:10.1002/mats.201400085). A simplified model to capture the trend of propagation theory was derived, while a previously published model for the termination theory was used. The predicted kinetic trends based on the two models were qualitatively compared with various published experiment trends. The comparison showed that neither models can fully explain the contradicting experimental trends reported in the literature.

Chapter 8 presents the simulation works done in investigating the factors affecting grafting density in SI-ATRP. Grafting density plays a crucial role in determining the resulting surface properties. However, it is difficult to accurately measure grafting density of polymers grafted on flat surfaces due to the limited amount of grafted polymers available. Therefore, it is not clear how grafting density is affected by the polymerization conditions. By investigating grafting density, we hope to provide an alternate explanation on the trends that could not be reproduced by the two theories proposed in Chapter 7. In the simplified models, grafting density is assumed to be a known quantity and it is not affected by polymerization condition. This chapter is a draft of manuscript that will be submitted to a peer-reviewed journal in the near future.

As a closing, the summary of major contributions made during this study and several recommendations on future research direction are provided in **Chapter 9**.

§ 1.4 Other works

Other works completed during this study, but not included in this thesis are listed below:

- Co-authored an article on the modeling of surface-initiated reversible addition-fragmentation chain transfer (RAFT) polymerization (Primary author: Dr. Dapeng Zhou, a visiting professor from Jiaxing University, China). This work is published in *Macromolecular Theory and Simulations* journal, **2012**, 21 (9), p.602-614 (doi:10.1002/mats.201200043)
- A tutorial article on the use of method of moments for modeling of polymerization and polymer modification systems. Published in *European Polymer Journal*, **2015**, 68, p.139-160 (doi:10.1016/j.eurpolymj.2015.04.018)
- Co-authored a review article (Primary author: Dr. Xiaohui Li, a visiting PhD student from Zhejiang University, China) on reactor engineering of controlled radical polymerization. This manuscript is currently under peer-review process in *Reaction Chemistry & Engineering* journal

§ 1.5 References

- [1] A. D. Jenkins, R. G. Jones, G. Moad, *Pure Appl Chem* **2010**, 82.

-
- [2] A. Goto, T. Fukuda, *Prog Polym Sci* **2004**, *29*, 329-385.
- [3] E. Mastan, X. Li, S. Zhu, *Prog Polym Sci* **2015**, *45*, 71-101.
- [4] A. Khabibullin, E. Mastan, K. Matyjaszewski, S. Zhu, "Surface-Initiated Atom Transfer Radical Polymerization", Springer Berlin Heidelberg, 2015, p. 1-48.
- [5] H. Fischer, *J Polym Sci, Part A: Polym Chem* **1999**, *37*, 1885-1901.
- [6] S. Zhu, *J Polym Sci, Part B: Polym Phys* **1999**, *37*, 2692-2704.
- [7] S. Zhu, *Macromol Theory Simul* **1999**, *8*, 29-37.
- [8] R. Gilbert, M. Hess, A. Jenkins, R. Jones, P. Kratochvil, R. Stepto, *Pure Appl Chem* **2009**, *81*, 351-353.
- [9] A. H. Müller, G. Litvinenko, D. Yan, *Macromolecules* **1996**, *29*, 2346-2353.
- [10] J. D. Jeyaprakash, S. Samuel, R. Dhamodharan, J. Rühle, *Macromol Rapid Commun* **2002**, *23*, 277-281.
- [11] J.-B. Kim, W. Huang, M. D. Miller, G. L. Baker, M. L. Bruening, *J Polym Sci, Part A: Polym Chem* **2003**, *41*, 386-394.
- [12] D. Zhou, X. Gao, W.-j. Wang, S. Zhu, *Macromolecules* **2012**, *45*, 1198-1207.
- [13] S. Turgman-Cohen, J. Genzer, *Macromolecules* **2010**, *43*, 9567-9577.

2 LITERATURE REVIEW ON THE MODELING OF CRP SYSTEMS

This chapter serves as a literature survey on the modeling works for controlled radical polymerization (CRP) systems. This chapter is a part of a published article entitled “Modeling and theoretical development in controlled radical polymerization” in *Progress in Polymer Science* journal, **2015**, 45, p.71-101 (doi:10.1016/j.progpolymsci.2014.12.003), reproduced with permission from Elsevier. In order to avoid significant repetitions, the last two parts of the published review on heterogeneous CRP and surface-initiated CRP are not included here. Minor modifications were made in the Introduction section to keep its consistency after these omissions. Literature review on surface-initiated ATRP is included in Chapter 6 to preserve the flow of this thesis.

Author contributions

Erlita Mastan prepared the first draft after discussions with Dr. Shiping Zhu on the content and organization of the review. Dr. Xiaohui Li provided the first revision, with the final revision done by Dr. Shiping Zhu.

§ 2.1 Abstract

Controlled radical polymerization (CRP) systems have gained increasing interests for the past two decades. Numerous publications may be found in the literature reporting experimental and modeling work on various CRP processes, including their use in surface modification through grafting. Knowledge of underlying mechanism behind polymerization systems is valuable for product design and process optimization. This information may be obtained through the combination of modeling and experimental studies. In this review, published studies on kinetic and stochastic based modeling for CRP systems are summarized. Their relevance in model discrimination of proposed mechanisms is discussed. This review also includes various parameter estimation studies, that is crucial to obtain accurate simulation predictions. Existing issues on the fundamental mechanism in CRP processes are also addressed.

§ 2.2 Introduction

The two extremes of chain growth polymerization systems with respect to the level of control in producing synthetic polymers are free radical polymerization (FRP) and

living polymerization (LP). In FRP, polymer chains are initiated, propagated, and terminated almost instantaneously. The initiation occurs throughout the polymerization, resulting in chains growing under different conditions, depending on when they are initiated. This, in turn, results in a broader distribution of polymer chain length, or equivalently degree of polymerization. Therefore, FRP only provides limited to no control on the properties of the synthesized product and involves 100% termination. However, due to its versatility in monomer selections and relative insensitivity to impurity, FRP is still widely used in industrial settings.

The term “living polymer” was first coined by Michael Szwarc in 1956,^[1] who studied anionic polymerization of styrene in tetrahydrofuran. The polymerization occurred in the absence of conventional bimolecular termination or any irreversible transfer, hence producing narrowly distributed living polymer. This living polymer may be extended in a subsequent polymerization, providing easy synthesis route for block copolymers. This discovery have inspired the developments of various living polymerization processes, including but not limited to, carbocationic polymerization, ring opening polymerization (ROP), and ring opening metathesis polymerization (ROMP). However, depending on their mechanisms, most LPs are very sensitive to impurities. Therefore, LP usually requires very stringent reaction conditions and only applicable to limited types of monomers.

Controlled radical polymerization (CRP), or reversible deactivation radical polymerization (RDRP), may be viewed as a middle ground, by combining the best of FRP and LP. It provides an alternative to FRP, since ideal CRP involves instantaneous initiation at the beginning of the polymerization and suppression of bimolecular termination. This results in a narrow molecular weight distribution (MWD) of polymer chains, owing to the simultaneous growth of all chains. On the other hand, CRP is not as restrictive as LP in terms of monomer selection and reaction condition. Because of the level of control and high degree of living character in the synthesized polymer, CRP is also suitable in producing block copolymers, star polymers, and other types of polymers with well-defined architectures. The three major types of CRP in the literature are nitroxide mediated polymerization (NMP, also known as stable free radical polymerization, SFRP),^[2,3] atom transfer radical polymerization (ATRP),^[4,5] and reversible addition fragmentation chain transfer (RAFT).^[6]

The relation between experimental and modeling approaches is clear, as illustrated in Figure 2-1. On one hand, modeling is essential for quality control, process design, and optimization of experiments. For example, the quality control of copolymerization using FRP in a semi-batch process is generally accomplished using model-based control, developed using the well-known pseudo-kinetic rate constant concept.^[7] On the other hand, simplifying assumptions are usually involved in model formulation, that must be justified through experimental data. Some models might have limited applicability, such that there may be a range of experimental conditions

for which the models give inaccurate predictions. Comparison of data obtained from experiments to those from simulation results is commonly used as a mean of model discrimination and/or for parameter estimation. More importantly, the underlying mechanism behind a system may be determined reliably through the combined approach of modeling and experiment. Using models, the polymerization kinetics (conversion profile) and the properties of polymers may be predicted and optimized.

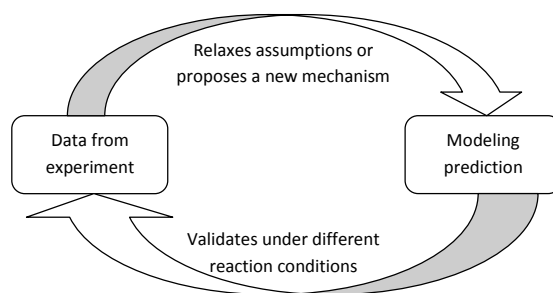


Figure 2-1. Ideal relation of experimentally obtained data and modeling predictions

This review focuses on kinetics and polymer chain properties that are commonly reported in experimental studies, *i.e.*, molecular weight distribution MWD (also known as molar mass distribution), number-average molecular weight M_n , weight-average molecular weight M_w , and dispersity \mathcal{D} (formerly better known as polydispersity index, PDI). For homopolymers, the first three properties are equivalent to chain length distribution CLD, number-average chain length r_n , and weight-average chain length r_w , respectively. The use of chain length-based properties is chosen in lieu of those based on molecular weight, with chain length referring to the number of monomeric units in a chain (equivalent to the degree of

polymerization). The definition of average properties, r_n , r_w , and \bar{D} , in terms of the CLD are shown in Equation (1)–(3), respectively, with $n(r)$ representing the mole fraction of polymer chains having r monomeric units. From these equations, it is obvious that knowledge of the CLD allows calculation of r_n , r_w , and \bar{D} , but the reverse is not true. Unless a distribution type is assumed, the full expression of CLD cannot be inferred from the average properties.

$$r_n \equiv \sum_{r=0}^{\infty} [r \times n(r)] \quad (1)$$

$$r_w \equiv \frac{1}{r_n} \sum_{r=0}^{\infty} [r^2 \times n(r)] \quad (2)$$

$$\bar{D} \equiv \frac{r_w}{r_n} \quad (3)$$

A summary of modeling work on CRP processes is provided in the following. First, a brief discussion on various modeling approaches for polymerization processes along with their predictive ability is presented. The second part deals with a short summary of modeling work on living polymerization relevant on modeling for CRP systems. The next part of the review summarizes the published modeling work, in attempts to understand the mechanisms involved in the three CRP types, NMP, ATRP, and RAFT, under homogeneous conditions.

§ 2.3 Modeling techniques

In this section, various modeling approaches, both kinetic and stochastic based approaches, commonly applied on polymerization processes in solutions/bulk are briefly discussed. The discussion includes the range of predictive ability for the polymer chain properties that are generally reported in experimental work, r_n , r_w , and \bar{D} . The modeling approaches discussed are by no means comprehensive, but they represent some of the most commonly used simulation methods for the polymerization systems presented in the literature. For modeling techniques that are generally used on surface-initiated CRP (SI-CRP) systems, such as Monte Carlo simulation with bond fluctuation model, coarse-grained molecular dynamics, etc., readers are encouraged to read a recent review by Bain et al.^[8]

2.3.1 Kinetic-based approach

The kinetic-based approaches, or also known as deterministic approaches, are methods that involve solving a set of algebraic/differential equations obtained from the mass balances. For a polymer population, the number of mass balances required is theoretically infinite, because each polymer chain could possess any number of monomeric units, from 1 to ∞ . Equation (4) shows an example of the infinite differential equations for polymer chains possessing r monomeric units, $[P_r]$, produced via disproportionation termination of two radicals, $[P^\bullet]$, with rate constant (also referred to as a rate coefficient) of k_{td} .

$$\frac{d[P_r]}{dt} = k_{td}[P_r^\bullet] \sum_{s=0}^{\infty} [P_s^\bullet] \quad r \in \mathbb{N} \quad (4)$$

The most obvious and straightforward method to solve the set of differential equations is by simultaneously solving these equations numerically. This method is referred to as direct integration of mass balances. This method tends to be computationally expensive, even with truncation of possible chain lengths of polymer to limit the number of differential equations. Moreover, the concentration of growing radicals with length r depends on that of radicals with length $r-1$. Therefore, all of the differential equations must be solved, since they are dependent on one another. Nevertheless, as computers have becoming increasingly more powerful, this method has been shown to be a viable approach with a reasonable calculation time. In addition, this method allows the model to account for the effect of chain length dependence of reaction rate constants. It is worth noting that if the reaction rate constants do not significantly vary with chain length, the polymerization rate may be predicted with only a few mass balance equations, but not the polymer chain-length properties.

It is clear that direct integration approach allows prediction of the full CLD, because it calculates chain concentrations for all possible chain lengths. It could also be expected that this method is more appropriate for polymerization systems that generate narrow CLD polymers than for those that produce polymers with broader CLD. This is because narrower CLD implies that a smaller range of chain lengths need to be

considered, thereby reducing the number of equations involved. Moreover, the CLD of linear polymers are easier to model than those of branched polymers.

It should be noted that there are many numerical integration techniques that may be used in the direct integration approach to solve the differential equations. Some of the differential equations may be reduced to algebraic equations via simplifying assumptions wherever applicable (*e.g.*, quasi steady state assumption for radical population), thus reducing the complexity and stiffness of the system. Another technique to simplify the system is by grouping chain lengths together to form several finite intervals,^[9] as demonstrated in fixed pivot, moving pivot, and orthogonal collocation on finite element (OCFE) methods. Kiparissides et al. showed comparison of the fixed pivot and OCFE methods for calculation of the full CLD in FRP systems.^[10]

Another method that is widely used in modeling polymerization systems is the method of moments. This method combines moment definitions with kinetically-derived mass balances, by rewriting the mass balances into moment balances. Equation (5) shows the definition of n^{th} order moment, $[Q]_n$, for polymer chains, P . The popularity of this method is mainly owing to its ability to simplify the large number of differential equations of mass balance into a smaller number of differential equations of moment balance. The profile of average properties of polymer may then be obtained by solving various orders of the moment balances.

$$[Q]_n \equiv \sum_{r=0}^{\infty} r^n [P_r] \quad (5)$$

The number-average chain length, r_n , may be obtained from the ratio of the first order moment to the zeroth order moment, and the weight-average chain length, r_w , may be calculated from the ratio of the second order moment to the first order moment. This means that the r_n , r_w , and \bar{D} may be calculated by solving only three differential equations, *i.e.*, balances for zeroth, first, and second order moments (along with mass balances for small reactants involved). This is a dramatic simplification in comparison to the infinitely large number of equations involved in the direct integration approach. Other types of chain length averages (*e.g.*, z-average chain length) may also be obtained by incorporating higher order moments. In addition, the method of moments has been used in the derivation of explicit expressions for the average chain properties (*e.g.*, r_n , r_w , and \bar{D}) as functions of time. Having explicit expressions facilitates understanding of the effect of various parameters on these properties.

It should be noted that the method of moments cannot predict the full CLD of a synthesized polymer. Moreover, this method is not able to account for explicit chain length-dependence of reaction rate constants. However, for CRP processes producing narrowly distributed polymer chains, this dilemma may be solved by approximating numerous chain lengths with a single number-average chain length, that could then be related to time. Alternatively, an extension of the method of moments to account

for the chain length dependence of reaction rate constants has been proposed by D'hooge et al.^[11]

Another approach to model polymerization processes is through the use of probability generating functions (PGF). Similar to the method of moments, the basis of PGF is in combination of statistical and kinetic approach, whereby the mass balances are rewritten as generating function balances. The definition of generating function, $G(z)$, of polymer chains, P , is shown by Equation (6). This definition is then used to transform mass balances into PGF balances. One of the properties of generating functions allows for inversion of PGF to obtain the full CLD of polymers, as shown by Equation (7).

$$G(z) \equiv \sum_{r=0}^{\infty} z^r [P_r] \quad (6)$$

$$[P]_r = \frac{1}{r!} \left. \frac{d^r G}{dz^r} \right|_{z=0} \quad (7)$$

Using software package is another alternative to conduct modeling investigation of a polymerization system. Arguably, Predici® is the most widely used software package in simulation studies of CRP. This software package was developed by Wulkow, based on discrete Galerkin h-p algorithm, that relies on the adaptive Rothe method for time discretization.^[12] Predici® is widely used because it allows prediction of the full CLD and other average chain properties, while offering a user-friendly interface.

2.3.2 Stochastic-based approach

Unlike kinetic-based approaches, the stochastic-based approach does not require solving a set of differential equations. This makes stochastic-based approach especially suitable for modeling complex systems, because it only requires knowledge of reaction probabilities, without having to derive and solve differential equations. Analytical expressions of chain properties have also been obtained using stochastic approaches.

Monte Carlo simulation is an example of probabilistic approach. A broad range of algorithms are available for Monte Carlo simulation, with Gillespie's algorithm being the most widely used in the application of Monte Carlo simulation to polymerization systems.^[13] This algorithm has repeatedly proved to be a powerful tool to predict not only the average properties, but also the full CLD in CRP systems. This method converts the rate of various possible reactions into the probability ϕ for a particular reaction, as shown by Equation (8) for ϕ_i for a reaction i among N possible reactions. Two uniformly distributed random numbers must then be generated. The first random number determines which reaction would occur, while the second random number gives the time before the next reaction takes place.

$$\phi_i = \text{rate}_i / \sum_{j=1}^N \text{rate}_j \quad i = \{1, 2, \dots, N\} \quad (8)$$

Other algorithms or modifications to apply Monte Carlo to polymerization systems continuously appear in the literature. He et al. combined Gillespie's algorithm with quasi steady state assumption to improve the simulation time, while Tobita developed Monte Carlo algorithm based on random sampling technique.^[14,15] Recently, Szymanski and Sosnowski proposed a method to account for radicals in Monte Carlo simulation.^[16] It is usually challenging to calculate the concentration of radicals in a Monte Carlo simulation, because it is orders of magnitude lower than that of other chemical species. Wang and Broadbelt proposed a new data storage scheme to reduce computational time in Monte Carlo simulation, subsequently improved by Reyniers et al.^[17,18]

It is worth noting that due to its probabilistic nature, there will always be differences in the results of Monte Carlo simulation from one run to another. Proper tuning of sample size is required to obtain reliable and accurate results. This is because the choice of sample size not only determines how accurate and precise the simulation results are, but also how fast the simulation runs. Larger sample size would give a more precise result at the expense of longer computation time. The optimum sample size for polymerization system changes with the reaction parameters or initial conditions used.

§ 2.4 Living polymerization

There have been numerous studies on the kinetics of living polymerization processes. The most well-known and widely accepted distribution of polymer produced by living polymerization is the Poisson distribution, as derived by Flory and shown in Equation (9).^[19] Flory derived that equation 16 years prior to the invention of living anionic polymerization.^[1,19] The equation was derived for living ROP of ethylene oxide, albeit not termed as such. The reaction mechanism used in the derivation of Poisson's distribution is shown in Figure 2-2.

$$n(r) = \frac{r_n^r}{r!} e^{-r_n} \quad (9)$$

Several modifications have been published on the fundamental derivation of Flory. Gold modified the Poisson distribution to account for unequal initiation and propagation rates (Scheme (1)).^[20] If the initiation is much slower, considerable broadening of molecular weight distribution from Poisson distribution may be observed. Another modification found in the literature is the inclusion of equilibrium reactions in living polymerization systems.^[21-31] Coleman and Fox considered several different cases of two-state mechanisms for living polymerization and obtained the molecular weight distribution under constant monomer concentration (Scheme (2)).^[21,22] Figini derived the dispersity expression of this system by assuming instantaneous equilibrium.^[23] Yan et al. extended the derivation for similar systems to investigate the validity of instantaneous equilibrium assumption.^[24]

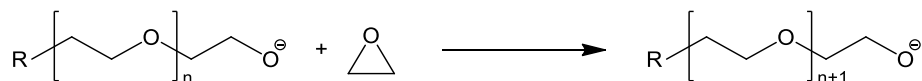


Figure 2-2. Living anionic ring opening polymerization of ethylene oxide

Szwarc and Hermans considered reaction mechanisms involving equilibrium between active and dormant species (Scheme (3)).^[25] Their work resulted in expressions for the dispersity under instantaneous equilibrium condition for systems with constant and varying monomer concentrations. Pickett used the same reaction mechanism to derive the analytical expression for molecular weight distribution under constant monomer concentration.^[26] A slightly different reaction mechanism was used by Figini and Schulz (Scheme (4)).^[27] They derived the dispersity under the assumption of instantaneous equilibrium, slow propagation/fast exchange, and constant monomer concentration. Puskas et al. continued the work by deriving the effect of monomer depletion on dispersity at complete conversion.^[28] Zhu and Wang further relaxed the assumption by investigating the effect of fast propagation and non-instantaneous equilibrium.^[29] They derived a dispersity expression at complete monomer conversion for the same mechanism.

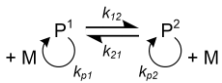
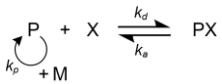
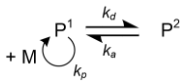
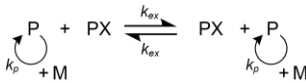
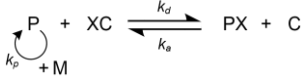
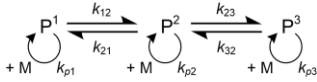
Müller et al. investigated the effects of slow equilibria for living polymerization involving degenerative transfer and dissociative mechanisms (Scheme (5) and Scheme (6)).^[30-32] The group also obtained expression for the CLD under constant monomer concentration using probability generating function method for the living polymerization with degenerative transfer.^[31] A more complicated reaction

mechanism involving three active species was considered by Böhm and continued by Yan et al. (Scheme (7)).^[33,34] All of these active species are in equilibrium with each other, and could propagate with different reactivities.

The modeling work discussed here is summarized with the generalized reaction mechanism in Table 2-1. A notable common ground between all these studies is the absence of termination, chain transfer, or any other side reaction, that is one of the main characteristics of living polymerizations. It should also be noted that under special conditions, these reaction mechanisms may be interchangeable. For example, under instantaneous equilibrium assumption, the derivation applicable for Scheme (3) is also applicable for Scheme (4) (because $[X^*]$ is constant). This list is by no means complete, but it is aimed to highlight some of the theoretical work on living polymerizations.

Living polymerizations are still being rigorously investigated. A published special issue in 2007 in *Progress of Polymer Science*, “50 years of Living Polymerization,” includes 7 detailed reviews of different types of living polymerization.^[35-41] In addition, So et al. recently published a comprehensive review of various living polymerization systems to synthesize low molecular weight polyethylenes.^[42] Interested readers are referred to these reviews for more detailed information on the development of living polymerization.

Table 2-1. Various modeling works on living polymerization

Scheme	Generalized mechanism	Authors	Assumption and notes	Resulting equation	Refs
(1)	$P_0 + M \xrightarrow{k_i} P_1$ 	Flory	$k_i = k_p$	CLD	[19]
		Gold	$k_i \neq k_p$	CLD	[20]
(2)		Coleman & Fox	Instantaneous equilibrium, constant $[M]$	CLD	[21,22]
		Figini	Instantaneous equilibrium	∅	[23]
		Yan et al.	Not instantaneous equilibrium	∅	[24]
(3)		Szwarc & Hermans	Instantaneous equilibrium	∅	[25]
		Pickett	Not instantaneous equilibrium, $[X^*]$ and $[M]$ are constant	CLD	[26]
(4)		Figini & Schulz	Instantaneous equilibrium, $k_p[M] \ll k_a$, constant $[M]$	∅	[27]
		Puskas et al.	Instantaneous equilibrium, $k_p[M] \ll k_a$	∅ at complete conversion	[28]
		Zhu & Wang	Not instantaneous equilibrium	∅ at complete conversion	[29]
(5)		Müller et al	Instantaneous equilibrium, corrected for slow equilibrium	∅ for slow equilibrium CLD under constant $[M]$	[30,31]
(6)		Müller et al	Instantaneous equilibrium Not instantaneous equilibrium	∅ for slow equilibrium	[32]
(7)		Böhm	Instantaneous equilibrium	∅	[33]
		Yan et al.	Instantaneous equilibrium	∅	[34]

§ 2.5 Homogeneous controlled radical polymerization (CRP)

Various types of controlled radical polymerization (CRP) may be described. In this review, the discussion is limited to modeling work on the three most studied types, namely nitroxide mediated polymerization (NMP, also known as stable free radical polymerization, SFRP),^[3] atom transfer radical polymerization (ATRP),^[4,5] and reversible addition fragmentation chain transfer (RAFT).^[6] Figure 2-3 to Figure 2-5 show the reaction mechanisms for these CRPs. From these figures, it can be seen that mechanisms of NMP and ATRP are similar. In NMP and ATRP, all chains are ideally initiated at a very early stage of polymerization and continue to grow throughout the polymerization. Equilibrium is achieved between radicals and capping agents (stable radical for NMP and deactivator for ATRP). On the other hand, the equilibrium in RAFT stems from chain transfer reaction between dormant and radical. Moreover, the initiator in RAFT is the same as that of conventional FRP, therefore initiation occurs continuously throughout the polymerization. The control and living character in RAFT relies on the large ratio of chain transfer agent (or RAFT agent) to the initiator.

Other modeling studies on different types of CRP, such as for iniferter polymerization, reversible chain transfer catalyzed polymerization (RTCP), iodide-mediated polymerization, and many others may be found, but will not be discussed in this review.^[43-53] In general, by assuming negligible bimolecular termination for CRP, the derivations made for living polymerization systems involving equilibrium become

applicable to CRP systems. However, this assumption is usually not valid because of the nature of radicals, making termination unavoidable in CRP.

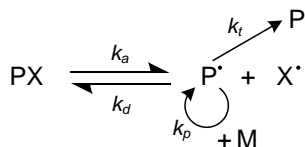


Figure 2-3. Mechanism of nitroxide-mediated polymerization (NMP).
X• is stable nitroxide radical

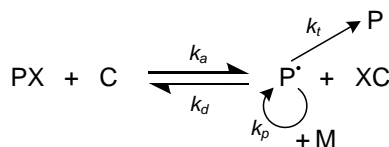


Figure 2-4. Mechanism of atom transfer radical polymerization (ATRP). X is halogen group and C is transition metal

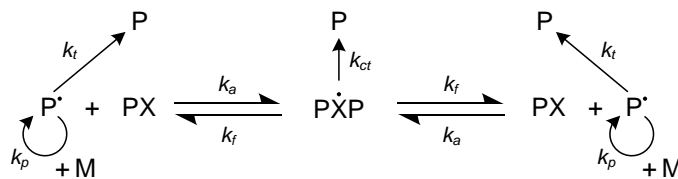


Figure 2-5. Mechanism of reversible addition-fragmentation chain transfer (RAFT) polymerization. X is RAFT agent without radical leaving group

In modeling studies, instantaneous equilibrium and quasi-steady state assumptions (QSSA) are commonly used to simplify derivations. Instantaneous equilibrium refers to fast initiation, for which initial concentrations of reactants are those observed at equilibrium. In a perfect living CRP system, this also implies constant reactant concentrations. In CRP with termination, reactant concentrations may drift from their equilibrium values. On the other hand, QSSA does not assume initial concentrations to be those at equilibrium. By applying QSSA, it is simply assumed that the variation of radical concentration with respect to time is slower than the rates of radical

generation and consumption. The radical concentration is still a function of time. This section will discuss both homopolymerization and copolymerization of CRP in homogeneous systems.

2.5.1 Nitroxide-mediated polymerization (NMP)

In a review in 2011, Grubbs summarized the reported strengths and weaknesses of NMP.^[54] Subsequently, in 2013 Nicolas et al. highlighted various aspects of the industrial applicability of NMP.^[55] This article will specifically highlight the modeling studies published in the literature.

Polymerization kinetics

Numerous efforts have been made to model NMP/SFRP since its introduction.^[2,3] Explicit expressions have been derived for conversion as a function of time, by assuming perfect living condition for NMP, as shown in Equation (10).^[56] The derivation is rooted in Müller's work on living polymerization involving degenerative transfer.^[30,31] Another assumption involved in this derivation is instantaneous equilibrium, that implies constant radical concentration. Yan et al. also published expressions for conversion, taking into account both instantaneous and non-instantaneous equilibrium for perfect living NMP systems.^[57] The kinetic equation under instantaneous equilibrium is the same as that developed by Georges et al., while that for non-instantaneous equilibrium is the same as that published by Shi et al.^[58]

The difference between the derivations of Yan et al. and Shi et al. lies in the initial stable radical concentration, with all the other assumptions being the same. None of these studies account for the effect of termination.

$$\ln\left(\frac{[M]_0}{[M]}\right) = k_p \left(\frac{K[RX]_0}{[X^\bullet]} \right) t \quad (10)$$

Zhu was among the first to investigate the effect of termination on NMP and ATRP through modeling via the method of moments.^[59,60] The influence of other reactions on the conversion and chain properties are also studied via simulations. Souaille and Fischer identified the persistent radical effect (PRE) as the source of the suppression of bimolecular termination in NMP (and also ATRP) relies on.^[61-64] In short, while the active radicals undergo propagation and termination, the stable radicals do not. Therefore, as the active radicals are depleted due to termination, the stable radicals accumulated, *i.e.*, a persistent radical effect (PRE). The persistent radical suppresses bimolecular termination by driving the equilibrium to favor dormant formation, *i.e.*, decreasing the active radical concentration. The decreased radical concentration reduces the polymerization rate, R_p , compared to conventional FRP. However, this suppresses the termination rate, R_t , even more significantly (note: $R_p \propto [R]$ vs. $R_t \propto [R]^2$). On considering PRE, it should be obvious that radical termination in NMP should not be neglected, and is responsible for the accumulation of stable radicals.

With consideration of termination in the mass balances (PRE), Fischer divided the polymerization into three stages: short time, quasi equilibrium, and long time.^[61,62]

During the quasi equilibrium stage, Fischer found that both active and stable radical concentrations change with time following Equation (11) and (12), respectively, due to the presence of termination. The resulting polymerization kinetics may be estimated based on concentration of radicals as shown in Equation (13). The major assumptions involved in this derivation are non diffusion-controlled reactions (constant k 's) and negligible change in dormant chain concentration ($[PX] \gg [X^\bullet]$). Similar equation was derived by Fukuda's group under quasi steady state assumption, and they compared the prediction with experimental data under negligible thermal initiation conditions.^[65-67]

$$[P^\bullet] = \left(\frac{K[RX]_0}{3k_t} \right)^{1/3} t^{-1/3} \quad (11)$$

$$[X^\bullet] = (3k_t)^{1/3} (K[RX]_0)^{2/3} t^{1/3} \quad (12)$$

$$\ln \left(\frac{[M]_0}{[M]} \right) = \frac{3}{2} k_p \left(\frac{K[RX]_0}{3k_t} \right)^{1/3} t^{2/3} \quad (13)$$

Comparison of Equations (10) and (13) shows that for constant radical concentration, the first-order kinetic is predicted to be linear, while PRE predicts a 2/3 order with respect to time. Constant radical concentration (Equation (10)) may be assumed for perfect living systems, or for those involving other reactions that could compensate for terminated radicals (*e.g.*, thermal initiation). It should be noted that in some cases, the equations derived for NMP system may be applicable for normal ATRP with only minor alterations. However, one must be aware of the underlying assumptions and initial conditions in the original derivations. For example, Equation (12) was derived

using zero initial concentration of the stable radical ($[X^\bullet]$), while in normal ATRP, deactivator is sometimes added at the beginning of polymerization to improve its living character. In that case, this equation could not be used by simple substitution for ATRP system.

It is well known that diffusion-controlled reactions could affect polymerization kinetics. An outstanding example is the experimentally-observed auto-acceleration effect in FRP due to diffusion-controlled termination (Trommsdorff effect). A general review on modeling diffusion-controlled reactions has been published for radical polymerization.^[68] Diffusion-controlled reactions have also been the subject of many theoretical studies for NMP systems. Butté et al. used Fermi's function to simulate the change in termination rate constant as a function of conversion.^[69] They employed the method of moments to obtain prediction of the reaction kinetics (conversion), number-average chain length, and dispersity. They also compared the theoretical results with various experimental data (including ATRP). Roa-Luna et al. investigated the effect of diffusion-controlled reactions on the living character of NMP system using Predici®.^[70] Diffusion-controlled reactions were included in the model using free-volume theory. In their subsequent study, they concluded that the effect of diffusion-controlled reactions in NMP of styrene is relatively insignificant in comparison to that observed in conventional FRP.^[71]

D'hooge et al. presented comprehensive modeling work on the effect of diffusion-controlled reactions in CRP systems.^[72] They compared the resulting polymer properties with different models used to account for diffusion-controlled reactions. The reactions investigated under diffusion-controlled conditions are termination, propagation, activation/deactivation for NMP and ATRP, and addition/fragmentation for RAFT. While diffusion-controlled termination was found to be significant, they concluded that the diffusion-controlled propagation is negligible, unless polymerization progressed to very high conversion and conducted at a sufficiently low temperature. The addition/fragmentation in RAFT is also prone to be under diffusion-control due to the large molecules involved in these reactions. The diffusion-controlled addition/fragmentation (or activation/deactivation for NMP and ATRP) significantly affects the dispersity of the resulting polymers.

Average chain properties of polymer

The commonly used expression for number-average chain length of polymer produced by NMP is shown in Equation (14). This equation is valid for an instantaneously initiated system, or at a late stage of polymerization ($t \gg 0$). Therefore, Equation (14) should not be used directly for CRP involving additional initiation occurring throughout the polymerization (*e.g.*, thermal initiator addition, thermal initiation of styrene in CRP, ICAR-ATRP), unless the amount of chains produced through this initiation is negligible. It should also be noted that the linear dependence of number-average molecular weight on conversion would still hold true

for CRP processes with a high degree of termination, provided that the termination occurs strictly via disproportionation.

For cases involving non-instantaneous initiation, the chain length expression derived by Müller for perfect living polymerization with dissociative mechanism (Scheme (6)) may be applied.^[32] This expression, shown in Equation (15) for NMP, was derived by applying correction on Equation (14) for a portion of initiator that has never been activated. It is easy to see that the average chain length predicted by Equation (15) is always higher than that predicted by Equation (14), due to the exclusion of non-initiated portion in Equation (15).

$$r_n = \frac{[M]_0 x}{[RX]_0} \quad (14)$$

$$r_n = \frac{[M]_0 x}{[RX]_0} \left(\frac{1}{1 - (1 - \alpha)(1 - x)^\beta} \right) \quad (15)$$

where $\alpha \equiv [R^*]/[RX]_0$ and $\beta \equiv k_d \alpha / k_p$

There are several dispersity expressions published in the literature for NMP systems. Under the perfect living assumption, the dispersity follows the same equation as that derived by Müller for dissociative living polymerization, shown in Scheme (6).^[32] It can be easily seen that Scheme (6) is in fact equivalent to a perfect living ATRP system (Figure 2-4 without termination). The dispersity expression for this case, shown by Equation (16) for NMP, has also been derived by Goto and Fukuda using probabilistic approach.^[73,74] An equivalent expression has also been reported by Matyjaszewski for

ATRP system.^[75,76] Other assumptions involved in the derivation include instantaneous equilibrium and that the moments of dormant are much larger than those of radical chains. For a perfect living system, instantaneous equilibrium also implies constant concentrations for all reactants, except for monomer. Therefore, Equation (16) implies that dispersity decreases as polymerization progresses.

$$\mathcal{D} = 1 + \frac{1}{r_n} + \frac{k_p[RX]_0}{k_d[X^*]} \left(\frac{2}{x} - 1 \right) = 1 + \frac{1}{r_n} + \frac{\ln(1-x)}{k_a t} \left(1 - \frac{2}{x} \right) \quad (16)$$

For systems with constant monomer concentration (or at an early polymerization stage, $x \rightarrow 0$), this dispersity expression becomes Equation (17).^[74,77,78] The assumptions involved are the same as those used to derive Equation (16), *i.e.*, instantaneous equilibrium and perfect living system. This equation clearly shows how higher number of activation cycles ($k_a t$) results in lower dispersity for polymers with the same number-average chain length. Equivalently, it can be said that systems with more monomeric unit added per activation cycle have broader distribution (higher dispersity). The number of monomeric units added per cycle is constant for this case as a result of the aforementioned assumptions. On the other extreme, an expression for dispersity of a perfect living NMP at complete conversion is shown in Equation (18).^[76] This equation serves to show dispersity dependence on the ratio of propagation to deactivation rates and its minimum value.

$$\mathcal{D}_{x \approx 0} = 1 + \frac{1}{r_n} + \frac{2}{k_a t} \quad (17)$$

$$\mathcal{D}_{x \rightarrow 1} = 1 + \frac{1}{r_n} + \frac{k_p[RX]_0}{k_d[X^*]} \quad (18)$$

Using the radical and deactivator concentrations based on PRE (Equation (11) and (12)), Fischer derived an expression for dispersity, shown in Equation (19), using the method of moments. The limiting cases are shown in Equation (20) and (21).^[62] The same dispersity expression has also been derived independently by Fukuda using a different approach.^[79] The derived expression accounts for the effect of termination on the polymerization kinetics, but not on the distribution itself.^[80] This is because of the approximation made in expressing the number of monomeric units in all polymer chains (the first order moment) is the same as that in the dormant chains.

$$\mathcal{D} = 1 + \frac{1}{r_n} + \frac{1}{x^2} \sqrt{\frac{\pi k_p^3 [RX]_0}{k_d k_a k_t}} \operatorname{erf} \left(\left(\frac{9 k_p^3 K [RX]_0}{k_t} t^2 \right)^{1/6} \right) \quad (19)$$

where: $\operatorname{erf}(u) \equiv \frac{2}{\pi_0} \int_0^u e^{-t^2} dt$ is the error function

$$\mathcal{D}_{t \rightarrow 0} = 1 + \frac{1}{r_n} + \frac{8}{3} (k_a t)^{-1} \quad (20)$$

$$\mathcal{D}_{t \rightarrow \infty} = 1 + \frac{1}{r_n} + \sqrt{\frac{\pi k_p^3 [RX]_0}{k_d k_a k_t}} \quad (21)$$

In a recently published work, Mastan et al. derived a dispersity expression for ATRP under constant monomer concentration to investigate the effect of termination, that has been rewritten for NMP in Equation (22).^[78] The additional assumption made in deriving the equation is that the reactant concentrations are constant. This equation

shows that there are two factors contributing to the broadening of distribution, *i.e.*, lack of control (indicated by low value z of activation cycles) and lack of living character (indicated by low value of chain end functionality, $\exp(-zf_t)$).

$$\mathcal{D}_{x \approx 0} = 1 + \frac{1}{r_n} + \frac{\sinh(zf_t) - zf_t(1 - f_t)}{\cosh(zf_t) - 1} \quad (22)$$

where: $f_t \equiv \frac{k_t[R^*]}{k_t[R^*] + k_d[X^]}$ is the fraction of active chains terminated per cycle

$z \equiv k_a t$ is the average number of activation cycles occurred after time t

$\sinh(u) \equiv \frac{e^u - e^{-u}}{2}$ and $\cosh(u) \equiv \frac{e^u + e^{-u}}{2}$ are hyperbolic sine and cosine

It may be easily proven that as $f_t \rightarrow 0$, the dispersity expression in Equation (22) is reduced to Equation (17). Table 2-2 summarizes various dispersity expressions along with the major assumptions involved in the derivation.

Table 2-2. Summary of dispersity expressions derived for NMP (and ATRP)

Major assumptions	Resulting dispersity	Ref
Perfectly living	Equation (16)	[73-76]
$k_t = 0, x = f(t), [R]$ and $[X^*] \neq f(t)$		
$x \sim 0$	Equation (17)	[74,77,78]
$x \rightarrow 1$	Equation (18)	[76]
Persistent radical effect	Equation (19)	[62,79]
$k_t \neq 0, x = f(t), [R]$ and $[X^*] = f(t)$		
$x \sim 0$	Equation (20)	[62,79]
$x \rightarrow 1$	Equation (21)	[62,79]
CSTR analogy	Equation (22)	[78]
$k_t \neq 0, x \approx 0, [R]$ and $[X^*] \neq f(t)$		

Chain length distribution of polymer

Knowledge of the full CLD offers much more information than r_n and dispersity. For example, the CLD allows observation of the distribution modality, that cannot be deduced from the average chain properties alone. Moreover, r_n and dispersity may be calculated from the CLD, but not the other way around. There are various ways to predict the CLD and it can be argued that to obtain the analytical expression is most desirable, be it based on reaction kinetics or probabilistic approach. However, this derivation is usually accompanied by many limiting assumptions.

Using random sampling method (a stochastic approach), Tobita derived an expression for the CLD under the constant monomer concentration condition, based on simplified reaction mechanism shown in Figure 2-6.^[77] Comparing this reaction mechanism with that of NMP (Figure 2-3), one can see the inherent assumptions in this derivation are complete living character and constant, stable radical concentration. The resulting expression is shown in Equation (23) when written for NMP. In this study, the effect of monomer transfer reaction was also investigated. The dispersity expression obtained from the CLD in Equation (23) is the same as Equation (17), because they were derived under the same assumptions, using different approaches.

$$n(r) = (\phi_p)^r e^{-z} \sum_{i=0}^{\infty} \binom{r+i-1}{r} \frac{(z\phi_d)^i}{i!} \quad (23)$$

where: $\phi_p \equiv \frac{k_p[M]}{k_p[M] + k_d[X^\bullet]}$ is the probability of radical to add a monomer unit

$\phi_d \equiv 1 - \phi_p$ is the probability of radical to undergo deactivation

$z \equiv k_a t$ is the average number of activation cycles occurs after time t

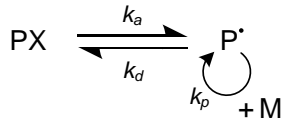


Figure 2-6. Reaction scheme of idealized CRP operating under PRE

By analogously relating the equilibrium in CRP in polymer chemistry to a series of continuous stirred tank reactors (CSTR) in chemical reaction engineering, Mastan et al. recently published analytical expressions for the CLD.^[78] These were derived for cases with and

without termination. The expression derived for the case without termination is the same as that derived by Tobita (Equation (23)), while the CLD for systems with termination is shown by Equation (24). The resulting dispersity expression for this CLD has been discussed and shown in Equation (22). The derivations were done under the condition of constant reactant concentrations.

$$n(r) = (\phi_p)^r e^{-z} \left[\sum_{i=0}^{\infty} \binom{r+i-1}{r} \frac{(z\phi_d)^i}{i!} + \frac{\phi_t}{\phi_d} \sum_{i=1}^{\infty} \frac{z^i}{i!} \sum_{j=1}^{\infty} \binom{r+j-1}{r} (\phi_d)^j \right] \quad (24)$$

where: $\phi_p \equiv \frac{k_p[M]}{k_p[M] + k_d[X^\bullet] + k_t[R^\bullet]}$ is the probability of radical to propagate

$\phi_d \equiv \frac{k_d[X^\bullet]}{k_p[M] + k_d[X^\bullet] + k_t[R^\bullet]}$ is the probability of radical to deactivate

$\phi_t \equiv 1 - \phi_p - \phi_d$ is the probability of radical to terminate

$z \equiv k_a t$ is the average number of activation cycles occurs after time t

In a subsequent study, Mastan et al. considered the effect of change in reactant concentrations by discretization of polymerization time into smaller periods.^[81]

During each period, the reactant concentrations may be considered as approximately constant, thus Equation (24) may be applied. This method only requires knowledge of how the concentrations and reaction rate constants change with conversion to obtain CLD. Therefore, this method is applicable for NMP, normal ATRP and other ATRP variants. The effect of variation in reaction rate constants on the full CLD may also be investigated using this approach.

Saldivar-Guerra et al. showed that direct integration may be used to predict the CLD with reasonable computation time (less than an hour) for CRP and conventional FRP systems.^[82] The full CLD could also be obtained through the use of coarse-graining technique, as shown by Reyniers et al. for NMP system.^[83] This method was introduced by the same group for ATRP to avoid the computationally expensive direct integration.^[11] These studies combined the coarse-graining technique with the extended method of moments and quasi steady state assumption to obtain the full CLD in NMP of styrene. The extended method of moments accounts for the dependence of reaction rate constants on the polymer chain length. The resulting algebraic and differential equations may be solved simultaneously to obtain the full CLD.

The inversion of probability generating functions has been employed to predict the CLD. Asteasuain et al. used Stehfest inversion algorithm to obtain the CLD from probability generating functions for NMP conducted in tubular systems.^[84] Side

reactions considered in the model development are termination by combination and transfer to monomer. Their approach allows calculation of the mole fraction of each chain length independently from the others. Therefore, the computation time may be tuned depending on the detail required in the CLD. Dias and Costa also simulated the CLD using probability generating functions for perfect living NMP system.^[85] The reaction mechanism they used was the same as Tobita's (Figure 2-6, thus involving the same assumptions). They investigated the effect of monomer depletion on the CLD and also showed that their approach allows prediction of the CLD in non-linear CRP (crosslinking), for which multimodal distribution is expected. Irzhak and Irzhak also used probability generating function to obtain the CLD in CRP cases.^[86]

Other methods for predicting the full CLD of NMP systems include Monte Carlo simulation^[14,15] and the software package, Predici®.^[87] Gillespie's algorithm,^[13] or similarly dynamic and kinetic Monte Carlo, are commonly used in simulation of polymerization systems. However, the high frequency of equilibrium in NMP results in a computationally expensive simulation. He et al. proposed a hybrid Monte Carlo algorithm to simulate NMP systems.^[14] The hybrid algorithm combines Gillespie's algorithm with quasi steady state assumption. Therefore, they proposed a combination of Gillespie's algorithm with an analytical estimation for the equilibrium reaction. A different Monte Carlo algorithm to predict CLD was developed by Tobita based on random sampling technique.^[15] In that study, the importance of monomer transfer reaction on the CLD was investigated. Another software based on Monte

Carlo simulation, developed by Drache and Drache called mcPolymer, is also capable to predict the complete CLD of various types of CRP's (NMP, ATRP, and RAFT) for both homo and copolymerization.^[88]

Other modeling studies in NMP

Many other modeling studies have been conducted to investigate the importance of certain reactions, the effect of different parameters and reaction conditions on NMP kinetics and average polymer chain properties. Fukuda et al. investigated the mechanism of NMP using combined experimental and theoretical approach.^[89] They postulated that the addition of thermal initiator is beneficial for the system to reach equilibrium, by compensating for the amount of terminated radicals. Kruse et al. used the method of moments to investigate the importance of thermal initiation and chain transfer to polymer in NMP of styrene.^[90] Through comparison to experimental data, they concluded that thermal initiation must be accounted in the model to obtain good agreement with experimental data. On the other hand, chain transfer reaction was shown to have negligible effect based on their simulation results.

Greszta and Matyjaszewski used Predici[®] to investigate the importance of termination and thermal initiation in NMP processes via comparison with experimental data.^[91] Hernández-Meza et al. also used Predici[®] to investigate NMP system involving microwave irradiation.^[92] Ahmad et al. investigated various possible causes to explain differences in the branching densities observed in CRP and FRP.^[93]

They concluded that the narrower distribution of polymer chains in CRP system lead to lower branching density. Reyes and Asua investigated similar phenomena using Monte Carlo simulation.^[94] Through their simulation, they argued that a short radical lifetime in CRP is responsible for the lower branching density, not the chain length dependent kinetics. Another simulation study showed that branching density in CRP also depends on the activation rate constant and various reaction conditions.^[95]

Parameter estimation is a recurring theme in modeling studies reported in the literature. Knowledge of accurate reaction rate constants is essential to obtain reliable simulation predictions. Goto and Fukuda showed how modeling predictions can be used in comparison with SEC data to find the activation rate constant of NMP systems.^[96,97] This was accomplished by determining the ratio of dormant concentration that have never been activated to the initial dormant concentration using SEC data. The kinetic plot based on PRE (Equation (13)) was used to estimate the equilibrium constant for NMP ($K = k_a/k_d$).^[98] However, this equation is not valid if there is significant change in the dormant concentration due to terminated chains. Matyjaszewski and Fukuda modified the PRE further by removing the assumption of constant dormant concentration for ATRP and NMP systems, as shown by Equation (25) for NMP.^[99,100] The resulting expression predicts the equilibrium constant more accurately than the original PRE equation, and is valid for longer period of time. This expression requires knowledge of the stable radical concentration, $[X^*]$.

$$\frac{([RX]_0)^2}{[RX]_0 - [X^\bullet]} + 2[RX]_0 \ln\left(\frac{[RX]_0 - [X^\bullet]}{[RX]_0}\right) - ([RX]_0 - [X^\bullet]) = 2k_t K^2 t \quad (25)$$

Benoit et al. obtained the equilibrium rate constants from PRE and used Predici® to simulate the effect of chain length dependent termination on NMP systems.^[101] Bonilla et al. used the method of moments to estimate the values of various reaction rate constants, and additionally conducted sensitivity analysis.^[102] Belincanta-Ximenes et al. used the method of moments with experimental data of NMP at various temperatures to evaluate the Arrhenius parameters.^[103] Ide and Fukuda estimated reactivity ratios in NMP copolymerization of styrene and 4,4'-divinylbiphenyl.^[104] Vivaldo-Lima and Penlidis published several studies on crosslinking kinetics of NMP and ATRP copolymerization via modeling using the method of moments.^[105-108] In these studies, they have considered multifunctional polymer molecules in the model derivation, and they also compared their simulation results to experimental data.

Modeling work is very helpful in understanding and designing a well-tailored copolymer composition distribution. It may be used to control comonomer feeding rates and polymerization conditions to achieve desired copolymer composition designs. Broadbelt and coworkers conducted many studies in this area using a stochastic approach, while Ye and Schork used a kinetic approach.^[109-113] Both groups focused on copolymer sequence distributions for various types of copolymer and ways to design experimental conditions for the syntheses. In a recent publication, Zapata-González et al. investigated the validity of using a terminal model for

copolymerization in NMP.^[114] They proposed some conditions that must be satisfied for the terminal model to be applicable for NMP systems. The initial stage of polymerization, for which quasi steady state assumptions are not applicable, is critical for the validity of terminal model in NMP. Moreover, they also demonstrated that high reactivity ratios lead to larger deviation from the terminal model.

Souaille and Fischer proposed that the living character and polymerization rate depend on the ratio of k_a to k_d , while the dispersity depends on the product of k_a and k_d .^[63,115] A higher ratio leads to lower living character but faster polymerization rate. On the other hand, a higher product of reaction rate constants gives a lower dispersity. From this relation, they created a graphical guideline

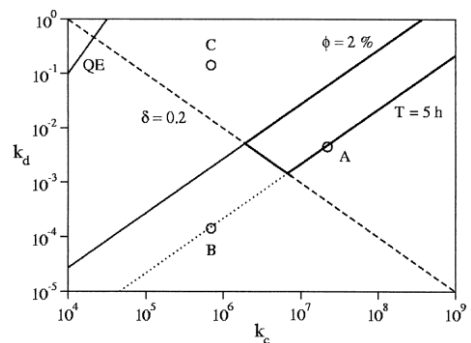


Figure 2-7. Graphical guideline for NMP process with 2% dead chains, 5 h to reach 90% conversion, and dispersity of 1.2 ($\delta = D - 1$)^[115]

for experiment design by plotting k_a vs k_d on a log-log scale for a set of pre-specified dispersity, dead chain fraction, and time required to reach 90% conversion, as shown in Figure 2-7. Gimes et al. further confirmed how the living character and controllability of NMP depend on the ratio and product of activation and deactivation rate constants, respectively.^[87] They used a similar concept as Fischer's graphical guideline and plotted the CLD for various cases using Predici[®] to test the level of living character and control of NMP systems. This group also showed how penultimate

effect could strongly change the value of equilibrium constant in NMP systems, thereby affecting the living character and degree of control.^[116]

Zhang and Ray conducted comprehensive kinetic modeling for CRP in batch reactor, semi batch reactor, continuous stirred tank reactor (CSTR), and plug flow reactor (PFR).^[117-119] This comprehensive model is not restricted to homopolymerization, but is also applicable for copolymerization process. They investigated the effect of residence time distribution (RTD) and found it to have only slight effect on the polymerization rate, but stronger effect on the dispersity. Schork and Smulders derived dispersity expressions of perfect living CRP in various reactor configurations using the method of moments.^[120] Their derivations showed the broadest distribution in a single CSTR system, for which narrower distributions may be obtained using PFR or a series of CSTRs. Similar finding for a single CSTR was also reported by Tobita through random sampling method.^[77] Continuous NMP in PFR to produce narrowly distributed polymer chains was investigated by Faliks et al. using an optimal control methodology.^[121] Narrow distribution and high conversion were optimized using a reactor design with variable mass flux of nitroxide radicals. Zitlalpopoca-Soriano et al. studied various parameters affecting NMP in tubular reactor, along with dynamic optimization of the process.^[122,123]

2.5.2 Atom transfer radical polymerization (ATRP)

There are many different types of ATRP derived from the original (“normal”) ATRP process. Most of these were developed to improve living character of the polymerization and control of polymer molecular weight, and/or to create a more environmentally friendly and economically feasible process by reducing the catalyst needed. Some of the variants of ATRPs include reverse ATRP, simultaneous reverse and normal initiation (SR&NI) ATRP, activators generated by electron transfer (AGET) ATRP, activator regenerated by electron transfer (ARGET) ATRP, and initiator for continuous activator regeneration (ICAR) ATRP. Some recent reviews include detailed discussion of the mechanisms of these ATRP derivatives.^[37,124] Other reviews highlight the challenges in industrialization,^[125] or focus on the use of ATRP to produce materials with highly tailored properties.^[126-128] To avoid overlaps, this part of the review mainly discusses the modeling studies of ATRP that have not been covered in the NMP section.

Normal ATRP

In both ATRP and NMP, a persistent radical effect governs the polymerization kinetics. The major kinetic difference between the two systems lies in the activation reaction. The activation of dormant chains in NMP to form radicals depends only on the dormant concentration. Meanwhile, the activation rate in ATRP is proportional to both dormant chain and catalyst concentrations (*i.e.*, transition metal at lower

oxidation state). The persistent radical in ATRP is the transition metal at higher oxidation state, also called a deactivator, that can deactivate radicals to form dormant chain.

Zhu used the method of moments to investigate the effect of termination and propagation rate on average chain properties of polymer.^[60] Vieira used the method of moments to investigate the effect of equilibrium constant values on various concentrations and polymer chain properties in an ATRP system.^[129] Based on the simulated dispersity and dormant chain concentration, they concluded that the value of equilibrium constant for ATRP to achieve good control should be between 10^{-7} – 10^{-9} . Yoshikawa et al. compared the kinetic prediction of ATRP systems with and without additional conventional initiator to experimental data. The comparison proved that adding small amount of initiator results in a linear first-order kinetics, while the system without initiator addition shows 2/3 order.^[130] These two trends are in agreement with Equation (10) and (13) derived for CRP under PRE conditions.

Shipp and Matyjaszewski investigated the kinetics of ATRP using a Predici® software package.^[131] They found that addition of thermal initiator could affect initial deactivator concentration at the beginning of polymerization. This, in turn, could significantly affect the apparent external order of polymerization, hence affecting the polymerization rate. The effect of initial deactivator concentration on the polymerization rate of ATRP has also been investigated by Zhang et al. through

modeling and experiment.^[132] They postulated that the kinetics is determined by PRE (analogous to Equation (13) for NMP) when the initial deactivator concentration is less than 10% of the initial catalyst concentration. However, if the amount of deactivator added at the beginning is more than 10% of the catalyst, the kinetics would show linear first-order kinetic (similar to Equation (10) for NMP system).

Lutz and Matyjaszewski used Predici® to investigate the effect of various possible reactions involved in the ATRP mechanism.^[133] They simulated the effect of chain length dependent termination, thermal initiation reaction, and reaction of polymer chain ends to form hydrobromic acid on the kinetics and chain properties of polymer synthesized via ATRP. The chain length dependence was found to increase the living character, while the thermal initiation and formation of hydrobromic acid were found to decrease the living character. Al-Harthi et al. also conducted modeling studies to investigate the effect of various reactions.^[134,135] Their studies focused mainly on ATRP systems with bifunctional initiator and the modeling was conducted using the method of moments and using Monte Carlo simulation to obtain the full CLD. López-Domínguez et al. studied ATRP system with microwave irradiation and compared two possible models for the system.^[136] The first model considers microwave radiation to generate radicals, while the second one takes into account the effect of microwave radiation on polymerization temperature.

An issue faced in ATRP is solubility of the metal complexes that are used as catalyst and deactivator. Snijder et al. derived kinetic model for ATRP system with partially insoluble deactivator, that results in a constant deactivator concentration.^[137] By assuming termination strictly by disproportionation, equal initial concentration of initiator and catalyst, and that the insoluble deactivator act as reservoir, Equation (26) was developed at a constant deactivator concentration (at its solubility limit). Fu et al. conducted simulation study for batch and semi-batch systems using Predici® with solubility limits assumed for both metal complexes.^[138] Through comparison with experimental data, they confirmed that while only the soluble part of metal complexes participates in the reaction, insoluble complexes act as a reservoir to keep the soluble component at approximately constant concentrations.

$$\ln\left(\frac{[M]_0}{[M]}\right) = \frac{k_p[XC]_{\text{lim}}}{2k_tK} \left[\left(\frac{6k_tK^2}{[XC]_{\text{lim}}^2}t + \frac{1}{[RX]_0^3} \right)^{1/3} - \frac{1}{[RX]_0} \right] \quad (26)$$

Wang et al. experimentally estimated the amount of dead chains formed during ATRP from the mass balance of halogen in the system.^[139,140] The experimentally determined dead chain fractions were compared to the predicted values calculated with Equation (27), derived by the same group under constant radical concentration assumption.^[141] Larger experimental dead chain fractions than the predicted ones were found, leading to the postulation of additional termination mechanism, termed a catalytic radical termination. In this mechanism, the termination of two radicals to form two dead chains is catalyzed by the presence of copper(I). This implies that a

low catalyst concentration should be used to improve living character, thus favoring new variants of ATRP (*e.g.*, ICAR and ARGET-ATRP). The expression to predict dead chain fraction with the consideration of catalytic radical termination at constant catalyst concentration is shown by Equation (28) (corrected for typo from the original article).

$$DCF = \frac{2k_t \ln^2(1-x)}{(k_p)^2 [RX]_0 t} \quad (27)$$

$$DCF = \frac{2k_t \ln^2(1-x)}{(k_p)^2 [RX]_0 t} + \frac{k_{t,CRT} [C]}{k_p [RX]_0} \ln\left(\frac{1}{1-x}\right) \quad (28)$$

In modeling studies of ATRP system, diffusion-controlled reactions have been shown to mask power-law behavior due to PRE. Shipp and Matyjaszewski used Predici® to investigate the effect of diffusion-controlled termination on ATRP kinetics.^[142] In this study, they modeled the change in termination rate constants by empirically derived chain length dependence. They showed that the variation of termination rate constants during polymerization could explain some deviations in experimental data from PRE prediction. The effect of diffusion-controlled termination on living character has also been studied by Najafi et al. using Monte Carlo simulation method with chain length dependent termination rate constant.^[143,144]

Delgadillo-Velásquez et al. used free-volume theory to model the diffusion-controlled reactions in ATRP system, including propagation, termination, activation, and deactivation reactions.^[145] Their simulation showed that diffusion-controlled

propagation and termination have opposite effects on living character of the system, with diffusion-controlled propagation deteriorating the living character. Al-Harhi et al. used the method of moments and free-volume theory to investigate the effect of these elementary reactions under diffusion-controlled condition in ATRP with bifunctional initiator.^[146] This group also used Monte Carlo simulation to investigate the effect of diffusion-controlled termination on the CLD for ATRP with monofunctional and bifunctional initiators.^[147,148] In these studies, an empirical relation between termination rate constant and conversion was used. Haddadi-Asl et al. also used a Monte Carlo simulation based on Gillespie's algorithm to investigate various parameters affecting termination in ATRP process.^[149] They showed the ability of Monte Carlo simulation to predict the CLD under the presence of a gel-effect and/or chain length dependent termination. D'hooge et al. modeled the diffusion-controlled termination in ATRP involving backbiting reactions using extension of the method of moments.^[150] This modeling approach allows inclusion of variation in kinetic rate constants in the moment balances. They concluded that termination becomes diffusion-controlled at an early stage of the polymerization, while deactivation reaction becomes diffusion-controlled at a higher conversion.

Johnston-Hall and Monteiro modeled diffusion-controlled termination based on a composite model, for which they defined two regimes, dilute and gel, to differentiate the termination rate constant variation.^[151] More discussion on this composite model is provided in another section of this review. This composite model for termination

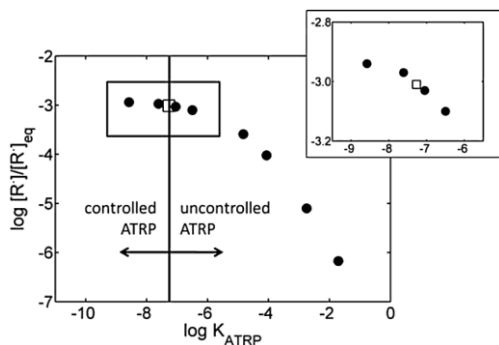


Figure 2-8. Graphical guideline to determine the limit of control for ATRP of MMA. The blank square indicates the limit of control^[152]

controlled. Bergenudd et al. also proposed a guideline to design well-controlled ATRP (similar concept as Figure 2-7), as shown in Figure 2-8.^[152] The level of control was defined as the ratio of actual degree of polymerization and perfect living system. The higher ratio means lower living character. A ratio greater than 1.25 is referred to as uncontrolled polymerization.

On the other hand, Zhong et al. also provided a graphical guideline, shown in Figure 2-9,^[141] from theoretical calculation focusing on the living character of ATRP system and its polymerization rate. From this plot, it is clear that a long polymerization time is required in order to suppress the amount of dead chains produced at the same monomer conversion.

rate constant variation was compared with empirical relation by Bergenudd et al.^[152] Both models predict more or less linear first-order kinetics, contrary to the 2/3 order due to PRE predicted for cases for which termination is not considered to be diffusion-

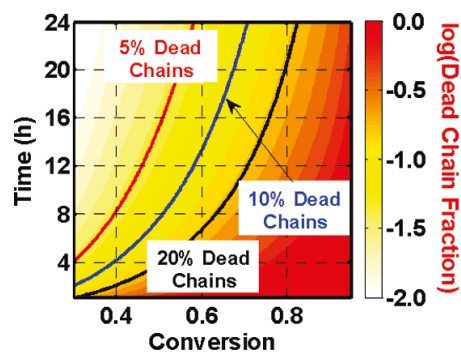


Figure 2-9. Limit of livingness as a function of polymerization rate for bulk ATRP of MMA^[141]

The common conclusion of these two studies is that slower systems would result in more living/controlled conditions.

Similar to NMP cases, there are many parameter estimation studies conducted for ATRP systems. Ohno et al. modeled initiator concentration and estimated the activation rate constant by comparison of the theoretical and experimental results determined from SEC.^[153] Kwark and Novak estimated the reaction rate constants of ATRP using non-linear regression.^[154] A regression approach was used by Reyniers et al. to determine the Arrhenius parameters for activation and deactivation reactions, using experimental data from ICAR-ATRP.^[155] Buback group studied the activation and deactivation equilibrium of various ATRP systems at high pressure.^[156-159] This group also studied the effect of solvent fraction on the equilibrium constant of ATRP.^[160] Shipp and Yu used a PRE-based model to estimate the average rate constant of bimolecular termination and the effect of initial catalyst concentration on its value.^[161] Systems with lower initial catalyst concentration show a higher termination rate constant, when estimated using their method. This observation was attributed to the deviation from PRE for a low initial catalyst concentration.

Ziegler and Matyjaszewski used Predici® and experimental data to estimate the reactivity ratios for copolymerization of methyl methacrylate and n-butyl acrylate in ATRP (ATRcoP).^[162] These values were found to be approximately the same as those found in conventional FRP. Fu et al. also reported similar findings from their study

with Predici® for styrene and butyl acrylate ATRcoP system.^[163] Roos et al. compared the reactivity ratios of monomer and macromonomers in ATRcoP and those in conventional free radical copolymerization.^[164] They found that the reactivity ratio of macromonomer is more affected by diffusion in FRP than that in ATRP system. Klumperman et al. investigated deviations of experimentally obtained data in ATRcoP from simulation results obtained using terminal model.^[165] They attributed the deviations to the non-equilibrium concentrations of reactants at the initial stage of ATRcoP.

A major advantage of CRP is the ability to fine-tune the copolymer composition profile. For batch copolymerization with ATRP, gradient copolymers may be produced only if there is composition drift. Wang et al. showed that in a semi-batch mode, various types of gradient copolymer composition profile may be obtained in ATRCoP.^[166] The model presented was derived based on the method of moments. It may be used to precisely design the composition profile of copolymers in semi-batch reactor by controlling the feed rates of comonomers. Al-Harhi et al. also published modeling work on ATRcoP, done by combining either the method of moments^[167] or dynamic Monte Carlo with the pseudo-kinetic rate constants method.^[168,169] The copolymerization systems studied were in batch and semi-batch modes to produce either random or gradient copolymers. Reyniers et al. used kinetic Monte Carlo to study the formation of block and block-like copolymers in ICAR-ATRP systems.^[170] They investigated two reactor configurations, a semi-batch reactor and a series of two

batch reactors. Zhou et al. also modeled the copolymers composition and their glass transition temperature in batch and semi-batch ATRcoP using pseudo-kinetic rate constants and the method of moments.^[171] Diffusion-controlled reactions were taken into account in this study using free volume theory. Steenberge et al. used Monte Carlo simulation to track the composition of copolymer synthesized by ATRcoP for various monomer combination systems.^[18] They introduced the concept of gradient deviation as an indicator for the quality of gradient copolymer produced. Modeling of branching/crosslinking to the onset of gelation in ATRP has also been subject of modeling studies, mainly conducted using Monte Carlo technique and by Predici[®].^[95,172-176]

Many experimental studies have been conducted on CRP in the presence of copper(0). However, there has been a debate on the mechanisms behind radical polymerization in the presence of copper(0)-mediated radical polymerization. As elaborated in the following, one group proposed that copper(0) acts primarily as a reducing agent, as in ARGET-ATRP a mechanism (and also as a supplementary activator, *i.e.*, via SARA-ATRP).^[177-179] The other group proposes that copper(I) disproportionate to form copper(0) and copper(II), that are then responsible for the equilibrium between dormant and radical chains, via so-called single electron transfer living radical polymerization (SET-LRP).^[180] Figure 2-10 compares the proposed mechanisms for ARGET-ATRP and SET-LRP.

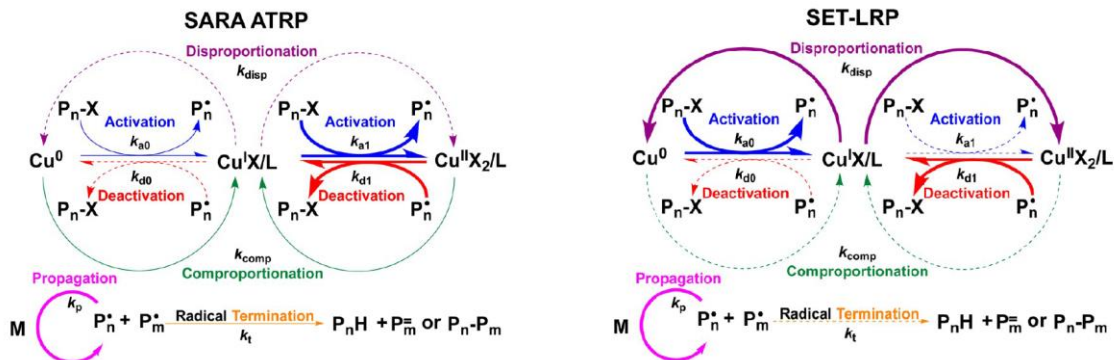


Figure 2-10. Reaction mechanism of ARGET-ATRP and SET-LRP^[177]

Theoretical studies on both SARA-ATRP and SET-LRP mechanisms have been published. Many studies favoured the ARGET-ATRP mechanism. Predici® was used to include all possible reaction pathways and it was concluded that the activation of dormant chains by copper(I) is much faster than that by copper(0).^[179] On the other side, Percec's group used quantum chemistry calculation and experimental data in comparing SET-LRP vs. ARGET-ATRP.^[180] They proposed that depending on the type of solvent used, copper(0) could serve as the main activator via outer sphere electron transfer process (OSET). However, OSET in this system is not possible, according to experimental and *ab initio* computational studies.^[181] Matyjaszewski et al., based on direct measurements of rates of disproportionation and activation and Predici simulation, demonstrated that copper(I) dominates the activation of radicals and contribution of disproportionation is negligible in DMSO as well as in water in ATRP of acrylates in the presence of copper(0).^[178] A similar conclusion was reached in polymerization of methacrylates.^[182]

Continuous ATRP has also been modeled by various researchers. Zhang and Ray developed a comprehensive model for various CRPs in different reactor configurations, as discussed in previous section.^[117,118] Dervaux et al. utilized Predici® to model a series of tubular reactors with supported ATRP catalyst inside the reactor to produce block-like copolymers.^[183] Catalyst support was also developed to facilitate recovery of catalysts.^[184] A recently published review by Chan et al. summarized many kinetic and experimental papers on various types of ATRP in continuous system.^[185]

Other types of ATRP

The different types of ATRP operate under the same basic mechanism to achieve equilibrium as normal ATRP. Tang and Matyjaszewski published a comprehensive modeling study of the normal ATRP (with and without initial deactivator), reverse ATRP, and simultaneous reverse and normal initiation (SR&NI) ATRP.^[186] Kinetic modeling was done using Predici® to differentiate the quasi steady state behavior for these types of ATRPs. Haehnel et al. modeled SET-LRP using Predici® to investigate the polymerization mechanism.^[187] The deviation of experimentally determined molecular weight from theoretically predicted value was attributed to the large role of conventional FRP mechanism at the initial stage of polymerization.

Li et al. modeled ARGET-ATRP system using the method of moments to study the effect of equilibrium constant and reduction rate coefficient on the control, living

character, and polymerization rate.^[188] Based on comparison of the modeling and experimental results, they concluded that systems with highly active but low equilibrium constant provide better control to polymerization than those with high equilibrium constant. On the other hand, a highly reactive reducing agent increases the polymerization rate, but decreases the living character. Payne et al. used Monte Carlo technique to investigate the mechanism behind ARGET-ATRP system.^[189] They found that there is a trade-off in polymerization rate with the amount of dead chains formed. Both of these variables are affected by the initial concentrations of reducing agent and deactivator. They also studied the effect of diffusion-controlled termination and different activation and deactivation rate constants for initiator and polymeric chains.

D'hooge et al. modeled ICAR-ATRP using the extended method of moments to take into account chain length dependent termination.^[190,191] They found that additional thermal initiator may be added in the middle of polymerization to maintain good control, even with low catalyst concentration.^[190] In addition, they provided guideline on optimization of ICAR-ATRP to obtain high polymerization rate at low catalyst concentration based on their modeling results.^[191] They also considered ICAR ATRCoP to produce gradient copolymers using semi-batch reactor.^[192] Using Monte Carlo approach, they found that high-quality copolymers with linear gradient may be obtained using monomer-starved feed conditions, but at the expense of the rate of polymerization. Payne et al. also utilized Monte Carlo simulation to investigate

copolymerization using ATRP variant, ARGET ATRcoP.^[193] Their study showed the effect of adding supplementary reducing agent during reaction on polymerization rate, living character, and controllability of the system.

2.5.3 Reversible addition-fragmentation chain transfer (RAFT)

There are many reviews of RAFT, some are general reviews, including many aspects of kinetics, mechanisms, and applications of RAFT,^[194-198] while others focus on design of the RAFT agent.^[199] The modeling studies for RAFT are summarized and discussed here, by first discussing theoretical predictions of polymer chain properties synthesized through RAFT, followed by parameter estimations of RAFT systems or using a RAFT process (RAFT-CLD-T). Modeling studies related to the controversy between slow fragmentation model (SFM) and intermediate termination model (ITM) are also highlighted.

Kinetics and chain properties

For a RAFT mechanism (Figure 2-5), the reaction may be treated as a simple living polymerization under degenerative transfer mechanism (Scheme (5)) for which the limiting case of perfect living character with fragmentation reaction is considered as infinitely fast ($k_f \rightarrow \infty$). Therefore, the full CLD derived by Müller et al. under constant monomer concentration is also applicable for RAFT under these extreme conditions.^[31] Tobita also derived an expression for the full CLD of RAFT

polymerization under perfect living assumption with constant monomer and radical concentrations.^[200] The difference between the CLD expressions derived for NMP (Equation (23)) and the one for RAFT (Equation (29)) lies on repetition of activation of radical from the intermediate radical. Tobita introduced the concept of an “overall” active period to account for this probability. In that study, he arrived at similar concept introduced by Goto et al., for which simple degenerative chain transfer may be used to represent RAFT mechanism with exchange rate constant to be equal to half of the addition rate constant ($k_{ex} = k_a/2$, Figure 2-11).^[201] This relation has also been proven by Gao and Zhu in another modeling study.^[202] Tobita also derived dispersity expression for RAFT in CSTR system, showing how the use of CSTR results in broader distribution than batch due to its residence time distribution.

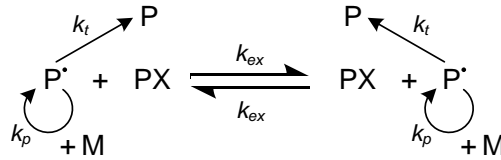


Figure 2-11. RAFT as simple degenerative transfer

$$n(r) = (\phi_{p,ov})^r e^{-z} \sum_{i=0}^{\infty} \binom{r+i-1}{r} \frac{(z(1-\phi_{p,ov}))^i}{i!} \quad (29)$$

where: $\phi_{p,ov} \equiv \frac{k_p[M]}{k_p[M] + k_a[PX]/2}$ is the overall probability of radical to add a monomer unit
 z is the average number of overall growth period

Peklak et al. demonstrated the use of a coarse-graining technique to obtain the full CLD.^[203] In the study, they discretized chain length (ranging from 1 to infinite) into finite intervals and solved mass balances for the chains in these intervals. Konkolewicz et al. also developed a method to obtain CLD for RAFT process, while accounting for termination effect.^[204,205] They discretized the polymerization period and used probabilistic approach to account for propagation of radicals. From their simulation results, they proposed the combination of ITM and SFM for the RAFT mechanism, *i.e.*, intermediate termination with oligomeric model (ITOM).

The full CLD has also been calculated via inversion of probability generating function by Fortunatti et al. for RAFT system.^[206] They used SFM as the mechanism for RAFT to investigate the effect of initiator and chain transfer agent on the kinetics and chain properties. Zapata-González et al. used direct integration of mass balances to obtain the full CLD for RAFT polymerization.^[207] They investigated the validity of quasi steady state approximations for the three models of RAFT mechanism, SFM, ITM, and ITOM. Johnston-Hall et al. also integrated mass balances for all chain lengths in order to plot the CLD of polymers synthesized via RAFT.^[208]

Vana et al. showed the ability of Predici® to predict the full CLD in RAFT.^[209] They found the importance of high activation rate constant (k_a) to achieve narrow dispersity, even at fixed value of equilibrium constant (k_a/k_f). Chaffey-Millar et al. simulated the full CLD of star polymers synthesized through RAFT polymerization

using Predici® software.^[210,211] Zetterlund et al. used the same software to simulate the full CLD of multiblock copolymers in RAFT polymerization.^[212] It should be noted that the use of Predici® in RAFT polymerization requires modification on how the reaction mechanism are described to account for the presence of intermediate radical.^[213] The full CLD has also been simulated for RAFT using Monte Carlo technique implemented in mcPolymer.^[88,214]

Zhang and Ray developed a comprehensive model for RAFT polymerization system using the method of moments.^[117,118,215] This versatile kinetic model developed is applicable for batch, semi-batch, and continuous reactors. Butté and Peklak derived models for various possible mechanisms that could cause inhibition and retardation in RAFT.^[216] The three mechanisms studied were SFM, ITM, and slow re-initiation. Slow re-initiation is a model that proposes slower propagation of R-group from RAFT agent than that of propagating radical chains. Based on their simulation results, they concluded that SFM could lead to inhibition, while ITM and slow re-initiation could induce retardation in polymerization rate.

An explicit expression for conversion profile in RAFT system has been derived by Wang and Zhu, as shown in Equation (30).^[217] The assumptions made to derive this expression include fast fragmentation of intermediate radicals and quasi steady state for radicals (propagating and intermediate) and dormant chains. They also derived the evolution of various reactant concentrations with time. In a more recent work,

Gao and Zhu has investigated the effect of simplifying RAFT mechanism to a simple degenerative chain transfer than addition-fragmentation reactions.^[202] They also derived an expression to estimate the chain transfer coefficient (ratio of exchange to propagation rate constants, k_{ex}/k_p) based on experimentally determined dispersity data.

$$x = 1 - \left(\frac{(\sqrt{1+\beta} + 1)(\sqrt{1+\beta \exp(k_d t)} - 1)}{(\sqrt{1+\beta} - 1)(\sqrt{1+\beta \exp(k_d t)} + 1)} \right)^{-\gamma} \quad (30)$$

$$\text{where: } \gamma = k_p \sqrt{\frac{k_f}{k_d k_{ct} k_a} \left(1 + \frac{k_t k_f}{2k_{ct} k_a [RX]_0} \right)} \text{ and } \beta = \left(1 + \frac{k_t k_f}{2k_{ct} k_a [RX]_0} \right)^2 \frac{[RX]_0}{f[I]_0} - 1$$

Monteiro and coworkers conducted experimental and modeling studies for system with difunctional RAFT agent.^[218,219] The modeling was carried out using the method of moments and by assuming simple degenerative chain transfer for RAFT mechanism. Through modeling and experimental results, they showed how the use of difunctional RAFT agent leads to a lower amount of dead chains. Adamy et al. used Predici® to estimate transfer constants of various xanthates as RAFT agents.^[220] Based on comparison of the estimated transfer constants, they concluded that the reactivity of radical to RAFT agent may be affected by the intermediate radicals.

Modeling studies on RAFT system involving microwave irradiation has been conducted by Hernández-Ortiz et al. and Zetterlund and Perrier.^[221,222] Comparison of simulation results based on various models and experimental data was conducted in those studies. Hernández-Ortiz et al. assumed that microwave irradiation plays role

in decomposition of monomer into radical. On the other hand, Zetterlund and Perrier used Predici® to compare 3 different effects that microwave irradiation could have on RAFT system, *i.e.*, decomposition of monomer into radical, increase in temperature, or increase in propagation and addition rate constants (k_p and k_a). Bitsch et al. studied various reactor configurations for RAFT system via the method of moments.^[223] The reactor configurations considered were PFR with a recycle stream and a series of CSTRs. The effects of backmixing on chain properties and polymerization kinetics were investigated and found to be significant.

Diffusion-controlled reactions in RAFT are investigated by Wang and Zhu using a semi-empirical correlation based on free-volume theory combined with the method of moments.^[224] They used reaction rate constants based on ITM and showed how both diffusion-controlled termination and activation accelerate polymerization rate, but have opposite effects on dispersity. Peklak et al. modeled the diffusion-controlled reactions using free-volume theory for two RAFT systems.^[225,226] They assumed dependence of reaction rate constants on the average chain length of all chains or on that of the chains directly involved in reaction. Chain length distribution must be taken into account in modeling the chain length dependence of reaction rate constants. Coote and coworkers studied the chain length dependence of addition and fragmentation reactions via high level ab initio molecular orbital calculation.^[227,228] In those studies, they concluded that the addition and fragmentation reactions are significantly affected by chain length during the initial stage of polymerization

Monteiro used the method of moments to show how versatile RAFT copolymerization (RAFTcoP) is in tailoring block copolymers.^[229] By manipulating comonomer concentration, the dispersity of each copolymer block may be predetermined. Feldermann et al. compared copolymer composition experimental data in conventional free radical copolymerization and RAFTcoP with those obtained from simulations using Predici®.^[230] The difference in reactivity ratios between FRP and RAFT was attributed to the presence of RAFT agent, that was postulated to provide additional reaction pathway for the radicals. The copolymers produced by RAFTcoP consist of slightly higher fraction of monomer with larger reactivity ratio than copolymers produced by conventional free radical copolymerization.

Schork's group used kinetic-based approach to model the sequence of copolymer composition produced by RAFTcoP.^[231-233] The model, referred to as sequence model, was developed using the method of moments and derived for batch, semi-batch, and various configuration of continuous reactors. Model-based control over copolymer composition in semi-batch reactor was also demonstrated by manipulating flow rates in feeding both monomers. They have also shown that combination of CSTR and PFR allows synthesis of copolymer with high conversion, low dispersity, and controlled copolymerization sequence.

Zhou et al. studied the effect of monomer, initiator, and RAFT agent concentrations on polymerization kinetics and polymer chain properties produced in RAFTcoP using the

method of moments.^[234] The model was developed for two consecutive batch reactions to produce triblock copolymers. Zetterlund and coworkers investigated the synthesis of multiblock polymers by RAFT.^[212] In the study, they simulated 10 cycles of monomer additions to form multiblock polymers. Chaffey-Millar et al. discussed the kinetics in formation of star polymers using RAFT via R-group approach to optimize reaction conditions.^[211] Star polymers synthesized through the Z-group approach were investigated by Vana and coworkers using Predici[®] and Monte Carlo with a shielding factor.^[235-237]

Kubo et al. have compared terminal and penultimate models in simulation of RAFTcoP for synthesis of random and block copolymers.^[238] They concluded that the terminal model is sufficient for estimation of the chain transfer coefficients. Li and Zhu and coworkers conducted several theoretical studies on copolymers produced via RAFTcoP using terminal model.^[239-241] They investigated the differences between batch and semi-batch on the conversion and copolymer composition profiles.^[239] This group has also developed an expression to obtain the dependence of chain transfer coefficient on monomer composition.^[240] In addition, they extended their study to model crosslinking in RAFTcoP, in order to investigate the effect of the RAFT agent concentration on the gelation point.^[241] Hernández-Ortiz et al. also published a modeling study to investigate the kinetics of crosslinking in RAFTcoP.^[242] The model was derived based on the method of moments and Flory-Stockmayer theory.

RAFT CLD-T

Vana et al. developed a method to determine chain length dependent termination rate using models for RAFT polymerization and experimental data, termed as a RAFT chain length dependent termination (RAFT CLD-T).^[243] The analytical expression was developed by use of quasi steady state assumption for radical concentration and by assuming a single chain length for all living chains. The quasi steady state assumption allows termination rate constant to be expressed in terms of polymerization rate and time. The assumption of single chain length enables exchange between time and chain length as the independent variable.

The use of RAFT polymerization to determine termination rate constant as a function of chain length has been demonstrated for various systems.^[208,244-252] Feldermann et al. investigated the influence of RAFT agent structure on the accuracy of the method.^[244] The decrease in accuracy lies on the assumption that all living chains possess equal chain length for systems that behave as both CRP and conventional FRP, due to the type of RAFT agent chosen. Johnston-Hall and coworkers extended the chain length dependence of termination rate constant to also account for the dependence on conversion.^[249,250] This model divides chain length into two regimes, dilute and gel, and is referred to as the composite model.

Slow fragmentation vs. Intermediate termination

There has been a disagreement amongst researchers on the cause of polymerization rate retardation observed with increasing RAFT agent concentration in some RAFT polymerizations. One group theorized that fragmentation of intermediate radical to form dormant and radical chains is a slow process, as illustrated in Figure 2-5 with a low value of k_f and zero for k_{ct} (slow fragmentation model, SFM). While the other group hypothesized that although the intermediate radical is short-lived, it could undergo termination with other radicals, as shown in Figure 2-5 with high value of k_f and non-zero value of k_{ct} (intermediate termination model, ITM). This debate has been discussed repeatedly in review papers, including other variations of these models, such as a “missing species” hypothesis, reversible intermediate termination, etc.^[194-198] Discussions on various methods to differentiate the mechanisms based on theoretical modeling and experimentation could also be found in these publications. For completeness, but for the sake of brevity, this part of the review briefly highlights some of the pertinent modeling work in this area.

Barner-Kowollik et al. estimated the RAFT equilibrium constant between addition and fragmentation reactions by comparing simulation results from Predici® and experimental data.^[253,254] The value of equilibrium constant found was high, indicating addition reaction occurs at a much faster rate than fragmentation ($k_a \gg k_f$). These values are also supported by ab-initio calculation by Coote et al. for activation and fragmentation rate constants.^[255,256] Around the same time, Monteiro et al.^[257,258]

along with Fukuda's group^[201,259] proposed cross-termination mechanism between active and intermediate radical to be responsible for the rate retardation based on various parameter estimations. The fragmentation rate constant found from these studies suggests a much shorter lifetime for the intermediate radical than that estimated by Barner-Kowollik et al.

There have been discussions on the values of kinetic rate constants in the literature to use to correctly represent the actual RAFT mechanism, *i.e.*, SFM vs ITM, some of which are highlighted here.^[260-266] Using the method of moments, Wang and Zhu investigated the effect of various reaction conditions and reaction rate constants in RAFT systems.^[260] For their simulations, they used reaction rate constants supporting the ITM as published by the groups of Monteiro and Fukuda. Barner-Kowollik et al. criticized the choice of reaction rate constants, mainly because fast fragmentation of intermediate radicals and cross-termination are considered by Wang (large k_f and $k_{ct} \neq 0$).^[261] In response to this comment, the groups of Zhu, Fukuda and Monteiro justified the use of these reaction rate constants through previously published experimental data.^[262] Their major argument was based on the level of intermediate radical concentration. It was clear that if SFM employed, the radical concentration in RAFT would reach an unreasonably high level. They also discussed the need for model discrimination in order to clarify the true mechanism behind rate retardation in RAFT.

Meiser and Buback published an EPR-based method to estimate the equilibrium constant for RAFT.^[264] Their experimental results showed a relatively low value for equilibrium constant, implying fast fragmentation of intermediate radicals (against SFM). However, using a quantum chemical calculation this method has been criticized by Junkers et al. to be model dependent.^[265] Their calculations were based on slow fragmentation of intermediate radicals, but with cross termination of radicals (SFM and ITM). A further response from Meiser and Buback criticized the use of SFM and ITM together due to significant retardation that would be observed.^[266] They also showed that the EPR-based method is not model dependent.

The model discrimination between SFM and ITM has also been studied by experimental and modeling work of heterogeneous RAFT system.^[267-272] Luo et al. compared their modeling results for miniemulsion RAFT with experimental data.^[267] The model was derived based on ITM or SFM, resulting in a zero-one emulsion behavior or pseudo-bulk behavior, respectively. The simulated results based on ITM agreed well with experimental data. It may be used to explain that miniemulsion polymerization has faster rate, but more severe rate retardation than bulk. On the other hand, the model derived from SFM does not show a compartmentalization effect, hence does not fit experimental data.

Through a different approach, Tobita and Yanase have also shown that the polymerization rates of miniemulsion RAFT are different when SFM or ITM are

applied in Monte Carlo simulation.^[268] The SFM-based simulation predicted an equal polymerization rate of miniemulsion and bulk, regardless of particle size.^[269-272] On the other hand, ITM-based simulation predicts that smaller particles would result in faster polymerization rates. In a collaboration with Suzuki et al., experiments were conducted for model discrimination by comparing polymerization rate in bulk and in miniemulsion.^[273] The experimental results showed an increase of polymerization rate for systems with small particle sizes, as predicted by ITM-based simulations.

Konkolewicz et al. proposed a combination of two models, for which the intermediate radical fragmentation is considered to be slow, but oligomeric radical chains could cross-terminate with the intermediate radicals (intermediate termination model with oligomeric model, ITOM).^[204] This model has been extended in their subsequent studies^[205,274] and used by Zapata-González et al. in their modeling work.^[207] Experimental validation of this model has been reported by Ting et al., who conducted RAFT in the absence of short radical chains through the use of macroinitiator, with little to no rate retardation.^[275]

§ 2.6 Concluding remarks

Modeling is essential in designing and optimizing reaction conditions for tailoring product properties nowadays. CRP modeling activities started in the 1990's, right after introduction of the respective mechanisms. In this area, modeling has played a particularly important role in explaining experimental observations. The combination

of modeling and experimental studies provides a powerful tool to investigate the actual mechanism and kinetics of polymerization systems. Despite the numerous studies on CRP being published every year, disagreements on the true mechanisms of some experimentally-observed phenomena still remain. To name a few, the debate on SFM vs ITM as the cause of rate retardation in RAFT and propagation vs. termination for SI-CRP mechanism. These controversies show that further studies are required to obtain conclusive proof on the actual underlying mechanisms, as may be done via model discrimination using carefully designed experiments.

Simulation of complex systems is easier with the significant improvement of processing power in today's computers, along with various commercially available software packages. However, one should be aware of the underlying assumptions involved in the software, to ensure that the reaction conditions of the cases considered are consistent with these assumptions. In conducting parameter estimation, it should be kept in mind that comparison of simulation results to limited experimental data for estimation of a large number of parameters requires extra caution in practice. It is likely that more than one set of parameters could represent the data within experimental uncertainty for a limited range of operational parameters.

§ 2.7 References

- [1] M. Szwarc, *Nature* **1956**, *178*, 1168-1169.

- [2] G. Moad, E. Rizzardo, D. H. Solomon, *Macromolecules* **1982**, *15*, 909-914.
- [3] M. Georges, R. P. N. Veregin, P. M. Kazmaier, G. K. Hamer, *Macromolecules* **1993**, *26*, 2987-2988.
- [4] J.-S. Wang, K. Matyjaszewski, *J Am Chem Soc* **1995**, *117*, 5614-5615.
- [5] M. Kato, M. Kamigaito, M. Sawamoto, T. Higashimura, *Macromolecules* **1995**, *28*, 1721-1723.
- [6] J. Chiefari, Y. K. B. Chong, F. Ercole, J. Krstina, J. Jeffery, T. P. T. Le, R. T. A. Mayadunne, G. F. Meijs, C. L. Moad, G. Moad, E. Rizzardo, S. H. Thang, *Macromolecules* **1998**, *31*, 5559-5562.
- [7] A. Hamielec, J. MacGregor, "Modelling Copolymerizations--Control of Composition, Chain Microstructure, Molecular Weight Distribution, Long Chain Branching and Crosslinking", in *Polymer Reaction Engineering: Influence of Reaction Engineering on Polymer Properties*, K. Reichert and W. Geiseler, Eds., Carl Hanser Verlag, New York, 1983, p. 21-71.
- [8] E. D. Bain, S. Turgman-Cohen, J. Genzer, *Macromol Theory Simul* **2013**, *22*, 8-30.
- [9] T. J. Crowley, K. Y. Choi, *Ind Eng Chem Res* **1997**, *36*, 1419-1423.
- [10] A. Krallis, D. Meimaroglou, V. Saliakas, C. Chatzidoukas, C. Kiparissides, *Computer Aided Chemical Engineering* **2006**, *21*, 1335-1340.
- [11] D. R. D'hooge, M.-F. Reyniers, G. B. Marin, *Macromol React Eng* **2009**, *3*, 185-209.
- [12] M. Wulkow, *Macromol Theory Simul* **1996**, *5*, 393-416.
- [13] D. T. Gillespie, *The Journal of Physical Chemistry* **1977**, *81*, 2340-2361.
- [14] J. He, H. Zhang, J. Chen, Y. Yang, *Macromolecules* **1997**, *30*, 8010-8018.
- [15] H. Tobita, *Macromol Theory Simul* **2006**, *15*, 23-31.
- [16] R. Szymanski, S. Sosnowski, *Macromol Theory Simul* **2012**, *21*, 510-515.
- [17] L. Wang, L. J. Broadbelt, *Macromol Theory Simul* **2011**, *20*, 54-64.
- [18] P. H. Van Steenberge, D. R. D'hooge, Y. Wang, M. Zhong, M.-F. o. Reyniers, D. Konkolewicz, K. Matyjaszewski, G. B. Marin, *Macromolecules* **2012**, *45*, 8519-8531.
- [19] P. J. Flory, *J Am Chem Soc* **1940**, *62*, 1561-1565.
- [20] L. Gold, *The Journal of Chemical Physics* **1958**, *28*, 91-99.
- [21] B. D. Coleman, T. G. Fox, "On the two-state mechanism for homogeneous ionic polymerization", in *Journal of Polymer Science Part C: Polymer Symposia*, Wiley Online Library, 1963, p. 4/345-360.

- [22] B. D. Coleman, T. G. Fox, *J Am Chem Soc* **1963**, *85*, 1241-1244.
- [23] V. R. Figini, *Die Makromolekulare Chemie* **1964**, *71*, 193-197.
- [24] D. Yan, H. Dong, G. Wang, Z. Zhou, *Chin Sci Bull* **1999**, *44*, 426-431.
- [25] M. Szwarc, J. Hermans, *Journal of Polymer Science Part B: Polymer Letters* **1964**, *2*, 815-818.
- [26] T. J. Pickett, *Journal of Polymer Science Part B: Polymer Physics* **1997**, *35*, 1711-1725.
- [27] R. V. Figini, G. V. Schulz, *Zeitschrift für Physikalische Chemie* **1960**, *23*, 233-256.
- [28] J. E. Puskas, G. Kaszas, M. Litt, *Macromolecules* **1991**, *24*, 5278-5282.
- [29] S. Zhu, W. Wang, *Journal of Polymer Science Part B: Polymer Physics* **1999**, *37*, 961-964.
- [30] A. H. Müller, R. Zhuang, D. Yan, G. Litvinenko, *Macromolecules* **1995**, *28*, 4326-4333.
- [31] A. H. Müller, D. Yan, G. Litvinenko, R. Zhuang, H. Dong, *Macromolecules* **1995**, *28*, 7335-7338.
- [32] A. H. Müller, G. Litvinenko, D. Yan, *Macromolecules* **1996**, *29*, 2346-2353.
- [33] L. Böhm, *Z Phys Chem* **1970**, *72*, 199-221.
- [34] D. Yan, P. Ye, H. a. Zhang, *Science in China Series B: Chemistry* **1998**, *41*, 278-284.
- [35] C. W. Bielawski, R. H. Grubbs, *Prog Polym Sci* **2007**, *32*, 1-29.
- [36] G. J. Domski, J. M. Rose, G. W. Coates, A. D. Bolig, M. Brookhart, *Prog Polym Sci* **2007**, *32*, 30-92.
- [37] W. A. Braunecker, K. Matyjaszewski, *Prog Polym Sci* **2007**, *32*, 93-146.
- [38] T. Yokozawa, A. Yokoyama, *Prog Polym Sci* **2007**, *32*, 147-172.
- [39] D. Baskaran, A. H. Müller, *Prog Polym Sci* **2007**, *32*, 173-219.
- [40] E. J. Goethals, F. Du Prez, *Prog Polym Sci* **2007**, *32*, 220-246.
- [41] S. Penczek, M. Cypriak, A. Duda, P. Kubisa, S. Słomkowski, *Prog Polym Sci* **2007**, *32*, 247-282.
- [42] L. C. So, S. Faucher, S. Zhu, *Prog Polym Sci* **2014**, *39*, 1196-1234.
- [43] J. H. Ward, N. A. Peppas, *Macromolecules* **2000**, *33*, 5137-5142.
- [44] M. Krajnc, I. Poljanšek, J. Golob, *Polymer* **2001**, *42*, 4153-4162.
- [45] E. Vivaldo-Lima, A. de Jesús Mendoza-Fuentes, *Polym React Eng* **2002**, *10*, 193-226.

- [46] A. Goto, K. Ohno, T. Fukuda, *Macromolecules* **1998**, *31*, 2809-2814.
- [47] A. Goto, H. Zushi, N. Hirai, T. Wakada, Y. Tsujii, T. Fukuda, *J Am Chem Soc* **2007**, *129*, 13347-13354.
- [48] A. Goto, Y. Tsujii, T. Fukuda, *Polymer* **2008**, *49*, 5177-5185.
- [49] P. Vana, A. Goto, *Macromol Theory Simul* **2010**, *19*, 24-35.
- [50] A. Goto, T. Wakada, T. Fukuda, Y. Tsujii, *Macromol Chem Phys* **2010**, *211*, 594-600.
- [51] A. Goto, H. Zushi, N. Hirai, T. Wakada, Y. Kwak, T. Fukuda, "Germanium- and Tin-Catalyzed Living Radical Polymerizations of Styrene and Methacrylates", in *Macromol Symp*, Wiley Online Library, 2007, p. 248/126-131.
- [52] Y. Kwak, A. Goto, T. Fukuda, Y. Kobayashi, S. Yamago, *Macromolecules* **2006**, *39*, 4671-4679.
- [53] Y. Kwak, M. Tezuka, A. Goto, T. Fukuda, S. Yamago, *Macromolecules* **2007**, *40*, 1881-1885.
- [54] R. B. Grubbs, *Polymer Reviews* **2011**, *51*, 104-137.
- [55] J. Nicolas, Y. Guillaneuf, C. Lefay, D. Bertin, D. Gigmes, B. Charleux, *Prog Polym Sci* **2013**, *38*, 63-235.
- [56] R. P. Veregin, P. G. Odell, L. M. Michalak, M. K. Georges, *Macromolecules* **1996**, *29*, 3346-3352.
- [57] D. Yan, H. Jiang, X. Fan, *Macromol Theory Simul* **1996**, *5*, 333-345.
- [58] A.-C. Shi, M. K. Georges, H. K. Mahabadi, *Polym React Eng* **1999**, *7*, 283-300.
- [59] S. Zhu, *J Polym Sci, Part B: Polym Phys* **1999**, *37*, 2692-2704.
- [60] S. Zhu, *Macromol Theory Simul* **1999**, *8*, 29-37.
- [61] H. Fischer, *Macromolecules* **1997**, *30*, 5666-5672.
- [62] H. Fischer, *J Polym Sci, Part A: Polym Chem* **1999**, *37*, 1885-1901.
- [63] M. Souaille, H. Fischer, *Macromolecules* **2000**, *33*, 7378-7394.
- [64] M. Souaille, H. Fischer, *Macromolecules* **2001**, *34*, 2830-2838.
- [65] K. Ohno, Y. Tsujii, T. Miyamoto, T. Fukuda, M. Goto, K. Kobayashi, T. Akaike, *Macromolecules* **1998**, *31*, 1064-1069.
- [66] T. Fukuda, A. Goto, K. Ohno, *Macromol Rapid Commun* **2000**, *21*, 151-165.
- [67] C. Yoshikawa, A. Goto, T. Fukuda, *Macromolecules* **2002**, *35*, 5801-5807.
- [68] D. S. Achilias, *Macromol Theory Simul* **2007**, *16*, 319-347.
- [69] A. Butté, G. Storti, M. Morbidelli, *Chem Eng Sci* **1999**, *54*, 3225-3231.

- [70] M. Roa-Luna, M. P. Díaz-barber, E. Vivaldo-Lima, L. M. Lona, N. T. McManus, A. Penlidis, *J Macromol Sci, Part A: Pure Appl Chem* **2007**, *44*, 193-203.
- [71] M. Roa-Luna, A. Nabifar, N. T. McManus, E. Vivaldo-Lima, L. M. Lona, A. Penlidis, *J Appl Polym Sci* **2008**, *109*, 3665-3678.
- [72] D. R. D'hooge, M.-F. Reyniers, G. B. Marin, *Macromol React Eng* **2013**, *7*, 362-379.
- [73] T. Fukuda, A. Goto, *Macromol Rapid Commun* **1997**, *18*, 683-688.
- [74] A. Goto, T. Fukuda, *Macromolecules* **1997**, *30*, 4272-4277.
- [75] K. Matyjaszewski, *J Macromol Sci, Part A: Pure Appl Chem* **1997**, *10*, 1785-1801.
- [76] K. Matyjaszewski, "The importance of exchange reactions in controlled/living radical polymerization in the presence of alkoxyamines and transition metals", in *Macromol Symp*, Wiley Online Library, 1996, p. 111/47-61.
- [77] H. Tobita, *Macromol Theory Simul* **2006**, *15*, 12-22.
- [78] E. Mastan, D. Zhou, S. Zhu, *J Polym Sci, Part A: Polym Chem* **2013**, *52*, 639-651.
- [79] T. Fukuda, *J Polym Sci, Part A: Polym Chem* **2004**, *42*, 4743-4755.
- [80] A. Goto, T. Fukuda, *Prog Polym Sci* **2004**, *29*, 329-385.
- [81] E. Mastan, D. Zhou, S. Zhu, *Macromol Theory Simul* **2014**, *23*, 227-240.
- [82] E. Saldívar-Guerra, R. Infante-Martínez, E. Vivaldo-Lima, A. Flores-Tlacuahuac, *Macromol Theory Simul* **2010**, *19*, 151-157.
- [83] L. Bentein, D. R. D'hooge, M.-F. Reyniers, G. B. Marin, *Macromol Theory Simul* **2011**, *20*, 238-265.
- [84] M. Asteasuain, M. Soares, M. K. Lenzi, M. Cunningham, C. Sarmoria, J. C. Pinto, A. Brandolin, *Macromol React Eng* **2007**, *1*, 622-634.
- [85] R. Dias, M. R. P. Costa, *Macromol Theory Simul* **2010**, *19*, 323-341.
- [86] T. Irzhak, V. Irzhak, *Polymer Science Series A* **2012**, *54*, 883-893.
- [87] D. Gimes, D. Bertin, C. Lefay, Y. Guillaneuf, *Macromol Theory Simul* **2009**, *18*, 402-419.
- [88] M. Drache, G. Drache, *Polymers* **2012**, *4*, 1416-1442.
- [89] T. Fukuda, T. Terauchi, A. Goto, K. Ohno, Y. Tsujii, T. Miyamoto, S. Kobatake, B. Yamada, *Macromolecules* **1996**, *29*, 6393-6398.
- [90] T. M. Kruse, R. Souleimonova, A. Cho, M. K. Gray, J. M. Torkelson, L. J. Broadbelt, *Macromolecules* **2003**, *36*, 7812-7823.
- [91] D. Greszta, K. Matyjaszewski, *Macromolecules* **1996**, *29*, 7661-7670.

- [92] J. J. Hernández-Meza, G. Jaramillo-Soto, P. R. García-Morán, J. Palacios-Alquisira, E. Vivaldo-Lima, *Macromol React Eng* **2009**, *3*, 101-107.
- [93] N. M. Ahmad, B. Charleux, C. Farcet, C. J. Ferguson, S. G. Gaynor, B. S. Hawkett, F. Heatley, B. Klumperman, D. Konkolewicz, P. A. Lovell, *Macromol Rapid Commun* **2009**, *30*, 2002-2021.
- [94] Y. Reyes, J. M. Asua, *Macromol Rapid Commun* **2011**, *32*, 63-67.
- [95] D. Konkolewicz, S. Sosnowski, D. R. D'hooge, R. Szymanski, M.-F. Reyniers, G. B. Marin, K. Matyjaszewski, *Macromolecules* **2011**, *44*, 8361-8373.
- [96] A. Goto, T. Terauchi, T. Fukuda, T. Miyamoto, *Macromol Rapid Commun* **1997**, *18*, 673-681.
- [97] A. Goto, T. Fukuda, *Macromolecules* **1997**, *30*, 5183-5186.
- [98] J.-F. Lutz, P. Lacroix-Desmazes, B. Boutevin, *Macromol Rapid Commun* **2001**, *22*, 189-193.
- [99] W. Tang, T. Fukuda, K. Matyjaszewski, *Macromolecules* **2006**, *39*, 4332-4337.
- [100] W. Tang, N. V. Tsarevsky, K. Matyjaszewski, *J Am Chem Soc* **2006**, *128*, 1598-1604.
- [101] D. Benoit, S. Grimaldi, S. Robin, J.-P. Finet, P. Tordo, Y. Gnanou, *J Am Chem Soc* **2000**, *122*, 5929-5939.
- [102] J. Bonilla, E. Saldivar-Guerra, A. Flores-Tlacuahuac, E. Vivaldo-Lima, R. Pfaendner, F. Tiscareño-Lechuga, *Polym React Eng* **2002**, *10*, 227-263.
- [103] J. Belincanta-Ximenes, P. V. Mesa, L. M. Lona, E. Vivaldo-Lima, N. T. McManus, A. Penlidis, *Macromol Theory Simul* **2007**, *16*, 194-208.
- [104] N. Ide, T. Fukuda, *Macromolecules* **1997**, *30*, 4268-4271.
- [105] J. C. Hernández-Ortiz, E. Vivaldo-Lima, L. M. Lona, N. T. McManus, A. Penlidis, *Macromol React Eng* **2009**, *3*, 288-311.
- [106] J. C. Hernández-Ortiz, E. Vivaldo-Lima, A. Penlidis, *Macromol Theory Simul* **2012**, *21*, 302-321.
- [107] A. J. Scott, A. Nabifar, J. C. Hernández-Ortiz, N. T. McManus, E. Vivaldo-Lima, A. Penlidis, *Eur Polym J* **2014**, *51*, 87-111.
- [108] J. C. Hernández-Ortiz, E. Vivaldo-Lima, M. A. Dubé, A. Penlidis, *Macromol Theory Simul* **2014**, *23*, 429-441.
- [109] L. Wang, L. J. Broadbelt, *Macromolecules* **2009**, *42*, 7961-7968.
- [110] A. S. Cho, L. J. Broadbelt, *Mol Simul* **2010**, *36*, 1219-1236.
- [111] L. Wang, L. J. Broadbelt, *Macromolecules* **2010**, *43*, 2228-2235.

- [112] L. Wang, L. J. Broadbelt, *Macromol Theory Simul* **2011**, *20*, 191-204.
- [113] Y. Ye, F. J. Schork, *Macromol React Eng* **2010**, *4*, 197-209.
- [114] I. Zapata-González, R. A. Hutchinson, K. Matyjaszewski, E. Saldívar-Guerra, J. Ortiz-Cisneros, *Macromol Theory Simul* **2014**, *23*, 245-265.
- [115] H. Fischer, M. Souaille, *Macromol Symp* **2001**, *174*, 231-240.
- [116] Y. Guillaneuf, D. Gimes, S. R. Marque, P. Tordo, D. Bertin, *Macromol Chem Phys* **2006**, *207*, 1278-1288.
- [117] M. Zhang, W. H. Ray, *J Appl Polym Sci* **2002**, *86*, 1630-1662.
- [118] M. Zhang, W. H. Ray, *J Appl Polym Sci* **2002**, *86*, 1047-1056.
- [119] M. Zhang, W. H. Ray, "The value of fundamental modeling in the design and operation of controlled free radical polymerization processes", in *Macromol Symp*, Wiley Online Library, 2002, p. 182/169-180.
- [120] F. J. Schork, W. Smulders, *J Appl Polym Sci* **2004**, *92*, 539-542.
- [121] A. Faliks, R. A. Yetter, C. A. Floudas, Y. Wei, H. Rabitz, *Polymer* **2001**, *42*, 2061-2065.
- [122] A. G. Zitalpopoca-Soriano, E. Vivaldo-Lima, A. Flores-Tlacuahuac, *Macromol React Eng* **2010**, *4*, 599-612.
- [123] A. G. Zitalpopoca-Soriano, E. Vivaldo-Lima, A. Flores-Tlacuahuac, *Macromol React Eng* **2010**, *4*, 516-533.
- [124] K. Matyjaszewski, *Macromolecules* **2012**, *45*, 4015-4039.
- [125] Y. Shen, H. Tang, S. Ding, *Prog Polym Sci* **2004**, *29*, 1053-1078.
- [126] V. Coessens, T. Pintauer, K. Matyjaszewski, *Prog Polym Sci* **2001**, *26*, 337-377.
- [127] F. J. Xu, K. G. Neoh, E. T. Kang, *Prog Polym Sci* **2009**, *34*, 719-761.
- [128] J. Ran, L. Wu, Z. Zhang, T. Xu, *Prog Polym Sci* **2014**, *39*, 124-144.
- [129] R. P. Vieira, A. Ossig, J. M. Perez, V. G. Grassi, C. L. Petzhold, A. Peres, J. M. Costa, L. M. Lona, *J Braz Chem Soc* **2013**, *24*, 2008-2014.
- [130] C. Yoshikawa, A. Goto, T. Fukuda, *Macromolecules* **2003**, *36*, 908-912.
- [131] D. A. Shipp, K. Matyjaszewski, *Macromolecules* **2000**, *33*, 1553-1559.
- [132] H. Zhang, B. Klumperman, W. Ming, H. Fischer, R. van der Linde, *Macromolecules* **2001**, *34*, 6169-6173.
- [133] J.-F. Lutz, K. Matyjaszewski, *Macromol Chem Phys* **2002**, *203*, 1385-1395.
- [134] M. Al-Harhi, J. B. Soares, L. C. Simon, *Macromol Theory Simul* **2006**, *15*, 198-214.
- [135] M. Al-Harhi, J. B. Soares, L. C. Simon, *Macromol React Eng* **2007**, *1*, 95-105.

- [136] P. López-Domínguez, E. Vivaldo-Lima, *Macromol React Eng* **2013**, *7*, 463-476.
- [137] A. Snijder, B. Klumperman, R. van der Linde, *Macromolecules* **2002**, *35*, 4785-4790.
- [138] Y. Fu, A. Mirzaei, M. F. Cunningham, R. A. Hutchinson, *Macromol React Eng* **2007**, *1*, 425-439.
- [139] Y. Wang, M. Zhong, Y. Zhang, A. J. Magenau, K. Matyjaszewski, *Macromolecules* **2012**, *45*, 8929-8932.
- [140] Y. Wang, N. Soerensen, M. Zhong, H. Schroeder, M. Buback, K. Matyjaszewski, *Macromolecules* **2013**, *46*, 683-691.
- [141] M. Zhong, K. Matyjaszewski, *Macromolecules* **2011**, *44*, 2668-2677.
- [142] D. A. Shipp, K. Matyjaszewski, *Macromolecules* **1999**, *32*, 2948-2955.
- [143] M. Najafi, V. Haddadi-Asl, M. Salami-Kalajahi, H. R. Mamaghani, *e-Polymers* **2009**, *9*, 355-374.
- [144] M. Najafi, H. Roghani-Mamaqani, V. Haddadi-Asl, M. Salami-Kalajahi, *Adv Polym Technol* **2011**, *30*, 257-268.
- [145] O. Delgadillo-Velázquez, E. Vivaldo-Lima, I. A. Quintero-Ortega, S. Zhu, *AIChE J* **2002**, *48*, 2597-2608.
- [146] M. Al-Harhi, J. B. Soares, L. C. Simon, *Macromol Chem Phys* **2006**, *207*, 469-483.
- [147] M. Al-Harhi, J. Soares, B.P. L. Simon, *Macromol Mater Eng* **2006**, *291*, 993-1003.
- [148] M. Al-Harhi, L. S. Cheng, J. B. Soares, L. C. Simon, *J Polym Sci, Part A: Polym Chem* **2007**, *45*, 2212-2224.
- [149] M. Najafi, H. Roghani-Mamaqani, M. Salami-Kalajahi, V. Haddadi-Asl, *Chin J Polym Sci* **2010**, *28*, 483-497.
- [150] D. R. D'hooge, M.-F. Reyniers, F. J. Stadler, B. Dervaux, C. Bailly, F. E. Du Prez, G. B. Marin, *Macromolecules* **2010**, *43*, 8766-8781.
- [151] G. Johnston-Hall, M. J. Monteiro, *Macromol Theory Simul* **2010**, *19*, 387-393.
- [152] H. Bergenudd, M. Jonsson, E. Malmström, *Macromol Theory Simul* **2011**, *20*, 814-825.
- [153] K. Ohno, A. Goto, T. Fukuda, J. Xia, K. Matyjaszewski, *Macromolecules* **1998**, *31*, 2699-2701.
- [154] Y.-J. Kwark, B. M. Novak, *Macromolecules* **2004**, *37*, 9395-9401.
- [155] C. Toloza Porras, D. R. D'hooge, P. H. Van Steenberge, M.-F. o. Reyniers, G. B. Marin, *Ind Eng Chem Res* **2014**, *53*, 9674-9685.

- [156] J. Morick, M. Buback, K. Matyjaszewski, *Macromol Chem Phys* **2011**, *212*, 2423-2428.
- [157] J. Morick, M. Buback, K. Matyjaszewski, *Macromol Chem Phys* **2012**, *213*, 2287-2292.
- [158] H. Schroeder, D. Yalalov, M. Buback, K. Matyjaszewski, *Macromol Chem Phys* **2012**, *213*, 2019-2026.
- [159] H. Schroeder, J. Buback, J. Schrooten, M. Buback, K. Matyjaszewski, *Macromol Theory Simul* **2014**, *23*, 279-287.
- [160] Y. Wang, Y. Kwak, J. Buback, M. Buback, K. Matyjaszewski, *ACS Macro Letters* **2012**, *1*, 1367-1370.
- [161] D. A. Shipp, X. Yu, *J Polym Sci, Part A: Polym Chem* **2004**, *42*, 5548-5558.
- [162] M. J. Ziegler, K. Matyjaszewski, *Macromolecules* **2001**, *34*, 415-424.
- [163] Y. Fu, M. F. Cunningham, R. A. Hutchinson, "Semibatch atom transfer radical copolymerization of styrene and butyl acrylate", in *Macromol Symp*, Wiley Online Library, 2007, p. 259/151-163.
- [164] S. G. Roos, A. H. Müller, K. Matyjaszewski, *Macromolecules* **1999**, *32*, 8331-8335.
- [165] B. Klumperman, G. Chambard, R. H. G. Brinkhuis, "Peculiarities in Atom Transfer Radical Copolymerization", in *Advances in Controlled/Living Radical Polymerization*, American Chemical Society, 2003, p. 180-192.
- [166] R. Wang, Y. Luo, B.-G. Li, S. Zhu, *AIChE J* **2007**, *53*, 174-186.
- [167] M. Al-Harhi, J. B. Soares, L. C. Simon, *Macromol React Eng* **2007**, *1*, 468-479.
- [168] M. Al-Harhi, M. J. Khan, S. H. Abbasi, J. B. Soares, *Macromol React Eng* **2009**, *3*, 148-159.
- [169] M. Al-Harhi, J. K. Masihullah, S. H. Abbasi, J. B. Soares, *Macromol Theory Simul* **2009**, *18*, 307-316.
- [170] C. Toloza Porras, D. R. D'hooge, P. H. Van Steenberge, M.-F. Reyniers, G. B. Marin, *Macromol React Eng* **2013**, *7*, 311-326.
- [171] Y.-N. Zhou, J.-J. Li, Z.-H. Luo, *J Polym Sci, Part A: Polym Chem* **2012**, *50*, 3052-3066.
- [172] I. Bannister, N. C. Billingham, S. P. Armes, *Soft Matter* **2009**, *5*, 3495-3504.
- [173] H. Gao, P. Polanowski, K. Matyjaszewski, *Macromolecules* **2009**, *42*, 5925-5932.
- [174] J. Poly, D. J. Wilson, M. Destarac, D. Taton, *J Polym Sci, Part A: Polym Chem* **2009**, *47*, 5313-5327.

- [175] P. Polanowski, J. K. Jeszka, K. Matyjaszewski, *Polymer* **2010**, *51*, 6084-6092.
- [176] P. Polanowski, J. K. Jeszka, K. Matyjaszewski, *Polymer* **2013**, *54*, 1979-1986.
- [177] D. Konkolewicz, Y. Wang, M. Zhong, P. Krys, A. A. Isse, A. Gennaro, K. Matyjaszewski, *Macromolecules* **2013**, *46*, 8749-8772.
- [178] D. Konkolewicz, Y. Wang, P. Krys, M. Zhong, A. A. Isse, A. Gennaro, K. Matyjaszewski, *Polymer Chemistry* **2014**, *5*, 4396-4417.
- [179] M. Zhong, Y. Wang, P. Krys, D. Konkolewicz, K. Matyjaszewski, *Macromolecules* **2013**, *46*, 3816-3827.
- [180] B. M. Rosen, V. Percec, *Chemical Reviews* **2009**, *109*, 5069-5119.
- [181] A. A. Isse, A. Gennaro, C. Y. Lin, J. L. Hodgson, M. L. Coote, T. Gulashvili, *J Am Chem Soc* **2011**, *133*, 6254-6264.
- [182] Y.-N. Zhou, Z.-H. Luo, *Macromolecules* **2014**, *47*, 6218-6229.
- [183] B. Dervaux, T. Junkers, C. Barner-Kowollik, F. E. Du Prez, *Macromol React Eng* **2009**, *3*, 529-538.
- [184] Y. Shen, S. Zhu, F. Zeng, R. H. Pelton, *Macromolecules* **2000**, *33*, 5427-5431.
- [185] N. Chan, M. F. Cunningham, R. A. Hutchinson, *J Polym Sci, Part A: Polym Chem* **2013**, *51*, 3081-3096.
- [186] W. Tang, K. Matyjaszewski, *Macromol Theory Simul* **2008**, *17*, 359-375.
- [187] A. P. Haehnel, S. Fleischmann, P. Hesse, K.-D. Hungenberg, C. Barner-Kowollik, *Macromol React Eng* **2013**, *7*, 8-23.
- [188] X. Li, W.-J. Wang, B.-G. Li, S. Zhu, *Macromol React Eng* **2011**, *5*, 467-478.
- [189] K. A. Payne, D. R. D'Hooge, P. H. M. Van Steenberge, M.-F. Reyniers, M. Cunningham, R. A. Hutchinson, G. B. Marin, *Macromolecules* **2013**, *46*, 3828-3840.
- [190] D. R. D'hooge, D. Konkolewicz, M.-F. Reyniers, G. B. Marin, K. Matyjaszewski, *Macromol Theory Simul* **2012**, *21*, 52-69.
- [191] C. Toloza Porras, D. R. D'hooge, M.-F. Reyniers, G. B. Marin, *Macromol Theory Simul* **2013**, *22*, 136-149.
- [192] D. R. D'hooge, P. H. Van Steenberge, M.-F. Reyniers, G. B. Marin, *Polymers* **2014**, *6*, 1074-1095.
- [193] K. A. Payne, P. H. Van Steenberge, D. R. D'hooge, M.-F. Reyniers, G. B. Marin, R. A. Hutchinson, M. F. Cunningham, *Polym Int* **2014**, *63*, 848-857.
- [194] C. Barner-Kowollik, M. Buback, B. Charleux, M. L. Coote, M. Drache, T. Fukuda, A. Goto, B. Klumperman, A. B. Lowe, J. B. Mcleary, *J Polym Sci, Part A: Polym Chem* **2006**, *44*, 5809-5831.

- [195] B. Klumperman, E. T. van den Dungen, J. Heuts, M. J. Monteiro, *Macromol Rapid Commun* **2010**, *31*, 1846-1862.
- [196] T. Junkers, *J Polym Sci, Part A: Polym Chem* **2011**, *49*, 4154-4163.
- [197] G. Moad, E. Rizzardo, S. H. Thang, *Aust J Chem* **2012**, *65*, 985-1076.
- [198] G. Moad, *Macromol Chem Phys* **2014**, *215*, 9-26.
- [199] M. Destarac, *Polymer Reviews* **2011**, *51*, 163-187.
- [200] H. Tobita, *Macromol React Eng* **2008**, *2*, 371-381.
- [201] A. Goto, K. Sato, Y. Tsujii, T. Fukuda, G. Moad, E. Rizzardo, S. H. Thang, *Macromolecules* **2001**, *34*, 402-408.
- [202] X. Gao, S. Zhu, *J Appl Polym Sci* **2011**, *122*, 497-508.
- [203] A. D. Peklak, A. Butté, G. Storti, M. Morbidelli, "A discretization method for computing chain length distributions", in *Macromol Symp*, Wiley Online Library, 2004, p. 206/481-494.
- [204] D. Konkolewicz, B. S. Hawkett, A. Gray-Weale, S. Perrier, *Macromolecules* **2008**, *41*, 6400-6412.
- [205] D. Konkolewicz, M. Siau, A. Gray-Weale, B. S. Hawkett, S. b. Perrier, *The Journal of Physical Chemistry B* **2009**, *113*, 7086-7094.
- [206] C. Fortunatti, C. Sarmoria, A. Brandolin, M. Asteasuain, *Comput Chem Eng* **2014**, *66*, 214-220.
- [207] I. Zapata-Gonzalez, E. Saldivar-Guerra, J. Ortiz-Cisneros, *Macromol Theory Simul* **2011**, *20*, 370-388.
- [208] G. Johnston-Hall, C. Barner-Kowollik, M. J. Monteiro, *Macromol Theory Simul* **2008**, *17*, 460-469.
- [209] P. Vana, T. P. Davis, C. Barner-Kowollik, *Macromol Theory Simul* **2002**, *11*, 823-835.
- [210] H. Chaffey-Millar, M. Busch, T. P. Davis, M. H. Stenzel, C. Barner-Kowollik, *Macromol Theory Simul* **2005**, *14*, 143-157.
- [211] H. Chaffey-Millar, M. H. Stenzel, T. P. Davis, M. L. Coote, C. Barner-Kowollik, *Macromolecules* **2006**, *39*, 6406-6419.
- [212] P. B. Zetterlund, G. Gody, S. Perrier, *Macromol Theory Simul* **2014**, *23*, 331-339.
- [213] M. Wulkow, M. Busch, T. P. Davis, C. Barner-Kowollik, *J Polym Sci, Part A: Polym Chem* **2004**, *42*, 1441-1448.
- [214] M. Drache, G. Schmidt-Naake, M. Buback, P. Vana, *Polymer* **2005**, *46*, 8483-8493.

- [215] M. Zhang, W. H. Ray, *Ind Eng Chem Res* **2001**, *40*, 4336-4352.
- [216] A. Butté, A. D. Peklak, *Macromol Theory Simul* **2006**, *15*, 285-302.
- [217] A. R. Wang, S. Zhu, *Macromol Theory Simul* **2003**, *12*, 663-668.
- [218] G. Johnston-Hall, M. J. Monteiro, "Tailoring molecular weight distribution and structure with difunctional reversible addition fragmentation chain transfer agent. A model study", in *ACS Symp Ser*, Oxford University Press, 2006, p. 944/421-437.
- [219] Y.-K. Goh, M. J. Monteiro, *Macromolecules* **2006**, *39*, 4966-4974.
- [220] M. Adamy, A. M. van Herk, M. Destarac, M. J. Monteiro, *Macromolecules* **2003**, *36*, 2293-2301.
- [221] J. C. Hernández-Ortiz, G. Jaramillo-Soto, J. Palacios-Alquisira, E. Vivaldo-Lima, *Macromol React Eng* **2010**, *4*, 210-221.
- [222] P. B. Zetterlund, S. Perrier, *Macromolecules* **2011**, *44*, 1340-1346.
- [223] B. Bitsch, C. Barner-Kowollik, S. Zhu, *Macromol React Eng* **2011**, *5*, 55-68.
- [224] A. R. Wang, S. Zhu, *Macromol Theory Simul* **2003**, *12*, 196-208.
- [225] A. D. Peklak, A. Butté, *Macromol Theory Simul* **2006**, *15*, 546-562.
- [226] A. D. Peklak, A. Butté, G. Storti, M. Morbidelli, *J Polym Sci, Part A: Polym Chem* **2006**, *44*, 1071-1085.
- [227] E. I. Izgorodina, M. L. Coote, *Macromol Theory Simul* **2006**, *15*, 394-403.
- [228] C. Y. Lin, M. L. Coote, *Aust J Chem* **2009**, *62*, 1479-1483.
- [229] M. J. Monteiro, *J Polym Sci, Part A: Polym Chem* **2005**, *43*, 5643-5651.
- [230] A. Feldermann, A. A. Toy, H. Phan, M. H. Stenzel, T. P. Davis, C. Barner-Kowollik, *Polymer* **2004**, *45*, 3997-4007.
- [231] Y. Ye, F. J. Schork, *Ind Eng Chem Res* **2009**, *48*, 10827-10839.
- [232] A. Zargar, F. J. Schork, *Macromol React Eng* **2009**, *3*, 118-130.
- [233] A. Zargar, F. J. Schork, *Ind Eng Chem Res* **2009**, *48*, 4245-4253.
- [234] Y.-n. Zhou, C.-m. Guan, Z.-h. Luo, *Eur Polym J* **2010**, *46*, 2164-2173.
- [235] D. Boschmann, P. Vana, *Macromolecules* **2007**, *40*, 2683-2693.
- [236] M. G. Fröhlich, P. Vana, G. Zifferer, *Macromol Theory Simul* **2007**, *16*, 610-618.
- [237] M. G. Fröhlich, M. M. Nardai, N. Förster, P. Vana, G. Zifferer, *Polymer* **2010**, *51*, 5122-5134.
- [238] K. Kubo, A. Goto, K. Sato, Y. Kwak, T. Fukuda, *Polymer* **2005**, *46*, 9762-9768.
- [239] R. Wang, Y. Luo, B. Li, X. Sun, S. Zhu, *Macromol Theory Simul* **2006**, *15*, 356-368.

- [240] J. Gao, Y. Luo, R. Wang, X. Zhang, B.-G. Li, S. Zhu, *Polymer* **2009**, *50*, 802-809.
- [241] R. Wang, Y. Luo, B.-G. Li, S. Zhu, *Macromolecules* **2008**, *42*, 85-94.
- [242] J. C. Hernández-Ortiz, E. Vivaldo-Lima, M. A. Dubé, A. Penlidis, *Macromol Theory Simul* **2014**, *23*, 147-169.
- [243] P. Vana, T. P. Davis, C. Barner-Kowollik, *Macromol Rapid Commun* **2002**, *23*, 952-956.
- [244] A. Feldermann, M. H. Stenzel, T. P. Davis, P. Vana, C. Barner-Kowollik, *Macromolecules* **2004**, *37*, 2404-2410.
- [245] G. Johnston-Hall, A. Theis, M. J. Monteiro, T. P. Davis, M. H. Stenzel, C. Barner-Kowollik, *Macromol Chem Phys* **2005**, *206*, 2047-2053.
- [246] A. Theis, A. Feldermann, N. Charton, M. H. Stenzel, T. P. Davis, C. Barner-Kowollik, *Macromolecules* **2005**, *38*, 2595-2605.
- [247] A. Theis, A. Feldermann, N. Charton, T. P. Davis, M. H. Stenzel, C. Barner-Kowollik, *Polymer* **2005**, *46*, 6797-6809.
- [248] A. Theis, T. P. Davis, M. H. Stenzel, C. Barner-Kowollik, *Polymer* **2006**, *47*, 999-1010.
- [249] G. Johnston-Hall, M. J. Monteiro, *Macromolecules* **2007**, *40*, 7171-7179.
- [250] G. Johnston-Hall, M. H. Stenzel, T. P. Davis, C. Barner-Kowollik, M. J. Monteiro, *Macromolecules* **2007**, *40*, 2730-2736.
- [251] G. Johnston-Hall, M. J. Monteiro, *J Polym Sci, Part A: Polym Chem* **2008**, *46*, 3155-3173.
- [252] T. Junkers, A. Theis, M. Buback, T. P. Davis, M. H. Stenzel, P. Vana, C. Barner-Kowollik, *Macromolecules* **2005**, *38*, 9497-9508.
- [253] C. Barner-Kowollik, J. F. Quinn, D. R. Morsley, T. P. Davis, *J Polym Sci, Part A: Polym Chem* **2001**, *39*, 1353-1365.
- [254] C. Barner-Kowollik, J. F. Quinn, T. U. Nguyen, J. P. Heuts, T. P. Davis, *Macromolecules* **2001**, *34*, 7849-7857.
- [255] M. L. Coote, *The Journal of Physical Chemistry A* **2005**, *109*, 1230-1239.
- [256] M. L. Coote, E. I. Izgorodina, E. H. Krenske, M. Busch, C. Barner-Kowollik, *Macromol Rapid Commun* **2006**, *27*, 1015-1022.
- [257] M. J. Monteiro, H. de Brouwer, *Macromolecules* **2001**, *34*, 349-352.
- [258] M. Monteiro, N. Subramaniam, J. Taylor, B. Pham, M. Tonge, R. Gilbert, *Polymer* **2001**, *42*, 2403-2411.
- [259] Y. Kwak, A. Goto, Y. Tsujii, Y. Murata, K. Komatsu, T. Fukuda, *Macromolecules* **2002**, *35*, 3026-3029.

- [260] A. R. Wang, S. Zhu, *J Polym Sci, Part A: Polym Chem* **2003**, *41*, 1553-1566.
- [261] C. Barner-Kowollik, M. L. Coote, T. P. Davis, L. Radom, P. Vana, *J Polym Sci, Part A: Polym Chem* **2003**, *41*, 2828-2832.
- [262] A. R. Wang, S. Zhu, Y. Kwak, A. Goto, T. Fukuda, M. S. Monteiro, *J Polym Sci, Part A: Polym Chem* **2003**, *41*, 2833-2839.
- [263] J. Pallares, G. Jaramillo-Soto, C. Flores-Cataño, E. Vivaldo Lima, L. M. Lona, A. Penlidis, *Journal of Macromolecular science part A: pure and applied chemistry* **2006**, *43*, 1293-1322.
- [264] W. Meiser, M. Buback, *Macromol Rapid Commun* **2011**, *32*, 1490-1494.
- [265] T. Junkers, C. Barner-Kowollik, M. L. Coote, *Macromol Rapid Commun* **2011**, *32*, 1891-1898.
- [266] W. Meiser, M. Buback, *Macromol Rapid Commun* **2012**, *33*, 1273-1279.
- [267] Y. Luo, R. Wang, L. Yang, B. Yu, B. Li, S. Zhu, *Macromolecules* **2006**, *39*, 1328-1337.
- [268] H. Tobita, F. Yanase, *Macromol Theory Simul* **2007**, *16*, 476-488.
- [269] H. Tobita, *Macromol Theory Simul* **2009**, *18*, 108-119.
- [270] H. Tobita, *Macromol Theory Simul* **2009**, *18*, 120-126.
- [271] H. Tobita, "Fundamentals of RAFT Miniemulsion Polymerization Kinetics", in *Macromol Symp*, Wiley Online Library, 2010, p. 288/16-24.
- [272] H. Tobita, *Macromol Theory Simul* **2011**, *20*, 709-720.
- [273] K. Suzuki, Y. Nishimura, Y. Kanematsu, Y. Masuda, S. Satoh, H. Tobita, *Macromol React Eng* **2012**, *6*, 17-23.
- [274] D. Konkolewicz, B. S. Hawkett, A. Gray-Weale, S. Perrier, *J Polym Sci, Part A: Polym Chem* **2009**, *47*, 3455-3466.
- [275] S. S. Ting, T. P. Davis, P. B. Zetterlund, *Macromolecules* **2011**, *44*, 4187-4193.

3 AN EXPLICIT EXPRESSION OF MOLECULAR WEIGHT DISTRIBUTION FOR ATRP SYSTEMS

This chapter is based on the manuscript entitled “Modeling molecular weight distribution and effect of termination in controlled radical polymerization: A novel and transformative approach”, which was published in the *Journal of Polymer Science, Part A: Polymer Chemistry*, **2014**, 52 (5), p.639-651 (doi:10.1002/pola.27046). This reproduction is done with permission from John Wiley and Sons. This chapter presents an explicit expression for molecular weight distribution for low conversion or continuous ATRP systems.

Author contributions

The idea and initial derivation were originated from Dr. Shiping Zhu, with the derivation completed by Erlita Mastan. Erlita performed the calculations and

prepared the first draft of the work. Dr. Dapeng Zhou provided the first revision, followed by the final revision from Dr. Shiping Zhu.

§ 3.1 Abstract

A theory for polymer molecular weight distribution (MWD) in atom transfer radical polymerization (ATRP) has been derived by using analogy to a series of continuous stirred tank reactors (CSTRs). This approach relates one activation cycle in ATRP to one reactor in CSTRs. The derived MWD expression includes effect of radical termination and allows detailed investigation on the factors that determine the polymer distribution, namely the level of “control” and “livingness”. The level of control means the average number of activation cycles experienced by individual chains. The degree of livingness is quantified by the fraction of terminated chains. It was found that the effect of livingness and control on MWD is complex. Large number of activation cycles does not guarantee a narrow distribution. There exists an optimum value of activation cycles to achieve the lowest polydispersity by balancing the control (achieved by increasing activation cycles) with the loss of livingness (also caused by increasing activation cycles). The distribution for ATRP is in-between Poisson and Flory distributions, determined by the level of control and livingness. In general, having high degree of livingness and maintaining control are both necessary conditions to obtain narrow molecular weight distribution.

§ 3.2 Introduction

Polymers are chain molecules and their chain length distribution, CLD (or equivalently, molecular weight distribution, MWD) plays a critical role in determining polymer performance in applications. In practice, we often use the number-average chain length, r_N (or the number-average molecular weight, M_N) and polydispersity index, PDI , in characterizing polymer's CLDs. The polydispersity index, PDI , is the ratio of weight-average chain length over number-average chain length, r_W/r_N (or M_W/M_N , where M_W is the weight-average molecular weight), which is closely related to standard deviation in the distribution and serves as an indication of how broadly distributed these chains are. These two average parameters alone, r_N and PDI , do not give enough information to obtain the full molecular weight distribution (MWD) of the polymer chains. Polymers having equal average chain length and polydispersity do not necessarily have the same distribution. A small difference in MWD could lead to very different materials application properties and/or processabilities. The knowledge of full MWD is highly desirable, whenever possible.

Living anionic polymerization (LAP) is a well-known type of polymerization that could synthesize very narrowly distributed polymer chains, which was first demonstrated by Szwarc in 1956.^[1] Due to the same charge on the chain-ends, the chains do not terminate with each other owing to electrostatic repulsion, thus creating a “living” polymerization. This polymerization requires very stringent conditions to avoid any possible chain transfer or other side reactions to preserve the

livingness. Moreover, this polymerization involves association of active chain-ends with counter-ions. Due to electrostatic attraction, this association occurs continuously and frequently, giving chains approximately equal probability to propagate. Coupling this with fast initiation in LAP, where all chains are initiated in the beginning of polymerization, makes LAP a “controlled” polymerization, in which polymer chain length development is well controlled in a predictable manner. “Living” and “control” are both necessary conditions for generating narrow MWDs. The full MWD of polymers synthesized by LAP follows Poisson distribution, shown by Equation (1), where $n(r)$ is the number fraction of chains having r monomer units.^[2,3] Additionally, the PDI could be calculated through Equation (2).^[2,3] The resulting polymer chains are not monodispersed, due to some inherent statistical broadening.

$$n_{Poisson}(r) = \frac{r_N^r}{r!} e^{-r_N} \quad (1)$$

$$PDI_{Poisson} = 1 + \frac{1}{r_N} \quad (2)$$

An alternative expression for CLD (note: CLD and MWD are used interchangeably in this work) is $w(r)$, which is the weight fraction of chains having r units. The relationship between $n(r)$ and $w(r)$ is unique, giving one allows us to calculate the other: $w(r) = r \times n(r) / \int_0^\infty (r \times n(r)) dr$ and $n(r) = (w(r)/r) / \int_0^\infty (w(r)/r) dr$.

On the other hand, free radical polymerization (FRP) is more flexible in the experiment conditions, but it involves a high level of termination. Moreover, the

initiation occurs throughout the polymerization, with each initiated chain rapidly grow and terminate almost instantaneously, resulting in each chain to grow under different conditions with 100% termination. In other words, FRP is not a living nor is it a controlled polymerization, hence creating polymers with broad distribution. The instantaneous full MWD has been found to agree with Flory-Schulz distribution, also known as the Flory's most probable distribution or random distribution.^[2,4] This distribution, shown by Equation (3), is much broader than Poisson distribution, as can be seen by comparing the *PDI* expressions shown in Equation (2) and (4).

$$n_{Flory}(r) = \left(1 - \frac{1}{r_N}\right)^{r-1} \frac{1}{r_N} \xrightarrow{r_N \gg 1} \frac{e^{-r/r_N}}{r_N} \quad (3)$$

$$PDI_{Flory} = 2 - \frac{1}{r_N} \xrightarrow{r_N \gg 1} 2 \quad (4)$$

In comparison, controlled radical polymerization (CRP), or reversible-deactivation radical polymerization (RDRP), as IUPAC has recently recommended,^[5] stands between FRP and LAP. Through an equilibrium between dormant and active chains, CRP gives a more equal probability of growth for all chains than in FRP. However, the radical termination cannot be completely eliminated like in the case of LAP, thereby it possesses a reduced level of livingness. Moreover, similar to LAP, all chains in CRP are initiated at the beginning of polymerization. These two conditions provide some control in the CRP. It is clear that CRP is more living and controlled than FRP, but lacks in both when compared to LAP. This leads to conclusion that the full MWD of CRP lies between Poisson and Flory distributions, as shown by Figure 3-1.^[6-9] Despite the

importance of MWD, most theoretical/modeling studies conducted for CRP have mainly focused on the kinetics and average properties, rather than the full MWD.^[10-31]

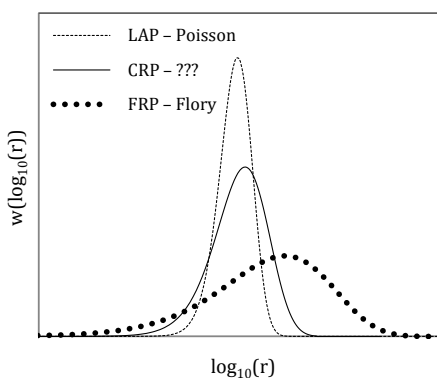


Figure 3-1. Various polymerization mechanisms and the resulting full molecular weight distributions

One of the most widely studied CRPs is atom transfer radical polymerization (ATRP), which operates under persistent radical effect, much like nitroxide mediated polymerization (NMP, also termed as stable free radical polymerization or SFRP).^[19-21] Due to their similar nature, the equations derived for one is usually applicable for the other. The expression to predict *PDI* for ATRP and NMP systems has been developed by different research groups, and is shown by Equation (5), where z is the average number of activation cycles in the polymerization time t .^[21-23,32] This equation was developed under the assumption that the radical concentration remains constant and that the termination is negligible, *i.e.*, treating CRP as a perfectly living polymerization.

$$PDI = 1 + \frac{1}{r_N} + \frac{1}{z} \left(1 - \frac{2}{x} \right) \ln(1-x) \xrightarrow{x \approx 0} 1 + \frac{1}{r_N} + \frac{2}{z} \quad (5)$$

Several simulation studies have been conducted to model the full MWD of polymers synthesized by CRPs.^[6,8,33-38] However, most of these works do not generate an expression for the MWD. In a previously published work, Tobita developed an expression for full MWD for CRP system under constant monomer concentration, by making use of propagation probability, ϕ_p and by assuming no termination.^[6] The resulting full MWD, number-average chain length and index are shown in Equation (6), (7), and (8), respectively. The equation predicts polydispersity the full MWD of a perfectly living CRP system. In other words, it only takes into account the effect of the degree of control, but disregards the broadening of MWD due to reduced livingness that is unavoidable in CRP.

$$n(r) = (1 - \phi_p) \phi_p^r z e^{-z} {}_1F_1[1+r, 2, (1 - \phi_p)z] \quad (6)$$

where: ${}_1F_1$ is the confluent hypergeometric function, given by:

$${}_1F_1[a, b, c] \equiv \sum_{i=1}^{\infty} \frac{(a+i-1)!}{(a-1)!} \frac{(b-1)!}{(b+i-1)!} \frac{c^i}{i!}$$

$$r_N = \frac{z \phi_p}{1 - \phi_p} \quad (7)$$

$$PDI = 1 + \frac{1}{r_N} + \frac{2}{z} \quad (8)$$

The *PDI* derived for this model is equivalent to that derived previously by other research groups for CRP under negligible change in the monomer concentration, which can be seen by obtaining the limit of Equation (5) for very small value of

conversion ($x \rightarrow 0$). Since the model assumes a living system, it can also be shown that the limit of *PDI* in Equation (8) approaches that of Poisson distribution in Equation (2), for an infinitely large z value, *i.e.*, when it becomes a perfectly controlled polymerization.

The control and livingness of polymerization have been previously studied through modeling approach for NMP system.^[38,39] Fischer introduced a phase diagram for NMP system based on the equilibrium rate constants to predict whether the system is living, controlled, or both,^[39] which has been studied and confirmed further by using PREDICI by Guillaneuf et al. in a recent study.^[38]

In this work, we developed an expression for the full MWD of polymers synthesized by CRP, by using ATRP as the model polymerization system. The model was developed by using analogy to a series of continuous stirred-tank reactors (CSTRs), which is a well-studied system in the chemical reactor engineering field. This allows us to use the known knowledge of CSTR system and apply it to the polymerization, in order to gain better understanding of the effects of radical termination and activation cycles on MWD in ATRP. By utilizing the equations obtained, we differentiate the effect of termination, or reduced livingness, and the effect of degree of control on the broadening of full MWD through simulations.

§ 3.3 Model development

The commonly accepted reaction mechanism for an ATRP system is shown in Table 3-1. Throughout the polymerization reaction, each chain experiences numerous activation cycles, with the dormant state, PX , being heavily favoured than the active/radical state, P^\bullet .

Table 3-1. Reaction mechanisms involved in atom transfer radical polymerization (ATRP)

Reactions in ATRP		Eqn No
Activation	$P_r X + C \xrightarrow{k_a} P_r^\bullet + XC$	(9)
Deactivation	$P_r^\bullet + XC \xrightarrow{k_d} P_r X + C$	(10)
Propagation	$P_r^\bullet + M \xrightarrow{k_p} P_{r+1}^\bullet$	(11)
Termination	$P_r^\bullet + P_s^\bullet \xrightarrow{k_t} P_r + P_s$	(12)

The model is developed by using analogy to a series of CSTRs, with each reactor representing one activation cycle in the ATRP mechanism. In developing the equations for full CLD, ATRP is chosen as the model system, but the resulting equations could be modified to suit other types of CRP.

Figure 3-2 shows the configuration of CSTRs in series used for the model development. The stream entering a reactor corresponds to the dormant chains, which are deactivated after the last cycle of activation. In this analogy, the dormant chains get activated upon entry to the reactor. The active chains, that is, the radicals, undergo propagation inside the reactor, with the possibility of adding 0 to an infinite

number of monomers. The chains then experience either deactivation or termination. The deactivated chains become dormant and can be reactivated to “enter the next reactor”, while the terminated chains are dead and sent to the by-product path, where it can no longer participate in further reactions. In other words, the content of reactor i represents the active chains that are growing via propagation in their i^{th} cycle of activation.

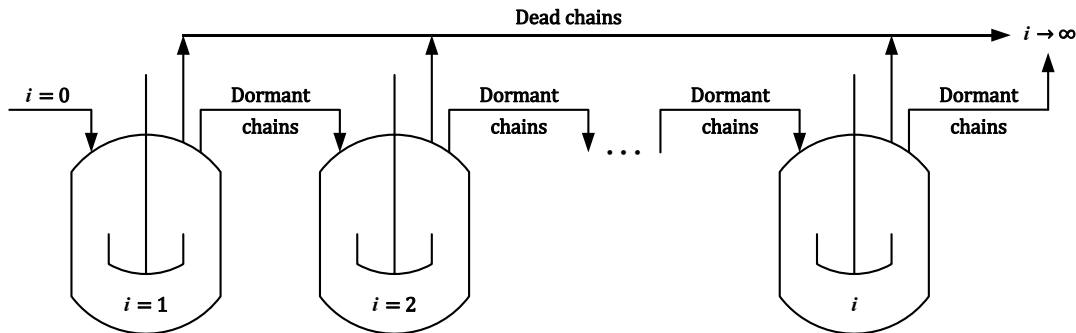


Figure 3-2. Understanding the mechanism behind ATRP system by using an analogy to a series of CSTRs

Figure 3-3 summarizes the parameters along with the parallel physical meanings in the CSTR system used in this analogy. The variable i represents the number of activation cycles that the chains have experienced, which is analogous to the reactor number in the CSTR system. Polymer chains that have gone through different activation cycles would have different CLDs, represented by $n_i(r)$ for chains that have undergone i activation cycles, which relates to the mole fraction of component r in the i^{th} reactor for the CSTR system. The fraction of chains that are terminated (dead) instead of deactivated (dormant) per activation cycle, f_t , is parallel to the fraction of

species leaving the i^{th} CSTR as by-product in this analogy. The by-product stream leaves a reactor and does not participate in subsequent reactions, much like the dead chains in ATRP system. The full MWD at any time of interest is the combination of both dormant and dead chains coming out of these reactors, which could vary from $i = 0$ to infinity, with $i = 0$ representing initiator molecules that have never been activated even once. It should be pointed out that there are also chains that have been activated but never propagate ($i \neq 0, r = 0$). This bivariable probability approach was first used in the work of Goto and Fukuda for a perfectly living NMP system.^[22]

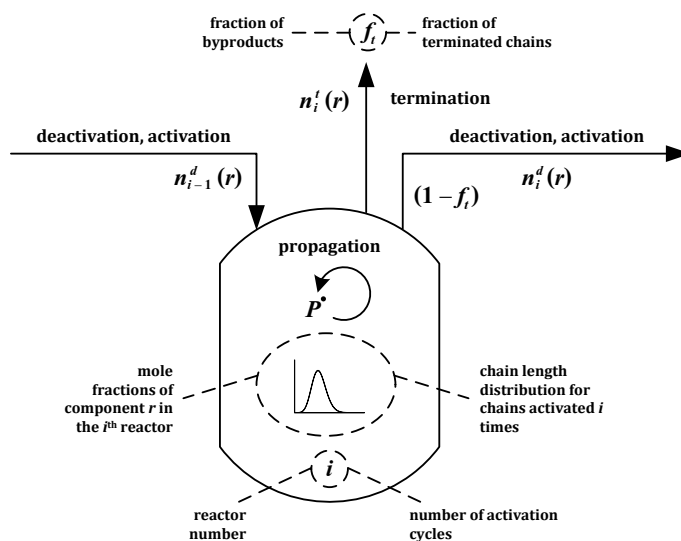


Figure 3-3. The analogy of the i^{th} reactor in a series of CSTRs to the i^{th} activation cycles in ATRP reaction system

The major assumptions involved in the development of the full MWD demonstrated in this work are that the reactant concentrations remain constant, the radical reaches its steady-state concentration in a short time, the reaction rate constants do not vary

throughout the polymerization and are chain-length independent, and other possible side reactions not listed in Table 3-1 have negligible effect on the CLD. Based on the constant reactants assumptions, the model developed in this work is valid for very dilute system with abundance of monomer and low concentration of initiator. The reaction conditions in which the radical reaches its steady-state concentration quickly have been thoroughly examined by another study.^[19]

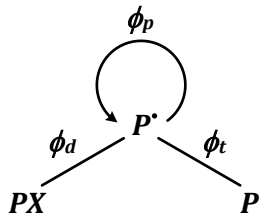


Figure 3-4. The possible paths available for a radical chain along with the probabilities

Figure 3-4 shows the possible paths available for an active chain in each cycle of activation. The parameters are defined by Equation (13), (14), and (15). Each of these parameters represents the probability of a radical to propagate, ϕ_p , deactivate, ϕ_d , or terminate, ϕ_t . The fraction of dead chains in

one activation cycle, f_t , as explained previously, can be expressed in terms of the probability of a radical to be terminated, as shown in Equation (16). The fraction of dormant chains in one activation cycle, f_d , as a result could be expressed by Equation (17). The average number of activation cycles, z , is used as the independent variable in lieu of reaction time, t . The two variables are related by Equation (18).

$$\phi_p \equiv \frac{k_p[M]}{k_p[M] + k_d[XC] + k_t[P^\bullet]} \quad (13)$$

$$\phi_d \equiv \frac{k_d[XC]}{k_p[M] + k_d[XC] + k_t[P^\bullet]} \quad (14)$$

$$\phi_t \equiv 1 - \phi_p - \phi_d \quad (15)$$

$$f_t \equiv \frac{\phi_t}{\phi_t + \phi_d} \quad (16)$$

$$f_d \equiv \frac{\phi_d}{\phi_t + \phi_d} = 1 - f_t \quad (17)$$

$$\frac{dz}{dt} = \frac{N_{Av}k_a[C][PX]}{N_{Av}[PX]} = k_a[C] \rightarrow z = k_a[C]t \quad (18)$$

In the model development, first a perfectly living system in the absence of termination is considered. With this assumption, the CSTRs configuration shown in Figure 3-2 could be used as analogy without the by-product stream (*i.e.*, the parameters involving termination, ϕ_t and f_t are equal to 0), hence simplifying the problem. This is followed by extension of the same concept to include the effect of termination on the CLD by use of by-product streams in the analogy. For brevity purpose, detailed derivation could be found in the Appendix section. The final equations obtained through this approach are summarized and tabulated in Table 3-2.

It is worth noting that as the parameters related to termination, ϕ_t and f_t , approach zero, the limits of Equations (22), (23) and (24) approach their counterparts, Equations (19), (20), and (21), which are derived under the same assumptions but for an ATRP system without termination (*i.e.*, a “perfectly living” CRP, $\phi_t \rightarrow 0$).

For system without termination, it can be seen that the resulting equations, shown by Equations (19), (20), and (21) in Table 3-2, are identical to the expressions obtained by Tobita.^[6] This serves as a proof of the validity for the analogy to a series of CSTRs

used in this work, because the model developed by Tobita was derived through a different approach, but under similar assumption as in this work, *i.e.*, constant reactant concentrations and for a perfectly living CRP.

**Table 3-2. Summary of the MWD equations for ATRP system,
derived from analogy to a series of CSTRs**

Without termination	
Full MWD	
	$n(r) = (\phi_p)^r e^{-z} \sum_{i=0}^{\infty} \binom{r+i-1}{r} \frac{(z\phi_d)^i}{i!} \quad (19)$
Number-average chain length	
	$r_N = \frac{z\phi_p}{1-\phi_p} \quad (20)$
Polydispersity index	
	$PDI = 1 + \frac{1}{r_N} + \frac{2}{z} \quad (21)$
With termination	
Full MWD	
	$n(r) = e^{-z} (\phi_p)^r \left(\sum_{i=0}^{\infty} \binom{r+i-1}{r} \frac{(z\phi_d)^i}{i!} + \frac{\phi_t}{\phi_d} \sum_{i=1}^{\infty} \frac{z^i}{i!} \sum_{j=1}^i \binom{r+j-1}{r} (\phi_d)^j \right) \quad (22)$
Number-average chain length	
	$r_N = \frac{\phi_p}{\phi_t} (1 - e^{-zf_t}) \quad (23)$
Polydispersity index	
	$PDI = 1 + \frac{1}{r_N} + \frac{\sinh(zf_t) - zf_t f_d}{\cosh(zf_t) - 1} \quad (24)$
Dead chain fraction	
	$DCF = 1 - e^{-zf_t} \quad (25)$

Moreover, the model without termination involves 2 independent variables, which are the average number of activation cycles, z , and the propagation probability, ϕ_p . Meanwhile, the model with termination involves the same independent variables, with the addition of another independent variable, which is the fraction of dead chains per activation cycle, f_t . The resulting parameters of interest in this study are the ones listed in Table 3-2, *i.e.*, the full CLD, number-average chain length, polydispersity index, and overall fraction of dead chains in the system (*DCF*). The reaction time is not listed as an independent variable in this study because z is linearly proportional to time, as shown in Equation (18).

§ 3.4 Simulation results and discussions

The broadness of MWD in CRP is known to depend on two things, the degree of control in polymerization (or the uniformity of chain growth) and the degree of livingness (or the fraction of dead chains). The degree of control mainly depends on the frequency of activation cycles, which is related to z . For the same r_N , a higher z value simply indicates a better controlled system. In other words, fewer monomeric units are added per cycle for better control. The degree of livingness depends on the product of z and f_t , as shown by Equation (25), for the fraction of dead chains present in the system.

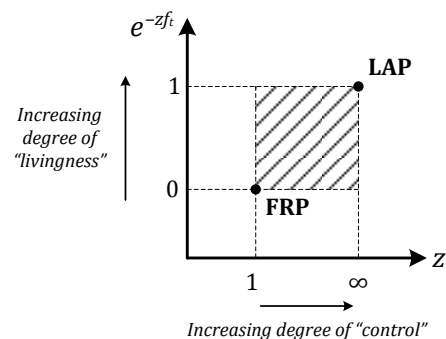


Figure 3-5. Conceptual graph of variables affecting the degree of control and livingness in ATRP

Figure 3-5 shows the degrees of livingness and control with the extreme cases shown by LAP and FRP along with variables affecting these factors, dormant chain fraction ($= \exp(-zft) = 1 - DCF$) and average number of activation cycles, z . Based on the reaction condition, an ATRP system can lie anywhere inside the shaded area depending on its degree of livingness and that of control exhibited. How these variables affect the MWD are investigated in this work through simulation.

3.4.1 Evolution of MWD in ATRP

Figure 3-6 shows the change of full MWDs with and without termination, as the polymerization proceeds in terms of activation cycles instead of reaction time (the two are linearly related, as shown by Equation (18)). The corresponding simulation parameters along with the resulting average chain length, polydispersity, and dead chain fraction are tabulated in Table 3-3. It can be clearly seen from the table that as the polymer chains undergo more activation cycles, the polydispersity index decreases if termination is not considered. However, if the termination is taken into account, the polydispersity index increases due to the increase in the dead chain fraction, DCF .

Table 3-3. Simulation results for the evolution of MWD after different activation cycles, corresponding to Figure 3-6

$\phi_p = 0.3$	Without termination ($f_t = 0$)			With termination ($f_t = 0.001$)		
	200 cycles	600 cycles	1000 cycles	200 cycles	600 cycles	1000 cycles
r_N	85.7	257.1	428.6	77.7	193.4	270.9
PDI	1.02	1.01	1.00	1.09	1.21	1.33
DCF	-	-	-	18%	45%	63%

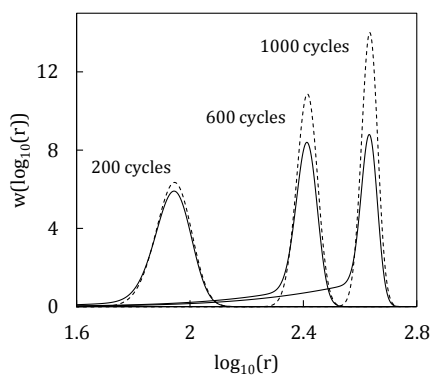


Figure 3-6. The evolution of chain length distribution with $\phi_p = 0.3$.

Dashed lines: without termination, $f_t = 0$. Solid lines: with termination, $f_t = 0.001$

Dead chains are formed throughout the polymerization. Therefore, as the polymerization proceeds, the presence of dead chains can be observed in the evolution of full MWD, shown in Figure 3-6. A clear tail on the left hand side is present in each distribution, represented by solid line (with termination), while it cannot be seen in the dashed line (without termination). The tail observed on the simulation is an indication of the presence of dead chains that stop growing due to termination. The broadening of the distribution in this case could be attributed to the loss of livingness in the polymerization.

3.4.2 Effect of activation cycles (z) on MWD

The effect of activation cycles on the full MWD is studied by varying the average number of activation cycles, z , required to achieve the same number-average chain length. This could be achieved, for example, by changing the monomer concentration. The simulation results for model with and without termination are shown in Figure 3-7 for number-average chain length of 100. For the model with termination, the fraction of dead chains formed per activation cycle, f_t , is kept constant for all cases at 0.002. Poisson distribution as exhibited by LAP and Flory's most probable distribution as exhibited by FRP with termination via disproportionation are also plotted in the same figure for comparison purposes.

By looking at Figure 3-7 (a) for cases without termination, an increase in z leads to a narrower distribution. This is as expected because an increase in z leads to an increase in the level of control. Another way of looking at it is by looking at the value for the propagation probability, ϕ_p , as listed in Table 3-4, which decreases as z increases, to achieve the same r_N , which implies fewer monomeric units are added in one activation cycle. It is well known that chains grow more evenly when fewer monomeric units are added per cycle, which yields a narrower distribution due to the increase of control in the system.

Table 3-4. Simulation results for the effect of number of activation cycles (z) for cases with and without termination, corresponding to Figure 3-7

$r_N = 100$	Without termination ($f_t = 0$)			With termination ($f_t = 0.002$)		
	$z = 10,000$	$z = 100$	$z = 10$	$z = 10,000$	$z = 100$	$z = 10$
ϕ_p	0.01	0.50	0.91	0.17	0.52	0.91
DCF	0	0	0	100%	18.13%	1.98%
PDI	1.01	1.03	1.21	2.01	1.10	1.22

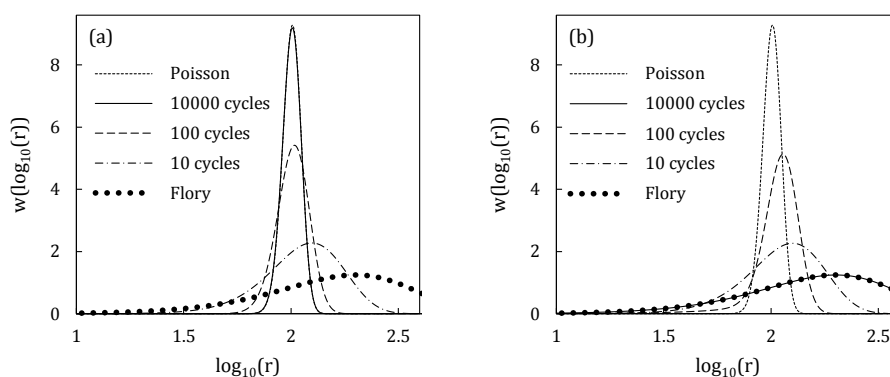


Figure 3-7. Comparison of chain length distribution with various average activation cycles to obtain the same number-average chain length of 100 for the case (a) without and (b) with termination ($f_t = 0.002$)

The relation between distribution and the number of activation cycles is not as straightforward when termination is considered. From Figure 3-7 (b), it can be observed that increasing the number of activation cycles, z , does not necessarily lead to a narrower distribution. This could be explained by looking at Equation (25), where it is clear that increasing z leads to an increase in the amount of dead chains in the system (DCF) for the same fraction of terminated chains per cycle, f_t . Therefore, in all ATRP systems, where termination is unavoidable, increasing the number of activation

cycles does not necessarily yield a narrower distribution. In fact, increasing z could have a detrimental effect in achieving narrow distribution, as could be observed in Figure 3-8, where there exists an optimum value of z to obtain low PDI . The initial decrease in PDI could be attributed to the control in polymerization. However, with more activation cycles, the loss of livingness would broaden the distribution, which results in the increase of PDI . System with higher fraction of dead chains per cycle, f_t , is more sensitive to the value of z and has lower optimum value of z to achieve a narrow distribution. It could also be observed that the PDI approaches 2 (which is the PDI of Flory's distribution) as more and more dead chains are formed.

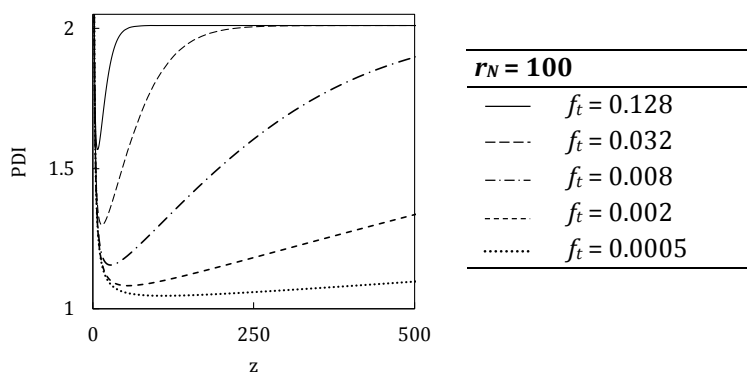
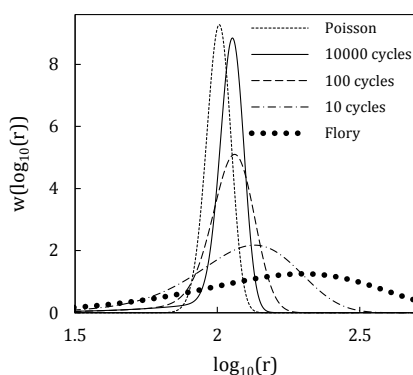


Figure 3-8. The effect of number of activation cycles on polydispersity of system with number-average chain length of 100 and various fractions of terminated chains per activation cycle, f_t

Due to the nature of ATRP, termination is unavoidable (*i.e.*, $f_t \neq 0$), which means there are 2 factors affecting MWD in ATRP, namely the level of control, which depends on the value of z , and the livingness, which depends on the product of z and f_t , as previously shown in Figure 3-5. These two factors are both affected by the activation

cycles (z), but in opposite manner. Increasing the activation cycles would improve the level of control, but at the same time it would reduce the livingness (*i.e.*, produce more dead chains). Therefore, in order to isolate the effect of control in ATRP from the livingness, the model with termination was also simulated by changing both z and f_t to keep the same level of livingness (*i.e.*, constant zf_t), while varying the level of control (*i.e.*, z). The simulation results for these cases are shown in Figure 3-9 for number-average chain length of 100 and constant dead chain fraction of 20%. It becomes clear that, with targeted chain length r_N and degree of livingness DCF , increasing degree of control, z , narrows molecular weight distribution, MWD.



DCF = 20%, $r_N = 100$			
z (cycles)	10,000	100	10
f_t	2.2×10^{-5}	2.2×10^{-3}	2.2×10^{-2}
ϕ_p	0.01	0.53	0.92
PDI	1.08	1.10	1.28

Figure 3-9. Comparison of chain distribution with various average activation cycles to obtain the same number-average chain length of 100 for the case with 20% overall dead chain fraction

The distribution for model without termination overlaps that of a perfectly living and controlled polymerization, *i.e.*, Poisson distribution, for large value of z (or under very good control), as shown in Figure 3-7 (a). On the other hand, with termination (DCF is kept constant), it is impossible to obtain Poisson distribution even if the z is

increased, as shown in Figure 3-9. This is attributed to the presence of dead chains, which is absent in LAP. The distribution of LAP only involves statistical broadening, while in ATRP, the presence of dead chains further broadens the distribution and make it deviate from Poisson distribution due to the loss of livingness.

On the other extreme, with very low value of z (or under very poor control), the simulation results for both cases, with and without termination, do not approach that of Flory's most probable distribution. This is because FRP, illustrated by Flory's distribution, is not only an uncontrolled polymerization, but also non-living, which involves all chains to be terminated. It should be kept in mind that instantaneous MWD for FRP involves all the initiated chains to be terminated during the short period of time. In other words, the terminated chains are 100% of the initiated chains and there is no livingness at all.

However, the distribution for case with high value of z (10,000 cycles) and 100% dead chains, shown in Figure 3-7 (b), approaches Flory's distribution, as can also be seen from the *PDI*. This is an interesting result, because FRP is not a controlled polymerization, while the simulation was done at high value of z ("very good control"). Based on intuition, when all chains destined to be terminated, the activation/deactivation cycles simply slow down the termination process but make no effect on the final distribution. This shows that the effect of control and livingness on the full MWD is not straightforward and is not independent from each other.

Livingness (small DCF) and control (large z) are both necessary conditions for a well-behaved ATRP system.

Moreover, the MWD of polymer chains in ATRP system could be even broader than that of FRP if the number of activation cycles is very low. This is evident from looking at Figure 3-8, where the polydispersity index of ATRP system is larger than 2 (Flory's PDI) for very low value of z . The reason for the broader distribution observed in CRP is because the polydispersity calculated for CRP system accounts for chains that have never been activated, while that for FRP only includes chains that have been initiated (activated once).

3.4.3 Effect of dead chain fraction on MWD

In this section, the effect of amount of dead chain on the full MWD for ATRP system is investigated through simulation. This is done to study the effect of livingness on the full MWD. In order to obtain different dead chain fractions while keeping z and number-average chain length constant, both ϕ_p and f_t must be varied. Figure 3-10 shows the comparison of full MWD for various dead chain fractions with equal number-average chain length and activation cycles. Other simulation parameters and properties are shown in Table 3-5.

Table 3-5. Simulation results for cases shown in Figure 3-10 with various dead chain fractions to investigate the effect of livingness

$z = 100$ cycles $r_N = 100$	$DCF = 0\%$	$DCF = 70\%$	$DCF = 99.9\%$
ϕ_p	0.50	0.63	0.87
f_t	0	0.01	0.07
PDI	1.03	1.41	2.00

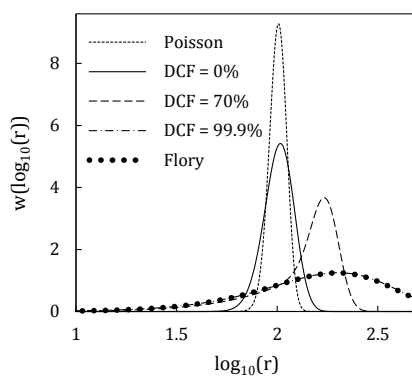


Figure 3-10. Comparison of MWD for cases with number-average chain length of 100 units after 100 activation cycles for various values of dead chain fractions

From Table 3-5 and Figure 3-10, it could be observed that the full MWD becomes broader with increasing dead chain fraction present in the system, as expected due to loss of livingness in the system. The extreme case of the simulation result at 100% terminated chains overlaps with the Flory's most probable distribution. This has been confirmed for different values of z , that the degree of control does not affect the resulting distribution for system with 100% dead chains. It is always the Flory's most probable distribution. Without livingness, control does not make difference to MWD. This is also evident from Figure 3-11, which shows the effect of dead chain fraction

(*DCF*) on the polydispersity index, for various activation cycles (*z*). Regardless of the number of activation cycles, the polydispersity approaches the value of 2 (Flory's *PDI*) when all the chains are terminated (*DCF* = 1).

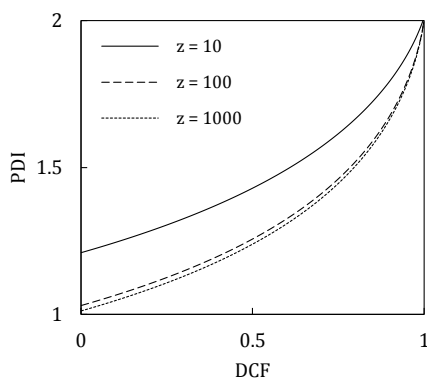


Figure 3-11. The effect of dead chain fraction on polydispersity of system with number-average chain length of 100 and various average activation cycles, *z*

Additionally, with 100 activation cycles, the distribution could not match that of a Poisson distribution, even at the absence of the terminated chains, shown in Figure 3-10. This could be attributed to poor control associated with low activation cycles, causing uneven chain growth, as shown in previous section for various values of *z*. Poisson distribution is the MWD of a perfectly living and controlled polymerization system, *i.e.*, LAP. On the other hand, if simulations are conducted for various values of f_t for systems that have undergone the same number of activation cycles, *z*, with the same propagation probability, ϕ_p , the resulting MWD and other properties vary as shown by Figure 3-12.

As expected, system with higher f_t values will yield polymer chains with lower number-average chain length and higher overall percentage of dead chains. The high dead chain fraction in turn affects the broadness of the distribution, as indicated by the higher PDI . The difference in PDI is enhanced further in cases with high f_t values because the number-average chain length is lower, hence making PDI to be more sensitive to the variation in chain length.

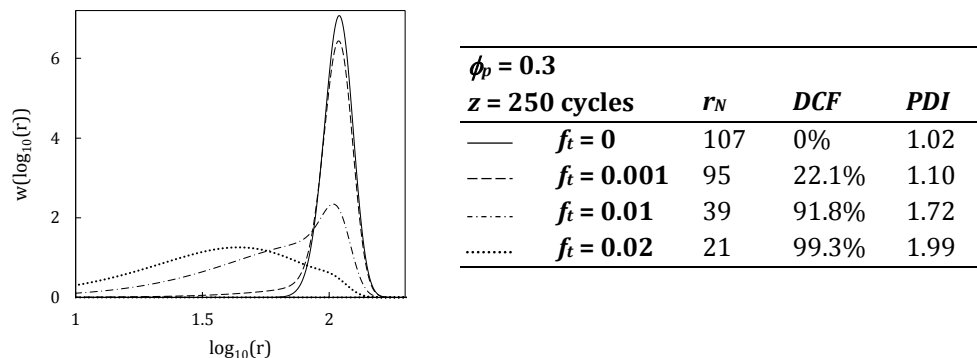


Figure 3-12. Comparison of models with and without termination with average activation cycles (z) of 250 and ϕ_p of 0.3 for various dead chain fractions per cycle, f_t

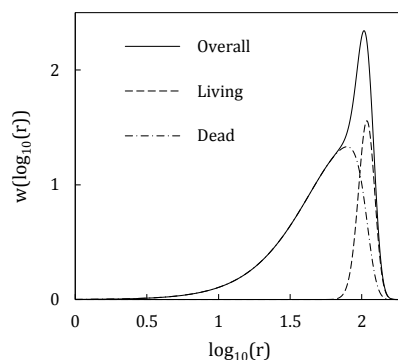


Figure 3-13. Simulation results of dormant, dead chains, and overall distributions for polymerization with average activation cycles (z) of 250, ϕ_p of 0.3, and f_t of 0.01 as shown in Figure 3-12

Equation (22) could also be used to separate the distributions of the dormant and the dead chains, details shown in Appendix. For example, in Figure 3-12 for case with f_t of 0.01, the full MWD shows a broad bimodality. By separating the expression of full MWD for the dormant chains from that of the dead chains, the two distributions could be plotted separately as shown in Figure 3-13, to observe the contribution from each population.

§ 3.5 Conclusions

Atom transfer radical polymerization (ATRP) has been extensively studied in the past 20 years due to its ability to produce polymer chains with narrow molecular weight distribution (MWD). It is speculated that the MWD function is between Poisson distribution of living anionic polymerization (LAP) and Flory's most probable distribution of free radical polymerization (FRP). However, there is no function reported on the full MWD that accounts for unavoidable termination reactions. This work presents such a desirable theory. The development was accomplished by analogously relating the activation cycle in ATRP to a series of continuous stirred tank reactor system (CSTRs). This analogy represents a novel and transformative approach. It allows concepts from the CSTR system, which is well studied in chemical reaction engineering field, to be applied to ATRP system in polymer chemistry. The concepts make it possible for the derivation of full MWD of chains synthesized by ATRP, while taking into account the effect of termination on the distribution. This was

achieved by using the concept of by-product streams to simulate the formation of dead chains, both of which are not participating in further reactions.

The full MWD expression thus obtained could be deconvoluted to separate the contribution of the dormant (or living) chains from the dead chains. It also allows investigation of the effect of various parameters on the broadening of the MWD. It was discovered that the full MWD does not depend only on how controlled the system is, but also on the livingness of the system. These two factors depend on the number of activation cycles and the fraction of dead chains in the system, respectively. The degree of livingness (amount of dead chains) and the degree of control are both necessary conditions, for yielding a narrow MWD in ATRP system.

With a fixed percentage of terminated chains per activation cycle, a large number of activation cycles in a system does not necessarily guarantee a narrow distribution. This is because the amount of dead chain fractions would increase as more activation cycles is involved. There exists an optimum value of activation cycles to achieve the lowest *PDI* by balancing the gain of control (achieved by increasing activation cycles), with the loss of livingness in the system (also caused by increasing activation cycles). Moreover, an ATRP system with low average activation cycle could have a broader distribution than of FRP, because all chains in FRP are initiated (activated) once, while in CRP, there is a distribution of activation cycles among the chains.

The distribution for ATRP found in this study is found to be in-between the narrow Poisson distribution and the broad Flory's most probable distribution. The Poisson distribution is the limit for ATRP distribution if a completely controlled and perfectly living system can be maintained. On the other extreme, Flory's most probable distribution is the limit for ATRP with 100% dead chains, regardless of the activation cycles, showing the suppression of control effect on the distribution with poor livingness. While this MWD theory is derived for ATRP, it is generally applicable to other controlled radical polymerization processes such as NMP and RAFT, etc.

§ 3.6 References

- [1] M. Szwarc, *Nature* **1956**, *178*, 1168-1169.
- [2] P. J. Flory, "*Principles of polymer chemistry*", Cornell Univ. Press, Ithaca, NY, 1953.
- [3] P. J. Flory, *J Am Chem Soc* **1940**, *62*, 1561-1565.
- [4] H. Tobita, *Macromolecules* **1995**, *28*, 5119-5127.
- [5] A. D. Jenkins, R. G. Jones, G. Moad, *Pure Appl Chem* **2010**, *82*.
- [6] H. Tobita, *Macromol Theory Simul* **2006**, *15*, 12-22.
- [7] G. Odian, "*Principles of polymerization*", 4th edition, John Wiley and Sons, Hoboken, NJ, 2004.
- [8] A. H. Müller, D. Yan, G. Litvinenko, R. Zhuang, H. Dong, *Macromolecules* **1995**, *28*, 7335-7338.
- [9] J. Qiu, B. Charleux, K. Matyjaszewski, *Prog Polym Sci* **2001**, *26*, 2083-2134.
- [10] A. R. Wang, S. Zhu, *J Polym Sci, Part A: Polym Chem* **2003**, *41*, 1553-1566.
- [11] S. Zhu, *J Polym Sci, Part B: Polym Phys* **1999**, *37*, 2692-2704.
- [12] S. Zhu, *Macromol Theory Simul* **1999**, *8*, 29-37.
- [13] X. Gao, S. Zhu, *J Appl Polym Sci* **2011**, *122*, 497-508.

- [14] A. H. Müller, R. Zhuang, D. Yan, G. Litvinenko, *Macromolecules* **1995**, *28*, 4326-4333.
- [15] K. Ohno, A. Goto, T. Fukuda, J. Xia, K. Matyjaszewski, *Macromolecules* **1998**, *31*, 2699-2701.
- [16] D. Yan, H. Jiang, X. Fan, *Macromol Theory Simul* **1996**, *5*, 333-345.
- [17] W. Tang, K. Matyjaszewski, *Macromol Theory Simul* **2008**, *17*, 359-375.
- [18] W. Tang, T. Fukuda, K. Matyjaszewski, *Macromolecules* **2006**, *39*, 4332-4337.
- [19] H. Fischer, *J Polym Sci, Part A: Polym Chem* **1999**, *37*, 1885-1901.
- [20] H. Fischer, *Macromolecules* **1997**, *30*, 5666-5672.
- [21] K. Matyjaszewski, *J Macromol Sci, Part A: Pure Appl Chem* **1997**, *10*, 1785-1801.
- [22] A. Goto, T. Fukuda, *Macromolecules* **1997**, *30*, 4272-4277.
- [23] T. Fukuda, A. Goto, *Macromol Rapid Commun* **1997**, *18*, 683-688.
- [24] D. R. D'hooge, D. Konkolewicz, M.-F. Reyniers, G. B. Marin, K. Matyjaszewski, *Macromol Theory Simul* **2012**, *21*, 52-69.
- [25] M. Zhong, K. Matyjaszewski, *Macromolecules* **2011**, *44*, 2668-2677.
- [26] G. Johnston-Hall, M. J. Monteiro, *Macromol Theory Simul* **2010**, *19*, 387-393.
- [27] G. Johnston-Hall, C. Barner-Kowollik, M. J. Monteiro, *Macromol Theory Simul* **2008**, *17*, 460-469.
- [28] T. Fukuda, A. Goto, K. Ohno, *Macromol Rapid Commun* **2000**, *21*, 151-165.
- [29] T. Fukuda, T. Terauchi, A. Goto, K. Ohno, Y. Tsujii, T. Miyamoto, S. Kobatake, B. Yamada, *Macromolecules* **1996**, *29*, 6393-6398.
- [30] M. J. Monteiro, *J Polym Sci, Part A: Polym Chem* **2005**, *43*, 5643-5651.
- [31] M. Zhang, W. H. Ray, *Ind Eng Chem Res* **2001**, *40*, 4336-4352.
- [32] M. Souaille, H. Fischer, *Macromolecules* **2002**, *35*, 248-261.
- [33] I. Zapata-Gonzalez, E. Saldivar-Guerra, J. Ortiz-Cisneros, *Macromol Theory Simul* **2011**, *20*, 370-388.
- [34] H. Tobita, *Macromol Theory Simul* **2006**, *15*, 23-31.
- [35] H. Chaffey-Millar, M. Busch, T. P. Davis, M. H. Stenzel, C. Barner-Kowollik, *Macromol Theory Simul* **2005**, *14*, 143-157.
- [36] P. Vana, T. P. Davis, C. Barner-Kowollik, *Macromol Theory Simul* **2002**, *11*, 823-835.
- [37] M. Al-Harhi, J. Soares, B.P, L. Simon, C, *Macromol Mater Eng* **2006**, *291*, 993-1003.

- [38] D. Gigmes, D. Bertin, C. Lefay, Y. Guillaneuf, *Macromol Theory Simul* **2009**, *18*, 402-419.
- [39] H. Fischer, "Criteria for livingness and control in nitroxide-mediated and related radical polymerizations", in *Advances in Controlled/Living Radical Polymerization*, American Chemical Society, 2003, p. 10-23.

§ 3.7 Appendix

Model without termination

In the absence of termination ($k_t = 0$, resulting in ϕ_t and f_t to be 0), the polymerization is analogous to a system of CSTRs configured in series without the by-product line. An initiator PX “flowing into a reactor” gets activated for the first time and adds monomer through propagation with a probability $\phi_p = k_p[M]/(k_p[M] + k_d[XC])$. The probability for this chain to grow r units in this cycle of activation (“inside the first reactor”) is $(\phi_p)^r$ (r can be from 0 to infinity). The chain is then deactivated at the exit (*i.e.*, “leaving the reactor”) with the probability of $\phi_d = 1 - \phi_p$. Therefore, the probability of chain that have undergone one activation cycle to have chain length r can be expressed mathematically as Equation (A1) and this is equivalent to the number fraction of chains having r monomeric units, if all chains have been activated once.

$$n_1(r) = \phi_d (\phi_p)^r \quad (\text{A1})$$

Similarly, as this chain gets activated for the second time (“entering the second reactor”), it experiences propagation again. After deactivation (or “at the exit of the reactor”), the number fraction of r -unit chains can be shown to follow Equation (A2),

where r is the total number of units added to the chain in both first and second cycles of activation (from both reactors).

$$n_2(r) = \sum_{s=0}^r n_1(s) \phi_d (\phi_p)^{r-s} = (\phi_d)^2 (\phi_p)^r (r+1) \quad (\text{A2})$$

Following the same method, it could be shown that after i^{th} activation cycle (at the exit of the i^{th} reactor), the probability of the chain having chain length r , *i.e.*, the number fraction of r -unit chains, follows Equation (A3). Equivalently, the weight fraction of r -unit chains that have been activated i times can be calculated based on Equation (A4).

$$n_i(r) = \sum_{s=0}^r n_{i-1}(s) \phi_d (\phi_p)^{r-s} = \binom{r+i-1}{r} (\phi_d)^i (\phi_p)^r \quad (\text{A3})$$

$$w_i(r) = [r \times n_i(r)] / \sum_{r=0}^{\infty} [r \times n_i(r)] = \binom{r+i-1}{i} (\phi_d)^{i+1} (\phi_p)^{r-1} \quad (\text{A4})$$

Based on their respective definitions, the number- and weight-average chain lengths, as well as the polydispersity of the chains that have experienced i cycles of activation (at the exit of i^{th} reactor) can be shown to follow Equation (A5), (A6), and (A7).

$$r_{N,i} \equiv \sum_{r=0}^{\infty} [r \times n_i(r)] = \frac{i \phi_p}{\phi_d} \quad (\text{A5})$$

$$r_{W,i} \equiv \sum_{r=0}^{\infty} [r \times w_i(r)] = \frac{1 + i \phi_p}{\phi_d} \quad (\text{A6})$$

$$PDI_i \equiv \frac{r_{W,i}}{r_{N,i}} = 1 + \frac{1}{i \phi_p} = 1 + \frac{1}{r_{N,i}} + \frac{1}{i} \quad (\text{A7})$$

It should be pointed out that in a polymerization system, not all chains would have experienced the same number of activation cycles. Some chains are activated more times than the others, which in turns create a distribution with respect to the number of activation cycles. This distribution could be obtained by solving the mass balances for chains that have been activated for different times. To elucidate this concept, the mass balance for initiator molecules that have never been activated, $[PX]_0$, can be shown to follow Equation (A8).

$$\frac{d[PX]_0}{dt} = -k_a[C][PX]_0 \quad (A8)$$

In order to simplify this equation and other subsequent mass balances, the independent variable can be changed from reaction time, t , to be the average number of activation cycles, z , that individual chain had undergone during the time. The relation between these two variables is shown by Equation (18) in the Model Development section.

$$\frac{dz}{dt} = \frac{N_{Av}k_a[C][PX]}{N_{Av}[PX]} = k_a[C] \rightarrow z = k_a[C]t \quad (18)$$

Equation (A8) can then be rewritten in terms of z and solved as shown by Equation (A9) to obtain an expression for the concentration of initiator molecules that have never been activated, $[PX]_0$.

$$\frac{d[PX]_0}{dz} = -[PX]_0 \rightarrow [PX]_0 = [PX]_{0,z=0} \exp(-z) \quad (A9)$$

where $[PX]_{0,z=0}$ is the initial initiator concentration. The concentration of the dormant chains that have been activated once, $[PX]_1$, could be obtained by solving the mass balance for these very chains, as shown by Equation (A10).

$$\frac{d[PX]_1}{dz} = [PX]_0 - [PX]_1 \rightarrow [PX]_1 = [PX]_{0,z=0} z \exp(-z) \quad (\text{A10})$$

Following the same approach, a general expression for the chains that have been activated i times could be obtained, as shown by Equation (A11), as a function of the average number of activation cycles, z . Note that this expression applies to all chains that have been activated i times, regardless of their chain lengths (r from 0 to infinity). The probability of chains that have been activated i times, p_i , could then be calculated as the number fraction of these chains out of all the chains in the system, expressed in Equation (A12). As expected, the distribution of number of activation cycles follows Poisson distribution, with average number of activation cycles of z . This is because the difference of activation cycles experienced by each chain is only due to statistical broadening of the activation reaction.

$$\frac{d[PX]_i}{dz} = [PX]_{i-1} - [PX]_i \rightarrow [PX]_i = [PX]_{0,z=0} \frac{z^i}{i!} \exp(-z) \quad (\text{A11})$$

$$p_i \equiv \frac{[PX]_i}{[PX]_{0,z=0}} = \frac{z^i}{i!} \exp(-z) \quad (\text{A12})$$

The probability of finding a chain with r -unit that have been activated i times among all chains in the system could be obtained by combining the probability of finding chains that have been activated i times, p_i , with the number fraction of r -unit chains

among chains that have been activated i times, $n_i(r)$. This combination could then be added for all possible number of activation cycles that any chain could have undergone (summation for i from 0 to infinity), yielding the expression for the full chain length distribution, $n(r)$, shown in Equation (A13). From this equation, the weight-fraction distribution for chains with r -units, regardless the number of activation cycles that they have undergone, follows Equation (A14).

$$n(r) = \sum_{i=0}^{\infty} [p_i \times n_i(r)] = (\phi_p)^r e^{-z} \sum_{i=0}^{\infty} \binom{r+i-1}{r} \frac{[z(1-\phi_p)]^i}{i!} \quad (\text{A13})$$

$$w(r) = (1-\phi_p)^2 (\phi_p)^{r-1} e^{-z} \sum_{i=0}^{\infty} \binom{r+i-1}{i} \frac{[z(1-\phi_p)]^{i-1}}{(i-1)!} \quad (\text{A14})$$

The number- and weight-average chain length and polydispersity could also be obtained from the MWD expression, as shown by Equations (A15), (A16), and (A17), respectively.

$$r_N = \frac{z\phi_p}{1-\phi_p} \quad (\text{A15})$$

$$r_W = \frac{1+\phi_p+z\phi_p}{1-\phi_p} \quad (\text{A16})$$

$$PDI = 1 + \frac{1}{r_N} + \frac{2}{z} \quad (\text{A17})$$

Comparing Equations (A7) and (A17) reveals that the distribution of chains activated i times is narrower than that of the overall chain population activated the same number of times ($z = i$), as seen from the higher PDI for overall chain ($2/z$ versus $1/i$). The broadening is attributed to the distribution of the number of activation cycles among chains in the system.

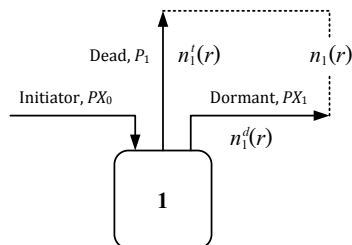
Model with termination

Figure A3-1. The activation of initiator molecules followed by deactivation or termination

The derivation shown in the previous section for the case without termination could be extended to the system of a series of CSTRs with by-product streams to account for the effect of termination on the MWD. For this case, there are two streams exiting each CSTR as shown in Figure 3-2, where the by-product stream represents chains that are irreversibly terminated instead of deactivated, hence unable to participate in further reaction. There are two distributions of chains involved in the i^{th} activation cycle, $n_i^d(r)$ and $n_i^t(r)$, for the dormant and dead chains, respectively. To elucidate the derivation of these distributions, the same approach would be taken as that used in the previous section.

The initiator molecules, PX , that are being activated for the first time (“entering the first reactor”) have the probability to grow 0 to infinite monomeric units “inside this reactor”. The probability that it will add r units in this activation cycle is given by is $(\phi_p)^r$, where ϕ_p is defined by Equation (13) in the Model Development section. However, in this case, these chains could either be deactivated to revert to dormant state with a probability of ϕ_d (“the stream exiting the first reactor to enter the second reactor”), or they could be terminated to form dead chains with a probability of ϕ_t (“the stream exiting the first reactor to join the by-product stream”). Therefore,

the number fractions of the dormant and dead chains with r -unit that have been activated could be expressed as shown by Equations (A18) and (A19). The overall chain length distribution for chains that have been activated once could be expressed as Equation (A20). This process is analogous to the first reactor, as illustrated by Figure A3-1. Note that Equation (A20) reduces to Equation (A1) when termination becomes negligible ($\phi_t \rightarrow 0$).

$$n_1^d(r) = \phi_d (\phi_p)^r \quad (\text{A18})$$

$$n_1^t(r) = \phi_t (\phi_p)^r \quad (\text{A19})$$

$$n_1(r) = n_1^d(r) + n_1^t(r) = (1 - \phi_p) (\phi_p)^r \quad (\text{A20})$$

From these equations, the number-average chain lengths of dormant and dead chains “exiting the first reactor” could be calculated separately, as shown by Equations (A21) and (A22). By doing so, the dead chain contribution to the overall chain population could be clearly observed.

$$r_{N,1}^d = \frac{\sum_{r=0}^{\infty} r n_1^d(r)}{\sum_{r=0}^{\infty} n_1^d(r)} = \frac{\phi_p}{1 - \phi_p} \quad (\text{A21})$$

$$r_{N,1}^t = \frac{\sum_{r=0}^{\infty} r n_1^t(r)}{\sum_{r=0}^{\infty} n_1^t(r)} = \frac{\phi_p}{1 - \phi_p} \quad (\text{A22})$$

After the first reactor, the number-average chain lengths of the dormant and dead chains are identical, which was expected since both streams are originated from the same reactor. However, only the dormant chains can be reactivated for the second time (“stream entering the second reactor”), and propagate further “inside the

reactor.” These chains could then be deactivated (“stream exiting the second reactor to enter the third reactor”) or terminated (“stream exiting the second reactor to join the by-product stream”), similar to the previous reactor. Therefore, the number fractions of dormant and dead chains with r monomeric units exiting from the second reactor can be calculated as shown by Equations (A23) and (A24), where r denotes the total number of monomeric units added in the first and second reactors.

$$n_2^d(r) = \sum_{s=0}^r n_1^d(s) \phi_d (\phi_p)^{r-s} = (\phi_d)^2 (\phi_p)^r (r+1) \quad (\text{A23})$$

$$n_2^t(r) = \sum_{s=0}^r n_1^t(s) \phi_t (\phi_p)^{r-s} = \phi_d \phi_t (\phi_p)^r (r+1) \quad (\text{A24})$$

The terminated chains from the first activation cycle (“by-product stream from the first reactor”) must be added to the ones from the second activation cycle (“by-product stream from the second reactor”) to obtain the cumulative dead chain distribution after the second cycle, because though it does not participate in the reaction, it is still present in the system (“by-product stream from the first reactor joining the by-product stream from the second reactor”), shown in Equation (A25). The overall distribution could then be obtained by including the dormant chain distribution to the cumulative dead chain distribution, as shown by Equation (A26), and illustrated in Figure A3-2.

$$n_{2,cum}^t(r) \equiv n_1^t(r) + n_2^t(r) = (\phi_p)^r [\phi_t + \phi_d \phi_t (r+1)] \quad (\text{A25})$$

$$n_2(r) = n_2^d(r) + n_{2,cum}^t(r) = (\phi_p)^r [\phi_d (\phi_d + \phi_t) (r+1) + \phi_t] \quad (\text{A26})$$

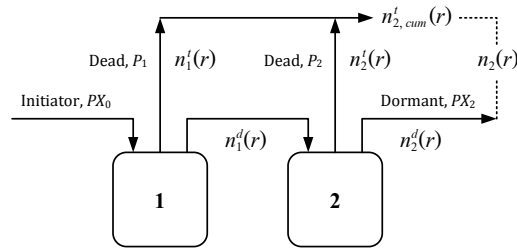


Figure A3-2. The analogy of dormant and dead chains that have been activated twice to a series of two reactors

Upon calculations of the number-average chain length of each chain population after the second activation cycle (“streams exiting the second reactor”), it can be clearly seen that the number-average chain length for the dormant and dead chains exiting the second reactor are equal, as shown in Equation (A27) and (A28). However, the dead chains from the first activation cycle (“by-product stream from the first reactor”) must also be accounted for in the calculation of the number-average chain length of the cumulative dead chain population, as shown by Equation (A29). By comparing Equation (A27) and (A29), it is obvious that the number-average chain length for the dead chains is lower than that for the dormant chains. This finding is as expected because the dead chains from the first activation cycle could no longer grow regardless of the number of activation cycles that the system has experienced (“by-product stream bypasses the other subsequent reactors”). The number-average chain length of the chains that have been activated twice falls in-between these two values, as shown by Equation (A30).

$$r_{N,2}^d = \frac{\sum_{r=0}^{\infty} r n_2^d(r)}{\sum_{r=0}^{\infty} n_2^d(r)} = \frac{2\phi_p}{1-\phi_p} \quad (\text{A27})$$

$$r_{N,2}^t = \frac{\sum_{r=0}^{\infty} r n_2^t(r)}{\sum_{r=0}^{\infty} n_2^t(r)} = \frac{2\phi_p}{1-\phi_p} \quad (\text{A28})$$

$$r_{N,2,cum}^t = \frac{\sum_{r=0}^{\infty} r n_{2,cum}^t(r)}{\sum_{r=0}^{\infty} n_{2,cum}^t(r)} = \left(1 + \frac{\phi_d}{\phi_t + 2\phi_d}\right) \left(\frac{\phi_p}{1-\phi_p}\right) \quad (\text{A29})$$

$$r_{N,2} = \sum_{r=0}^{\infty} r n_2(r) = \left(1 + \frac{\phi_d}{\phi_t + \phi_d}\right) \left(\frac{\phi_p}{1-\phi_p}\right) = (1 + f_d) \left(\frac{\phi_p}{1-\phi_p}\right) \quad (\text{A30})$$

Moreover, as shown in Equation (A31) and (A32), after 2 activation cycles the polydispersity of the cumulative dead chains is also higher than that of the dormant chains. This could also be explained by the presence of dead chains from the first activation cycle, creating a broader distribution for the dead chains than for the dormant chains.

$$PDI_2^d = 1 + \frac{1}{2\phi_p} \quad (\text{A31})$$

$$PDI_{2,cum}^t = 1 + \frac{1}{2\phi_p} + \left(\frac{1-\phi_p}{2\phi_p}\right) \left(\frac{3\phi_d + \phi_t + 2\phi_d\phi_p}{(3\phi_d + \phi_t)^2}\right) \quad (\text{A32})$$

Continuing the derivation with the same approach, the distribution expressions for dormant, dead and cumulative dead chains could be obtained after i cycles of activation, as shown by Equations (A33), (A34) and (A35), respectively. The fraction of dead chains in one activation cycle, f_t , as defined by Equation (16), could also be used to relate the distributions of dormant and dead chains, as expressed in Equation (A34). Moreover, normalizing the distribution of dormant and dead chains, Equation (A33) and (A34), would yield the exact same distribution. Therefore, it could also be

shown that the dormant and dead chains exiting the same reactor have the same number-average chain length, as calculated by Equation (A36) and (A37). However, due to the accumulation of dead chains formed in the previous activation cycles (“previous reactors”), the overall population of dead chains would have lower average with broader distribution when compared to the dormant chains.

$$n_i^d(r) = \binom{r+i-1}{r} (\phi_p)^r (\phi_d)^i \quad (\text{A33})$$

$$n_i^t(r) = \binom{r+i-1}{r} \phi_t (\phi_p)^r (\phi_d)^{i-1} = \frac{f_t}{f_d} n_i^d(r) \quad (\text{A34})$$

$$n_{i,cum}^t(r) \equiv \sum_{j=1}^i n_j^t(r) = \frac{\phi_t}{\phi_d} (\phi_p)^r \sum_{j=1}^i \binom{r+j-1}{r} (\phi_d)^j \quad (\text{A35})$$

$$r_{N,i}^d = \sum_{r=0}^{\infty} r n_i^d(r) / \sum_{r=0}^{\infty} n_i^d(r) = \frac{i \phi_p}{1 - \phi_p} \quad (\text{A36})$$

$$r_{N,i}^t = \sum_{r=0}^{\infty} r n_i^t(r) / \sum_{r=0}^{\infty} n_i^t(r) = \frac{i \phi_p}{1 - \phi_p} \quad (\text{A37})$$

The overall distribution of chains that have been activated i times is then expressed as Equation (A38), with the resulting number-average chain length shown by Equation (A39).

$$\begin{aligned} n_i(r) &= n_i^d(r) + n_{i,cum}^t(r) \\ &= (\phi_p)^r \left[\binom{r+i-1}{r} (\phi_d)^i + \frac{\phi_t}{\phi_d} \sum_{j=1}^i \binom{r+j-1}{r} (\phi_d)^j \right] \end{aligned} \quad (\text{A38})$$

$$r_{N,i} = \sum_{r=0}^{\infty} r n_i(r) = \frac{\phi_p}{\phi_t} [1 - (f_d)^i] \quad (\text{A39})$$

Similar to the previous case without termination, the distribution of the number of activation cycles in polymerization follows the Poisson distribution. Therefore, the probability of finding chains that have been activated i times, p_i , also follows Equation (A12).

$$p_i = \frac{z^i}{i!} \exp(-z) \quad (\text{A12})$$

The full MWD of the overall chain population, $n(r)$, is obtained with the same approach as the derivation for the model without termination. The product of chain length distribution for the i^{th} activation cycles, $n_i(r)$, with the probability of finding chains that have been activated i times, p_i , could be added for all possible activation cycles (i from 0 to infinity). The summation results in the number fraction of chains with r -monomeric units, $n(r)$, regardless of the number of activation cycles, as shown in Equation (A40).

$$\begin{aligned} n(r) &= \sum_{i=0}^{\infty} [p_i \times n_i(r)] \\ &= e^{-z} (\phi_p)^r \left[\sum_{i=0}^{\infty} \binom{r+i-1}{r} \frac{(z\phi_d)^i}{i!} + \frac{\phi_t}{\phi_d} \sum_{i=1}^{\infty} \frac{z^i}{i!} \sum_{j=1}^i \binom{r+j-1}{r} (\phi_d)^j \right] \end{aligned} \quad (\text{A40})$$

Using this method, the MWD could also be deconvoluted to obtain separate distributions of the dormant and dead chains. The distributions of the overall dormant and dead chains are calculated by Equation (A41) and (A42) respectively. Therefore, it becomes clear that the second term of the full MWD, shown in Equation (A40), corresponds to the effect of termination on the distribution.

$$n^d(r) = \sum_{i=0}^{\infty} [p_i \times n_i^d(r)] = e^{-z} (\phi_p)^r \sum_{i=0}^{\infty} \binom{r+i-1}{r} \frac{(z\phi_d)^i}{i!} \quad (\text{A41})$$

$$n^t(r) = \sum_{i=0}^{\infty} [p_i \times n_{i,cum}^t(r)] = e^{-z} (\phi_p)^r \frac{\phi_t}{\phi_d} \sum_{i=1}^{\infty} \frac{z^i}{i!} \sum_{j=1}^i \binom{r+j-1}{r} (\phi_d)^j \quad (\text{A42})$$

The expression for the full MWD of overall chain population is also used to derive expressions for the number- and weight-average chain length, and polydispersity, shown by Equation (A43), (A44) and (A45) respectively.

$$r_N = \frac{\phi_p}{\phi_t} (1 - e^{-zf_t}) \quad (\text{A43})$$

$$r_w = 1 + \frac{2\phi_p}{\phi_t} \left(1 - \frac{zf_t f_d e^{-zf_t}}{(1 - e^{-zf_t})} \right) \quad (\text{A44})$$

$$PDI = 1 + \frac{1}{r_N} + \frac{\sinh(zf_t) - zf_t f_d}{\cosh(zf_t) - 1} \quad (\text{A45})$$

where: $\sinh(x)$ and $\cosh(x)$ are the hyperbolic sine and cosine of x , and are defined as:

$$\sinh(x) \equiv \frac{e^x - e^{-x}}{2} \quad \text{and} \quad \cosh(x) \equiv \frac{e^x + e^{-x}}{2}$$

Moreover, the fraction of terminated chains present in the system could be calculated by the summation of mole fractions of the terminated chains for all possible chain lengths (r from 0 to infinity). Therefore, the resulting dead chain fraction, DCF , could be expressed by Equation (A46).

$$DCF = \sum_{r=0}^{\infty} n^t(r) = 1 - \exp(-zf_t) \quad (\text{A46})$$

4 MOLECULAR WEIGHT DISTRIBUTION FOR ATRP AT A MODERATE TO HIGH CONVERSION

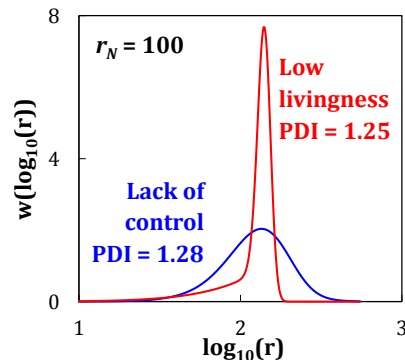
In this chapter, a method was proposed to extend the applicability of work done in the previous chapter to systems with varying reactants' concentrations (*i.e.*, moderate to high conversion ATRP). This chapter is a reproduction of a published article in the *Macromolecular Theory and Simulations* journal, **2014**, 23 (3), p.227-240 (doi:10.1002/mats.201300166), with permission from John Wiley and Sons.

Author contributions

Similar to Chapter 3, this chapter was prepared under the supervision of Dr. Dapeng Zhou and Dr. Shiping Zhu, who provided insightful ideas, discussions, and revisions. Erlita finished the derivation, calculations, and prepared the first draft of this chapter.

§ 4.1 Abstract

In a previous work, we developed a model of full molecular weight distribution (MWD) for atom transfer radical polymerization (ATRP) with radical termination, using analogy to a series of continuous stirred tank reactors (CSTRs). The model assumed constant reaction rates, which was applicable to low conversion batch or steady-state continuous processes. In this work, we generalized the model to any polymerization conditions, provided variations of the reaction rates with conversion are known. Using this extended model, we demonstrated the effect of monomer conversion on the MWD, for the cases with and without radical termination. The conversion dependence of MWD was found to be significant. The broadening of distribution was correlated to the lack of control and/or the loss of livingness. Both control and livingness are necessary conditions for narrow MWD. It was also found that the effects of these two factors are very different, yielding different distribution shapes, even with similar average chain lengths (r_N) and polydispersity indexes (PDI).



§ 4.2 Introduction

Controlled radical polymerization (CRP), or also termed reversible deactivation radical polymerization (RDRP) as have been recommended by IUPAC,^[1] is a type of

polymerization process that allows formation of polymers with narrow chain length distribution (CLD, or equivalently molecular weight distribution, MWD). In other words, polymers produced via CRP would possess similar chain lengths to each other, as indicated by its low polydispersity index (between 1.0 and 1.5). Polydispersity index (*PDI*) is a measure of how broadly distributed the polymer chains are, or also termed as dispersity (\mathcal{D}) by IUPAC.^[2] The narrow distribution has been attributed to the reduced level of termination and to the equilibrium involved in CRP reaction mechanisms, which allows radical/active chains to be deactivated and form dormant chains. The equilibrium between the dormant and radical chains provides control to the system, where the active chain end is capped very frequently, allowing very few monomeric units to be added per activation cycle. Moreover, all the chains in CRP are initiated at the beginning of polymerization, allowing all chains to grow under the same condition, further contributing to the narrow CLD possessed.

The three most commonly studied CRP types are nitroxide-mediated polymerization (NMP),^[3] atom transfer radical polymerization (ATRP),^[4] and reversible-addition fragmentation chain transfer (RAFT).^[5] An increasing numbers of papers have been published in these areas, along with numerous reviews that summarize the progress in the area.^[6-9] The growing interest in CRP is mainly driven by its potential in industrial application to improve the properties of existing materials and to create new polymeric materials with carefully tailored properties. Some industrial successes have been accomplished in commercializing CRP processes, such as Kaneka's XMAP

from ATRP, Rhodiblock RS of Rhodia, Arkema's Blocbuilder from NMP, etc.^[10] Researchers continue working on reaction engineering and industrial aspects of CRP processes for further commercialization. Examples are the developments of reactor technologies^[11-13] and high monomer conversion polymerization operations.^[14]

Based on the number of papers published, the most widely studied types of CRP is ATRP, followed by RAFT and NMP.^[15] For the past two decades, many different types of ATRP have been developed, such as normal ATRP, reverse ATRP, activators regenerated by electron transfer (ARGET) ATRP, initiators for continuous activator regeneration (ICAR) ATRP, etc.^[6] Despite the different types, the basic mechanisms of these ATRPs are still similar, differing only in the initiation/activation system. The basic mechanism that is applicable for all the ATRP types is shown in Figure 4-1, with C and XC representing the activator and deactivator catalysts, respectively. The activator and deactivator, which create an equilibrium between dormant, PX , and radical, P^{\bullet} , are transition metal complexes with appropriate ligand. As can be seen from Figure 4-1, the termination in ATRP is not completely eliminated. The suppression of termination in ATRP relies on the persistent radical effect.^[16,17]

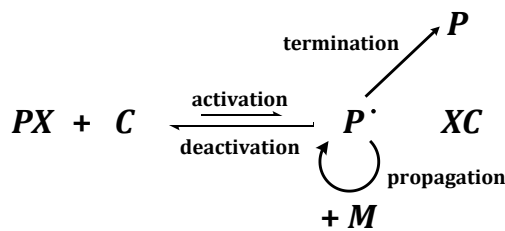


Figure 4-1. Basic reaction mechanism of ATRP system

Modeling of CRP has been of great interest because it allows deeper understanding of the reaction mechanism and kinetics, as recently demonstrated for RAFT system.^[18] There are many different modeling approaches taken in the investigation of CRP systems, from the early use of kinetic modeling and method of moments,^[19-32] to the more recent modeling studies, which utilized Monte Carlo method, PREDICI software, and other approaches.^[33-48] Out of all these studies, only some discussed the modeling of CLD, even though the knowledge of CLD is essential in determining polymer properties and in understanding reaction mechanism and kinetics. Several methods that have been employed in the literature to predict the CLD in CRP system include, but not limited to, Monte Carlo method, probability generating functions, and direct integration method.^[39-45]

Our group has recently developed an analytical expression for the full CLD of ATRP with termination by analogously relating the activation/deactivation cycles in ATRP to a series of continuous stirred tank reactors (CSTRs).^[45] By using this analogy, the well-known concepts for CSTRs are applicable to ATRP system, allowing the derivation of full CLD, while accounting for the effect of termination, as shown in Equation (1).

$$n(r) = e^{-z} (\phi_p)^r \left[\sum_{i=0}^{\infty} \binom{r+i-1}{r} \frac{(z\phi_d)^i}{i!} + \frac{\phi_t}{\phi_d} \sum_{i=1}^{\infty} \frac{z^i}{i!} \sum_{j=1}^i \binom{r+j-1}{r} (\phi_d)^j \right] \quad (1)$$

$$z = k_a [C] t \quad (2)$$

$$\phi_p = \frac{k_p [M]}{k_p [M] + k_d [XC] + k_t [P^*]} \quad (3)$$

$$\phi_d = \frac{k_d[XC]}{k_p[M] + k_d[XC] + k_t[P^*]} \quad (4)$$

$$\phi_t = 1 - \phi_p - \phi_d \quad (5)$$

$$f_t = \frac{\phi_t}{\phi_t + \phi_d} \quad (6)$$

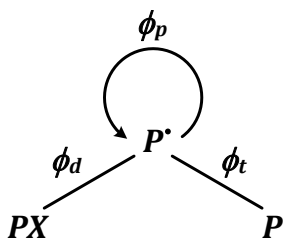


Figure 4-2. Possible reaction pathways of a radical to propagate to add monomeric units, to deactivate with catalyst to form dormant chain, PX , or to terminate with another radical to form dead chain, P

In that work, the average number of activation cycles that the chains have undergone, z , was used in lieu of reaction time, t , as defined by Equation (2). The different probabilities of a radical to participate in various reactions are defined by Equation (3)-(5), also illustrated in Figure 4-2, with the

subscripts representing propagation, deactivation, and termination, respectively. The fraction of chains that are terminated in one activation cycle, f_t , is defined by Equation (6).

The analytical expression developed in that work has been utilized to study the effects of “livingness” and “control” on the broadening of CLD. However, this model was developed under the assumption that the probabilities of radical undergoing different reactions are constant. This in turn requires the reactants concentrations to be constant, which limits the applicability of Equation (1) to low conversion batch systems or steady state continuous systems. As polymerization proceeds to high

conversion in batch process, significant amount of monomer is consumed and more polymer chains are irreversibly terminated to form dead chains. The depletion of monomer concentrations and accumulation of dead chains result in a significant change in reactants concentrations, thereby invalidating the use of Equation (1) for high conversion ATRP system. Furthermore, various reactions could also become diffusion controlled at high conversions, and thus the reaction rate constants could be changing too during polymerization. Variations in concentrations and rate constants change the probability parameters in the above equations. In this work, we make a great effort in extending this analytical model to account for these changes. This allows the model to be usable in predicting CLD of high conversion batch processes.

§ 4.3 Model development

The generally accepted reaction mechanism for ATRP system, shown in Figure 4-1, is used in the model derivation of this work. The elementary reactions are listed in Table 4-1. In ATRP, the key to livingness and control of polymerization lies in the equilibrium between the dormant state, PX , and the active/radical state, P^\bullet , which heavily favours the dormant state. The other possible side reactions not listed in Table 4-1 are assumed to pose negligible effect on the CLD.

For the CLD expression shown by Equation (1) to be usable for high conversion systems, the polymerization is discretized into several short intervals, during which the reactants concentrations can be assumed to be approximately constant.

Therefore, the previously developed theory could be independently applied to each interval, generating the CLD of the chains grown during that interval. These expressions are then combined to obtain the cumulative CLD for the whole period of reaction time. The discretization concept is illustrated in Figure 4-3.

Table 4-1. Reactions involved in atom transfer radical polymerization (ATRP)

Reactions in ATRP		Eqn No
Activation	$P_r X + C \xrightarrow{k_a} P_r^* + XC$	(7)
Deactivation	$P_r^* + XC \xrightarrow{k_d} P_r X + C$	(8)
Propagation	$P_r^* + M \xrightarrow{k_p} P_{r+1}^*$	(9)
Termination	$P_r^* + P_s^* \xrightarrow{k_t} P_r + P_s$	(10)

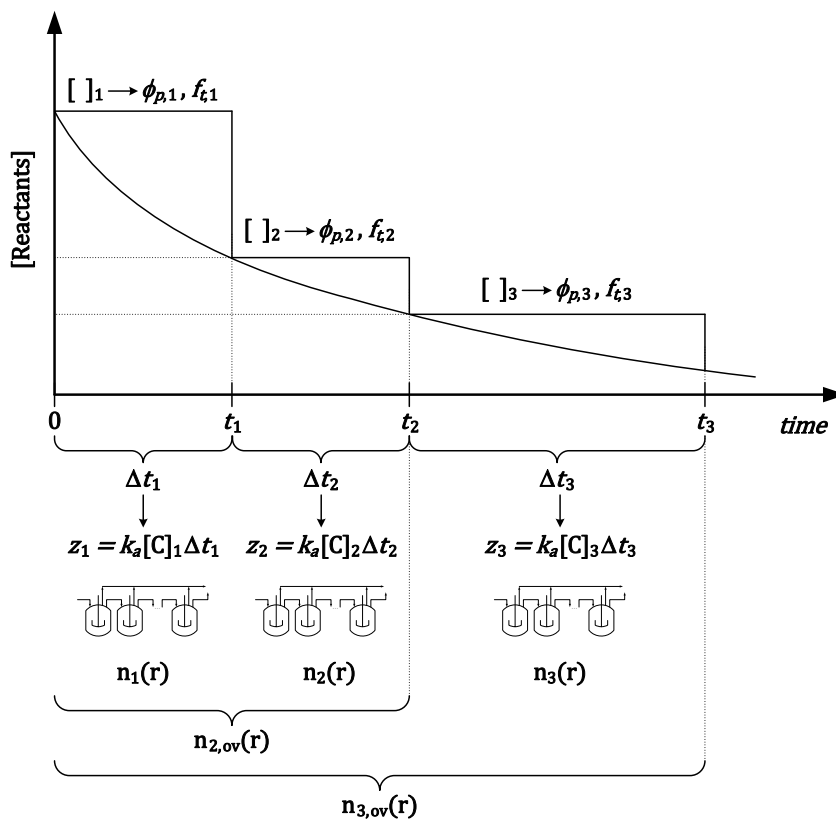


Figure 4-3. Discretization of polymerization period to smaller time intervals to obtain CLD

The detailed derivation of the model is divided into two parts, first is the simplest case for the system without any termination (perfectly “living” system), while the second accounts for the effect of termination on CLD. In both cases, the intervals chosen are based on the total monomer conversion value, with 1 interval representing 1% of monomer conversion. This is done to reduce the number of CSTRs series at high conversion, since the change in concentration becomes slower towards the end of polymerization.

4.3.1 No termination ($k_t = 0 \rightarrow \phi_t = 0, f_t = 0$)

For a perfectly living system under constant reactants concentrations, the full CLD of that system could be shown to follow Equation (11), with the number-average chain length and polydispersity index expressed by Equation (12) and (13). These equations were first derived by Tobita using a random sampling technique and later by us using analogy to a series of CSTRs.^[39,45] From Equation (11), it can be seen that for the system without termination, the full CLD is described by two independent variables, namely the polymerization time, or equivalently represented by the average number of activation cycles involved, z , and the probability of radical to add monomeric unit, ϕ_p .

$$n(r) = e^{-z} (\phi_p)^r \sum_{i=0}^{\infty} \binom{r+i-1}{r} \frac{(z(1-\phi_p))^i}{i!} \quad (11)$$

$$r_N = \frac{z\phi_p}{1-\phi_p} \quad (12)$$

$$PDI = 1 + \frac{1}{r_N} + \frac{2}{z} \quad (13)$$

With the discretization as illustrated by Figure 4-3, the distribution of chain growth during one interval follows Equation (11), with different values of ϕ_p and z for different intervals. For the first interval, the full CLD and the number-average chain length are shown by Equation (14) and (15), respectively.

$$n_1(r) = f(z_1, \phi_{p,1}) = e^{-z_1} (\phi_{p,1})^r \sum_{i=0}^{\infty} \binom{r+i-1}{r} \frac{(z_1(1-\phi_{p,1}))^i}{i!} \quad (14)$$

$$r_{N,1} = \frac{z_1 \phi_{p,1}}{1 - \phi_{p,1}} \quad (15)$$

$$\text{where: } z_1 = k_a [C]_1 \Delta t_1 \quad \text{and} \quad \phi_{p,1} = \frac{k_p [M]_1}{k_p [M]_1 + k_d [XC]_1}$$

Similarly for the second interval, the distribution of monomer added during that interval follows Equation (16), while the number-average chain length is shown by Equation (17). The only difference between the first and second intervals is the independent variable values, z and ϕ_p . The reactants concentrations used for the calculation of z_2 and $\phi_{p,2}$ are obtained by solving a set of differential equations, shown in Appendix, at the beginning of the second interval ($t = t_1$).

$$n_2(r) = f(z_2, \phi_{p,2}) = e^{-z_2} (\phi_{p,2})^r \sum_{i=0}^{\infty} \binom{r+i-1}{r} \frac{(z_2(1-\phi_{p,2}))^i}{i!} \quad (16)$$

$$r_{N,2} = \frac{z_2 \phi_{p,2}}{1 - \phi_{p,2}} \quad (17)$$

$$\text{where: } z_2 = k_a[C]_2 \Delta t_2 \quad \text{and} \quad \phi_{p,2} = \frac{k_p[M]_2}{k_p[M]_2 + k_d[XC]_2}$$

In order to obtain the overall distribution, the two distributions from the first and second intervals must be combined. Polymer chains that possess r monomeric units at the end of the second interval are chains that grow s units during the first interval and added $(r - s)$ units during the second interval, as illustrated by Figure 4-4.

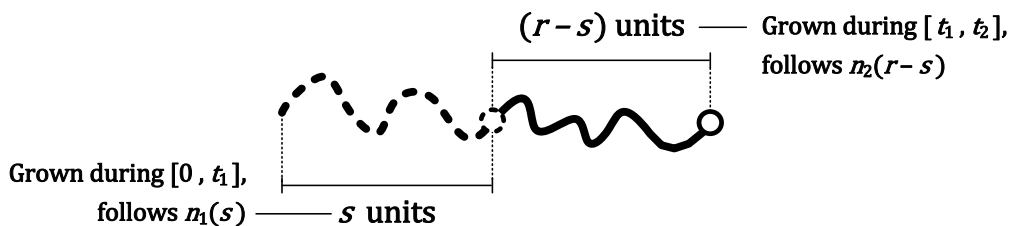


Figure 4-4. Chain growth history for chains with r monomeric units after 2 intervals in a perfectly living ATRP

In Figure 4-4, the dashed line is part of the polymer chain that is grown during the first interval (0 to t_1), therefore described by Equation (14). Meanwhile the solid line represents the portion of polymer grown during the second interval (t_1 to t_2), hence follows Equation (16). The overall distribution could be obtained by taking into account all possible combinations (s from 0 to r), as mathematically shown by Equation (18). The number-average chain length at the end of the second interval could be calculated as a simple summation of number-average chain length from the first and second intervals, as shown by Equation (19). This is possible because no dead chain is considered in this case, thus both intervals involve the same chain population.

$$n_{2,ov}(r) = \sum_{s=0}^r [n_1(s) \times n_2(r-s)] \quad (18)$$

$$r_{N,2,ov} = r_{N,1} + r_{N,2} \quad (19)$$

Following the same trend, a general expression for the CLD of the chains grown during the j^{th} interval is shown by Equation (20), resulting in the number-average chain length expression shown by Equation (21).

$$n_j(r) = f(z_j, \phi_{p,j}) = e^{-z_j} (\phi_{p,j})^r \sum_{i=0}^{\infty} \binom{r+i-1}{r} \frac{(z_j(1-\phi_{p,j}))^i}{i!} \quad (20)$$

$$r_{N,j} = \frac{z_j \phi_{p,j}}{1 - \phi_{p,j}} \quad (21)$$

where: $z_j = k_a [C]_j \Delta t_j$ and $\phi_{p,j} = \frac{k_p [M]_j}{k_p [M]_j + k_d [XC]_j}$

$$n_{j,ov}(r) = \sum_{s=0}^r [n_{j-1,ov}(s) \times n_j(r-s)] \quad (22)$$

$$r_{N,j,ov} \equiv \sum_{r=0}^{\infty} [r \times n_{j,ov}(r)] \quad \text{or} \quad r_{N,j,ov} = \sum_{i=1}^j r_{N,i} \quad (23)$$

The cumulative CLD from the beginning to the end of the j^{th} interval (*i.e.*, $t = [0, t_j]$) follows Equation (22). Moreover, due to the absence of dead chains in this system, the overall number-average chain length is simply the summation of those from each interval, as shown by Equation (23).

4.3.2 With termination

When termination is taken into account, there are two different chain populations that have to be considered, the living (dormant) chains and the dead (terminated) chains. In our previous work, the dormant and terminated chain distributions can be separated for the system under constant reactants concentrations, as shown by Equation (24), obtained through the analogy to a series of CSTRs with by-product streams. The number-average chain length and living chain fraction (*LCF*) have been shown to follow Equation (25) and (26) respectively.^[45]

$$n(r) = n^d(r) + n^t(r) = e^{-z}(\phi_p)^r \left[\sum_{i=0}^{\infty} \binom{r+i-1}{r} \frac{(z\phi_d)^i}{i!} + \frac{\phi_t}{\phi_d} \sum_{i=1}^{\infty} \frac{z^i}{i!} \sum_{j=1}^i \binom{r+j-1}{r} (\phi_d)^j \right] \quad (24)$$

$$\text{where: } n^d(r) = f(z, \phi_p, f_t) = e^{-z}(\phi_p)^r \sum_{i=0}^{\infty} \binom{r+i-1}{r} \frac{(z\phi_d)^i}{i!}$$

$$n^t(r) = f(z, \phi_p, f_t) = e^{-z}(\phi_p)^r \frac{\phi_t}{\phi_d} \sum_{i=1}^{\infty} \frac{z^i}{i!} \sum_{j=1}^i \binom{r+j-1}{r} (\phi_d)^j$$

$$r_N = \frac{\phi_p}{f_t(1-\phi_p)}(1 - LCF) \quad (25)$$

$$LCF = \exp(-zf_t) \quad (26)$$

With the discretization, the growth of polymer chains during one interval could be expressed by the previously developed theory, as shown by Equation (24). Therefore, the distributions of dormant and dead chains grown during the first interval follow Equation (27) and (28), respectively. The number-average chain length of the total chain population and the fraction of the living chains (*LCF*) produced during the first

interval are shown by Equation (29) and (30), respectively. Based on Equation (27) and (28), it can be observed that the independent variables affecting the distribution are the same as the case without termination, with the additional variable f_t , which is the fraction of terminated chains per cycle.

$$n_1^d(r) = f(z_1, \phi_{p,1}, f_{t,1}) = e^{-z_1} (\phi_{p,1})^r \sum_{i=0}^{\infty} \binom{r+i-1}{r} \frac{(z_1 \phi_{d,1})^i}{i!} \quad (27)$$

$$n_1^t(r) = f(z_1, \phi_{p,1}, f_{t,1}) = e^{-z_1} (\phi_{p,1})^r \frac{\phi_{t,1}}{\phi_{d,1}} \sum_{i=1}^{\infty} \frac{(z_1)^i}{i!} \sum_{j=1}^i \binom{r+j-1}{r} (\phi_{d,1})^j \quad (28)$$

$$r_{N,1} = \frac{[M]_2 - [M]_1}{[PX]_1} = \frac{\phi_{p,1}}{f_{t,1}(1 - \phi_{p,1})} (1 - LCF_1) \quad (29)$$

$$LCF_1 = \frac{[PX]_2}{[PX]_1} = \exp(-z_1 f_{t,1}) \quad (30)$$

Similarly, the distribution of monomer added during the second interval follows Equation (31) and (32), for the dormant and terminated chains at the end of the second interval, respectively. As is the case without termination, the differences between chain growth in the two intervals are the concentrations used to calculate the independent variable values, z , ϕ_p , and f_t . The concentrations used to obtain the CLD of the second interval are calculated by solving the differential equations at the beginning of the second interval ($t = t_1$), and the concentrations are assumed to be constant through the second interval ($t = [t_1, t_2]$).

$$n_2^d(r) = f(z_2, \phi_{p,2}, f_{t,2}) = e^{-z_2} (\phi_{p,2})^r \sum_{i=0}^{\infty} \binom{r+i-1}{r} \frac{(z_2 \phi_{d,2})^i}{i!} \quad (31)$$

$$n_2^t(r) = f(z_2, \phi_{p,2}, f_{t,2}) = e^{-z_2} (\phi_{p,2})^r \frac{\phi_{t,2}}{\phi_{d,2}} \sum_{i=1}^{\infty} \frac{(z_2)^i}{i!} \sum_{j=1}^i \binom{r+j-1}{r} (\phi_{d,2})^j \quad (32)$$

It should be noted that the chains involved in the second interval are only those that remain as dormant chains at the end of the first interval, *i.e.*, excluding the dead chains formed in the first interval. Therefore, the total chain populations considered in the second interval are all based on these dormant chains, $[PX]_2$. Careful consideration must be taken when defining the number-average chain length and living chain fraction of the second interval. The number-average chain length for this interval is the average number of monomeric units added per chains that were dormant at the beginning of the second interval. Similarly, the living chain fraction calculated in the second interval is the fraction of chains that remains as dormant chains based on these total chains. These can be mathematically expressed as Equation (33) and (34).

$$r_{N,2} = \frac{[M]_3 - [M]_2}{[PX]_2} = \frac{\phi_{p,2}}{f_{t,2}(1 - \phi_{p,2})} (1 - LCF_2) \quad (33)$$

$$LCF_2 = \frac{[PX]_3}{[PX]_2} = \exp(-z_2 f_{t,2}) \quad (34)$$

In order to combine the distribution of the two intervals, it should be noted that the dormant chains at the end of the second interval must have been dormant at the end of the first interval. However, the terminated chains could have been one of two different possibilities. First type of terminated chains consists of the chains that were dormant at the end of the first interval, participated in reactions but terminated during the second interval. Second type consists of the chains that are already terminated at the end of the first interval, hence not growing in the second interval. These chains must still be included in the overall distribution to obtain full CLD of the

total populations. The three types of chains are illustrated in Figure 4-5. The portion drawn in dashed line represents the part grown during the first interval, while the solid line denotes the part grown during the second interval.

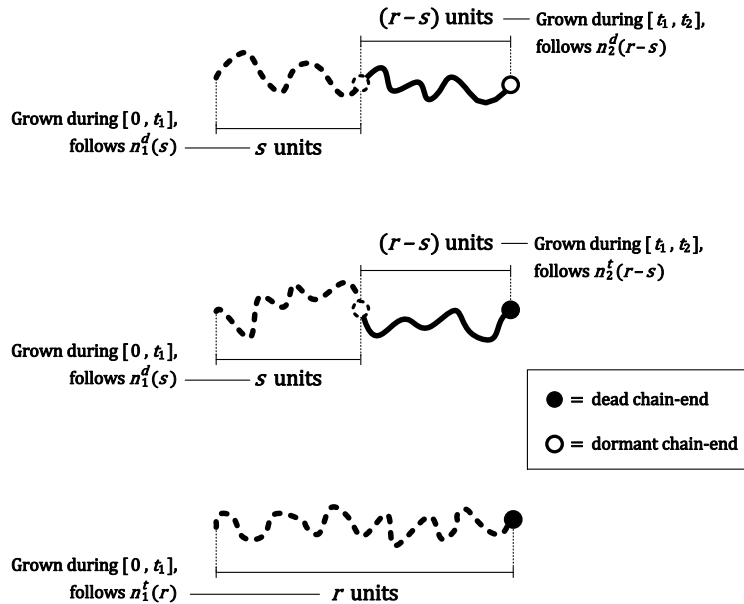


Figure 4-5. Different possible chain growth history for chains with r monomeric units after 2 intervals. Filled circle denotes dead chain-end while hollow circle denotes dormant chain-end

Based on Figure 4-5, the cumulative distributions of the dormant and dead chains at the end of the second interval could be expressed mathematically as all possible combinations of the distributions from the first and second intervals (s from 0 to r), along with the distribution of chains that were dead by the end of the first interval, shown by Equation (35) and (36). The overall distribution for the total chain populations is simply the summation of the distributions of dormant and terminated chains at the end of the second interval, as expressed by Equation (37).

$$n_{2,ov}^d(r) = \sum_{s=0}^r [n_1^d(s) \times n_2^d(r-s)] \quad (35)$$

$$n_{2,ov}^t(r) = n_1^t(r) + \sum_{s=0}^r [n_1^d(s) \times n_2^t(r-s)] \quad (36)$$

$$n_{2,ov}(r) = n_{2,ov}^t(r) + n_{2,ov}^d(r) \quad (37)$$

The overall number-average chain length could be obtained based on its definition. It could also be obtained from the combination of the two number-average chain lengths from the two intervals, while accounting the fraction of the chains that participated in the second interval, as shown by Equation (38). The overall living chain fraction could be calculated by Equation (39) as a product of the living chain fractions of the first and second intervals.

$$r_{N,2,ov} \equiv \sum_{r=0}^{\infty} [r \times n_{2,ov}(r)] \quad \text{or} \quad r_{N,2,ov} = r_{N,1} + r_{N,2} LCF_1 \quad (38)$$

$$LCF_{2,ov} \equiv \sum_{r=0}^{\infty} n_{2,ov}^d(r) \quad \text{or} \quad LCF_{2,ov} = \frac{[PX]_3}{[PX]_1} = LCF_1 \times LCF_2 \quad (39)$$

The expression for the third interval could be obtained by following the same approach. The full CLD expressions for chain grown during the third interval for dormant and terminated chains are shown by Equation (40) and (41) respectively. The overall distributions for the dormant and dead chains are obtained by utilizing the cumulative distribution up to the second interval, shown by Equation (42) and (43). The total number-average chain length and living chain fraction at the end of the third interval could be estimated based on Equation (44) and (45), respectively.

$$n_3^d(r) = f(z_3, \phi_{p,3}, f_{t,3}) = e^{-z_3} (\phi_{p,3})^r \sum_{i=0}^{\infty} \binom{r+i-1}{r} \frac{(z_3 \phi_{d,3})^i}{i!} \quad (40)$$

$$n_3^t(r) = f(z_3, \phi_{p,3}, f_{t,3}) = e^{-z_3} (\phi_{p,3})^r \frac{\phi_{t,3}}{\phi_{d,3}} \sum_{i=1}^{\infty} \frac{(z_3)^i}{i!} \sum_{j=1}^i \binom{r+j-1}{r} (\phi_{d,3})^j \quad (41)$$

$$n_{3,ov}^d(r) = \sum_{s=0}^r [n_{2,ov}^d(s) \times n_3^d(r-s)] \quad (42)$$

$$n_{3,ov}^t(r) = n_{2,ov}^t(r) + \sum_{s=0}^r [n_{2,ov}^d(s) \times n_3^t(r-s)] \quad (43)$$

$$r_{N,3,ov} \equiv \sum_{r=0}^{\infty} [r \times n_{3,ov}(r)] \quad \text{or} \quad r_{N,3,ov} = r_{N,2,ov} + r_{N,3} LCF_{2,ov} \quad (44)$$

$$LCF_{3,ov} \equiv \sum_{r=0}^{\infty} n_{3,ov}^d(r) \quad \text{or} \quad LCF_{3,ov} = LCF_{2,ov} \times LCF_3 \quad (45)$$

Following the same trend, general expressions for the overall distributions of dormant and dead chains after j^{th} interval could be shown to follow Equation (46) and (47), with the distribution of the total chain populations shown by Equation (48). The total number-average chain length and living chain fraction at the end of the j^{th} interval could be expressed as Equation (49) and (50).

$$n_{j,ov}^d(r) = \sum_{s=0}^r [n_{(j-1),ov}^d(s) \times n_j^d(r-s)] \quad (46)$$

$$n_{j,ov}^t(r) = n_{(j-1),ov}^t(r) + \sum_{s=0}^r [n_{(j-1),ov}^d(s) \times n_j^t(r-s)] \quad (47)$$

$$n_{j,ov}(r) = n_{j,ov}^d(r) + n_{j,ov}^t(r) \quad (48)$$

$$r_{N,j,ov} \equiv \sum_{r=0}^{\infty} [r \times n_{j,ov}(r)] \quad \text{or} \quad r_{N,j,ov} = \sum_{i=1}^j [r_{N,i} \times LCF_{(i-1),ov}] \quad (49)$$

$$LCF_{j,ov} \equiv \sum_{r=0}^{\infty} n_{j,ov}^d(r) \quad \text{or} \quad LCF_{j,ov} = \prod_{i=1}^j LCF_i \quad (50)$$

For both cases without and with termination, the overall distribution of polymer chains, represented by Equation (22) and (48), could be obtained once the full CLD of each interval is obtained. By using the approach outlined in this section, these effects could be studied for high conversion batch systems, in which the reactants concentrations are changing, resulting in variation of reaction probability values. The resulting average properties obtained from this method are compared with those obtained by method of moments to ensure the discretization do not introduce significant errors. Method of moments has been relied on to study the kinetics of various CRP systems as discussed in the Introduction section. The moments equations are included in the Appendix.

Similar to our previous work, the control level in a polymerization system is quantified by how many monomers are added to chain per activation cycle ($= \phi_p / (1 - \phi_p)$). Higher growth probability, ϕ_p , value implies more monomer is added per activation cycle, which in turn means a low level of control. The livingness of a system is quantified by the amount of chains that are still living, or the living chain fraction (*LCF*), which depends on both the number of activation cycles, z , and the fraction of terminated chains per cycle, f_t .

It should be noted that the model developed here is a general model for all types of ATRP system (*e.g.*, normal ATRP, ARGET ATRP, ICAR ATRP, etc). The only information that the model requires is the dependence of concentrations and reaction rate

constants with respect to monomer conversion, or more generally, the reaction rates as functions of conversion. The reaction rate constants are known to change as the viscosity of the system increases due to diffusion limitations, as have been noted by various researchers.^[30-32,47,48] In this work, for purpose of simplicity, only changes in concentrations as functions of conversion are considered, while the reaction rate constants are considered to be unaffected.

§ 4.4 Simulation results and discussion

The reaction rate constants used in all simulations conducted in this work are listed in Table 4-2. These reaction rate constants are the typical values for ATRP of MMA at 60°C.

Table 4-2. Reaction rate constants used in simulation of ATRP system

Reaction rate constants	Values
k_p (L·mol ⁻¹ s ⁻¹) ^[49]	834
k_a (L·mol ⁻¹ s ⁻¹)	1.0
k_d (L·mol ⁻¹ s ⁻¹)	10 ⁶
k_t (L·mol ⁻¹ s ⁻¹)	0 or 10 ⁸

The CLDs predicted by analytical model, which assumes constant reaction conditions, is compared to that predicted by the model developed in this work, which accounts for the change in reaction probabilities (ϕ_p and f_t) as functions of conversion. The comparison is done for both cases with and without termination, in order to investigate the effect of conversion on the development of CLD in batch processes,

where the change in reactants concentrations could not be neglected. In most cases, for the conversion-dependent model, or also referred to as the extended model, the reaction probability values are recalculated every 1% conversion by solving the differential equations derived from reaction kinetics.

4.4.1 Without termination

For the cases without termination, there are 2 independent variables affecting the distribution, namely the number of activation cycles (z) and the probability of growth (ϕ_p). The importance of reaction probability values in predicting CLD for a perfectly living system is investigated by comparing the analytical model with constant reaction probabilities with the solution of the extended model with variable reaction probabilities. The comparison is shown in Figure 4-6 (a), with the simulation results tabulated in Table 4-3. The discretization of the simulation parameter, ϕ_p , for the living system is illustrated by a step function in Figure 4-6 (b), while the dashed line represents the evolution of ϕ_p calculated from the reactants concentrations obtained by solving the set of differential equations. For the analytical model, only a constant value of reaction probability can be used per simulation, which is chosen to be the value calculated at the beginning of the polymerization ($x = 0\%$) for this initial comparison

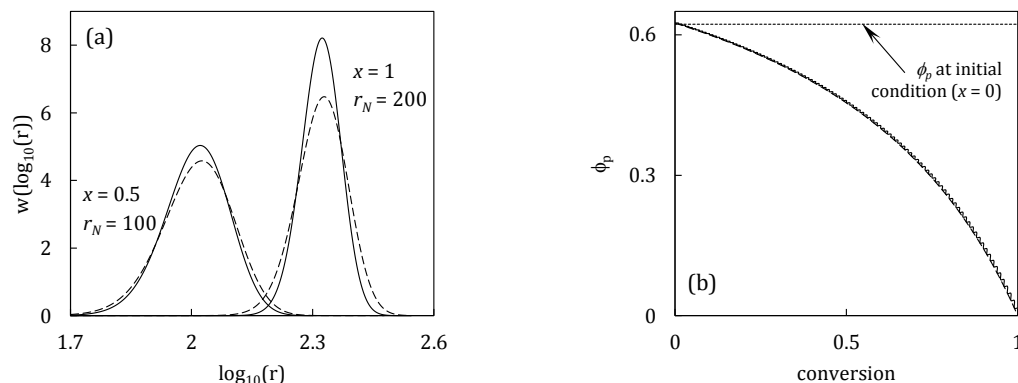


Figure 4-6. Simulation results of a perfectly living ATRP system. $[M] = 4.7$ M, $[M]:[RX]:[C]:[XC] = 200:1:1:0.1$. (a) Comparison of CLDs obtained by analytical and extended models after 50% and 100% conversion. Solid lines denote extended model with variable probability, dashed lines denote analytical model with probability calculated at $x = 0\%$. (b) Evolution of propagation probability with conversion

Table 4-3. Simulation results for perfectly living ATRP corresponding to Figure 4-6 (a)

$\phi_p = 0.63-0.02$	Polydispersity	
	Analytical	Extended
$r_N = 100$, $x = 50\%$	1.04	1.03
$r_N = 200$, $x = 100\%$	1.02	1.01

As can be observed from Figure 4-6 (a) above, the difference between the CLDs obtained from analytical and extended models becomes more obvious at higher conversion. This is because the concentrations deviate further from their initial values as conversion increases. The analytical model generates a slightly broader distribution than the extended one because as the monomer is consumed, the propagation probability, ϕ_p , decreases, as shown in Figure 4-6 (b). In terms of control level, this implies a more controlled condition because lower ϕ_p means fewer monomeric units is added per activation cycle ($= \phi_p / (1 - \phi_p)$).

Beside the initial value of ϕ_p , two other ϕ_p values are tested for the analytical model in comparison with the extended model. These values are calculated based on the reactants concentrations at 50% and 100% conversions for the system with $r_N = 200$ (corresponding to 100% conversion). The comparison is shown in Figure 4-7 (a). The evolution of probability values with monomer conversion is shown in Figure 4-7 (b).

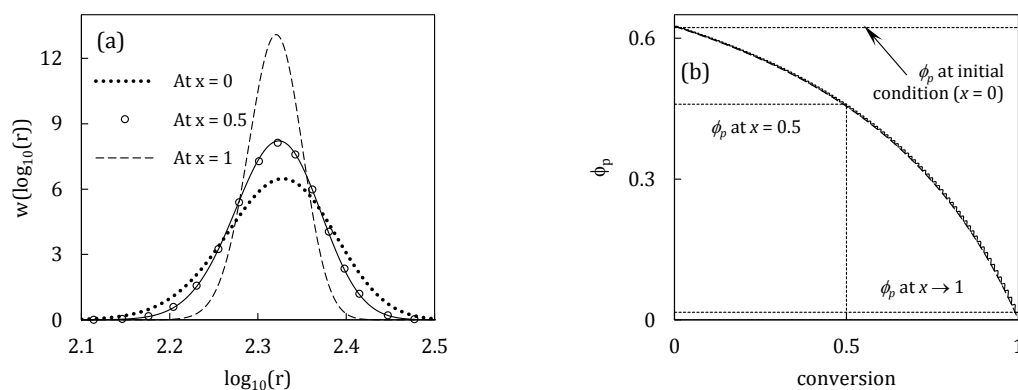


Figure 4-7. (a) Simulation results of CLD for perfectly living ATRP system after 100% conversion ($r_N = 200$). Solid line denotes extended model with variable probability, dashed lines denote analytical model with constant probability calculated from various conversions. (b) Evolution of propagation probability with conversion.

Polymerization recipe: $[M] = 4.7 \text{ M}$, $[M]:[RX]:[C]:[XC] = 200:1:1:0.1$

From Figure 4-7 (a), the use of ϕ_p calculated at half-way conversion ($x = 50\%$) for analytical model approximates the CLD obtained by the extended model. However, this is only due to the relatively simple relationship between ϕ_p and conversion for a perfectly living system, since the deactivator concentration does not change significantly with conversion in the absence of termination. Therefore, the propagation probability for a perfectly living system could be simplified from

Equation (3) to follow Equation (51) as a function of conversion. This expression results in a linear function of level of control ($= \phi_p/(1 - \phi_p)$) with respect to conversion, which explains why the simulation parameters in the analytical model calculated at the half-way conversion point gives a good estimate for the CLD predicted by the extended model.

$$\phi_p = f(x) = \frac{k_p[M]}{k_p[M] + k_d[XC] + k_t[P^\bullet]} \xrightarrow{\text{no termination, } k_t=0} \frac{\phi_p}{1 - \phi_p} = \frac{k_p[M]_0}{k_d[XC]_0}(1 - x) \quad (51)$$

When termination is taken into account, the concentrations of other reactants also change with conversion, resulting in a more complicated non-linear dependence of the simulation parameters on conversion. Therefore, the analytical model with parameters calculated at any conversion point would not be expected to exhibit similar CLDs as the extended model. For simplicity purpose, all subsequent comparisons of analytical and extended models will only be shown for the analytical model calculated with parameters based on the initial polymerization condition.

4.4.2 With termination

When termination is considered, there are 3 independent variables that are required to obtain the CLD of ATRP system by using Equation (24), namely the average number of activation cycles (z), growth probability in a cycle (ϕ_p), and fraction of terminated chains in a cycle (f_t). Conversion, or equivalently number-average chain length, is set to be an independent variable for comparison purpose to replace time, and

equivalently z . Similar to the case without termination, the CLD predictions from analytical and extended models are compared by using initial simulation parameters for the analytical model, as shown in Figure 4-8, with the simulation results summarized in Table 4-4. The dependence of the simulation parameters, ϕ_p and f_t , with conversion are shown in Figure 4-9, with the discretization of these parameters for the extended model shown as step functions.

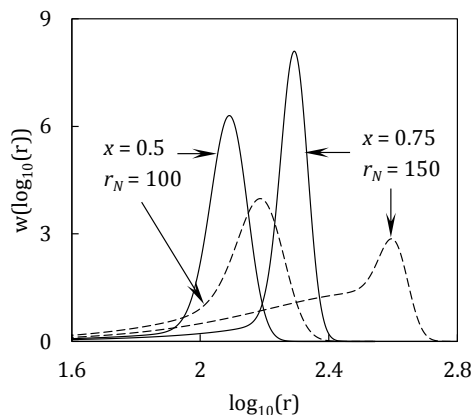


Figure 4-8. Comparison of CLDs obtained by analytical and extended models after 50% and 75% conversion. Recipe: $[M] = 4.7$ M, $[M]:[RX]:[C]:[XC] = 200:1:1:0.1$. Solid lines denote conversion-dependent solution of the extended model, dashed lines denote analytical model with parameters calculated at initial condition

Table 4-4. Simulation results for ATRP system by model with termination, corresponding to Figure 4-8. Recipe: $[M] = 4.7$ M, $[M]:[RX]:[C]:[XC] = 200:1:1:0.1$

$\phi_p = 0.62-0.02$ $f_t = 1E-2-5E-5$	Polydispersity		Living chain fraction	
	Analytical	Extended	Analytical	Extended
$r_N = 100$, $x = 50$ %	1.33	1.16	40%	73%
$r_N = 150$, $x = 75$ %	1.69	1.20	9%	64%

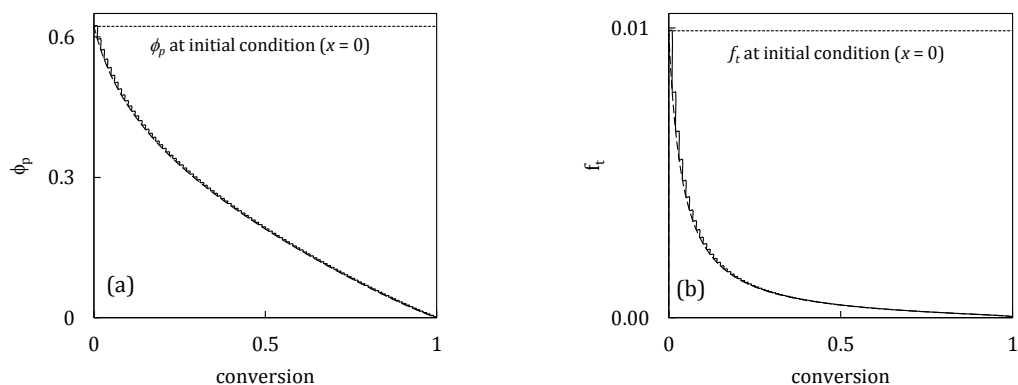


Figure 4-9. Evolution of simulation parameters with conversion, corresponding to Figure 4-8.
(a) Propagation probability. (b) Fraction of dead chains per activation cycle

The comparison presented in Figure 4-8 show that the difference in CLDs from the extended and analytical models is more obvious at higher conversion. However, in this case the difference is not only caused by the monomer consumption but also by the accumulation of dead chains in the system. Based on Table 4-4, the amount of living chains predicted by the analytical model is much less than that predicted by the extended model. This is also evident from the longer, more obvious tails on the CLDs predicted by the analytical model (dashed lines) shown in Figure 4-8, indicating large amount of dead chains that stopped growing prematurely. The overestimation of dead chains amount in the analytical model is due to its use of the initial f_t and thus not taking account the rapid decrease of f_t with conversion, as shown by Figure 4-9 (b). Therefore, for analytical model with parameters calculated based on the initial condition, termination is assumed to occur at its maximum rate, yielding lower livingness than if the conversion dependence of the dead chains formation rate is considered.

It should be noted that while ϕ_p is a good indicator of how controlled the system is, the simulation parameter f_t is not a good measure of the livingness in the system. The level of livingness can be better gauged by the fraction of living chains remaining at that conversion (*LCF*). Moreover, higher degree of control comes at the cost of slower polymerization rate, since fewer monomeric units are added per cycle in a more controlled system.

4.4.3 Lack of control versus loss of livingness

In our previous study, the broadening of CLD is attributed to the low level of control or low livingness under constant reactants concentrations.^[45] In this section, the degree of control and livingness are varied by varying the amount of catalyst present in the system to observe the effect on the CLD with the parameters changing with conversion. The ratio between catalyst and deactivator is kept constant between the two cases at 10:1 ratio. The resulting CLD and the average properties are reported in Figure 4-10 and Table 4-5, respectively. The dependence of simulation parameters, ϕ_p and f_t , with conversion are shown in Figure 4-11.

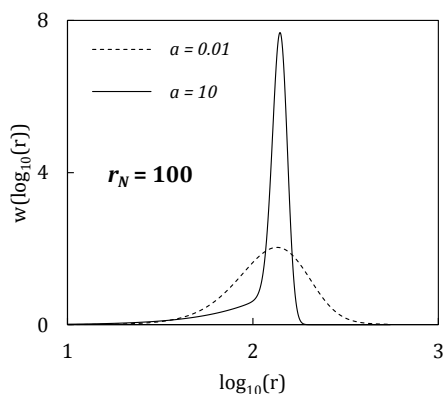


Figure 4-10. Chain length distribution of polymers simulated with the extended model, accounting for conversion dependence, at 50% conversion ($r_N = 100$), with different catalyst and deactivator concentrations. Recipe: $[M] = 4.7 \text{ M}$, $[M]:[RX]:[C]:[XC] = 200 : 1 : a : 0.1a$

Table 4-5. Simulation results for ATRP systems corresponding to Figure 4-10

$x = 50\%$	Polydispersity	Living chain fraction
$a = 0.01$	1.28	98%
$a = 10$	1.25	52%

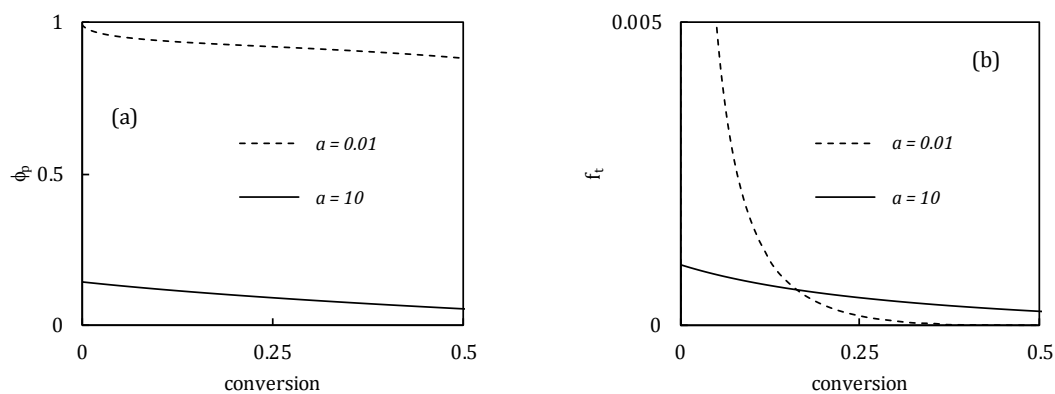


Figure 4-11. Evolution of simulation parameters with conversion corresponding to Figure 4-10. (a) Propagation probability. (b) Fraction of dead chains per activation cycle

It should be noted that despite the similar value of polydispersity indexes between the two cases presented in Table 4-5, 1.25 and 1.28, the distributions of polymer chains from these two cases are very different. The broadening observed in Figure 4-10 for the system with very low catalyst and deactivator concentrations (dashed line, $a = 0.01$) could be attributed to the non-uniformity in chain growth, as indicated by the high value of growth probability, ϕ_p , shown in Figure 4-11. The high value of ϕ_p implies that a large number of monomeric units are added in one activation cycle, thus the chains do not grow at a uniform rate. This translates to a poorly-controlled system, leading to broadening of the chain length distribution observed.

On the other hand, for the case with high catalyst and deactivator concentrations (solid line, $a = 10$), the system shows a good level of control, indicated by the narrow distribution shown in Figure 4-10, and by the low value of ϕ_p in Figure 4-11. Contrary to the previous case, the low value of ϕ_p indicates only a few monomeric units are added to a chain in one activation cycle, leading to a well-controlled system giving a narrow distribution. However, the system involves a large degree of termination, as indicated by the long tail in Figure 4-10 and low living chain fraction (*LCF*) in Table 4-5.

Upon observation, comparison between the amount of living chains and the value of f_t of the two cases seem to contradict each other. A system with low catalyst and deactivator concentrations has higher f_t value, yet exhibits high degree of livingness

(higher LCF). It should be noted that the degree of livingness, quantified by LCF , depends on both f_t and the average number of activation cycles (z) required to achieve a certain conversion or average chain length. In a well-controlled system, the average number of activation cycles required is higher because there are fewer monomeric units added per activation cycles (low ϕ_p). This shows that there exists a relation between the level of control and livingness. When termination is considered, very high degree of control (high number of activation cycles) could be detrimental to livingness of the system.

From the comparison, it becomes evident that the broadening of CLD could be attributed to the poor control, such as exhibited by the case with low catalyst and deactivator concentrations in Figure 4-10, or it could be due to the loss of livingness, observed in the case with high catalyst and deactivator concentrations in Figure 4-10. The effects of livingness and control on the CLD are not independent from each other, since a high degree of control could lead to the loss of livingness, resulting in broadening of the distribution. Moreover, the knowledge of average properties itself might not be enough, since two polymer populations with similar average chain length and polydispersity index could have different distributions, as clearly shown in Figure 4-10, depending on what causes the broadening.

§ 4.5 Conclusion

Growing research interests in ATRP for the past two decades is driven by its ability to polymerize chains with similar lengths, creating a narrowly distributed polymer chains. The knowledge of chain length distribution (CLD, or equivalently MWD) is crucial in determining polymer properties and is potentially beneficial in gaining better understanding of the reaction mechanism. In this work, a previously developed analytical model for CLD in ATRP is extended by applying the expression to small time intervals, during which the concentrations could be approximated as constant values. The cumulative CLD is obtained through combination of all the analytically calculated CLDs throughout the polymerization. By doing so, the variations of reactants concentrations with conversion are accounted for in this approach.

Through simulation using this extended model, it has been shown that the broadening of CLD in ATRP could be attributed to the lack of control in the system or the loss of livingness during the polymerization. Although the two phenomena result in the increase of polydispersity, the shape of the distribution is not the same. The lack of control results in a broader distribution due to non-uniform growth, while the system with low livingness still exhibits a very narrow distribution for the dormant chains, along with extended tails due to the presence of dead chains that stopped growing prematurely. Moreover, it has been shown that the control and livingness are not independent from each other. High degree of control could not only result in long polymerization time, but also could lead to loss of livingness. Control and livingness

are both necessary conditions for a narrow CLD in ATRP, as well as in other type of controlled radical polymerization processes.

This approach, which yields a conversion-dependent model, provides a general model to predict the chain length distribution of any type of ATRP, *e.g.*, normal ATRP, ARGET ATRP, ICAR ATRP, etc, as long as the change in reactants concentrations as functions of monomer conversion are known. In other words, by obtaining the reaction conditions as functions of monomer conversion through any approach, the CLD of that system could be predicted using this extended model, regardless of how the activator/deactivator equilibrium is achieved. Moreover, changes in reaction rate constants due to diffusion-limitation could also be incorporated in the extended model to account for gel-effect and glass effect that could occur in any radical polymerization processes.

§ 4.6 References

- [1] A. D. Jenkins, R. G. Jones, G. Moad, *Pure Appl Chem* **2010**, *82*.
- [2] R. Gilbert, M. Hess, A. Jenkins, R. Jones, P. Kratochvil, R. Stepto, *Pure Appl Chem* **2009**, *81*, 351-353.
- [3] M. Georges, R. P. N. Veregin, P. M. Kazmaier, G. K. Hamer, *Macromolecules* **1993**, *26*, 2987-2988.
- [4] J.-S. Wang, K. Matyjaszewski, *J Am Chem Soc* **1995**, *117*, 5614-5615.
- [5] J. Chiefari, Y. K. B. Chong, F. Ercole, J. Krstina, J. Jeffery, T. P. T. Le, R. T. A. Mayadunne, G. F. Meijs, C. L. Moad, G. Moad, E. Rizzardo, S. H. Thang, *Macromolecules* **1998**, *31*, 5559-5562.
- [6] W. A. Braunecker, K. Matyjaszewski, *Prog Polym Sci* **2007**, *32*, 93-146.

- [7] R. B. Grubbs, *Polymer Reviews* **2011**, *51*, 104-137.
- [8] C. Barner-Kowollik, S. Perrier, *J Polym Sci, Part A: Polym Chem* **2008**, *46*, 5715-5723.
- [9] M. Beija, J.-D. Marty, M. Destarac, *Prog Polym Sci* **2011**, *36*, 845-886.
- [10] M. Destarac, *Macromol React Eng* **2010**, *4*, 165-179.
- [11] Y. Shen, S. Zhu, R. Pelton, *Macromol Rapid Commun* **2000**, *21*, 956-959.
- [12] Y. Shen, S. Zhu, *AIChE J* **2002**, *48*, 2609-2619.
- [13] N. Chan, M. F. Cunningham, R. A. Hutchinson, *Polymer Chemistry* **2012**, *3*, 486-497.
- [14] A. Mohammad Rabea, S. Zhu, *Ind Eng Chem Res* **2013**, *53*, 3472-3477.
- [15] K. Matyjaszewski, *Macromolecules* **2012**, *45*, 4015-4039.
- [16] H. Fischer, *Macromolecules* **1997**, *30*, 5666-5672.
- [17] W. Tang, T. Fukuda, K. Matyjaszewski, *Macromolecules* **2006**, *39*, 4332-4337.
- [18] K. Suzuki, Y. Nishimura, Y. Kanematsu, Y. Masuda, S. Satoh, H. Tobita, *Macromol React Eng* **2012**, *6*, 17-23.
- [19] S. Zhu, *J Polym Sci, Part B: Polym Phys* **1999**, *37*, 2692-2704.
- [20] S. Zhu, *Macromol Theory Simul* **1999**, *8*, 29-37.
- [21] A. H. Müller, R. Zhuang, D. Yan, G. Litvinenko, *Macromolecules* **1995**, *28*, 4326-4333.
- [22] A. H. Müller, D. Yan, G. Litvinenko, R. Zhuang, H. Dong, *Macromolecules* **1995**, *28*, 7335-7338.
- [23] D. Yan, H. Jiang, X. Fan, *Macromol Theory Simul* **1996**, *5*, 333-345.
- [24] M. Souaille, H. Fischer, *Macromolecules* **2002**, *35*, 248-261.
- [25] M. Souaille, H. Fischer, *Macromolecules* **2000**, *33*, 7378-7394.
- [26] J. Bonilla, E. Saldivar-Guerra, A. Flores-Tlacuahuac, E. Vivaldo-Lima, R. Pfaendner, F. Tiscareño-Lechuga, *Polym React Eng* **2002**, *10*, 227-263.
- [27] T. Fukuda, T. Terauchi, A. Goto, K. Ohno, Y. Tsujii, T. Miyamoto, S. Kobatake, B. Yamada, *Macromolecules* **1996**, *29*, 6393-6398.
- [28] M. Zhang, W. H. Ray, *Ind Eng Chem Res* **2001**, *40*, 4336-4352.
- [29] A. R. Wang, S. Zhu, *J Polym Sci, Part A: Polym Chem* **2003**, *41*, 1553-1566.
- [30] O. Delgadillo-Velázquez, E. Vivaldo-Lima, I. A. Quintero-Ortega, S. Zhu, *AIChE J* **2002**, *48*, 2597-2608.
- [31] A. R. Wang, S. Zhu, *Macromol Theory Simul* **2003**, *12*, 196-208.

- [32] D. A. Shipp, K. Matyjaszewski, *Macromolecules* **1999**, *32*, 2948-2955.
- [33] W. Tang, K. Matyjaszewski, *Macromol Theory Simul* **2008**, *17*, 359-375.
- [34] D. R. D'hooge, D. Konkolewicz, M.-F. Reyniers, G. B. Marin, K. Matyjaszewski, *Macromol Theory Simul* **2012**, *21*, 52-69.
- [35] M. Al-Harhi, J. Soares, B.P. L. Simon, C, *Macromol Mater Eng* **2006**, *291*, 993-1003.
- [36] K. A. Payne, D. R. D'Hooge, P. H. M. Van Steenberge, M.-F. Reyniers, M. Cunningham, R. A. Hutchinson, G. B. Marin, *Macromolecules* **2013**, *46*, 3828-3840.
- [37] M. J. Monteiro, *J Polym Sci, Part A: Polym Chem* **2005**, *43*, 5643-5651.
- [38] P. B. Zetterlund, S. Perrier, *Macromolecules* **2011**, *44*, 1340-1346.
- [39] H. Tobita, *Macromol Theory Simul* **2006**, *15*, 12-22.
- [40] H. Tobita, *Macromol Theory Simul* **2006**, *15*, 23-31.
- [41] I. Zapata-Gonzalez, E. Saldivar-Guerra, J. Ortiz-Cisneros, *Macromol Theory Simul* **2011**, *20*, 370-388.
- [42] C. Sarmoria, M. Asteasuain, A. Brandolin, *Can J Chem Eng* **2012**, *90*, 263-273.
- [43] M. Asteasuain, M. Soares, M. K. Lenzi, M. Cunningham, C. Sarmoria, J. C. Pinto, A. Brandolin, *Macromol React Eng* **2007**, *1*, 622-634.
- [44] H. Chaffey-Millar, M. Busch, T. P. Davis, M. H. Stenzel, C. Barner-Kowollik, *Macromol Theory Simul* **2005**, *14*, 143-157.
- [45] E. Mastan, D. Zhou, S. Zhu, *J Polym Sci, Part A: Polym Chem* **2013**, *52*, 639-651.
- [46] D. Konkolewicz, B. S. Hawkett, A. Gray-Weale, S. Perrier, *J Polym Sci, Part A: Polym Chem* **2009**, *47*, 3455-3466.
- [47] D. R. D'hooge, M.-F. Reyniers, G. B. Marin, *Macromol React Eng* **2009**, *3*, 185-209.
- [48] G. Johnston-Hall, M. J. Monteiro, *Macromol Theory Simul* **2010**, *19*, 387-393.
- [49] D. R. Taylor, K. Y. van Berkel, M. M. Alghamdi, G. T. Russell, *Macromol Chem Phys* **2010**, *211*, 563-579.

§ 4.7 Appendix

The differential equations used in the recalculation of simulation parameters in this work were derived from reactions listed in Table 4-1. These differential equations are

obtained from the mass balance of each chemical species. The mass balance for monomer, which could also be re-written for conversion, is shown in Equation (A1). The mass balances for activator and deactivator catalyst, $[C]$ and $[XC]$, and for dormant $[PX]$, radical $[P^\bullet]$, and dead $[P]$ chain overall populations are shown in Equation (A2)–(A6), respectively. The simulation parameters were calculated by using the concentration profiles obtained from simultaneously solving these differential equations.

$$\frac{d[M]}{dt} = -k_p[M][P^\bullet] \rightarrow \frac{dx}{dt} = k_p[P^\bullet](1-x) \quad (\text{A1})$$

$$\frac{d[C]}{dt} = k_a[P^\bullet][XC] - k_d[PX][C] \quad (\text{A2})$$

$$\frac{d[XC]}{dt} = k_d[PX][C] - k_a[P^\bullet][XC] \quad (\text{A3})$$

$$\frac{d[PX]}{dt} = k_a[P^\bullet][XC] - k_d[PX][C] \quad (\text{A4})$$

$$\frac{d[P^\bullet]}{dt} = k_a[PX][C] - k_d[P^\bullet][XC] - k_t[P^\bullet][P^\bullet] \quad (\text{A5})$$

$$\frac{d[P]}{dt} = k_t[P^\bullet][P^\bullet] \quad (\text{A6})$$

The use of method of moments in determining the average properties of polymers produced by ATRP has been thoroughly explained in previous work.^[20] Therefore, only brief discussion is offered in this work. The definition of j^{th} order moments for dormant, radical, and dead polymer chains are shown by Equation (A7)–(A9).

$$[PQ_jX] = \sum_{r=0}^{\infty} r^j [PX_r] \quad (\text{A7})$$

$$[PQ_j^*] = \sum_{r=0}^{\infty} r^j [P_r^*] \quad (\text{A8})$$

$$[PQ_j] = \sum_{r=0}^{\infty} r^j [P_r] \quad (\text{A9})$$

The mass balances of the three chain types, dormant, radical, and dead, are written for chains with r -monomeric units, shown in Equation (A10)–(A12), respectively.

$$\frac{d[PX_r]}{dt} = k_d [P_r^*] [XC] - k_a [PX_r] [C] \quad (\text{A10})$$

$$\frac{d[P_r^*]}{dt} = k_p [M] ([P_{r-1}^*] - [P_r^*]) + k_a [PX_r] [C] - k_d [P_r^*] [XC] - k_t [P^*] [P_r^*] \quad (\text{A11})$$

$$\frac{d[P_r]}{dt} = k_t [P^*] [P_r^*] \quad (\text{A12})$$

The differential equations for zeroth, first, and second moments for the three chain populations could be obtained by combining the mass balances in Equation (A10)–(A12) with the moments' definitions from Equation (A7)–(A9). These differential equations are shown by Equation (A13)–(A21). It should be noted that the zeroth moments yields the overall concentrations of these chains, *i.e.*, Equation (A13)–(A15) are the same as Equation (A4)–(A6).

$$\frac{d[PQ_0X]}{dt} = \frac{d[PX]}{dt} = k_d [PQ_0^*] [XC] - k_a [PQ_0X] [C] \quad (\text{A13})$$

$$\frac{d[PQ_0^*]}{dt} = \frac{d[P^*]}{dt} = k_a [PQ_0X] [C] - k_d [PQ_0^*] [XC] - k_t [PQ_0^*] [PQ_0^*] \quad (\text{A14})$$

$$\frac{d[PQ_0]}{dt} = \frac{d[P]}{dt} = k_t [PQ_0^*] [PQ_0^*] \quad (\text{A15})$$

$$\frac{d[PQ_1X]}{dt} = k_d[PQ_1^*][XC] - k_a[PQ_1X][C] \quad (A16)$$

$$\frac{d[PQ_1^*]}{dt} = k_p[M][PQ_0^*] + k_a[PQ_1X][C] - k_d[PQ_1^*][XC] - k_t[PQ_0^*][PQ_1^*] \quad (A17)$$

$$\frac{d[PQ_1]}{dt} = k_t[PQ_0^*][PQ_1^*] \quad (A18)$$

$$\frac{d[PQ_2X]}{dt} = k_d[PQ_2^*][XC] - k_a[PQ_2X][C] \quad (A19)$$

$$\frac{d[PQ_2^*]}{dt} = k_p[M]([PQ_0^*] + 2[PQ_1^*]) + k_a[PQ_2X][C] - k_d[PQ_2^*][XC] - k_t[PQ_0^*][PQ_2^*] \quad (A20)$$

$$\frac{d[PQ_2]}{dt} = k_t[PQ_0^*][PQ_2^*] \quad (A21)$$

By solving Equation (A13)–(A21) simultaneously, the evolution of zeroth, first, and second order moments with time could be obtained. From these moments, the number-average chain length, weight-average chain length, and polydispersity could be calculated by using Equation (A22), (A23), and (A24), respectively.

$$r_N = \frac{[PQ_1X] + [PQ_1^*] + [PQ_1]}{[PQ_0X] + [PQ_0^*] + [PQ_0]} \quad (A22)$$

$$r_W = \frac{[PQ_2X] + [PQ_2^*] + [PQ_2]}{[PQ_1X] + [PQ_1^*] + [PQ_1]} \quad (A23)$$

$$PDI = \frac{r_W}{r_N} \quad (A24)$$

5 AN EXPLICIT POLYDISPERSITY EQUATION FOR ATRP SYSTEMS

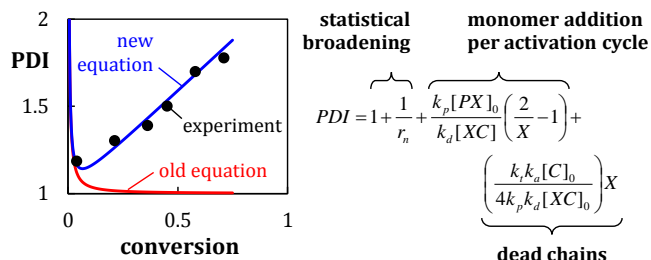
This chapter presents a new polydispersity equation derived for ATRP systems that accounts for the conversion, number of monomer added per activation cycle, and the contribution of dead chains. This is a reproduction of a published manuscript in *Macromolecules* journal, **2015**, 48 (18), p.6440-6449 (doi:10.1021/acs.macromol.5b01525) entitled “A molecular weight distribution polydispersity equation for the ATRP system: Quantifying the effect of radical termination”, with permission from ACS publisher. The Supporting Information referred in the manuscript is included at the end of this chapter.

Author contributions

Erlita Mastan derived the equations and prepared the first draft under Dr. Shiping Zhu’s supervision. Dr. Shiping Zhu revised and finalized the manuscript.

§ 5.1 Abstract

Polydispersity quantifies the breadth of polymer molecular weight distribution, making it an important and frequently quoted chain microstructural



property for characterization. An explicit expression of such an important variable is desirable for ease of calculation, correlation with experiment data, and/or parameter estimation. A review of published literatures shows that great efforts have been put forth by many researchers to derive these equations for various polymerization mechanisms. In atom transfer radical polymerization (ATRP), polydispersity depends on three factors: monomer conversion, number of monomer addition per activation/deactivation cycle, and amount of dead chains. The existing expressions available in the literature only account for, at most, two of these three factors, with the contribution from dead chains commonly neglected. This assumption results in polydispersity monotonically decreasing with conversion, which is often not observed in experiments. In this work, a new equation for polydispersity, which accounts for contributions of all the three aforementioned factors, is proposed. The validity of assumptions involved in the derivation is evaluated by comparing the polydispersity profiles to those simulated by the method of moments. In addition, this new equation is used to correlate several experiment data sets for verification, namely from ATRP of 2-hydroxyethyl methacrylate, methyl methacrylate, and *N*-

isopropylacrylamide, showing better agreement than the existing equation. Although the equation derived here is strictly applicable to homogeneous (bulk and solution) normal ATRP, with further effort it may be extended to other types of ATRP, as well as NMP and RAFT systems.

§ 5.2 Introduction

Polymers are chain molecules rich in microstructural properties that can be tailored for various applications. The properties of polymeric materials depend not only on the average chain microstructural properties, but also on their distributions. For example, narrowly distributed polymers have different material properties from broadly distributed polymers with the same average molecular weight. The broadness of molecular weight distribution (MWD, or chain length distribution CLD, both used interchangeably in this work) is often simply quantified by its polydispersity value, which is also known as polydispersity index, PDI, or dispersity,^[1] instead of the complete MWD. A broader distribution is characterized by a higher PDI value, with PDI of 1 representing a uniform distribution, *i.e.*, all chains have the same molecular weight or chain length.

The polymer MWD is determined by polymerization mechanisms. For example, living anionic polymerization yields narrowly distributed polymer chains,^[2] while conventional free radical polymerization is known to produce broadly distributed polymer chains.^[3] Throughout this article, the term free radical polymerization is

used to refer to the conventional free radical polymerization, for brevity purposes. Another example is atom transfer radical polymerization (ATRP or reversible-deactivation radical polymerization in general), which can be thought of as a middle ground between these two cases.^[4,5] It has been shown that under constant reactants concentrations, the polydispersity in ATRP can fall between living anionic polymerization and free radical polymerization, depending on the reaction conditions.^[6,7]

In a perfectly living anionic polymerization, no termination and no chain transfer reactions are observed and the initiation step is approximately instantaneous (*i.e.*, all polymer chains are initiated at the beginning of polymerization). Individual chains continue to grow throughout the period of polymerization. As derived by Flory, the MWD of this system follows Poisson distribution,^[2] which gives PDI expression shown in Equation (1), with r_n as the number-average chain length of the polymer population.

$$PDI_{LAP} = 1 + \frac{1}{r_n} \quad (1)$$

Contrary to the living anionic polymerization, the initiation step in free radical polymerization occurs throughout the period of polymerization, with each polymer chain growing and terminating almost instantaneously. Typically, it takes less than a second for an individual chain to grow from its initiation to termination. For a small time interval, the concentrations of reactants are almost constant and the MWD of

polymers produced during this period can be expressed by the Flory's most probable distribution.^[8] If termination occurs strictly by disproportionation, the PDI is 2. The cumulative polydispersity expression can be derived to follow Equation (2) by using the method of moments, where X is the monomer conversion. The derivation of this expression can be found in the Supporting Information.

$$PDI_{FRP} = \frac{1}{r_n} + \left(\frac{2}{X} - 1 \right) (-\ln(1-X)) \xrightarrow{X \approx 0} PDI_{FRP} \approx 2 \quad (2)$$

ATRP is a well-studied polymerization method with numerous papers being published every year.^[9] Several expressions for polydispersity have been derived under various assumptions.^[10,11] The PDI expression under constant reactants' concentrations with a perfectly living condition (*i.e.*, no radical termination and chain transfer reactions) was derived for ATRP (or for similar systems), as shown by Equation (3).^[6,7,12-14] Goto and Fukuda treated the polymer chains as "block" polymers in deriving the PDI expression.^[13,14] In Equation (3), the variable z represents the number of activation/deactivation cycles after reaction time t , which can be calculated using Equation (4) for ATRP system. It can be clearly seen from Equation (3) that for the same average chain length, r_n , systems with higher number of activation/deactivation cycles possess lower PDI. Therefore, the higher number of activation/deactivation cycles for every monomer addition in a chain results in a more controlled ATRP. When discussed as a broadening factor, it is usually more convenient to think of this factor as its reverse equivalent, *i.e.*, the number of

monomer addition per cycle. That is to say, more monomer added in one activation/deactivation cycle results in a broader PDI.

$$PDI = 1 + \frac{1}{r_n} + \frac{2}{z} \quad (3)$$

$$z \equiv \int k_a [C] dt \approx k_a [C]_0 t \quad (4)$$

where k_a is the activation rate constant of dormant chains

$[C]_0$ and $[C]$ are the catalyst concentration at the beginning and at time t , respectively

Strictly speaking, termination is unavoidable in a radical polymerization, no matter it is ATRP or free radical polymerization. Recently, the effect of radical termination on the MWD of ATRP was investigated.^[7,12] A PDI expression for constant reactants' concentrations was derived, shown in Equation (5). The variable f_t represents the fraction of chains undergoing termination, instead of deactivation in an activation cycle. Equation (5) shows how the polydispersity of ATRP (as any other controlled radical polymerization) depends on two factors in such systems, namely the number of activation/deactivation cycles (z) and the livingness of the system (quantified by the fraction of living chains, $\exp(-zf_t)$ ^[7]). A high number of activation/deactivation cycles and high livingness are both necessary conditions for a controlled polymerization system giving narrow MWD.^[7,12] When termination is assumed to be negligible, it is easy to see that Equation (5) approaches Equation (3), which was derived under the same condition except for the absence of termination.

$$PDI = 1 + \frac{1}{r_n} + \frac{\sinh(zf_t) - zf_t(1 - f_t)}{\cosh(zf_t) - 1} \xrightarrow{k_t=0} PDI = 1 + \frac{1}{r_n} + \frac{2}{z} \quad (5)$$

$$\text{where } f_t \equiv \frac{k_t [P^\bullet]}{k_d [XC] + k_t [P^\bullet]}$$

k_t and k_d are the rate constants of termination and deactivation
 $[P^\bullet]$ and $[XC]$ are the concentrations of radical and deactivator
 $\sinh(x)$ and $\cosh(x)$ are the hyperbolic sine and cosine of x

At the extreme case of a very large number of activation/deactivation cycles with no termination ($f_t = 0, z \rightarrow \infty$), Equation (5) approaches that of Equation (1). At the other extreme, for the systems with low livingness (*i.e.*, high amount of dead chains, $\exp(-zf_t) \rightarrow 0$), the PDI value approaches 2 at any instant, *i.e.*, Equation (2). This clearly shows how ATRP provides compromise between living anionic polymerization and free radical polymerization. Additionally, this also demonstrates that polymers with either broad or narrow distribution can be synthesized via ATRP by simply adjusting the two factors: the number of activation/deactivation cycles and the livingness. These factors can be simply varied via reactants' types and/or reaction conditions, making ATRP a very suitable method to tailor the MWD of polymer chains.

When the change in monomer concentration is taken into consideration, the PDI expression for a perfectly living ATRP has been shown to follow Equation (6). This equation was first derived by Müller et al for living polymerization with dissociative mechanism, and by Fukuda and Goto for NMP.^[6,14-16] With the exception of monomer concentration, other reactants are assumed to be at constant concentrations in the derivation. It can be shown that the limit of Equation (6) as the conversion is pushed to zero becomes Equation (3) (*i.e.*, at constant monomer concentration).

$$PDI = 1 + \frac{1}{r_n} + \frac{k_p[PX]_0}{k_d[XC]_0} \left(\frac{2}{X} - 1 \right) \xrightarrow{x \approx 0} PDI = 1 + \frac{1}{r_n} + \frac{2}{z} \quad (6)$$

As evident from Equation (6), polydispersity is expected to continually decrease as polymerization progresses when no other factor is present (*i.e.*, absence of termination). However, this monotonically decreasing polydispersity is not usually observed in the experiments.^[17-19] This demonstrates that termination plays an important role in the polydispersity of ATRP and it needs to be quantified. By considering the termination effect on reaction kinetics, Fischer and Fukuda derived another polydispersity expression.^[20,21] However, the resulting equation does not account for the contribution of dead chains on the broadening of polydispersity itself, hence also showing monotonic decrease with increasing conversion.^[10,11]

In this work, we propose a new polydispersity expression that accounts for effects of all the monomer conversion, monomer addition per activation/deactivation cycle, and amount of dead chains in ATRP systems. Thus far, at most only two of the three factors are considered in the polydispersity equations available from the literature. Our derivation was accomplished by *blending* dormant and dead chain subpopulations, where each subpopulation consists of *block* polymers (or also referred to as segments). The resulting equation is compared to the existing equation in the literature to investigate the contributions of different broadening factors. Moreover, the validity of assumptions involved are evaluated by comparing the profile with results from the method of moments under various polymerization

conditions. The derived equation is verified by correlating several ATRP experiment data obtained from the literature, namely, ATRP of 2-hydroxyethyl methacrylate (HEMA),^[17] methyl methacrylate (MMA),^[18] and *N*-isopropylacrylamide (NIPAM).^[19]

§ 5.3 Mathematical formulations

As illustrated in Figure 5-1, as polymerization proceeds in living anionic polymerization, the polymer chains grow longer and longer, while the number of chains stays constant. Therefore, the overall polymer chain population can be thought of as *block* polymers of various segments formed at different time intervals. On the other hand, Figure 5-2 depicts how the number of chains in free radical polymerization keeps increasing with reaction time, since more and more chains are being born, grew, and terminated at every time interval. Therefore, the overall chains can be thought of as a *blend* of the subpopulations, which consist of dead chains formed at different time intervals throughout the polymerization.

In ATRP, the polymer chains grow in a similar fashion as living anionic polymerization, where the chains grow longer and longer as polymerization progresses. However, termination is unavoidable due to the radical nature in ATRP, thus causing some of the chains to stop growing. The number of dead chains increases throughout the polymerization, similar to free radical polymerization. Therefore, the overall chain synthesized via ATRP can be thought of as a *blend* of the dead and

dormant polymer mixtures, where each mixture consists of polymers possessing different number of segments (or *blocks*), as depicted in Figure 5-3.

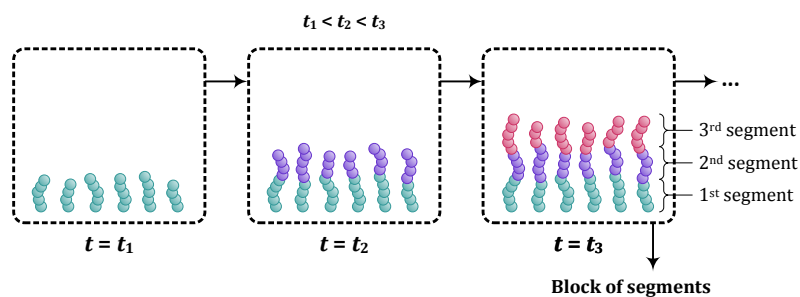


Figure 5-1. Initiation and growth steps in a perfectly living anionic polymerization

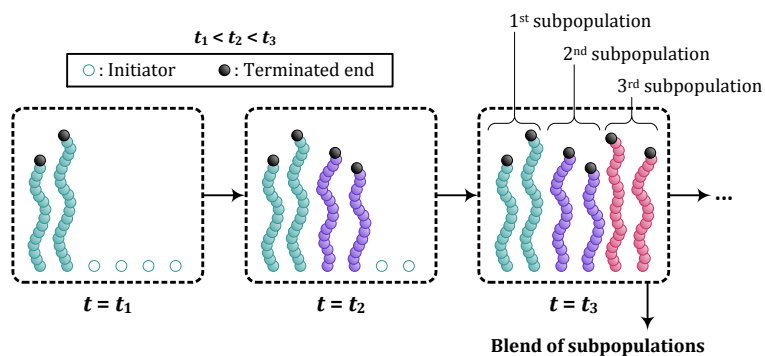


Figure 5-2. Initiation, growth, and termination steps in a free radical polymerization

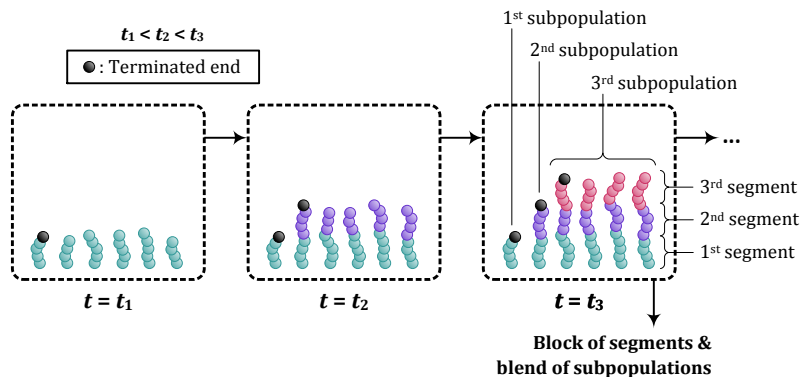


Figure 5-3. Initiation, growth, and termination steps in an ATRP

The *blend* and *block* strategy to derive the PDI expression for ATRP systems is implemented by discretizing the polymerization time into shorter time intervals. Based on this discretization, the overall polymer population can be divided into multiple subpopulations, depending on when it is terminated. For example, the polymer population can be divided into three subpopulations if the polymerization time is divided into three time intervals, as illustrated in Figure 5-4. The first subpopulation contains polymer chains that are terminated in the first time interval (between 0 and t_1). The second subpopulation contains polymer chains that are terminated in the second time interval (terminated between t_1 and t_2). This subpopulation can be thought of as diblock polymer (or block polymer with two *blocks* or segments). Finally, the third subpopulation contains polymer chains that are still growing in the third time interval (can either be dormant or terminated at the end). This subpopulation can be viewed as triblock polymer (*block* polymer with three segments). The overall polymer population synthesized is simply the *blend* of these subpopulations.

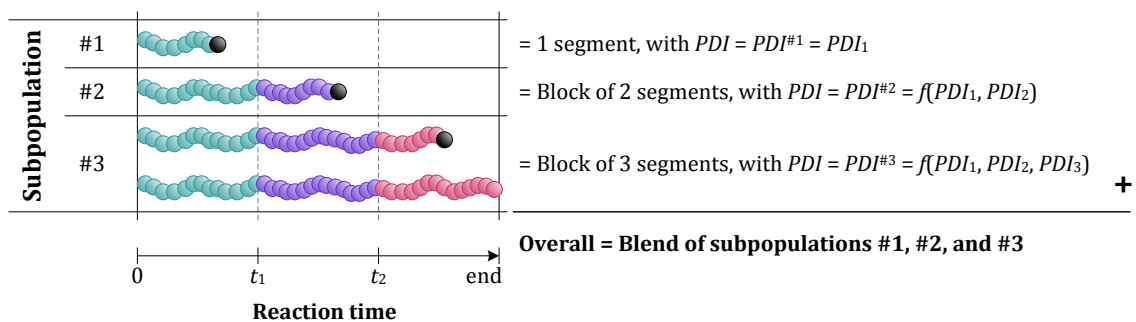


Figure 5-4. Use of *blend* and *block* strategy for an ATRP system with three subpopulations

As the reaction time is divided into more intervals, the duration of each interval becomes shorter. For a sufficiently short time interval, the concentration of reactants in that interval can be assumed to be constant. By using the same reaction mechanism as that used in the previous work, the polydispersity of the segment grown at that time interval can be obtained.^[7,12] For the purpose of simplicity, the polydispersity of each segment is assumed to be equal, regardless if it remains dormant or undergoes termination in that time interval, *i.e.*, polydispersity of the i^{th} segment is given by Equation (7) (follows Equation (3) from the literature). This approximation is valid for ATRP systems with sufficiently fast initiation.

$$PDI_i = 1 + \frac{1}{r_{n,i}} + \frac{2}{\Delta Z_i} \quad (7)$$

Using the *block* strategy, the polydispersity of subpopulation # n can be expressed as a function of the chain microstructural properties of each segment, shown by Equation (8). This equation can be obtained by relating the distributions of each segment to that of the block polymer, as provided in the Supporting Information. An equivalent relation has been used by Goto and Fukuda.^[13,14]

$$PDI^{\#n} = 1 + \frac{1}{(r_n^{\#n})^2} \sum_{i=1}^n (r_{n,i})^2 (PDI_i - 1) \quad (8)$$

where $r_{n,i}$ and PDI_i are the number-average chain length and polydispersity of segment i , respectively

These subpopulations are then *blended* to find the resulting polydispersity of the mixture. Based on the known equation for a blend of polymer mixtures, the polydispersity of the whole polymer population can be calculated using Equation (9) (for a blend of N subpopulations). For the first $N-1$ subpopulations, the mole fractions of these subpopulations are simply the fractions of dead chains formed at the respective time intervals (out of all chains). The known equation for a blend of polymer is commonly written on weight-basis, while it is more convenient in our derivation to use the mole-basis. The transformation to the mole-basis is included in the Supporting Information.

$$PDI^{blend} = \frac{1}{(r_n^{blend})^2} \sum_{i=1}^N n^{#i} (r_n^{#i})^2 PDI^{#i} \quad (9)$$

where $n^{#i}$, $r_n^{#i}$, and $PDI^{#i}$ are the mole fraction, number-average chain length, and polydispersity of subpopulation $\#i$, respectively

At this point, it is convenient to define variable β in Equation (10), which quantifies the number of monomer addition per activation/deactivation cycle. Higher β results in a broader polydispersity.

$$\beta \equiv \frac{k_p[M]}{k_d[XC] + k_t[P^\bullet]} \approx \frac{k_p[M]}{k_d[XC]} \quad (10)$$

Using the combined *blend* and *block* strategy outlined here and taking the limit of each time interval to be zero (or equivalently an infinite number of intervals, $N \rightarrow \infty$), the summation sign becomes integration. Therefore, the polydispersity of polymers synthesized by ATRP can be written as Equation (11). This equation has been

integrated numerically for systems with fast initiation step, giving results that agree well to those obtained via the method of moments, thus validating the derivation strategy used here. Each of the term in this equation is responsible for broadening the distribution since they are always positive. The broadening factors related to these terms are discussed in the next section.

$$\begin{aligned}
 PDI &= 1 + \frac{1}{r_n} + \frac{2}{r_n} \left(\frac{1}{X} \int_0^x \beta dx \right) + \left(\frac{2}{X^2} \int_0^x \left(\int_0^x \frac{[P]}{[PX]} dx \right) dx \right) \quad \text{or} \\
 PDI &= 1 + \frac{1}{r_n} + \left(\frac{2}{X^2} \frac{k_p [PX]_0}{k_d} \int_0^x \frac{(1-x)}{[XC]} dx \right) + \left(\frac{2}{X^2} \int_0^x \left(\int_0^x \frac{[P]}{[PX]} dx \right) dx \right) \quad (11)
 \end{aligned}$$

It can be easily seen that in the absence of termination, *i.e.*, $[P] = 0$, the fourth term disappears and Equation (11) can be integrated to give Equation (6). For the systems following a first-order kinetic behaviour, the amount of dead chains has been expressed as a function of conversion (and/or time).^[22] Therefore, the polydispersity can be simplified as Equation (12) using Gaussian quadrature with 1 node. The detailed derivation is included in the Supporting Information.

$$PDI = 1 + \frac{1}{r_n} + \frac{k_p [PX]_0}{k_d [XC]} \left(\frac{2}{X} - 1 \right) + \left(\frac{k_t k_a [C]_0}{4k_p k_d [XC]_0} \right) X \quad [XC]_0 \neq 0 \quad (12)$$

Equation (12) is the most desired form of polydispersity as a function of conversion and it is convenient to use for experimentalists. Every parameter in this equation is known, either from experiment condition (initiator concentration $[PX]_0$, catalyst concentration $[C]_0$, and deactivator concentration $[XC]_0$) or as reaction rate constants

(propagation k_p , activation k_a , deactivation k_d , and termination k_t). The propagation and termination rate constants are available for various monomer systems from polymer handbooks. If the activation and deactivation rate constants are known, this equation has predictive power. On the other hand, if these parameters are not known, this equation can be used to correlate the experiment data to extract the k_a and k_d separately. It should also be emphasized that Equation (12) is applicable for homogeneous (bulk or solution) normal ATRP. With some efforts, similar equation can be obtained for other ATRP variants (*e.g.*, AGET, ARGET, ICAR ATRP), as well as for nitroxide-mediated radical polymerization (NMP) systems. Extension to reversible addition-fragmentation chain transfer radical (RAFT) polymerization may require much more effort because of the presence of intermediate radicals and the nature of continuous initiation.

§ 5.4 Results and discussions

The polydispersity expression, Equation (12), derived in this work is compared with the existing expression, Equation (6), to analyze the contribution of each broadening factor. Moreover, the error due to the assumptions behind these equations are investigated by using simulated PDI values from the method of moments as a reference. The method of moments is a simple yet powerful tool in modeling polymerization kinetics.^[23] The results from the method of moments are free from most assumptions, except for the constant reaction rate parameters. Having said that, this method requires simultaneously solving a set of ordinary differential equations,

which are often not solvable analytically. The two PDI equations are also compared for correlation of several experimental data published in the literature. For comparison with experimental data, the reaction rate constants are first estimated by their typically reported values in the literature. These values are then adjusted by correlating the conversion kinetics data using the method of moments. The estimated reaction rate constants are then used in the calculation of polydispersity profiles.

5.4.1 Analysis of the derived PDI equations

The assumptions involved in derivations of various polydispersity equations for ATRP are summarized in Table 5-1. Other assumptions involved in these derivations are constant reaction rate parameters (not affected by neither chain length nor by conversion) and the absence of other side reactions (chain transfer, termination by combination, etc.). Other common assumptions among these equations are instantaneous initiation and constant dormant, radical, catalyst, and deactivator concentrations. It can be shown that when termination is considered negligible ($k_t = 0$), Equation (5) and (12) are reduced to Equation (3) and (6), respectively. In this work, Equations (6) and (12) will be compared because they both account for the effect of conversion.

Table 5-1. Comparison of the underlying assumptions in the derivation of various polydispersity expressions for ATRP systems

Polydispersity expressions	$[M]$	$k_t = k_{td}$	Sources
Equation (3)	$\neq f(t)$	$= 0$	[6,7,13,14]
Equation (5)	$\neq f(t)$	$\neq 0$	[7]
Equation (6)	$= f(t)$	$= 0$	[6,14,15]
Equation (12)	$= f(t)$	$\neq 0$	This work

Part of the third term of Equation (11) that is inside the brackets represents the average of number of monomer addition per activation/deactivation cycle throughout the polymerization. It is easy to see that the higher this number is, the broader the polydispersity will be. Thus, this broadening term can be attributed to the number of monomer addition per cycle, β . In a perfectly living polymerization, the monomer concentration decreases as the polymerization proceeds, while the catalyst and deactivator concentrations remain relatively constant. This leads to the decrease of average β with increasing conversion, thus lowering its contribution to PDI. This explains the monotonic decrease of polydispersity profile with conversion in a perfectly living polymerization system, as predicted by Equation (6). It can also be observed from a mathematics standpoint, where the derivative of this term with respect to X is always negative (*i.e.*, decreasing term). This effect of the monomer addition per activation/deactivation cycle, *i.e.*, the third term of Equation (11), was referred to as loss of *control* in our previous works.^[7,12] Another indirect effect of conversion on polydispersity is through chain length. As polymerization proceeds and

chains grow longer, the polydispersity decreases because the relative length differences between the chains decrease.

On the other hand, it is easy to see that the fourth term of Equation (11) represents the contribution of dead chains on the distribution broadening. This term does not depend on how fast or slow the reaction proceeds, but only on the dead chain fraction at a given conversion. The effect of dead chains on polydispersity is easily pictured. Since dead chains stop growing, it results in an uneven growth for the overall population, thus broadening the distribution. Therefore, it makes sense to observe how the contribution of dead chains to polydispersity is cumulative and monotonically increase with conversion.

At the beginning of polymerization, there is only small amount of dead chains, thus contributing insignificantly to the polydispersity. Therefore, the number of monomer addition per cycle dominates the PDI value at this early stage, as it decreases rapidly to reach its minimum value. However, as the contribution from monomer addition per cycle decreases with conversion, the broadening due to dead chains starts to dominate in determining the polydispersity value. This leads to the commonly observed trend of early decrease in polydispersity, followed by plateau or a slow increase at high conversions (depending on how far the persistent radical effect suppresses the termination rate). Experimentally speaking, this trend may be further complicated or masked due to diffusion-controlled termination and deactivation,

where the latter may occur at intermediate to high conversion.^[24] Diffusion-controlled termination results in lower amount of dead chains, while diffusion-controlled deactivation broadens polydispersity,^[25] because it increases both the monomer addition per cycle and the amount of dead chains.

5.4.2 Comparison with the method of moments

The predicted polydispersity values from Equations (6) and (12) are compared with the results obtained from the method of moments. These explicit expressions allow easy calculation of polydispersity profiles with simple and widely available spreadsheet software (*e.g.*, Microsoft Excel). On the other hand, even though the method of moments provides results that are free from most assumptions, it requires the use of software that can perform numerical integration of a set of stiff ordinary differential equations. The differential equations for the method of moments are included in the Supporting Information. The simulation parameters are chosen around the range of those typically found for ATRP systems and listed on Table 5-2. The predictions are compared for three different values of activation rate constant (k_a) and equilibrium constant (K_{ATRP}).

Table 5-2. Reaction parameters used in the comparison of polydispersity predictions with numerical integration of moments' balances

Simulation parameters	Values
$[M]_0$ (M)	3.0
$[M]_0 : [PX]_0 : [C]_0 : [XC]_0$	500 : 1 : 1 : 0.2
k_p ($M^{-1} s^{-1}$)	1600
k_t ($M^{-1} s^{-1}$)	1×10^8
k_a ($M^{-1} s^{-1}$)	0.5, 5, or 50
$K_{ATRP} (\equiv k_a/k_d)$	1×10^{-6} , 5×10^{-6} , or 1×10^{-5}

By varying activation rate constant at the same equilibrium constant, the assumption of instantaneous initiation can be investigated. For this comparison, the calculations are done with the parameters from Table 5-2 at equilibrium constant of 5×10^{-6} . The variation of k_a does not significantly affect the kinetics and the dead chain formation, as evident from Figure 5-5. The comparison of polydispersity profiles from the explicit equations and the method of moments for these cases are shown in Figure 5-6. At a higher k_a value, the initiation is faster thus resulting in a better agreement of the explicit equations with the method of moments. Moreover, the profiles calculated from the new expression (Equation (12), represented by the blue lines) conform better with the method of moments compared to those calculated by Equation (6), shown by the red dotted lines.

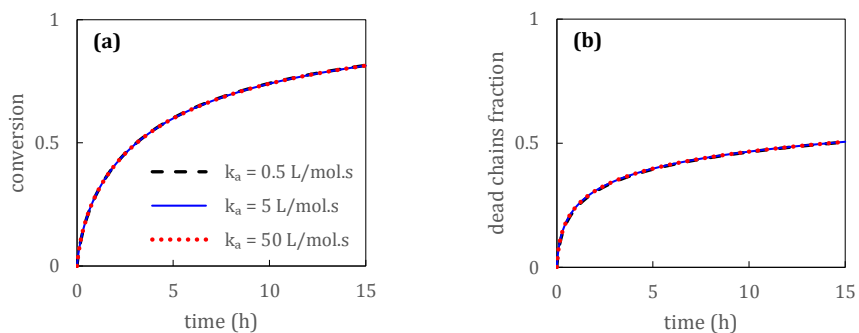


Figure 5-5. Kinetic and dead chain fraction plots for typical ATRP systems under different activation rate constants with $K_{ATRP} = 5 \times 10^{-6}$

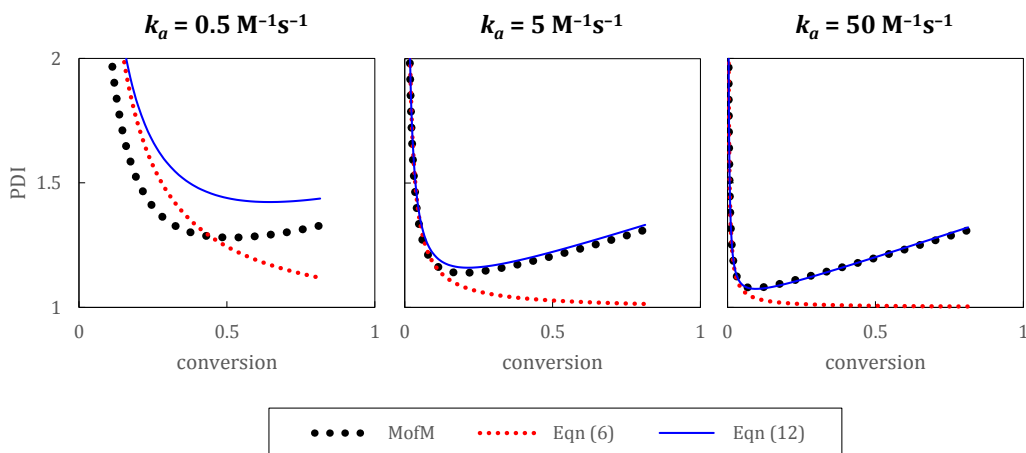


Figure 5-6. Polydispersity profiles for typical ATRP systems under different activation rate constants with $K_{ATRP} = 5 \times 10^{-6}$

The polydispersity profiles are also calculated from Equation (6) and (12) for three different equilibrium constant values at activation rate constant of $5 \text{ M}^{-1}\text{s}^{-1}$, as plotted in Figure 5-7. The fractions of terminated chains are obtained from the integration of mass balances after 15 hours of reactions. Similar to the previous comparison, it can be seen that the new equation (Equation (12)) provides more accurate predictions

than the existing expression (Equation (6)) in all the three cases when the method of moments is used as a reference.

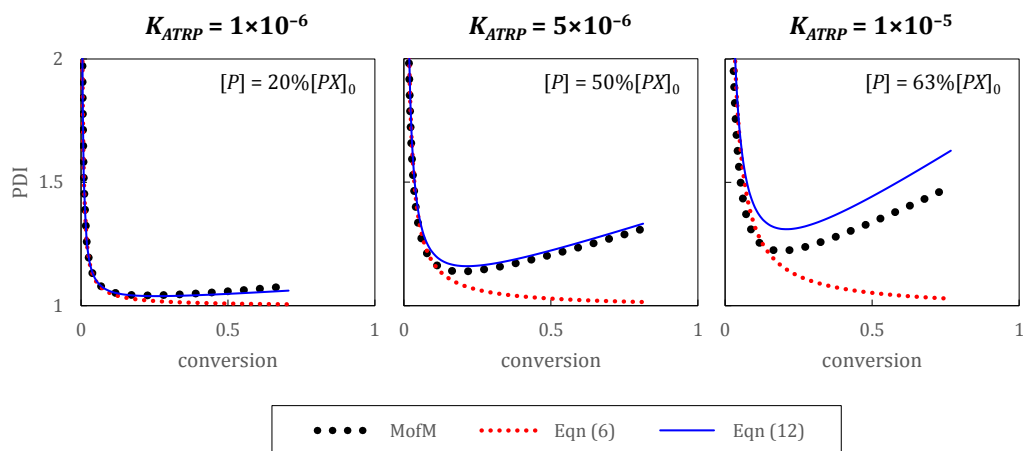


Figure 5-7. Polydispersity profiles for typical ATRP systems under different equilibrium constants with $k_a = 5 \text{ M}^{-1}\text{s}^{-1}$

The accuracy of these explicit equations is lower for cases with higher equilibrium constants. This is due to the assumption of constant reactants' concentrations made in the derivation, *i.e.*, the persistent radical effect (PRE) is neglected. This assumption results in an overestimation of termination (thus overestimate its contribution to the PDI broadening), because the deactivator concentration actually increases due to PRE, which in turn suppresses the termination. This discrepancy is more pronounced in systems with higher termination (higher equilibrium constant), because there is more deactivator accumulated in those systems.

5.4.3 Polymerization of HEMA

The kinetic and polydispersity data for ATRP of 2-hydroxyethyl methacrylate (HEMA) were collected from Beers et al.^[17] The polymerization was conducted at room temperature in DMF with copper (I) bromide and copper (II) bromide as catalyst and deactivator. The initiator and ligand chosen were ethyl 2-bromoisobutyrate and bipyridine, respectively. Other experiment details can be found in the original publication. Differential mass balances were used to correlate the kinetic data of this system to estimate the reaction rate parameters, as shown in Figure 5-8.

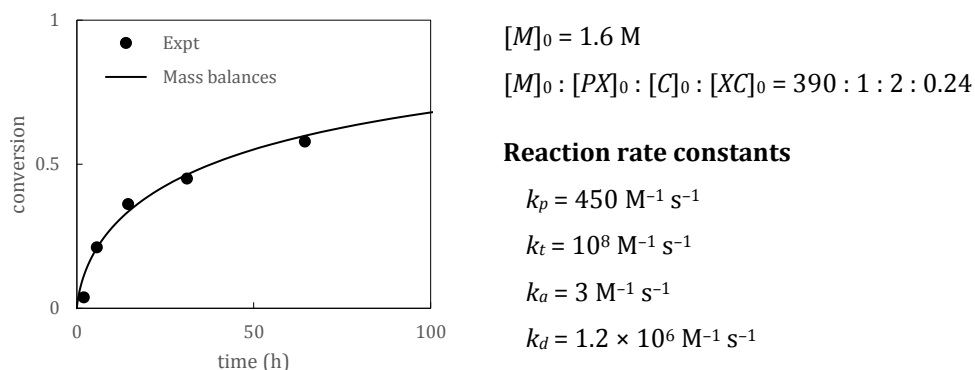


Figure 5-8. Estimation of the reaction rate parameters for ATRP of HEMA in DMF at room temperature from the kinetic data. Experiment data were obtained from Beers et al.^[17]

The estimated reaction rate constants from the kinetic data correlation are used in Equations (6) and (12) to obtain prediction of the polydispersity. These predictions are compared with the polydispersity data from the experiment, as shown in Figure 5-9. Equation (6) predicts continuous decreases in PDI with increasing conversion, which disagree with the reported experiment data. Experiment shows increasing

value of polydispersity with conversion, which can be attributed to the presence of dead chains, as predicted by Equation (12).

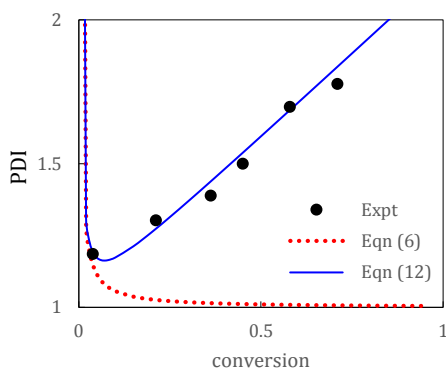


Figure 5-9. Comparison of experimentally obtained polydispersity with the predictions from Equations (6) and (12) for ATRP of HEMA in DMF at room temperature.

Experiment data were obtained from Beers et al.^[17]

Another possible cause of the polydispersity increase is diffusion-controlled deactivation reaction. This reaction has been proposed to cause the increase in polydispersity of polymers synthesized by bulk ATRP at higher conversion.^[25] However, the data used here was collected from experiment conducted under dilute conditions (bulk concentration of HEMA is 8.2 M, whereby the experiment data were collected for ATRP at 1.6 M HEMA concentration). Therefore, diffusion-controlled deactivation is ruled out as the cause of increasing trend observed in this system.

5.4.4 Polymerization of MMA

The kinetics and polydispersity data for ATRP of methyl methacrylate (MMA) were collected from the study by Gromada et al.^[18] The ATRP was conducted at 90°C in anisole (50% v/v) with copper (I) chloride and copper (II) chloride as catalyst and deactivator. The initiator and ligand chosen were ethyl 2-bromoisobutyrate and BzA₆TREN. Other experiment details can be found in the original publication. Differential mass balances were used to correlate the kinetic data of this system to estimate the reaction rate parameters, as shown in Figure 5-10. The propagation rate constant, k_p , is assumed to be equal to the bulk polymerization and calculated based on the equation proposed in the kinetic study of MMA polymerization.^[26]

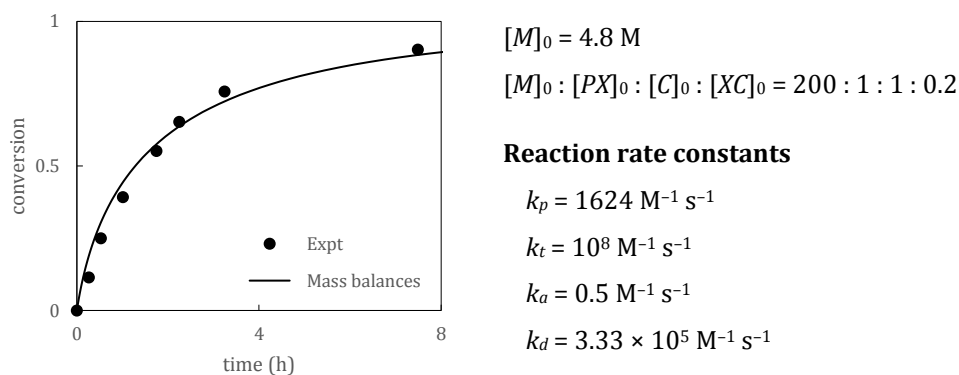


Figure 5-10. Estimation of the reaction rate parameters for ATRP of MMA in anisole at 90°C from the kinetic data. Experiment data were obtained from Gromada et al.^[18]

Similar to previous section, the estimated rate constants from the kinetic data are used in Equations (6) and (12) to obtain PDI predictions, which are then compared to the experiment data. These profiles are plotted in Figure 5-11, with the

experimentally measured polydispersity showing a plateau at a value of approximately 1.15. Similar to the previous case, Equation (12) provides better correlation with the experiment data than Equation (6) does.

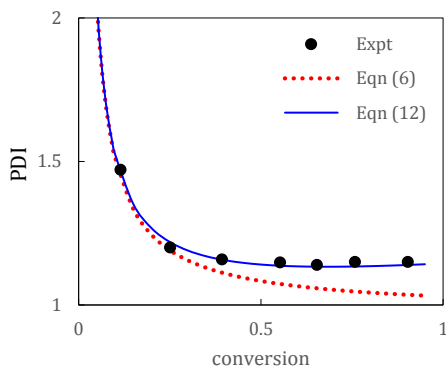


Figure 5-11. Comparison of experimentally obtained polydispersity with the predictions from Equations (6) and (12) for ATRP of MMA in anisole at 90°C. Experiment data were obtained from Gromada et al.^[18]

5.4.5 Polymerization of NIPAM

The kinetics and polydispersity data for ATRP of *N*-isopropylacrylamide (NIPAM) were collected from the experimental work of Bontempo et al.^[19] The polymerization was conducted at 20°C in dimethyl sulfoxide (DMSO) with copper (I) chloride and copper (II) chloride as catalyst and deactivator. Biotinylated initiator and Me₆TREN ligand were used in the polymerization. Other experiment details can be found in the original publication. Differential mass balances were used to correlate the kinetic data of this system to estimate the reaction rate parameters, as shown in Figure 5-12.

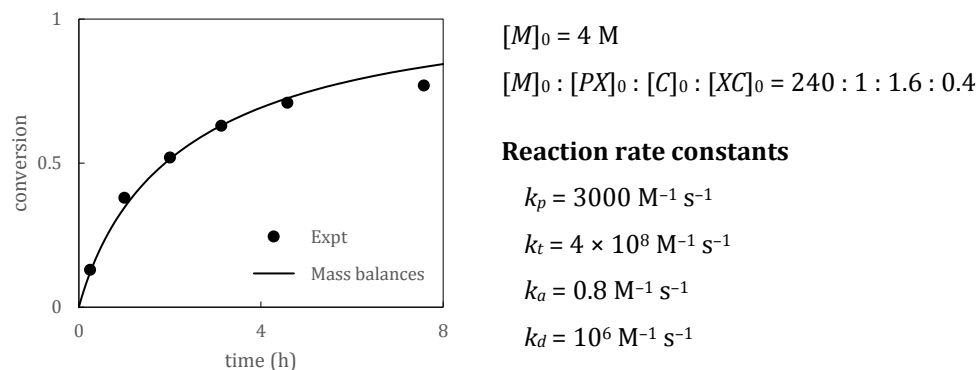


Figure 5-12. Estimation of the reaction rate parameters for ATRP of NIPAM in DMSO at 20°C from the kinetic data. Experiment data were obtained from Bontempo et al.^[19]

Similar to the previous sections, the estimated reaction rate constants from the kinetic data are used in Equations (6) and (12) to obtain prediction of the polydispersity. These predictions are compared with the experiment data, as shown in Figure 5-13, to again show better performance of Equations (12) compared to Equation (6) in predicting the experiment trend. Up to moderate conversions, Equation (12) provides a decent prediction for the experiment data. However, at higher conversions, a rapid increase in polydispersity can be observed in the experiment, which is neither predicted by Equation (6) nor Equation (12). This increase may be attributed to the increase in solution viscosity, thus resulting in complication due to diffusion-controlled reactions.

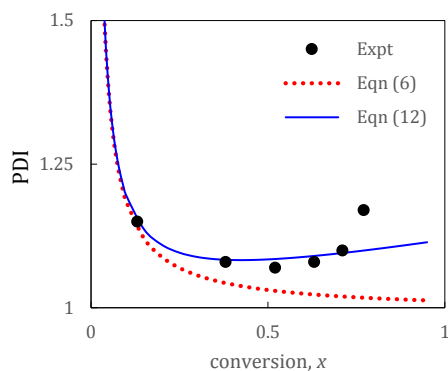


Figure 5-13. Comparison of experimentally obtained polydispersity with the predictions from Equations (6) and (12) for ATRP of NIPAM in DMSO at 20°C. Experiment data were obtained from Bontempo et al.^[19]

§ 5.5 Conclusion

There are three known factors affecting the polydispersity in ATRP system, namely monomer conversion, monomer addition per activation/deactivation cycle, and amount of dead chains. In this work, an easy-to-use explicit expression for polydispersity (Equation (12)) that accounts for all the three factors is derived by using *blend* and *block* strategy. The prediction from this equation is compared with the widely used PDI expression (Equation (6)) that accounts for the first two factors (*i.e.*, including monomer conversion and monomer addition per cycle, but excluding dead chains). Comparison is first done with the simulated profiles from the method of moments. The results from the method of moments are used as the benchmarks to evaluate the validity of assumptions made in the derivation. The newly derived Equation (12) agrees much better with the method of moments than the existing Equation (6).

In addition, these two equations are also used to correlate several experiment data sets from the literature, namely for the ATRP of HEMA, MMA, and NIPAM. For all three data sets, the new equation (Equation (12)) provides better correlations than the existing PDI equation (Equation (6)). This is because the polydispersity will monotonically decrease with conversion when the contribution of dead chains is neglected. Therefore, when the measured polydispersity does not decrease with conversion but showing an increase or plateau instead, the presence of dead chains in the system must be accounted for in the broadening of the polydispersity.

§ 5.6 Supporting Information

Included in this supporting information are:

- Polydispersities of block polymers and blend of polymers
- Detailed derivation using *blend* and *block* strategy
- Differential mass and moments balances

5.6.1 Polydispersities of block polymers and blend of polymers

Derivations of the polydispersity of block polymers as a function of those of the segments and the polydispersity of a blend of polymers as a function of those of the subpopulations are presented.

Block polymers

Derivation will first be given for diblock polymers (polymer with two segments, each with a known polydispersity), as depicted in Figure A5-1. The molecular weight distribution of the block polymers can be written as a function of those of the segments, shown in Equation (S-1). It follows from this equation and their respective definitions that the number- and weight-average chain lengths of the block polymers can be expressed as shown in Equation (S-2) and (S-3), respectively. Simplification method for the double summations in these equations can be found in another work.^[23]

$$n^{block}(r) = \sum_{s=0}^r [n_1(s) \times n_2(r-s)] \quad (S-1)$$

$$r_n^{block} \equiv \sum_{r=0}^{\infty} [r \times n^{block}(r)] = \sum_{r=0}^{\infty} r \sum_{s=0}^r [n_1(s) \times n_2(r-s)] = r_{n,1} + r_{n,2} \quad (S-2)$$

$$r_w^{block} \equiv \frac{\sum_{r=0}^{\infty} [r^2 \times n^{block}(r)]}{\sum_{r=0}^{\infty} [r \times n^{block}(r)]} = \frac{1}{r_n^{block}} \sum_{r=0}^{\infty} r^2 \sum_{s=0}^r [n_1(s) \times n_2(r-s)]$$

$$r_w^{block} = \frac{1}{r_n^{block}} (r_{w,1}r_{n,1} + r_{w,2}r_{n,2} + 2r_{n,1}r_{n,2}) \quad (S-3)$$

where $r_{n,i}$ and $r_{w,i}$ are the number- and weight-average chain lengths of the i^{th} segment, respectively ($i = 1, 2$)

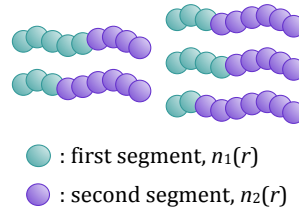


Figure A5-1. Diblock polymers

Polydispersity of the resulting block polymer can be expressed as those possessed by the segments by using its definition, Equation (S-2), and Equation (S-3), as shown in Equation (S-4).

$$PDI^{block} \equiv \frac{r_w^{block}}{r_n^{block}} = 1 + \frac{1}{(r_n^{block})^2} [(r_{n,1})^2 (PDI_1 - 1) + (r_{n,2})^2 (PDI_2 - 1)] \quad (S-4)$$

where PDI_i is the polydispersity of the i^{th} segment ($i = 1, 2$)

Following similar derivation, it can be shown that the number-average chain length and polydispersity of block polymers with N -segments follow Equation (S-5) and (S-6), respectively.

$$r_n^{block} = \sum_{i=1}^N r_{n,i} \quad (S-5)$$

$$PDI^{block} = 1 + \frac{1}{(r_n^{block})^2} \sum_{i=1}^N (r_{n,i})^2 (PDI_i - 1) \quad (S-6)$$

Blend of polymers

When blending two or more polymer subpopulations (as depicted in Figure A5-2 for a mixture of 2 subpopulations), the number-average chain length ($r_{n,i}$), polydispersity (PDI_i), and weight fraction (w_i , or mole fraction, n_i) of each subpopulation determines

the resulting polydispersity. The widely used equations for the number-average and polydispersity of a blend of N subpopulations are given by Equation (S-7) and (S-8) for weight-basis calculation, respectively.

$$\frac{1}{r_n^{blend}} = \sum_{i=1}^N \frac{w_i}{r_{n,i}} \quad (\text{S-7})$$

$$PDI^{blend} = \left(\sum_{i=1}^N w_i \times r_{w,i} \right) \left(\sum_{i=1}^N \frac{w_i}{r_{n,i}} \right) \quad (\text{S-8})$$

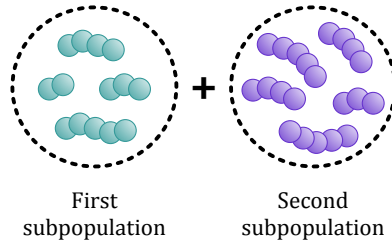


Figure A5-2. Blend of two polymer subpopulations

In this work, it is more convenient to use the mole fractions instead of the weight fractions of the subpopulations, where these two are related by Equation (S-9). Therefore, Equation (S-7) and (S-8) are rewritten as Equation (S-10) and (S-11) for mole-basis relations, respectively.

$$n_i = w_i r_n^{blend} / r_{n,i} \quad (\text{S-9})$$

$$r_n^{blend} = \sum_{i=1}^N (n_i \times r_{n,i}) \quad (\text{S-10})$$

$$PDI^{blend} = \frac{1}{(r_n^{blend})^2} \sum_{i=1}^N n_i (r_{n,i})^2 PDI_i \quad (\text{S-11})$$

5.6.2 Detailed derivation using *blend* and *block* strategy

In this derivation, the polymerization period is divided into several time intervals (Δt_i). Similar approach has been used to obtain the full molecular weight distribution of ATRP system.^[12] As time intervals are taken to the extreme limit of zero, the polydispersity expression can be obtained via integration. The polymers are treated as a *blend* of *block* polymers. Each segment of the block polymers possess a certain distribution that can be expressed based on our previous work.^[27] The terminated chains are treated separately from the dormant, allowing properties of the whole polymer population to be obtained by blending the dormant and dead chains subpopulations. Goto and Fukuda introduced the use of block polymer to treat polymer chains in a perfectly living nitroxide-mediated polymerization system.^[13] This is first derived for perfectly living systems as a proof of concept, followed by derivation for systems with termination.

Without termination

When considering a perfectly living system, all chains continue to grow from the start of the polymerization to the end. Previous work showed that the polymer segment grown at an interval with constant reactants concentrations possess number-average chain length and polydispersity as given by Equation (S-12) and (S-13).^[27]

$$r_{n,i} = \frac{k_a[C]_i}{k_d[XC]_i} k_p[M]_i \Delta t_i \quad (\text{S-12})$$

$$PDI_i = 1 + \frac{1}{r_{n,i}} + \frac{2}{k_a[C]_i \Delta t_i} \quad (S-13)$$

In order to obtain the polydispersity expression, the polymerization time is divided into N intervals, where each interval produces chain segment with properties given by Equation (S-12) and (S-13). The polymer can then be considered as block polymers with N segments. For block polymers, the number-average chain length and polydispersity can be expressed in terms of the properties possessed by each block as shown in Equation (S-5) and (S-6) from the previous section. The properties of each block of the polymer from Equation (S-12) and (S-13) can be substituted into these equations to give Equation (S-14) and (S-15).

$$r_n^{block} = \sum_{i=1}^N r_{n,i} = \sum_{i=1}^N \frac{k_a[C]_i}{k_d[XC]_i} k_p[M]_i \Delta t_i \quad (S-14)$$

$$\begin{aligned} PDI^{block} &= 1 + \frac{1}{(r_n^{block})^2} \sum_{i=1}^N (r_{n,i})^2 (PDI_i - 1) \\ &= 1 + \frac{1}{r_n^{block}} + \frac{2}{(r_n^{block})^2} \sum_{i=1}^N \frac{(k_p[M]_i)^2}{(k_d[XC]_i)^2} k_a[C]_i \Delta t_i \end{aligned} \quad (S-15)$$

By taking the limit of time interval to be zero (*i.e.*, infinitely many intervals), the summations become integrations. Combining this with the equilibrium relation for radical concentration ($[P^*] = k_a[PX][C]/k_d[XC]$) and mass balances, the expressions for the number-average chain length and polydispersity of the block polymer can be shown to follow Equation (S-16) and (S-17). The concentrations of reactants other than monomer are assumed to be constant in this case.

$$\begin{aligned}
 r_n &= \lim_{\Delta t_i \rightarrow 0} r_n^{block} = \lim_{\Delta t_i \rightarrow 0} \left(\sum_{i=1}^N \frac{k_a [C]_i}{k_d [XC]_i} k_p [M]_i \Delta t_i \right) \\
 &= \int_0^t \frac{k_a [C]}{k_d [XC]} k_p [M] dt = \frac{[M]_0 X}{[PX]_0}
 \end{aligned} \tag{S-16}$$

$$\begin{aligned}
 PDI &= \lim_{\Delta t_i \rightarrow 0} PDI^{block} = 1 + \frac{1}{r_n} + \frac{k_p [PX]_0}{k_d [XC]_0} \left(\frac{2}{X} - 1 \right) \\
 &= 1 + \frac{1}{r_n} + \frac{-\ln(1-X)}{k_a [C]_0 t} \left(\frac{2}{X} - 1 \right)
 \end{aligned} \tag{S-17}$$

Equation (S-17) for polydispersity derived in this perfectly living ATRP case is equivalent to those derived by other researchers using different approaches for living polymerization systems.^[14,15] This agreement serves as validation of the derivation strategy used in this work.

With termination

When termination is taken into account in the derivation, the number-average chain length and polydispersity of chain segment grown at time interval i can be shown to follow Equation (S-18) and (S-19). The derivation of these expressions and their physical significance can be found in our previous publication.^[27]

$$r_{n,i} = \frac{k_p [M]_i}{k_t [P^\bullet]_i} (1 - \exp(-\Delta z_i f_{t,i})) \tag{S-18}$$

$$PDI_i = 1 + \frac{1}{r_{n,i}} + \frac{1 - \exp(-2\Delta z_i f_{t,i}) - 2\Delta z_i f_{t,i} (1 - f_{t,i}) \exp(-\Delta z_i f_{t,i})}{(1 - \exp(-\Delta z_i f_{t,i}))^2} \tag{S-19}$$

where: $\Delta z_i \equiv k_a [C]_i \Delta t_i$ and $f_{t,i} \equiv \frac{k_t [P^\bullet]_i}{k_d [XC]_i + k_t [P^\bullet]_i}$

As the time interval is taken to approach zero, these equations can be simplified to be Equation (S-20) and (S-21), which are the same as those found in a perfectly living system (Equation (S-12) and (S-13)). For simplicity, the dead chain fraction will be represented by T (for terminated fraction), while the dormant fraction is referred to as D ($= 1 - T$). Moreover, the properties of the chain segment are assumed to be approximately the same for short time interval, regardless if it's a dead or dormant chain, to simplify the derivation process. This assumption is valid for systems with instantaneous initiation.

$$\lim_{\Delta t_i \rightarrow 0} r_{n,i} = \frac{k_a [C]_i}{k_d [XC]_i} k_p [M]_i \Delta t_i = \frac{[M]_0 \Delta x_i}{[PX]_i} \quad \text{for } k_d [XC]_i \gg k_t [P^*]_i \quad (\text{S-20})$$

$$\lim_{\Delta t_i \rightarrow 0} PDI_i = 1 + \frac{1}{r_{n,i}} + \frac{2}{k_a [C]_i \Delta t_i} \quad (\text{S-21})$$

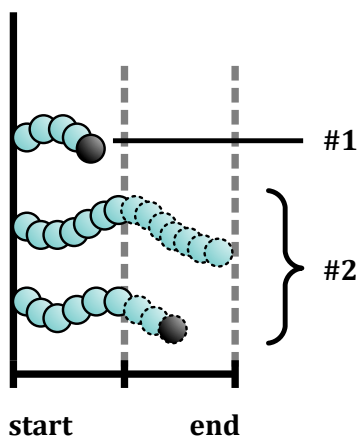


Figure A5-3. Polymer subpopulations when the time is divided into two intervals

The polymerization time is first divided into two intervals. In this case, the polymer chains can be classified into two different subpopulations, as illustrated in Figure A5-3. The first subpopulation, #1, consists of polymers that are terminated in the first time interval. The second subpopulation, #2, consists of the rest of the chains, *i.e.*, chains that remain as dormant and chains that are terminated in the second time interval. Therefore, subpopulation #2 can be

viewed as block copolymer with two segments. The associated number fractions,

number-average chain length, and polydispersity of these subpopulations can be tabulated as shown below. Numbers (1, 2, ...) are used to denote the properties of each segment, while numbers preceded with # sign (#1, #2, ...) are used to indicate the different subpopulations.

Subpopulation (# <i>i</i>)	Number fraction, $n^{#i}$	Number-average chain length, $r_n^{#i}$	Polydispersity, $PDI^{#i}$
#1 – Terminated in the first interval. Block(1)	$n^{#1} = T_1$	$r_n^{#1} = r_{n,1}$	$PDI^{#1} = PDI_1$
#2 – Grew in the second interval. Block(1, 2)	$n^{#2} = L_1$	$r_n^{#2} = r_{n,1} + r_{n,2}$	$PDI^{#2} = 1 + \frac{(r_{n,1})^2(PDI_1 - 1) + (r_{n,2})^2(PDI_2 - 1)}{(r_n^{#2})^2}$
T – Total	1	Blend(#1, #2)	

The blend formulas for the number-average chain length and polydispersity are introduced earlier in Equation (S-10) and (S-11), respectively.

$$r_n^{blend} = \sum_{i=1}^N (n_i \times r_{n,i}) \quad (\text{S-10})$$

$$PDI^{blend} = \frac{1}{(r_n^T)^2} \sum_{i=1}^N n_i (r_{n,i})^2 PDI_i \quad (\text{S-11})$$

Using the above equations for polymer blend from the 2 subpopulations (Equation (S-10) and (S-11) with $N = 2$), the number-average chain length and the polydispersity

can be expressed as those possessed by the two segments, given by Equation (S-22) and (S-23).

$$r_n^T = n^{\#1} r_n^{\#1} + n^{\#2} r_n^{\#2} = r_{n,1} + L_1 r_{n,2} \quad (\text{S-22})$$

$$\begin{aligned} PDI^T &= \frac{n^{\#1} (r_n^{\#1})^2 PDI^{\#1} + n^{\#2} (r_n^{\#2})^2 PDI^{\#2}}{(r_n^T)^2} \\ &= 1 + \frac{(r_{n,1})^2 (PDI_1 - 1) + L_1 (r_{n,2})^2 (PDI_2 - 1)}{(r_n^T)^2} + \frac{T_1 L_1 (r_{n,2})^2}{(r_n^T)^2} \end{aligned} \quad (\text{S-23})$$

Similarly, the derivation can be done as the polymerization time is divided into smaller time intervals. For three time intervals (*i.e.*, 3 segments of growth), three polymer subpopulations can be considered, as tabulated below.

Subpopulation (# <i>i</i>)	Number fraction, $n^{\#i}$	Number-average chain length, $r_n^{\#i}$	Polydispersity, $PDI^{\#i}$
#1 – Terminated in the first interval. Block(1)	$n^{\#1} = T_1$	$r_n^{\#1} = r_{n,1}$	$PDI^{\#1} = PDI_1$
#2 – Terminated in the second interval. Block(1, 2)	$n^{\#2} = L_1 T_2$	$r_n^{\#2} = \sum_{i=1}^2 r_{n,i}$	$PDI^{\#2} = 1 + \frac{1}{(r_n^{\#2})^2} \sum_{i=1}^2 (r_{n,i})^2 (PDI_i - 1)$
#3 – Grew in the third interval. Block(1, 2, 3)	$n^{\#3} = L_1 L_2$ $= L_2^{ov}$	$r_n^{\#3} = \sum_{i=1}^3 r_{n,i}$	$PDI^{\#3} = 1 + \frac{1}{(r_n^{\#3})^2} \sum_{i=1}^3 (r_{n,i})^2 (PDI_i - 1)$
T – Total	1	Blend(#1, #2, #3)	

The properties of the resulting polymer blend (*i.e.*, the whole polymer population) can then be expressed as the properties of the three polymer segments, shown by Equation (S-24) and (S-25).

$$r_n^T = n^{\#1} r_n^{\#1} + n^{\#2} r_n^{\#2} + n^{\#3} r_n^{\#3} = \sum_{i=1}^3 L_{i-1}^{ov} r_{n,i} \quad (\text{S-241})$$

$$PDI^T = \frac{n^{\#1} (r_n^{\#1})^2 PDI^{\#1} + n^{\#2} (r_n^{\#2})^2 PDI^{\#2} + n^{\#3} (r_n^{\#3})^2 PDI^{\#3}}{(r_n^T)^2}$$

$$PDI^T = 1 + \frac{1}{(r_n^T)^2} \sum_{i=1}^3 \left(L_{i-1}^{ov} (r_{n,i})^2 (PDI_i - 1) + T_{i-1}^{ov} L_{i-1}^{ov} (r_{n,i})^2 \right) + \frac{2L_2^{ov} T_1^{ov} r_{n,2} r_{n,3}}{(r_n^T)^2} \quad (\text{S-25})$$

Following similar approach, the properties of the polymer blend when the reaction time is divided into N intervals can be derived to follow Equation (S-26) and (S-27), for the number-average chain length and polydispersity, respectively. From Equation (S-27), it can be seen that the last term represent the contribution of dead chains to the broadening of the distribution, since it involves the dead chain fraction, T .

$$r_n^T = \sum_{i=1}^N L_{i-1}^{ov} r_{n,i} \quad (\text{S-26})$$

$$PDI^T \approx 1 + \frac{1}{(r_n^T)^2} \sum_{i=1}^N L_{i-1}^{ov} (r_{n,i})^2 (PDI_i - 1) + \frac{2}{(r_n^T)^2} \sum_{i=1}^N L_{i-1}^{ov} r_{n,i} \sum_{j=1}^i T_{j-1}^{ov} r_{n,j} \quad (\text{S-27})$$

By substituting Equation (S-20) to Equation (S-26) and by taking the limit of each time interval duration to approach zero, the number-average chain length of the polymer blend can be expressed as Equation (S-28). The resulting expression is the same as that found for the case without termination, which is as expected since termination by disproportionation does not affect the relation between the number-average chain

length and conversion. The equilibrium relation for radical concentration ($[P^\bullet] = k_a[PX][C]/k_d[XC]$) was used to solve the equation. In addition, the overall dormant fraction, L_{i-1}^{ov} , is substituted by the concentration ratio of $[PX]/[PX]_0$.

$$r_n = \lim_{\Delta t_i \rightarrow 0} r_n^T = \lim_{\Delta t_i \rightarrow 0} \sum_{i=1}^N \frac{[PX]}{[PX]_0} \frac{[M]_0 \Delta x_i}{[PX]} = \int_0^X \frac{[M]_0}{[PX]_0} dx = \frac{[M]_0 X}{[PX]_0} \quad (S-28)$$

Similarly, Equation (S-20) and (S-21) can be substituted into Equation (S-27) and the limit as time interval approaches zero can be taken to obtain the polydispersity expression, as shown by Equation (S-29).

$$\begin{aligned} PDI &= \lim_{\Delta t_i \rightarrow 0} PDI^T \\ &= 1 + \frac{1}{(r_n)^2} \lim_{\Delta t_i \rightarrow 0} \sum_{i=1}^N L_{i-1}^{ov} (r_{n,i})^2 (PDI_i - 1) + \frac{2}{(r_n)^2} \lim_{\Delta t_i \rightarrow 0} \sum_{i=1}^N L_{i-1}^{ov} r_{n,i} \sum_{j=1}^i T_{j-1}^{ov} r_{n,j} \\ PDI &= \lim_{\Delta t_i \rightarrow 0} PDI^T = 1 + \frac{1}{r_n} + A + B \end{aligned} \quad (S-29)$$

$$\text{where } A \equiv \frac{2}{X^2} \frac{k_p [PX]_0}{k_d} \int_0^X \frac{(1-x)}{[XC]} dx \text{ and } B \equiv \frac{2}{X^2} \int_0^X \left(\int_0^x \frac{[P]}{[PX]} dx \right) dx$$

Each term in Equation (S-29) contribute to the broadening of polydispersity, since they are all positive terms. The first two terms are observed for the polydispersity of Poisson's distribution, thus can be attributed to statistical broadening. From the main text, it has been shown that the third term (A) represents the contribution from *number of monomer added per cycle*, while the fourth term (B) can be attributed to the *dead chains* contribution. The term A can be integrated analytically, while B is approximated by using Gaussian quadrature with 1 node. Substituting the resulting A

and B terms back to the Equation (S-29) for cases with and without initial deactivator gives Equation (12) in the main text. It can be shown that the derivative of A is always negative, indicating a monotonically decreasing function, while the opposite is true for B .

5.6.3 Differential mass and moments balances

The definitions of the i^{th} moment of the radical, dormant, dead, and total chains are given by Equation (S-30)-(S-33), respectively. Detailed use of the method of moments can be found elsewhere.^[23,28]

$$Y_i \equiv \sum_{r=0}^{\infty} r^i [P_r^*] \quad (\text{S-30})$$

$$QX_i \equiv \sum_{r=0}^{\infty} r^i [PX_r] \quad (\text{S-312})$$

$$Q_i \equiv \sum_{r=0}^{\infty} r^i [P_r] \quad (\text{S-32})$$

$$Q_i^T \equiv Y_i + QX_i + Q_i \quad (\text{S-33})$$

The mass and moments balances used in the method of moments for comparison purpose in this work are summarized in Table A5-1. The polydispersity profile can be obtained by numerically integrating equations in Table A5-1 and using the resulting moments in Equation (S-34).

$$PDI = \frac{Q_2^T Q_0^T}{(Q_1^T)^2} \quad (\text{S-343})$$

Table A5-1. Differential mass and moments balances for an ATRP system

Species	Balances
Small molecules	
Monomer	$\frac{d[M]}{dt} = -k_p[M]Y_0$
Catalyst	$\frac{d[C]}{dt} = k_d[XC]Y_0 - k_a[C]QX_0$
Deactivator	$\frac{d[XC]}{dt} = k_a[C]QX_0 - k_d[XC]Y_0$
r-unit chains	
Radical	$\frac{d[P_r^\bullet]}{dt} = k_p[M][P_{r-1}^\bullet] - k_p[M][P_r^\bullet] + k_a[C][PX_r] - k_d[XC][P_r^\bullet] - k_t[P_r^\bullet]Y_0$
Dormant	$\frac{d[PX_r]}{dt} = k_d[XC][P_r^\bullet] - k_a[C][PX_r]$
Dead	$\frac{d[P_r]}{dt} = k_t[P_r^\bullet]Y_0$
Zeroth moment	
Radical	$\frac{dY_0}{dt} = k_a[C]QX_0 - k_d[XC]Y_0 - k_t(Y_0)^2$
Dormant	$\frac{dQX_0}{dt} = k_d[XC]Y_0 - k_a[C]QX_0$
Dead	$\frac{dQ_0}{dt} = k_t(Y_0)^2$
First moment	
Radical	$\frac{dY_1}{dt} = k_p[M]Y_0 + k_a[C]QX_1 - k_d[XC]Y_1 - k_tY_1Y_0$
Dormant	$\frac{dQX_1}{dt} = k_d[XC]Y_1 - k_a[C]QX_1$
Dead	$\frac{dQ_1}{dt} = k_tY_1Y_0$
Second moment	
Total	$\frac{dQ_2^T}{dt} = 2k_p[M]Y_1 + k_p[M]Y_0$

§ 5.7 References

- [1] R. Gilbert, M. Hess, A. Jenkins, R. Jones, P. Kratochvil, R. Stepto, *Pure Appl Chem* **2009**, *81*, 351-353.
- [2] P. J. Flory, *J Am Chem Soc* **1940**, *62*, 1561-1565.
- [3] S. Zhu, A. Hamielec, "4.32 - Polymerization Kinetic Modeling and Macromolecular Reaction Engineering", in *Polymer Science: A Comprehensive Reference*, K.M. Möller, Ed., Elsevier, Amsterdam, 2012, p. 779-831.
- [4] J.-S. Wang, K. Matyjaszewski, *J Am Chem Soc* **1995**, *117*, 5614-5615.
- [5] M. Kato, M. Kamigaito, M. Sawamoto, T. Higashimura, *Macromolecules* **1995**, *28*, 1721-1723.
- [6] H. Tobita, *Macromol Theory Simul* **2006**, *15*, 12-22.
- [7] E. Mastan, D. Zhou, S. Zhu, *J Polym Sci, Part A: Polym Chem* **2014**, *52*, 639-651.
- [8] P. J. Flory, "*Principles of polymer chemistry*", Cornell Univ. Press, Ithaca, NY, 1953.
- [9] K. Matyjaszewski, N. V. Tsarevsky, *J Am Chem Soc* **2014**, *136*, 6513-6533.
- [10] A. Goto, T. Fukuda, *Prog Polym Sci* **2004**, *29*, 329-385.
- [11] E. Mastan, X. Li, S. Zhu, *Prog Polym Sci* **2015**, *45*, 71-101.
- [12] E. Mastan, D. Zhou, S. Zhu, *Macromol Theory Simul* **2014**, *23*, 227-240.
- [13] A. Goto, T. Fukuda, *Macromolecules* **1997**, *30*, 4272-4277.
- [14] T. Fukuda, A. Goto, *Macromol Rapid Commun* **1997**, *18*, 683-688.
- [15] K. Matyjaszewski, *J Macromol Sci, Part A: Pure Appl Chem* **1997**, *10*, 1785-1801.
- [16] A. H. Müller, G. Litvinenko, D. Yan, *Macromolecules* **1996**, *29*, 2346-2353.
- [17] K. L. Beers, S. Boo, S. G. Gaynor, K. Matyjaszewski, *Macromolecules* **1999**, *32*, 5772-5776.
- [18] J. Gromada, J. Spanswick, K. Matyjaszewski, *Macromol Chem Phys* **2004**, *205*, 551-566.
- [19] D. Bontempo, R. C. Li, T. Ly, C. E. Brubaker, H. D. Maynard, *Chem Commun* **2005**, 4702-4704.
- [20] H. Fischer, *J Polym Sci, Part A: Polym Chem* **1999**, *37*, 1885-1901.
- [21] T. Fukuda, *J Polym Sci, Part A: Polym Chem* **2004**, *42*, 4743-4755.
- [22] M. Zhong, K. Matyjaszewski, *Macromolecules* **2011**, *44*, 2668-2677.

- [23] E. Mastan, S. Zhu, *Eur Polym J* **2015**, *68*, 139-160.
- [24] P. B. Zetterlund, *Macromolecules* **2010**, *43*, 1387-1395.
- [25] A. Mohammad Rabea, S. Zhu, *Ind Eng Chem Res* **2014**, *53*, 3472-3477.
- [26] S. Beuermann, M. Buback, T. P. Davis, R. G. Gilbert, R. A. Hutchinson, O. F. Olaj, G. T. Russell, J. Schweer, A. M. van Herk, *Macromol Chem Phys* **1997**, *198*, 1545-1560.
- [27] E. Mastan, D. Zhou, S. Zhu, *J Polym Sci, Part A: Polym Chem* **2013**, *52*, 639-651.
- [28] S. Zhu, *Macromol Theory Simul* **1999**, *8*, 29-37.

6 LITERATURE REVIEW ON SI-ATRP

This chapter marks the beginning of the second part of this thesis, namely the investigation of surface-initiated ATRP (SI-ATRP). The review presented is based on a collaboration work with researchers from Carnegie Mellon University (Dr. Amir Khabibullin as the primary author and Dr. Krzysztof Matyjaszewski. See **Author contributions** below for detailed division). The published review, entitled “Surface-initiated atom transfer radical polymerization,” is published as a chapter in *Controlled Radical Polymerization at and from Solid Surfaces* book, **2015**, p.29-79 (doi:10.1007/12_2015_311), vol. 270 of the series *Advances in Polymer Science*. This reproduction is done with permission from Springer. Several modifications from the original chapter have been made to ensure brevity and to ensure its relevance with the other chapters in this thesis.

Author contributions

Researchers from Carnegie Mellon University contributed Section 1, 2, 3, and 6 of the original chapter, while researchers from McMaster University contributed Section 4 and 5. Erlita Mastan prepared the first draft for these two sections, which were then revised by Dr. Shiping Zhu. This chapter of the thesis only includes a part of Section 3, the whole Section 4, and Section 6 of the original chapter. A part of Section 3 and 6 from the collaborators are included here for the sake of completeness of this thesis. Section 3 (§6.2 in this chapter) gives the fundamental of SI-ATRP, serving as a brief introduction, while Section 6 (§6.4 here) provides conclusion. Section 4 gives the relevant literature review to the subsequent chapters of this thesis, *i.e.*, on the effect of various reactions on SI-ATRP kinetics.

§ 6.1 Abstract

Surface-initiated atom transfer radical polymerization (SI-ATRP) is a robust and versatile method for preparation of various hybrid materials with controlled molecular characteristics of the tethered polymer chains. The two determining properties of polymer brush are the thickness and the grafting density (*i.e.*, how thick and how densely grafted the polymer brush is). This review mainly covers the elementary reactions involved in SI-ATRP, such as initiation, propagation, termination, transfer, and activation/deactivation equilibria for grafting on various

surface geometries. The effects of these reactions on the resulting polymer brush properties are discussed based on various published results.

§ 6.2 Surface-initiated ATRP (SI-ATRP)

The versatility of surface-initiated atom transfer radical polymerization (SI-ATRP) as a method for grafting polymer brushes from the surface arises from its ability to precisely control the chain topology and composition of polymer brushes. This ability is a major tool to engineer the structure and properties of the resulting hybrid materials. This technique allows the grafting of (co) polymer, block, gradient, and statistical copolymer brushes from the surface of various substrates.^[1,2] The brushes can have different topologies, including linear, branched, hyperbranched, and crosslinked chains.^[3,4] Miktoarm hybrid systems can be created by introducing two different polymer chains to the substrate surface using SI-ATRP^[5-7] or SI-ATRP combined with other polymerization techniques.^[8] These materials are responsive to solvent change and can be turned into Janus nanoparticles by variation of solvent composition.^[6]

Control over the polymer brush thickness is achieved by controlling both the grafting density and the molecular weight (or equivalently, chain length) of the brush. Similar to its solution counterpart, the molecular weight of brush produced via SI-ATRP can be controlled by varying the polymerization time. Control over grafting density is essential for regulation of the number of polymer brushes on the surface. This can be

achieved by using a mixture of active and inactive (“dummy”) initiators to functionalize the substrate surface. The number of active ATRP initiators, and thus the number of polymer chains on the surface, is varied by controlling the corresponding fraction of active initiators in the mixture. Another approach for controlling grafting density is partial removal of tethered initiators from the surface by specific treatment (UV light, temperature, chemical).

SI-ATRP can be carried out on wide variety of surfaces, including flat surfaces, nanoparticles, cylindrical surfaces, or on the surface inside nanopores. The presence of ATRP initiator is the only requirement for successful introduction of polymer brushes via SI-ATRP. However, the choice of surface geometry can influence the parameters controlling the architecture of the grafted polymer brushes. For example, the grafting density for polymer brushes on a flat surface is usually below 0.5 chain/nm², whereas convex systems, such as functionalized nanoparticles, can have a significantly higher grafting density, approaching 1 chain/nm². However, such systems are prone to macroscopic gelation, even at only 0.1% of interparticle radical termination. In concave systems (*e.g.*, inside cylindrical or spherical pores), steric hindrance plays a significant role, reducing the level of control over polymer brush MW and MWD. However, in some systems good control was reported.^[9]

§ 6.3 Reactions in SI-ATRP

In this section, the basic reactions involved in SI-ATRP are discussed, namely initiation, propagation, termination, transfer, equilibrium, and other reactions. Most of the section is further divided on the basis of the curvature of the substrate.

6.3.1 Initiation

The surface properties introduced by the grafted layer depend on how long the chains are and how crowded the surface is (*i.e.*, the polymer chain length and its grafting density). Grafted chain length can be easily controlled using ATRP. On the other hand, predicting and tailoring the surface to possess a certain grafting density remains one of the major challenges in SI-ATRP. This is because all of the factors affecting grafting density are not fully understood.

On a flat substrate, the measurement of grafting density is challenging because of the limited amount of grafted polymers. In order to estimate the grafting density, it is either assumed that grafted chains have the same properties as free chains when polymerization is conducted simultaneously in both phases,^[7,10-13] or that an accurate relationship between swollen and dry thicknesses of polymer layer is known.^[14] For systems having large surface-to-volume ratios (*e.g.*, nanoparticles), polymers can be cleaved from the substrate and characterized to give an estimate of grafting density, after the experiments are conducted.

The polymer grafting density is strongly related to the initiator density, which can be controlled by varying the initiator concentration and immobilization time, or by introducing an inert analog along with the initiator species.^[15-22] The inert molecules, or spacers, are usually chosen to have a structure similar to the initiator moieties, but do not possess the transferable group for initiating ATRP. The similar chemical structure of spacer and initiator allows the assumption of similar chemical reactivity with the surface of the substrate. Therefore, the fraction of initiator spacer used during immobilization is generally assumed to be the same as the fraction immobilized on the substrate. However, prediction of how many immobilized initiators grow into polymer chains (*i.e.*, grafting efficiency) still cannot be made.

The terms “grafting efficiency” and “initiation efficiency” are used interchangeably in the literature, mainly referring to how many of the tethered initiator sites successfully grow into polymer chains. There are two ways to calculate the initiation efficiency from experimental data. The first is by directly considering the ratio of the polymer grafting density to the initiator density.^[23-26] The second is by comparing the theoretical molecular weight to the molecular weight measured from cleaved polymer chains.^[27-29] These two methods should theoretically represent the same value. Lower initiation efficiency is usually obtained at high initiator density, but increases with reduced initiator density up to the point where the efficiency becomes independent of the initiator density.^[15-17,26] This is because steric hindrance dictates the maximum concentration of polymer chains that can be grafted onto a substrate.

Apart from the initiator density, the types of monomer and initiator can affect initiation efficiency.^[13,30,31] The type of catalyst could indirectly affect the initiation efficiency, as shown by a study of aqueous SI-ATRP of methyl methacrylate (MMA).^[24] The SI-ATRP system with CuCl as catalyst showed slower polymerization rate but better controllability and higher initiator efficiency than the system with CuBr. The difference in initiation efficiency observed was thought to be caused by the difference in polymerization rate, whereby faster polymerization leads to a decrease in initiator efficiency. In addition, a difference in polymerization rate as a result of a difference in catalyst-to-deactivator ratio has also been shown to affect the resulting grafting density.^[32] Solvent type is another factor that could influence the grafting density. When SI-ATRP of OEGMA is conducted in a more polar solvent, the resulting grafting density is lower because of the bulkier tethered polymer coils in that system, which imposed steric hindrance for the other initiation sites.^[11]

The length and phobicity of the link between the initiator and solid surface can also affect the initiation efficiency, as studied by Green and coworkers for SI-ATRP of MMA and of styrene from silica nanoparticles.^[24,25] In the MMA system, their experimental results showed a monotonous increase in grafting density and initiation efficiency with longer initiator linkers, as a result of the increased hydrophobicity of the longer spacer. On the other hand, the system utilizing styrene as monomer showed little difference between shortest and longest linker, as each led to a similar grafting density of 0.7-0.8 chains/nm², with an initiation efficiency of 26-35%. However, the

system with the middle-length link resulted in a much lower grafting density of 0.2 chains/nm², with initiation efficiency around 10%. This difference was postulated to be caused by conformational change, in which the Br end group is hidden in the case of middle-length linker. Comparison of the initiation efficiency between the two studies is shown in Figure 6-1.

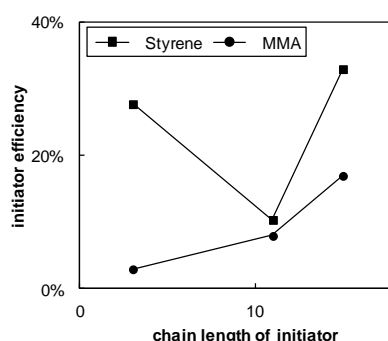


Figure 6-1. Effect of initiator spacer length on the initiation efficiency of SI-ATRP of styrene and MMA with CuBr. Detailed experimental conditions can be found in the original publications^[24,25]

Surface curvature plays an important role in determining initiation efficiency. The initiation efficiency of SI-ATRP from a flat substrate has been estimated to be around 10%.^[33-35] On the other hand, the initiation efficiency that could be obtained from a convex substrate is close to, or even more than, 30%.^[23-26,29,36] Even higher initiation efficiency values of approximately 80% for particles have also been reported in several studies.^[27,28,37] In particle systems, some studies have reported a constant increase in initiation efficiency with time,^[23,25] whereas others reported it to increase as polymerization progresses to higher conversion.^[27,28,36] This again shows the uncertainty in predicting initiation efficiency.

Some studies have reported an initiation efficiency of 3-8.5% for concave substrates within ordered mesoporous silica nanoparticles, with mesopore diameter ranging from 1.8 to 2.3 nm.^[38,39] Another study reported 22-37% initiation efficiency when SI-ATRP was conducted in ordered mesoporous silica with 15 nm cylindrical pores.^[9] These experimental results point to the conclusion that concave systems, with more severe confinement effects, exhibit lower initiation efficiency. This comparison might of course be influenced by the other factors mentioned above, because they are collected from experiments conducted under different conditions. However, similar findings have been reported in a simulation study of grafting from concave substrate with a “perfectly living” polymerization.^[40] As shown in Figure 6-2, the simulation results predicted lower grafting density, σ_g , in systems with higher curvature (smaller R), for the same initiator density, σ_i . It should be noted that in an experimental setting, the dependence of initiator density on the curvature and the influence of termination reactions may further complicate the actual result.

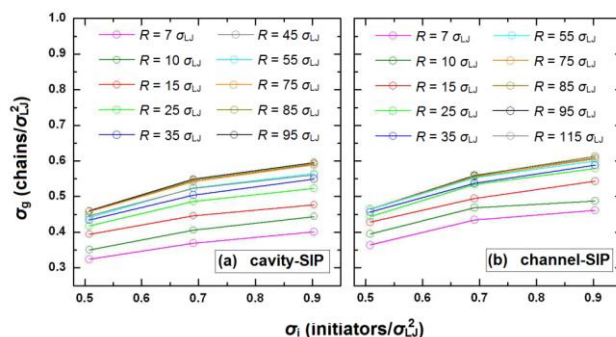


Figure 6-2. Effect of confinement on grafting efficiency (σ_g/σ_i), as simulated for surface-initiated polymerization within a spherical cavity or channel with various curvatures; R : radius of the cavity. Reprinted with permission from ^[40]

6.3.2 Propagation

Despite the numerous studies conducted using SI-ATRP, there are several fundamental points that still cannot be definitively answered. For example, what causes the grafted layer to stop growing, even when there is an abundance of monomer in the solution phase? Another fundamental question is related to the validity of assuming grafted and free chains to have comparable properties.^[18,41-43] This assumption is especially important as it is commonly made for graft polymerization on flat substrates, because it allows estimation of the grafting density of the polymer chains even when the amount of polymer collected from flat substrates is not enough for further characterization.

On the other hand, nanoparticle systems have a much larger surface-to-volume ratio than flat systems, allowing a sufficient amount of polymer to be collected for further characterization. Therefore, the assumption can be experimentally verified for these systems. As a matter of fact, much of the data on polymers obtained from SI-ATRP conducted on particle systems show an excellent agreement with the properties of polymers formed in the solution phase.^[44] However, this does not guarantee the same trend for polymers grown from flat substrates, because the degree of confinement on polymer chains grown from a convex substrate is less severe than that on a flat substrate. Owing to its positive curvature, polymers grown on convex substrates experience less and less confinement as the chain grows longer and the initiation site is farther away from the surface.

In SI-ATRP from a flat surface, one end of each individual polymer chain is fixed onto a substrate. This forces the polymer chains to grow in close proximity to one another, creating crowding of polymer chains and forcing them to assume a chain-extended brush conformation. The brush conformation is evident from the greater thickness of the grafted polymer layer on a flat substrate than the radius of gyration of the free polymer. The calculation of grafting density shows that each polymer chain occupies a smaller projected area than that predicted by its radius of gyration, further confirming the chain-extended brush conformation.

The steric crowding of polymer chains gives rise to unique properties not seen in grafted polymers with lower grafting density.^[44,45] However, the crowding of surface polymer chains can also lead to starvation of monomer, or earlier formation of a glassy state, which in turn hinders the propagation of additional surface chains. Moreover, some of the surface chains could have their active ends buried inside the dense polymer layer, thereby reducing the available monomer concentration for that radical to propagate. This is one of the two theories often used to explain many experimental trends in the literature, often referred to as the “school of propagation” because of the decrease in propagation rate. The other school of thought, referred to as the “school of termination,” is discussed in the next section. A recent publication has collected experiment data and compared predictions based on these two schools of thought.^[46] The result is inconclusive, as no model can fully explain the various contradicting experimental trends reported in the literature.

Based on the reduced rate of propagation, one could explain the slowing down of the growth rate for grafted chains at negligible monomer conversion. This school of thought could also shed light on when the assumption of equal properties of free and grafted chains can be considered valid. As a result of the difference in the availability of monomer for the chains solution and for the tethered surface chains, the chain length and dispersity of the two polymer populations may not be comparable. The reduction in the concentration of available monomers for the grafted chains is expected to result in chains that are shorter than the free chains in solution.

Recent simulation studies based on the understanding of the school of propagation have shown that the assumption of equal properties of grafted and free polymers is often invalid in a perfectly living polymerization.^[42,43] Simulation results show that the grafted polymers are always shorter and have broader distribution than their solution counterparts when polymerization is conducted simultaneously from a surface and in solution. The difference depends on the fraction of polymers present as grafted chains, η , and on the grafting density, σ , as shown by Figure 6-3. Higher grafting density leads to more confinement and reduced propagation rate as a result of monomer limitations, resulting in shorter grafted chains. On the other hand, a lower fraction of congested surface chains leads to less difference in properties between surface and free chains. Therefore, the assumption of surface chains having similar properties to free chains is true only when the surface chains exhibit low grafting density, which is not usually the case in experimental settings. However, it should be

noted that some experimental studies of SI-ATRP on flat surfaces have reported controlled growth to a very thick polymer brush, for example, 700 nm of poly(hydroxyethyl methacrylate) (PHEMA) brush on a gold surface^[47] and 700 nm of poly(dimethylaminoethyl methacrylate) (PDMAEMA) on a silicon surface.^[48]

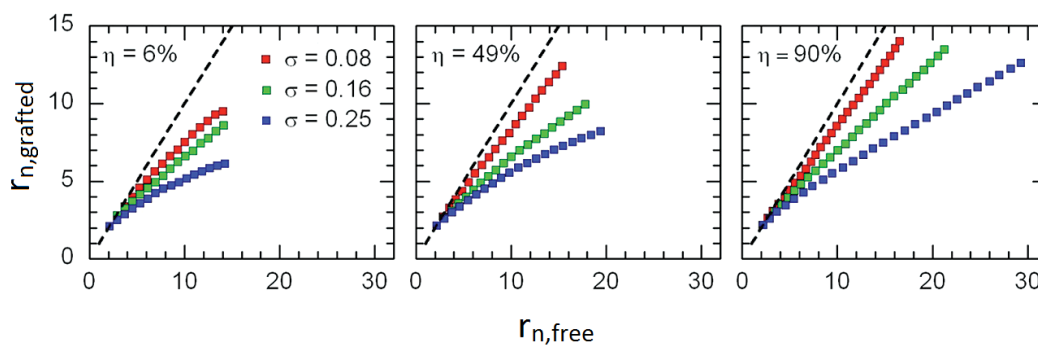


Figure 6-3. Model predictions of the chain length of grafted and free polymers in simultaneous surface-initiated polymerization with various grafting densities (σ) and fractions of grafted polymer (η). Reprinted with permission from ^[43]

For systems with concave substrates, the effect of confinement is expected to be even more severe than that for flat substrates. A theoretical study based on molecular dynamics simulations has systematically investigated surface-initiated living polymerization on concave substrates for polymerization occurring strictly on the surface.^[40] The simulation results verified the confinement effect on the grafted polymer: shorter chains are obtained in systems with higher degrees of confinement (*i.e.*, smaller surface radius). However, the results are counter-intuitive for the dispersity, where the resulting grafted polymers have narrower distribution with increasing confinement for the same amount of reaction time or at the same monomer

conversion. This trend is attributed to the slower polymerization rate in a more confined system, which leads to more uniform growth. It should be noted that the simulation was conducted in the absence of termination reactions, which could significantly affect the resulting dispersity in an experimental setting.

6.3.3 Termination

Termination is unavoidable in ATRP systems because of the very nature of radicals. Termination in SI-ATRP is highly dependent on the geometry of the substrates. For example, the confined environment of concave substrate leads to closer proximity of polymer chains, which could lead to higher possibility of termination. On flat or convex substrates, the termination could occur via multiple modes. The modes of termination and experimental data supporting the role of termination in kinetics of SI-ATRP are discussed in the following sections.

Termination on flat substrates

The termination of living chains during SI-ATRP could offer an explanation for some of the experimentally observed phenomena. For example, termination provides plausible explanation for the experimentally observed decrease in the growth rate of the grafted polymer layer, even when no significant monomer depletion is expected in the bulk contacting solution. This experimental trend has been repeatedly reported in the literature for various types of substrates and monomers,^[10,49-51] and has also

been supported by an experimentally measured decrease in the concentration of halide groups on the surface.^[52]

On flat substrates, the possible termination modes depend on the polymerization locus. For SI-ATRP accompanied by simultaneous polymerization in the contacting solution, termination could occur between two surface radicals, two solution radicals, or between a surface and a solution radical. On the other hand, the termination could only occur between two surface radicals for surface-confined SI-ATRP. These possible termination modes are illustrated in Figure 6-4.

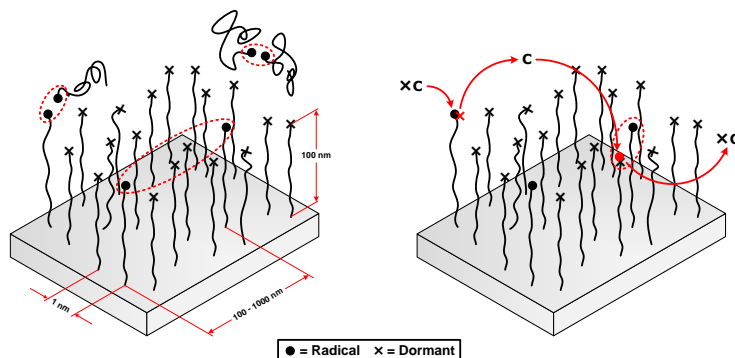


Figure 6-4. Left (a): Possible termination modes involved in SI-ATRP on a flat substrate.

The estimated distances shown are calculated based on the assumption of high grafting density (1 chain/nm²), a typical ratio of radical to dormant chains in ATRP ($[P\cdot]/[PX] = 10^4$ to 10^6), and typical brush thickness of 100 nm.

Right (b): Migration of surface radicals through activation/deactivation in SI-ATRP promotes termination between surface radicals. Reprinted with permission from ^[53]

Termination modes between two solution radicals and between solution and surface radicals are easily imaginable, because at least one of the participants is a mobile free

chain. On the other hand, it is harder to picture how two randomly formed radicals that are fixed to a substrate can reach each other to undergo termination, especially if they are located far from one another. As discussed in the section on propagation, with one end of the polymer chain fixed onto a substrate, the polymer chain cannot move as freely as chains in solution, even though the local concentration of polymer chains is much higher as a result of crowding. Only a very small portion of the chains have active ends at any instant, with most of the chains being capped and dormant. In fact, as demonstrated by Zhou et al., estimation of the distance between radicals on a highly grafted flat substrate indicates that termination between two surface radicals is highly improbable, as denoted in Figure 6-4(a).^[53] It is hard to picture how two surface-constrained radicals can reach each other for termination to occur.

Gao and colleagues proposed a mechanism by which two radical centers that are originally present on surface chains that are far apart could have a high probability of “hopping” to other fixed chains on the substrate.^[41,53] Although the chains do not move because of their attachment to the surface, the active (radical) ends could move as a result of the activation/deactivation involved in the basic ATRP mechanism. Faster migration of active centers from one chain to another, resulting from more frequent activation/deactivation of surface chains, could increase the probability of two radicals being adjacent to one another, as illustrated in Figure 6-4 (b). Therefore, the termination rate is proposed to be proportional to the migration rate, which in turn depends on the rate of activation/deactivation, as shown by Equation (1).^[53]

$$k_t \propto \text{migration rate} \propto [C]_{sol} \quad (1)$$

For SI-ATRP, a constant ratio of catalyst to deactivator is supposed to imply a constant polymerization rate. This is because only a small amount of polymer chains are present on the surface and therefore do not affect the catalyst-to-deactivator ratio throughout the polymerization medium. However, experimental data have shown that an increase in catalyst concentration can result in a faster leveling-off of the growth rate.^[54] This concept of migration-assisted termination has been used to explain the experimental data, where a decrease in growth rate of surface chains is observed with increasing catalyst concentration at a constant ratio of catalyst to deactivator, as shown in Figure 6-5.

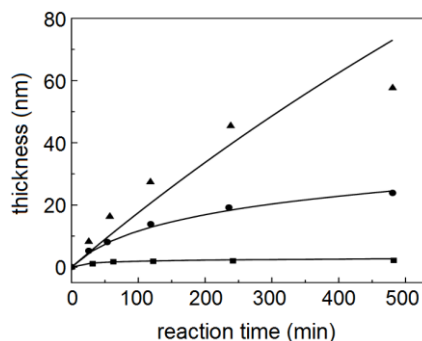


Figure 6-5. Growth kinetics of grafted polymer for different catalyst concentrations in SI-ATRP of methyl acrylate (MA) from gold substrate, with [MA] = 2 M and [CuBr₂/Me₆TREN]/[CuCl/Me₆TREN] = 0.3. Lines show the predicted result from the model. Data points were experimentally obtained: *squares* 40 mM, *circles* 2 mM, *triangles* 0.1 mM^[53,54]

Another possible explanation for the trend observed in Figure 6-5 is the recently proposed mechanism of catalytic radical termination in solution ATRP.^[55] The

proposed termination mechanism for solution ATRP might also be applicable for SI-ATRP. According to that mechanism, the presence of catalyst can increase the amount of termination, which contributes to the observed decrease in growth rate. Another factor to be considered is the possibility that the resulting grafting density is affected by different concentrations of catalyst. However, as mentioned previously, the grafting density is not known a priori, nor can it be measured accurately for a flat substrate.

The termination rate constant has also been proposed to depend on the grafting density (σ) according to Equation (2), from comparison of the model-predicted thickness with experimental data.^[53] The exponential decrease in termination rate constant (k_t) as grafting density increases could be a result of conformational change of the polymer chains.

$$k_t \propto \exp(-\gamma\sigma) \quad (2)$$

Based on the school of termination philosophy, Equation (3) and (4) have been developed by two different groups to predict the thickness growth profile.^[52,53] These two equations were derived from kinetic equations using quasi-steady state assumption (QSSA) $k_{act}[PX][C] = k_{deact}[P^\bullet][XC]$, and are applicable for cases with negligible conversion. The first group applied QSSA to the mass balance of radicals to obtain an expression for the dry grafted layer thickness, δ , as shown in Equation (3). On the other hand, the second expression, shown by Equation (4), was obtained by

applying QSSA to the balance of dead chains. Both equations predict the growth rate of the grafted layer thickness to decrease with polymerization time, which offers an explanation for the tapering off observed in the growth kinetics of the grafted layer in experiments.

$$\delta \propto \frac{k_p[M]_0[P^\bullet]_0 t}{1 + k_t[P^\bullet]_0 t} \quad (3)$$

$$\delta \propto \ln \left(1 + \sigma k_t \left(\frac{k_a[C]}{k_d[XC]} \right)^2 t \right) \quad (4)$$

Although data is scarce, some studies have reported the properties of grafted chains formed by SI-ATRP after cleaving the polymer brush grown on large or multiple planar substrates. [15,18,33,56-58] Unfortunately, such a comparison of grafted chain properties with those of free polymers is very limited, because some of these studies conducted polymerization strictly on the surface.[15,33,58] Other studies have reported that collected grafted chains are longer than the free chains produced during simultaneous polymerization.[18,56,57] Similar findings have also been reported when surface-initiated nitroxide-mediated polymerization was employed instead of SI-ATRP.[59,60]. A different trend was reported by Yamago et al., who found free and grafted chains to possess similar properties when using surface-initiated organotellurium-mediated living radical polymerization (SI-TERP).[61]

One way to confirm negligible termination has been reported by Kang et al.[58] The authors conducted a SI-ATRP of styrene on a silicon wafer from a photo-cleavable

initiator. The molecular weight of the cleaved polymers was used to calculate the grafting density. For their polystyrene system, which mainly terminates via coupling, constant grafting density implies negligible termination. It should be noted that this method is not valid for other monomers that terminate via disproportionation, since disproportionation would not affect the grafting density value calculated using this method.

Termination on nanoparticles

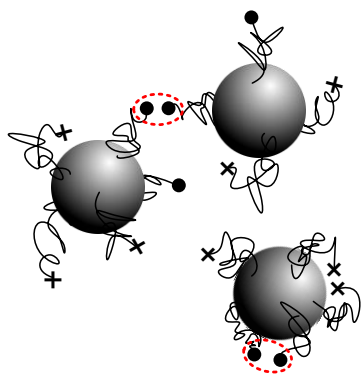


Figure 6-6. Interparticle and intraparticle termination modes between two surface radicals in SI-ATRP on nanoparticles

In SI-ATRP involving nanoparticles, there are two possible modes for termination between two surface radicals: interparticle and intraparticle termination. Intraparticle termination is basically similar to termination between two surface radicals observed on flat substrates, with the additional limitation of a curvature effect. On the other hand, interparticle termination occurs between chains that are fixed on two different

nanoparticles. The termination modes in such a particle system are illustrated in Figure 6-6.

A problem that often arises in conducting SI-ATRP on particles is macroscopic gelation, which occurs as a result of interparticle termination via coupling or

combination. This can result in an increase in viscosity, leading to diffusion-controlled reactions and loss of polymerization control. The large number of initiation sites on one particle makes it faster for the system to gel as compared with a solution polymerization system. By assuming approximately 1,600 initiation sites per particle, the gelation point can be estimated using Flory's gelation theory as occurring when only 0.125% of the chains undergo interparticle coupling termination.^[37] Therefore, macroscopic gelation has been reported even when no bimodality is reported in the MWD of the cleaved grafted chains.^[27]

Several ways have been proposed for reducing the macroscopic gelation, including using a dilute concentration of particles, or stopping the reaction at low monomer conversion.^[27,28,36] Free initiator in the solution is also often added to the reaction to form free polymers and prevent network formation.^[62,63] However, both of these methods can increase the cost of synthesizing pure polymer-grafted nanoparticles. Bombalski et al. have shown that macroscopic gelation can be avoided by conducting SI-ATRP in a miniemulsion system as a result of radical compartmentalization, as illustrated in Figure 6-7.^[37]

Another strategy that is effective for avoiding macroscopic gelation is conducting the polymerization in a high pressure system.^[26] When SI-ATRP is conducted under high pressure the polymerization occurs with an increase in propagation rate, whereas the termination rate is suppressed. This leads to a faster polymerization with better living

characteristics. Successful synthesis of PMMA grafted chains, with molecular weight above 1 million and low dispersity (<1.3), on silica nanoparticles has been reported using miniemulsion AGET-ATRP in a vessel pressurized to 6 kbar.^[26] The livingness of the tethered chains, or retention of high chain-end functionality, was confirmed by conducting SI-ATRP of methyl acrylate using the PMMA-grafted nanoparticles as surface initiator.

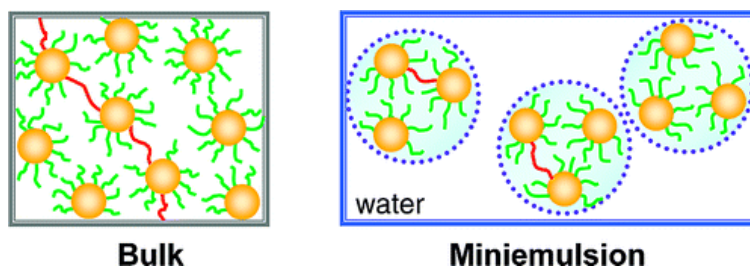


Figure 6-7. Interparticle coupling in SI-ATRP on nanoparticles for bulk and miniemulsion systems. The compartmentalization of particles in a miniemulsion prevents macroscopic gelation from occurring. Reprinted with permission from ^[37]

Chakkalakal et al. have observed bimodality in the MWD of grafted polymer on silica nanoparticles at higher conversion (above 25%).^[36] However, the bimodal distribution was attributed to intraparticle coupling and/or to the coupling termination between surface and solution radicals. The termination occurring via interparticle coupling was considered negligible in their study, based on dynamic light scattering (DLS) results. They also observed that more termination occurred for smaller nanoparticles than for larger particles, as suggested by earlier broadening and bimodality of the MWD.

Termination on concave substrates

In the case of systems involving concave substrates, such as porous particles or cylindrical channels, the confinement effect is expected to be much more severe than that for flat substrates. In addition to the obvious mass transport issue that results from a more confined space, the probability of termination could also increase. Therefore, a less living and less controlled polymerization is expected in systems involving concave substrates.

Multiple studies have reported a population of shorter grafted polymer chains with broader distribution in comparison with free/solution polymer chains.^[38,39,64] Gorman et al. conducted SI-ATRP from a silicon wafer, porous silicon, and anodically etched aluminum oxide. The results were compared with those of ATRP conducted in solution under similar conditions. The grafted polymer chains from a flat substrate were shown to be shorter than the free chains formed in the parallel solution polymerization. The polymers obtained from concave substrates have an even lower molecular weight and broader distribution.

Charleux group has conducted several studies of SI-ATRP in mesoporous silica nanoparticles.^[38,39] Instead of conducting parallel polymerizations, they conducted simultaneous polymerization in solution and from the surface. Their findings were similar to those of Gorman et al., showing grafted chains to have significantly lower molecular weight with broader distribution than the chains formed in solution.

Moreover, for some of the experiments, the grafted chains were shown to display multimodal distribution, as characterized using gel permeation chromatography (GPC) (see Figure 6-8). The lower molecular weight peak observed in the distribution did not shift, even at higher conversion, indicating the presence of dead chains. From this GPC curve, they estimated that approximately 50% of the chains had been terminated. Characterization of the grafted chains using mass spectroscopy also provided proof that some of the grafted chains had undergone termination by disproportionation.

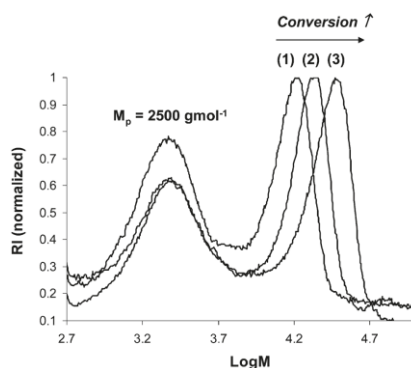


Figure 6-8. Molecular weight distributions of grafted chains for SI-ATRP of MMA from a concave substrate. Detailed experimental conditions are provided in the original literature. $M_{p,l}$ indicates the molar mass at the peak for the living chains. (1) 50%, $M_{p,l} = 16,320$ g/mol; (2) 62%, $M_{p,l} = 21,880$ g/mol; (3) 91%, $M_{p,l} = 30,020$ g/mol. The lower peak ($M_p = 2500$ g/mol) indicates the presence of dead chains. Reprinted with permission from [39]

Simulation of polymerization from a concave substrate could prove to be a challenging task because of the complexity of the system. However, Liu et al. used coarse-grained molecular dynamic simulation to investigate the effect of curvature on polymer growth and dispersity.^[40] Unfortunately, the polymerization was considered

to be a perfectly living polymerization (*i.e.*, in the absence of termination and other side reactions), thus it does not help in elucidating the role of termination in SI-ATRP.

6.3.4 Exchange

At the beginning of normal ATRP, only catalyst and initiator are present in the solution. As the polymerization progresses, some of the chains undergo bimolecular termination, resulting in accumulation of the deactivator. The accumulation of deactivator, termed the persistent radical effect,^[65] is important in reaching an equilibrium between dormant and active chains. Indeed, control in ATRP systems relies on creating an equilibrium between dormant and active chains, as they reversibly react with catalyst and deactivator, respectively. The broadness of the MWD (*i.e.*, dispersity) is often used as an indicator of how controlled the polymerization is. For cases with negligible termination and high degrees of polymerization, the dispersity (\mathcal{D}) of polymer chains synthesized through ATRP as a function of conversion (*conv*) follows Equation (5), with the polymerization rate (R_p) shown by Equation (6).^[66,67] Based on Equation (5), in order to obtain a high degree of control over the polymerization (low dispersity), there must be a sufficient concentration of deactivator (XC) present in the system. However, it is clear from Equation (6) that there is a trade-off between the polymerization rate and degree of control:

$$\mathcal{D} = 1 + \frac{k_p[PX]_0}{k_d[XC]} \left(\frac{2}{conv} - 1 \right) \quad (5)$$

$$R_p = k_p[M][PX] \left(\frac{k_a[C]}{k_d[XC]} \right) \quad (6)$$

In SI-ATRP from a flat substrate, the amount of initiator present on the surface is not nearly enough to provide sufficient accumulation of deactivator in the contacting system. This leads to an uncontrolled polymerization. Two procedures are commonly used to mitigate the uncontrolled SI-ATRP from flat substrates: the addition of free initiator^[68] and the addition of deactivator.^[50] The presence of free initiator provides solution chains that do terminate and, hence, accumulate enough deactivator to control the polymerization. For this reason, the free initiator is also often referred to as “sacrificial” initiator. Other than for maintaining control of the polymerization process, free initiator is also added to systems with flat substrates to provide an estimate of the properties of grafted chains. The validity of this estimation has been discussed in previous sections. On the other hand, the addition of deactivator can provide enough deactivator to control the polymerization without requiring surface chains to undergo termination. However, the addition of too much extra deactivator could result in retardation of the polymerization rate (Equation (6)).

One of the main differences between SI-ATRP from flat substrates involving addition of free initiator and addition of extra deactivator lies in the formation of free polymer. The free chains in solution greatly affect the polymerization kinetics of both chain populations. Because of the small amount of surface chains, the monomer conversion in SI-ATRP with extra deactivator is negligible. However, free initiator in solution can

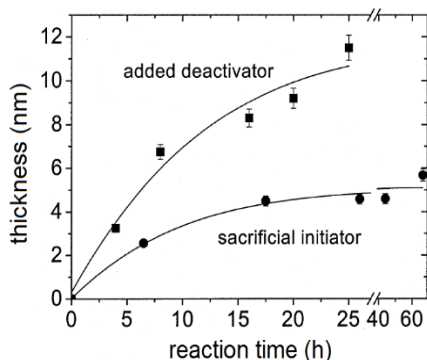


Figure 6-9. Growth profiles of grafted polystyrene on a silicon wafer with addition of sacrificial initiator (circles) or deactivator (squares). Reprinted with permission from [69]

consume significant amounts of monomer and cause monomer depletion. For this reason, a thicker polymer layer is usually obtained when the polymerization is conducted using SI-ATRP with added deactivator.^[69,70] Figure 6-9 shows a comparison between the growth profiles obtained from these two methods.

As noted above, in SI-ATRP with addition of deactivator, the consumption of monomer is negligible; therefore, the growth profile of the polymer layer with time is expected to be linear in an ideal case (no crowding or termination effects). On the other hand, monomer conversion in SI-ATRP with free initiator is not negligible. Hence, the growth profile of the polymer layer with conversion is expected to be linear in an ideal case, where the polymerization rates of solution and surface chains are the same. Deviation from linearity in the growth profile with time or with conversion (added deactivator or sacrificial initiator, respectively) could be explained by applying the philosophy of either the school of propagation or school of termination, as previously discussed.

In particle systems, as a result of the large surface-to-volume ratio, a sufficient number of surface initiators might be present to generate the required concentration

of deactivator in the solution. However, free initiator and/or excess deactivator are still often added to this system. Free initiator is often added for SI-ATRP of particles for multiple reasons. One reason is to provide better control over the polymerization, another is to prevent macroscopic gelation resulting from interparticle coupling.

The type of catalyst has also been shown to affect the equilibrium in SI-ATRP. Huang et al. compared the use of CuBr with CuCl for SI-ATRP of MMA from silica nanoparticles.^[24] The grafted chains on the nanoparticles were cleaved and their dispersity used as an indicator of polymerization controllability. They found that CuBr resulted in faster polymerization but produced a less uniform polymer layer and higher dispersity. Several researchers have attributed poorer control to differences in the local concentrations of catalyst and deactivator, which can affect the equilibrium experienced by the surface chains. According to experimental results from Behling et al., surface-initiated polymerization occurs faster than solution polymerization.^[18] The difference in polymerization rate was attributed to deviation of the ratio of local concentrations of catalyst and deactivator available to the surface chains, as shown in Figure 6-10. They postulated that in the “viscous front” (shaded area in Figure 6-10) the local concentration of catalyst (C) is higher than that in the bulk, whereas the opposite is true for the local concentration of deactivator (XC). Because of the reduced deactivation rate in the viscous front, the surface radical concentration increases, which results in a faster propagation rate for surface-tethered chains than for chains present in the contacting solution.

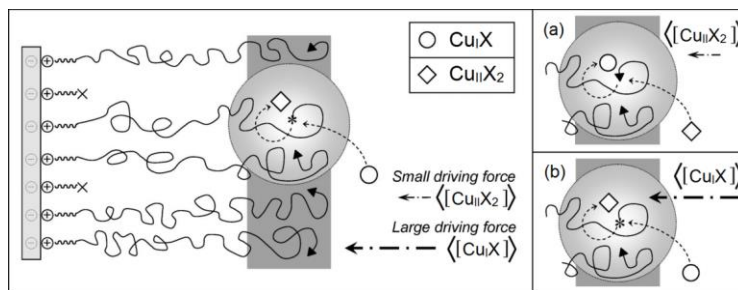


Figure 6-10. The growing viscous front for SI-ATRP postulated by Behling et al. The local concentration of catalyst in the shaded area is higher than that in the bulk solution, whereas the local concentration of deactivator is lower than that in the bulk. (a) conversion of catalyst (\diamond) to deactivator (\circ) (b) conversion of deactivator to catalyst. Reproduced with permission from [18]

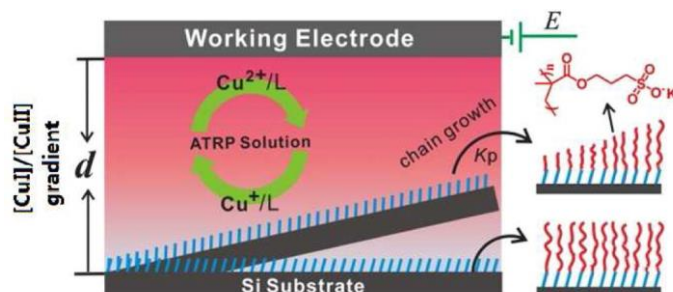


Figure 6-11. Generation of a gradient of catalyst-to-deactivator concentration ratio induced by adjusting the distance between the surface and the electrode, resulting in a gradient in the thickness of the grafted polymer layer. Reproduced with permission from [71]

Li et al. investigated the effect of catalyst-to-deactivator concentration ratio on the growth of a polymer layer on a flat substrate.^[71] They induced a gradient of the concentration ratio of activator to deactivator by using electrochemically mediated ATRP (eATRP) and tilting the substrate toward the electrode (as illustrated in Figure 6-11). In eATRP, the catalyst is regenerated electrochemically from the deactivator.^[72] By adjusting the distance, the surface closer to the electrode experiences a higher

concentration ratio of catalyst to deactivator, thereby experiencing a faster polymerization, as indicated by the thickness gradient in the grafted polymer layer.

6.3.5 Transfer

Several studies have investigated the importance of chain transfer reactions in solution ATRP. The importance of chain transfer to ligand was reported by Matyjaszewski and coworkers for ATRP of n-butyl acrylate.^[73] This chain transfer reaction was proposed to be the cause of the deviation observed in the first-order kinetic plot when excess ligand (pentamethyldiethylenetriamine, PMDETA) was used in the polymerization recipe. The mechanism of the chain transfer reaction to PMDETA was further investigated by Sharma et al.^[74] Chain transfer to PMDETA has been proposed to induce a higher degree of control for SI-ATRP systems containing acrylate monomers.^[75] This was achieved by conducting the SI-ATRP at a higher ratio of ligand to catalyst, $[PMDETA]/[CuBr] = 3$, in the absence of excess deactivator and free initiator. Other SI-ATRP studies have also used similar polymerization recipes, with elevated levels of PMDETA for an *N*-isopropylacrylamide (NIPAM) system showing great success.^[14,76-78]

The extent of chain transfer reactions in SI-ATRP could affect the polymerization kinetics and the resulting grafting density of polymers. However, further studies need to be conducted in order to fully understand the role of chain transfer reactions in the SI-ATRP mechanism.

6.3.6 Other side reactions

For some monomers (*e.g.*, styrene) thermal self-initiation is unavoidable. This results in simultaneous polymerization in solution and on the surface, even in the absence of added free ATRP initiator. The presence of free polymers might not be desirable, as they can alter the properties of the bulk nanoparticle system, hence requiring further separation steps. Moreover, the presence of free polymer chains affects the characterization of grafted polymer properties, including the estimation of grafting density, potentially generating large errors.^[29,79] Therefore, when seeking to determine the properties of a hybrid system, the presence of free polymer chains must be quantified to account for their effect on the system, or to ensure that they have been fully separated from the system. Figure 6-12 illustrates how even the presence of a small amount of free polymer chains can bridge the voids between grafted nanoparticles at certain particle size/graft chain molecular weight, thereby altering the material properties.

In nanoparticle systems, the separation of free polymers and grafted nanoparticles can be tricky and time-consuming. Therefore, it is necessary to understand factors affecting thermal self-initiation in order to control its rate. Tchoul and coworkers used size exclusion chromatography (SEC) to quantify the amount of free polystyrene chains formed during the SI-ATRP of styrene from nanoparticles (shown in Figure 6-13).^[29] They demonstrated the accuracy of using SEC to quantify the small amount of free polymer chains. They have also shown that interparticle distance is greatly

affected by the presence of free polymer chains, as indicated by the results of their TEM studies.^[79] By quantifying the formation of free polystyrene, they optimized the reaction conditions to suppress the thermal self-initiation of styrene. Using the dependence of thermal self-initiation rate on time and temperature the authors minimized the rate by using a lower reaction temperature combined with the use of a more active catalyst system.^[29,79]

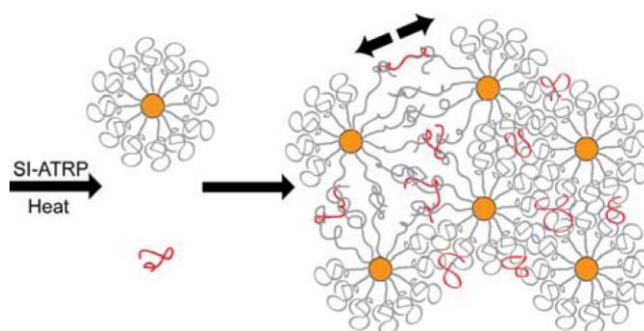


Figure 6-12. Presence of free polymer chains in a grafted nanoparticles system. The free chains act as bridges for the grafted nanoparticles to form a network. Reproduced with permission from ^[79]

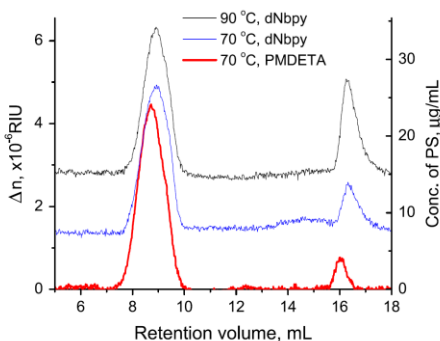


Figure 6-13. SEC results for polystyrene grafted from silica nanoparticles with different polymerization recipes. The concentration axis on the right is only applicable to peaks at 16-17 mL. Reprinted with permission from ^[29]

Chakkalakal et al. conducted SI-ATRP of MMA and styrene from silica nanoparticles, and their GPC curves showed a bimodality in the MWD of grafted polystyrene on silica nanoparticles at high conversion.^[36] The SI-ATRP was conducted at an elevated temperature, with free polymers formed by thermal self-initiation of styrene at 90°C. Even though there was significant bimolecular termination occurring via a coupling mechanism, as indicated by the bimodal MWD, the DLS result did not show evidence of interparticle termination. Therefore, the coupling could occur only by intraparticle coupling or by coupling of a surface radical with solution radical.

Mu et al. demonstrated the formation of polymer nanocapsules using SI-ATRP to grow a polymer brush from particles, crosslinking of the tethered polymer brush, followed by etching of the particles.^[80] Silica nanoparticles can work as a template for the preparation of polymeric nanocapsules. In an extension of this concept, formation of nanonetwork polymers was demonstrated by Matyjaszewski and coworkers, as shown in Figure 6-14.^[81] In addition to forming a nanocapsule by etching the silica particles after crosslinking, the authors also showed that a nanonetwork of carbon materials can be obtained by carbonizing the polymer prior to etching the core of the nanoparticles. The resulting material was a core-shell system with a mesoporous core from the silica template and a microporous shell from the intraparticle crosslinking of the tethered carbon precursor polymer brush.

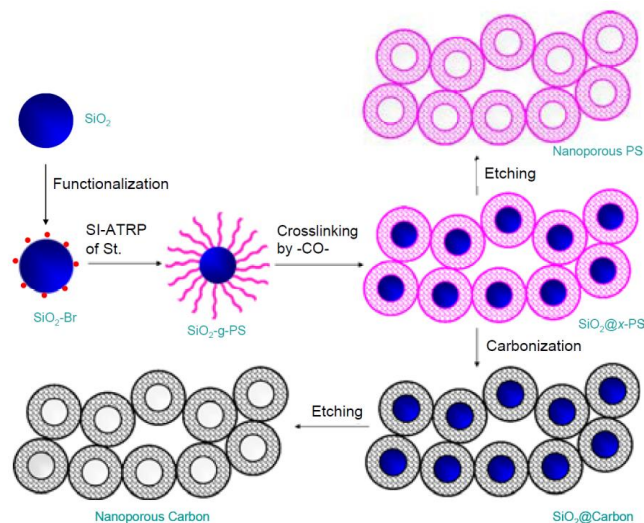


Figure 6-14. Formation of nanonetwork polymers and carbon materials using SI-ATRP from silica nanoparticles. Reproduced with permission from [81]

§ 6.4 Conclusions

SI-ATRP is a very rapidly developing area of the polymer and materials sciences. The scope of the procedure is constantly evolving, benefiting from new advances in ATRP, such as new catalysts and new initiating techniques, but also from seeking to meet an increasing demand for new advanced nanostructured materials. New ATRP techniques such as eATRP and photoATRP that are mediated by external stimuli have been successfully applied for modification and patterning of surfaces. The modified surfaces can provide extraordinary properties in terms of adhesion, lubrication, antifouling, and antimicrobial behavior. As described in this review, modification of flat, concave, and convex surfaces with polymeric brushes dramatically alters the surface properties of the substrates and provides good dispersibility of nanoparticles, creates responsiveness in membranes, and provides other properties to composite

materials. Although the general polymerization kinetics and mechanisms of homogeneous ATRP and SI-ATRP are similar, there are some peculiarities that can alter the molecular properties of the tethered polymer chains. These differences are based on the specific distribution of active centers anchored to surfaces, diffusion, congestion, and other phenomena. SI-ATRP sometimes resembles other CRP systems but also carries some specific behavior associated with the activator/deactivator nature of ATRP catalysts. Better understanding of such mechanistic features will help in the design and synthesis of new and more efficient hybrid materials.

§ 6.5 References

- [1] C. M. Hui, J. Pietrasik, M. Schmitt, C. Mahoney, J. Choi, M. R. Bockstaller, K. Matyjaszewski, *Chem Mater* **2014**, *26*, 745-762.
- [2] J. Pyun, K. Matyjaszewski, *Chem Mater* **2001**, *13*, 3436-3448.
- [3] H. Dong, M. Zhu, J. A. Yoon, H. Gao, R. Jin, K. Matyjaszewski, *J Am Chem Soc* **2008**, *130*, 12852-12853.
- [4] H. Mori, D. C. Seng, M. Zhang, A. H. E. Mueller, *Langmuir* **2002**, *18*, 3682-3693.
- [5] D. Julthongpiput, Y.-H. Lin, J. Teng, E. R. Zubarev, V. V. Tsukruk, *Langmuir* **2003**, *19*, 7832-7836.
- [6] I. Luzinov, S. Minko, V. V. Tsukruk, *Prog Polym Sci* **2004**, *29*, 635-698.
- [7] P. Ye, H. Dong, M. Zhong, K. Matyjaszewski, *Macromolecules* **2011**, *44*, 2253-2260.
- [8] B. Zhao, T. He, *Macromolecules* **2003**, *36*, 8599-8602.
- [9] M. Kruk, B. Dufour, E. B. Celer, T. Kowalewski, M. Jaroniec, K. Matyjaszewski, *Macromolecules* **2008**, *41*, 8584-8591.
- [10] R. Chen, W. Feng, S. Zhu, G. Botton, B. Ong, Y. Wu, *J Polym Sci, Part A: Polym Chem* **2006**, *44*, 1252-1262.
- [11] W. Feng, R. Chen, J. L. Brash, S. Zhu, *Macromol Rapid Commun* **2005**, *26*, 1383-1388.

- [12] J. R. Ell, D. E. Mulder, R. Faller, T. E. Patten, T. L. Kuhl, *Macromolecules* **2009**, *42*, 9523-9527.
- [13] M. R. Tomlinson, K. Efimenko, J. Genzer, *Macromolecules* **2006**, *39*, 9049-9056.
- [14] S. Wang, Y. Zhu, *Langmuir* **2009**, *25*, 13448-13455.
- [15] D. M. Jones, A. A. Brown, W. T. S. Huck, *Langmuir* **2002**, *18*, 1265-1269.
- [16] Z. Bao, M. L. Bruening, G. L. Baker, *Macromolecules* **2006**, *39*, 5251-5258.
- [17] H. Jia, A. Wildes, S. Titmuss, *Macromolecules* **2012**, *45*, 305-312.
- [18] R. E. Behling, B. A. Williams, B. L. Staade, L. M. Wolf, E. W. Cochran, *Macromolecules* **2009**, *42*, 1867-1872.
- [19] B. Lego, M. François, W. G. Skene, S. Giasson, *Langmuir* **2009**, *25*, 5313-5321.
- [20] T. Wu, K. Efimenko, P. Vlček, V. Šubr, J. Genzer, *Macromolecules* **2003**, *36*, 2448-2453.
- [21] I. Lilge, M. Steuber, D. Tranchida, E. Sperotto, H. Schönherr, *Macromol Symp* **2013**, *328*, 64-72.
- [22] B. R. Coad, K. E. Styan, L. Meagher, *ACS Applied Materials & Interfaces* **2014**, *6*, 7782-7789.
- [23] K. Ohno, T. Morinaga, K. Koh, Y. Tsujii, T. Fukuda, *Macromolecules* **2005**, *38*, 2137-2142.
- [24] C. Huang, T. Tassone, K. Woodberry, D. Sunday, D. L. Green, *Langmuir* **2009**, *25*, 13351-13360.
- [25] D. Sunday, S. Curras-Medina, D. L. Green, *Macromolecules* **2010**, *43*, 4871-4878.
- [26] J. Pietrasik, C. M. Hui, W. Chaladaj, H. Dong, J. Choi, J. Jurczak, M. R. Bockstaller, K. Matyjaszewski, *Macromol Rapid Commun* **2011**, *32*, 295-301.
- [27] J. Pyun, S. Jia, T. Kowalewski, G. D. Patterson, K. Matyjaszewski, *Macromolecules* **2003**, *36*, 5094-5104.
- [28] A. El Harrak, G. Carrot, J. Oberdisse, C. Eychenne-Baron, F. Boué, *Macromolecules* **2004**, *37*, 6376-6384.
- [29] M. N. Tchoul, M. Dalton, L.-S. Tan, H. Dong, C. M. Hui, K. Matyjaszewski, R. A. Vaia, *Polymer* **2012**, *53*, 79-86.
- [30] S. E. Averick, C. G. Bazewicz, B. F. Woodman, A. Simakova, R. A. Mehl, K. Matyjaszewski, *Eur Polym J* **2013**, *49*, 2919-2924.
- [31] C. Sugnaux, L. Lavanant, H.-A. Klok, *Langmuir* **2013**, *29*, 7325-7333.

- [32] N. Cheng, O. Azzaroni, S. Moya, W. T. S. Huck, *Macromol Rapid Commun* **2006**, *27*, 1632-1636.
- [33] J.-B. Kim, M. L. Bruening, G. L. Baker, *J Am Chem Soc* **2000**, *122*, 7616-7617.
- [34] R. R. Shah, D. Merrezeys, M. Husemann, I. Rees, N. L. Abbott, C. J. Hawker, J. L. Hedrick, *Macromolecules* **2000**, *33*, 597-605.
- [35] J. Hou, Q. Shi, P. Stagnaro, W. Ye, J. Jin, L. Conzatti, J. Yin, *Colloids and Surfaces B: Biointerfaces* **2013**, *111*, 333-341.
- [36] G. L. Chakkalakal, M. Alexandre, C. Abetz, A. Boschetti-de-Fierro, V. Abetz, *Macromol Chem Phys* **2012**, *213*, 513-528.
- [37] L. Bombalski, K. Min, H. Dong, C. Tang, K. Matyjaszewski, *Macromolecules* **2007**, *40*, 7429-7432.
- [38] F. Audouin, H. Blas, P. Pasetto, P. Beaunier, C. Boissière, C. Sanchez, M. Save, B. Charleux, *Macromol Rapid Commun* **2008**, *29*, 914-921.
- [39] P. Pasetto, H. l. n. Blas, F. Audouin, C. d. Boissière, C. m. Sanchez, M. Save, B. Charleux, *Macromolecules* **2009**, *42*, 5983-5995.
- [40] H. Liu, Y.-L. Zhu, J. Zhang, Z.-Y. Lu, Z.-Y. Sun, *ACS Macro Letters* **2012**, *1*, 1249-1253.
- [41] X. Gao, W. Feng, S. Zhu, H. Sheardown, J. L. Brash, *Macromol React Eng* **2010**, *4*, 235-250.
- [42] S. Turgman-Cohen, J. Genzer, *J Am Chem Soc* **2011**, *133*, 17567-17569.
- [43] S. Turgman-Cohen, J. Genzer, *Macromolecules* **2012**, *45*, 2128-2137.
- [44] Y. Tsujii, K. Ohno, S. Yamamoto, A. Goto, T. Fukuda, "Structure and Properties of High-Density Polymer Brushes Prepared by Surface-Initiated Living Radical Polymerization", in *Surface-Initiated Polymerization I*, R. Jordan, Ed., Springer Berlin Heidelberg, Berlin, Heidelberg, 2006, p. 1-45.
- [45] D. Schneider, M. Schmitt, C. M. Hui, R. Sainidou, P. Rembert, K. Matyjaszewski, M. R. Bockstaller, G. Fytas, *ACS Macro Letters* **2014**, *3*, 1059-1063.
- [46] E. Mastan, L. Xi, S. Zhu, *Macromol Theory Simul* **2015**.
- [47] W. Huang, J.-B. Kim, M. L. Bruening, G. L. Baker, *Macromolecules* **2002**, *35*, 1175-1179.
- [48] G. J. Dunderdale, C. Urata, D. F. Miranda, A. Hozumi, *ACS Applied Materials & Interfaces* **2014**, *6*, 11864-11868.
- [49] P. Jain, J. Dai, G. L. Baker, M. L. Bruening, *Macromolecules* **2008**, *41*, 8413-8417.

- [50] K. Matyjaszewski, P. J. Miller, N. Shukla, B. Immaraporn, A. Gelman, B. B. Luokala, T. M. Siclovan, G. Kickelbick, T. Vallant, H. Hoffmann, T. Pakula, *Macromolecules* **1999**, *32*, 8716-8724.
- [51] W. Feng, J. Brash, S. Zhu, *J Polym Sci, Part A: Polym Chem* **2004**, *42*, 2931-2942.
- [52] D. Xiao, M. J. Wirth, *Macromolecules* **2002**, *35*, 2919-2925.
- [53] D. Zhou, X. Gao, W.-j. Wang, S. Zhu, *Macromolecules* **2012**, *45*, 1198-1207.
- [54] J.-B. Kim, W. Huang, M. D. Miller, G. L. Baker, M. L. Bruening, *J Polym Sci, Part A: Polym Chem* **2003**, *41*, 386-394.
- [55] Y. Wang, N. Soerensen, M. Zhong, H. Schroeder, M. Buback, K. Matyjaszewski, *Macromolecules* **2013**, *46*, 683-691.
- [56] D. Koylu, K. R. Carter, *Macromolecules* **2009**, *42*, 8655-8660.
- [57] K. Yamamoto, Y. Miwa, H. Tanaka, M. Sakaguchi, S. Shimada, *J Polym Sci, Part A: Polym Chem* **2002**, *40*, 3350-3359.
- [58] C. Kang, R. M. Crockett, N. D. Spencer, *Macromolecules* **2014**, *47*, 269-275.
- [59] C. Devaux, J. P. Chapel, E. Beyou, P. Chaumont, *The European Physical Journal E* **2002**, *7*, 345-352.
- [60] Y. Miwa, K. Yamamoto, M. Sakaguchi, S. Shimada, *Macromolecules* **2001**, *34*, 2089-2094.
- [61] S. Yamago, Y. Yahata, K. Nakanishi, S. Konishi, E. Kayahara, A. Nomura, A. Goto, Y. Tsujii, *Macromolecules* **2013**, *46*, 6777-6785.
- [62] K. Ohno, T. Akashi, Y. Huang, Y. Tsujii, *Macromolecules* **2010**, *43*, 8805-8812.
- [63] K. Ohno, H. Tabata, Y. Tsujii, *Colloid Polym Sci* **2013**, *291*, 127-135.
- [64] C. B. Gorman, R. J. Petrie, J. Genzer, *Macromolecules* **2008**, *41*, 4856-4865.
- [65] H. Fischer, *Macromolecules* **1997**, *30*, 5666-5672.
- [66] K. Matyjaszewski, *J Macromol Sci, Part A: Pure Appl Chem* **1997**, *10*, 1785-1801.
- [67] T. Fukuda, A. Goto, *Macromol Rapid Commun* **1997**, *18*, 683-688.
- [68] M. Ejaz, S. Yamamoto, K. Ohno, Y. Tsujii, T. Fukuda, *Macromolecules* **1998**, *31*, 5934-5936.
- [69] J. D. Jeyaprakash, S. Samuel, R. Dhamodharan, J. R uhe, *Macromol Rapid Commun* **2002**, *23*, 277-281.
- [70] R. Chen, W. Feng, S. Zhu, G. Botton, B. Ong, Y. Wu, *Polymer* **2006**, *47*, 1119-1123.

-
- [71] B. Li, B. Yu, W. T. S. Huck, W. Liu, F. Zhou, *J Am Chem Soc* **2013**, *135*, 1708-1710.
- [72] A. J. D. Magenau, N. C. Strandwitz, A. Gennaro, K. Matyjaszewski, *Science* **2011**, *332*, 81-84.
- [73] J. Huang, T. Pintauer, K. Matyjaszewski, *J Polym Sci, Part A: Polym Chem* **2004**, *42*, 3285-3292.
- [74] R. Sharma, A. Goyal, J. M. Caruthers, Y.-Y. Won, *Macromolecules* **2006**, *39*, 4680-4689.
- [75] Q. Yu, Y. Zhang, H. Chen, Z. Wu, H. Huang, C. Cheng, *Colloids and Surfaces B: Biointerfaces* **2010**, *76*, 468-474.
- [76] X. J. Wang, P. W. Bohn, *Advanced Materials* **2007**, *19*, 515-520.
- [77] C. Xue, N. Yonet-Tanyeri, N. Brouette, M. Sferrazza, P. V. Braun, D. E. Leckband, *Langmuir* **2011**, *27*, 8810-8818.
- [78] X. Liu, Q. Ye, B. Yu, Y. Liang, W. Liu, F. Zhou, *Langmuir* **2010**, *26*, 12377-12382.
- [79] C. M. Hui, A. Dang, B. Chen, J. Yan, D. Konkolewicz, H. He, R. Ferebee, M. R. Bockstaller, K. Matyjaszewski, *Macromolecules* **2014**, *47*, 5501-5508.
- [80] B. Mu, R. Shen, P. Liu, *Colloids and Surfaces B: Biointerfaces* **2009**, *74*, 511-515.
- [81] D. Wu, C. M. Hui, H. Dong, J. Pietrasik, H. He, H. J. Ryu, Z. Li, M. Zhong, M. Jaroniec, T. Kowalewski, K. Matyjaszewski, *Polymer Preprints* **2011**, *52*, 693-694.

7 PROPAGATION VERSUS TERMINATION IN SI-ATRP

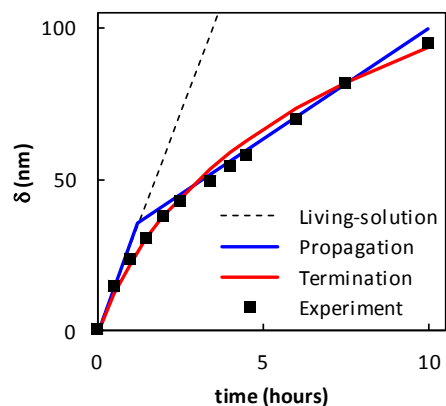
In this chapter, two simplified models developed from existing theories, namely propagation and termination theories, are compared to experiment trends from literature. This chapter is published in *Macromolecular Theory and Simulations* journal, **2015**, 24 (2), p.89-99 (doi:10.1002/mats.201400085) under the title “What limits the chain growth from flat surfaces in surface-initiated ATRP: Propagation, termination or both?”. This reproduction is done with permission from John Wiley and Sons.

Author contributions

This work is completed under the guidance of Dr. Li Xi and Dr. Shiping Zhu. Erlita Mastan prepared the first draft of the manuscript, followed by revisions from Dr. Li Xi and from Dr. Shiping Zhu.

§ 7.1 Abstract

Surface-initiated controlled radical polymerization, such as ATRP, has been proven to be a powerful method for preparation of well-controlled functional grafted polymers. There are thousands of experimental works published, by varying polymers, surfaces, and applications. In comparison, theoretical developments are very lacking. Many fundamental questions still remain to be answered. These questions include, but not limited to: What determine the surface initiator efficiency? How many chains per square nanometer can be fully grown? What is the maximum thickness can polymer grow to? If chains are simultaneously grown from surface and solution, which has higher molecular weight? Answers to these questions are most helpful for innovation and further development in this important area. In this work, we employed recently developed theories to explain experimentally observed kinetic profiles of polymer layer thickness growth. What limits the growth of surface chains? Is it the monomer starvation in grafting layer that slow down propagation? Or is it the termination of radicals that stop the chain growth? It was found that no existing models could fully explain the often contradictory experimental observations. It is our hope that this work will provoke further discussions and inspire more effort in resolving the fundamental issues of this area.



§ 7.2 Introduction

Modifications of surfaces via surface-initiated controlled radical polymerization, particularly surface-initiated atom transfer radical polymerization (SI-ATRP), have been the focus of many research studies, as indicated by the recent reviews.^[1-7] This method is versatile owing to the numerous possible combinations of substrates and polymers. Moreover, the use of ATRP, which is one of the most commonly studied reversible deactivation radical polymerization (RDRP), allows precise tailoring of chain microstructural properties of the polymers, giving practically endless possibilities of materials that can be designed. However, despite the numerous publications, factors affecting the mechanism behind the SI-ATRP process are still not well understood. For example, in the SI-ATRP from flat surfaces, most experimental works showed limited polymer layer thicknesses from tens to hundreds of nanometers. Very few literatures reported polymer layer thicknesses over five hundred nanometers. The thickness increases with polymerization time not always in a linear fashion. An initial linear increase in thickness is often followed by a levelling off in the growth rate. In other words, the growth rate slows down during SI-ATRP, in the presence of abundant monomer.

What cause the rate reduction and limit the polymer layer thickness? In many applications, thicker layers may be desirable. Would it be possible to grow polymer chains as long as we want, and to graft a polymer layer as thick as desired? What are the mechanisms that stop chains from growing in the presence of abundant

monomer? With thousands of papers published on SI-ATRP and other types of surface-initiated controlled radical polymerization, this is unarguably one of the most important fundamental questions, which unfortunately remain to be resolved.

In published literatures, there are two groups of theories, attempting to provide a mechanistic explanation. The first group assumes the polymerization as a perfectly living system, *i.e.*, without any radical termination. However, they consider crowding from grafted chains, thus starving of monomers in the grafted layer, to affect the kinetics.^[8-13] The chain-crowded monomer-starved environment reduces the available monomer molecules for radical chain ends, which are buried inside the polymer layer, thereby reducing the growth rate. The second group models surface polymerization without the chain crowding effect, but with radical termination playing an important role in the growth kinetics of the grafted layer.^[14-19] Based on intuition, radicals constrained to surface are not free to move around. However, it is believed that while the chains are not free to move, radical centers could migrate through the radical activation and deactivation reactions facilitated by catalytic species in solution. For simplicity purpose, the first group is termed *propagation theory* (*i.e.*, diffusion-controlled propagation due to the monomer starving condition, caused by crowding of grafted chains inside the polymer layer), while the second group is termed *termination theory* (*i.e.*, the surface radicals migrate with the help of catalytic species in solution and thus be terminated). It should be noted that while the

two theories assigned different factors to affect growth kinetics of the grafted layer, they are not mutually exclusive.

Knowledge of the actual mechanisms is valuable for optimization of the process and to allow design of experiments to better tailor the polymer properties. Modeling provides a powerful tool in understanding polymerization mechanisms. Model-based experiment design would reduce the cost of trial and error needed to obtain the desired products. Mechanistic investigation behind a process can be best conducted through combination of modeling and experiment.

The use of flat substrates in studying the mechanism of SI-ATRP is advantageous over particles or porous substrates, because it reduces complication from having to account possible curvature effects on the kinetics. However, only small number of initiation sites could be incorporated on flat substrate. This poses a problem in maintaining control over polymerization and in characterizing the grafted polymer due to its low amount of polymer materials. In order to counter the control problem, either sacrificial initiator^[20] or excess deactivator^[21] could be added to the solution. When sacrificial initiator is added to the solution, ATRP occurs simultaneously in solution and on surface. The solution (free) polymers are often characterized and its properties used as estimates for surface (grafted) polymers. The validity of this approximation has been questioned by several modeling and experiment studies.^[9,10,17,19,22]

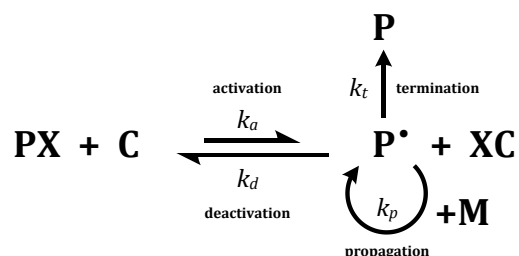
On the other hand, SI-ATRP in the presence of excess deactivator does not yield free polymers, because polymerization occurs strictly on the surface. Due to low amount of initiation sites, no significant consumption of monomer in solution is expected. This contributes to thicker grafted layer than that with sacrificial initiator, as reported by many experiments.^[16,23,24] Therefore, SI-ATRP with excess deactivator is more favorable in producing thicker grafted layers. However, despite the negligible consumption of monomer, numerous kinetic data have shown tapering off of the growth rate with time, instead of the expected constant growth rate.^[15,16,24-29]

In this study, we make effort in examining these two major groups with a model-based approach. SI-ATRP with excess deactivator on a flat surface is the focus of the present study. However, this issue is general with all types of surface-initiated controlled radical polymerization. We first derive simple version kinetic models based on the two theories, *propagation* and *termination*. The comparison and contrast of model predictions with the reported experimental observations reveal important insights into the mechanisms.

§ 7.3 Model formulation

Two phases are considered in this study, the bulk phase and the grafted layer phase. The bulk phase consists only of monomer (M), catalyst (C), and deactivator (XC). Meanwhile, the grafted layer consists of the same reactants and the polymer chains, both radical chains (P^\bullet) and dormant chain (PX). The subscript in the notation

indicates the phase of interest, with b denoting the bulk phase and g referring to the grafted layer. The reactions involved in ATRP are shown in Scheme 7-1. Other side reactions not included in the scheme are considered to be negligible. The bulk phase



Scheme 7-1. Reaction mechanisms for ATRP

acts as a reservoir of reactants, with no reaction occurring. Due to the small amount of surface initiator, monomer consumption is expected to be negligible in the SI-ATRP conducted without sacrificial initiator (*i.e.*, monomer concentration in the bulk phase is constant, that is, $[M]_b$ is time independent).

In this study, the grafted polymer is characterized through the dry polymer layer thickness, instead of the average chain length, to facilitate comparison with experiment data published in literatures. Using mass balance, the growth kinetics could be shown to follow Equation (1), where δ is dry thickness of the polymer layer, R_p is propagation rate, m is monomer molar mass, and ρ is density of the dry polymer. The propagation rate is the rate of monomer addition to the grafted layer per unit area, which could be calculated from propagation rate constant (k_p) and monomer and radical concentrations in the grafted layer.

$$\frac{d\delta}{dt} = \frac{m}{\rho} \times R_p = \frac{m}{\rho} (k_p [M]_g [P^\bullet]_g) \quad (1)$$

Three models based on Equation (1) are considered in this study, namely, *living-solution* model, *propagation* model, and *termination* model. As the name suggests, the *living-solution* model considers condition equivalent to living polymerization conducted in solution, *i.e.*, with no radical termination and no chain crowding effect. The *propagation* model refers to the model derived by taking into account monomer starving environment inside the polymer layer due to crowding of grafted chains. The *termination* model is adopted from the previously published work,^[18] which accounts for the radical termination reaction occurring between grafted chains. This termination reaction results in a decrease of radical concentration. Assumptions considered in the derivation of these models are summarized in Table 7-1, with explanations available in the subsequent sections.

Table 7-1. Underlying assumptions for various models discussed in this study

Factors considered	Living-solution	Propagation	Termination
Less reactants in grafted layer (crowding)	No	Yes ^a	No
Termination of grafted chains	No	No	Yes
Spatial distribution of reactants	No	No	No
Diffusion-limitation	No	No	No
Polymer conformations	No	Yes ^b	No
Transition between conformations	No	No	No

^a Partition coefficients of catalyst and deactivator are assumed to be the same

^b Rod conformation is assumed to have similar effect as mushroom conformation

Other studies have proposed the importance of local concentration of reactants.^[30,31] However, for simplicity purposes, spatial variation of reactants inside the grafted layer is not included in this study. In other words, the reactants are assumed to be

homogeneously distributed in the grafted layer. Moreover, the grafting density is assumed to be known a priori. Information of grafting density is crucial, but to the best of our knowledge, there is no theory to predict the grafting density as of yet.

7.3.1 Living-solution model

This model is derived by assuming no chain crowding and no radical termination. In other words, the monomer concentration in grafted layer is assumed to be similar to that in the bulk (*i.e.*, $[M]_g \approx [M]_b$), and that the radical concentration is constant. The resulting growth profile for this model is shown in Equation (2) with the radical concentration estimated using a quasi-steady state assumption. The quasi-steady state assumption is applied to the equilibrium reaction shown in Scheme 1. This model serves as a basis for comparison and contrast between the *propagation* and *termination* models, representing the extreme case of the two models.

$$\delta = \frac{m}{\rho} \left(k_p [M]_b \frac{k_a [C]_b [PX]_g}{k_d [XC]_b} \right) t \quad (2)$$

7.3.2 Propagation model

The conformation of grafted polymer chains depends on the distance between neighboring chains and the radius of gyration, which in turn depend on the grafting density and chain length, respectively. Therefore, the conformation of grafted chains changes throughout the course of polymerization as the polymer chains grow longer. At the beginning of polymerization, grafted chains exhibit rod conformation. As the

chains grow longer, they assume mushroom conformation in the absence of interactions between grafted chains (distance between neighboring chains is larger than the radius of gyration), or brush conformation in the presence of chain interactions. To simplify this model, the initial rod-like conformation at the beginning of polymerization is lumped together with the mushroom conformation. This simplification is expected to have little effect on the growth kinetics on the basis that crowding is not significant during both rod and mushroom regimes.

In brush conformation, the concentrations of available reactants (monomer, catalyst and deactivator) in the grafted layer are reduced due to chain crowding. The concentration ratios between grafted layer and bulk are defined as their partition coefficients. On the account of having similar sizes and chemical structures, the partition coefficients of catalyst and deactivator are assumed to have the same value. Therefore, their concentration ratio remains constant, resulting in negligible net effect on the growth rate. The expression of partition coefficient for monomer, γ , is derived based on mass balance, shown in Equation (3), which depends on the average chain length of the grafted polymer (r_N), dormant concentration ($[PX]_g$), wet thickness of the grafted layer (δ_{wet}), and monomer concentration in the bulk phase ($[M]_b$). Detailed derivation on the relation between wet thickness and average chain length of the grafted polymer is provided in the appendix.

$$\gamma = 1 - \frac{r_N [PX]_g}{\delta_{wet} [M]_b} \quad (3)$$

The transformation from mushroom to brush is assumed to occur at a critical thickness, δ^* . The transition stage from mushroom to brush is not modeled in this study, leading to abrupt change in the slope. In reality, the transition is smooth, but we believe this simplification should suffice to capture the trend for the *propagation* model as a first approximation. Using these assumptions, the dry thickness profile is shown in Equation (4).

$$\delta = \begin{cases} \frac{m}{\rho} \left(k_p[M]_b [PX]_g \frac{k_a[C]_b}{k_d[XC]_b} \right) t & \text{For } 0 \leq \delta \leq \delta^* \\ \frac{m}{\rho} \left(k_p[M]_b [PX]_g \frac{k_a[C]_b}{k_d[XC]_b} \right) \gamma t + \delta^*(1 - \gamma) & \text{For } \delta \geq \delta^* \end{cases} \quad (4)$$

7.3.3 Termination model

An explicit expression for the *termination* model was derived by Zhou et al., as shown in Equation (5).^[18] Detailed derivation of this expression, including the assumptions involved, could be found in the original publication.

$$\delta = \alpha \ln(1 + \beta t) \quad (5)$$

$$k_t = A[C] \exp(-\omega \tau) \quad (6)$$

$$\text{where } \alpha = \frac{m k_p [M]_b k_d [XC]_b}{\rho k_t k_a [C]_b} \quad \text{and} \quad \beta = k_t [PX]_g \left(\frac{k_a [C]_b}{k_d [XC]_b} \right)^2$$

$$A = \frac{k_t^o}{[C]^o \exp(-\omega \tau^o)}$$

k_t^o is termination rate constant for the system at $[C] = [C]^o$ and $\tau = \tau^o$

Based on comparison of the model to experiment data, Zhou et al. found that the termination rate constant (k_t) depends on both catalyst concentration ($[C]$) and grafting density (τ), as shown by Equation (6).^[18] The catalyst concentration dependence is rooted from the concept termed the “migration-assisted termination”. The activation-deactivation reactions of grafted chains facilitate the movement of active (radical) centers from one chain to another. Therefore, even though the chains are fixed onto surface, the active centers move more rapidly with a higher catalyst concentration due to more frequent activation-deactivation reactions. This “migration” of radical centers gives higher probability of two neighboring chains to have radical centers at the same time, which results in a higher termination rate. Zhou et al. have also compared the model to some experiment results, and suggested that the termination rate constant decreases with increasing grafting density following an exponential function. The reason for this exponential decrease is still unknown, but may be caused by the decrease in segmental diffusion rate of radical chains for termination due to increased crowding at higher grafting density.

The expressions from *living-solution*, *propagation*, and *termination* models provide an easily observed effect of each reaction parameter on the grafted layer growth. The explicit expressions also allow investigation of the effect of each variable separately, such as reaction rate constants, etc. The polydispersity of grafted layer could be obtained by using the method of moments, but it is not calculated in this study because of lack of experiment data for validation. It should also be noted that the

living-solution model could be obtained by simplifying the *propagation* and *termination* models to the extreme condition of negligible chain crowding and that of radical termination, respectively. Mathematically speaking, the limits of Equation (4) and (5) as γ and k_t approach 1 and 0 become Equation (2).

§ 7.4 Results and discussions

Simulation results from the three models described above are compared with the experiment trend collected from literatures for SI-ATRP conducted with excess deactivator.

7.4.1 Kinetics of growth rate

Most experiment studies have shown an initial linear increase in thickness followed by deceleration in the growth rate, even with negligible monomer consumption.^[15,16,24-29] By examining Equation (2), the *living-solution* model is not able to predict the rate reduction. However, both *propagation* and *termination* models could predict the decrease in growth rate as polymerization proceeds, as can be seen from Equation (4) and (5). A comparison of these models with experiment data^[25] obtained for SI-ATRP of MPC monomer on silicon wafer is shown in Figure 7-1, with the simulation parameters listed on Table 7-2.

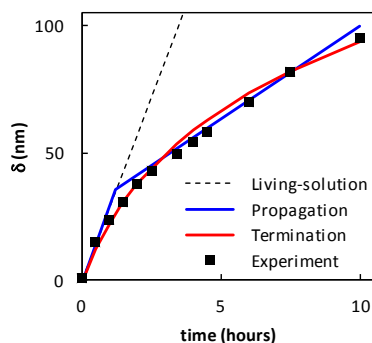


Figure 7-1. Comparison of growth profiles predicted using living-solution, propagation, and termination models to previously published SI-ATRP experiment data.^[25] Simulation parameters are shown in Table 7-2

Table 7-2. Simulation parameter for the model prediction of SI-ATRP experiment data^[25]

Model parameters	Value	Source
All models		
k_p (L/mol·s)	1600	[18]
k_a (L/mol·s)	1	[18]
k_d (L/mol·s)	3×10^5	This work
m (g/mol)	295	[25]
ρ (g/L)	1300	[25]
$[M]_b$ (mol/L)	1.33	[25]
$[M]:[C]:[XC]$	200:1:0.1	[25]
τ (chains/nm ²)	0.3	[25]
Propagation model		
c_1 (dm)	5×10^{-8}	This work
c_2 (dm/(chain/nm ²) ^{1/3})	7.5×10^{-9}	This work
Termination model		
k_t (dm ² /mol·s)	3×10^{13}	This work

Albeit offering decent fits to the experiment data, the *propagation* and *termination* models attributed the deceleration to the different mechanisms. The *propagation*

model assigned the decrease to the crowding of polymer chains in the grafted layer, creating a monomer-starving condition around the active chains. However, the *termination* model proposed the decreased number of active chains due to radical termination, which leads to the decrease in growth rate.

7.4.2 Effect of grafting density

The two defining parameters of grafted polymers are how thick and how packed the polymer layer is, *i.e.*, thickness (δ) and grafting density (τ). While thickness is easy to measure in experiment setting, grafting density is harder to determine, especially for the systems involving flat substrates. The grafting density is correlated to the number-average chain length (r_N) and thickness (or more accurately mass of the grafted polymer) as shown in Equation (7). Here, N_{Av} refers to the Avogadro's number (6.022×10^{23} chains/mole).

$$\tau = [PX]_g \times N_{Av} = \frac{\delta \times \rho}{r_N \times m} \times N_{Av} \quad (7)$$

Due to an insufficient amount of grafted polymers for GPC analysis, the average chain length of grafted polymer is usually not reported, which leaves two unknowns in Equation (7). Solutions to this problem include using immobilized surface initiator density instead of grafting density, or using model-based approach to calculate grafting density from the swollen and dry thickness measurements of the grafted layer.^[26,27,29] The chain length of grafted polymers could then be estimated from

Equation (7), or it could also be represented by the normalized thickness, which is defined as the dry thickness divided by grafting density in this study.

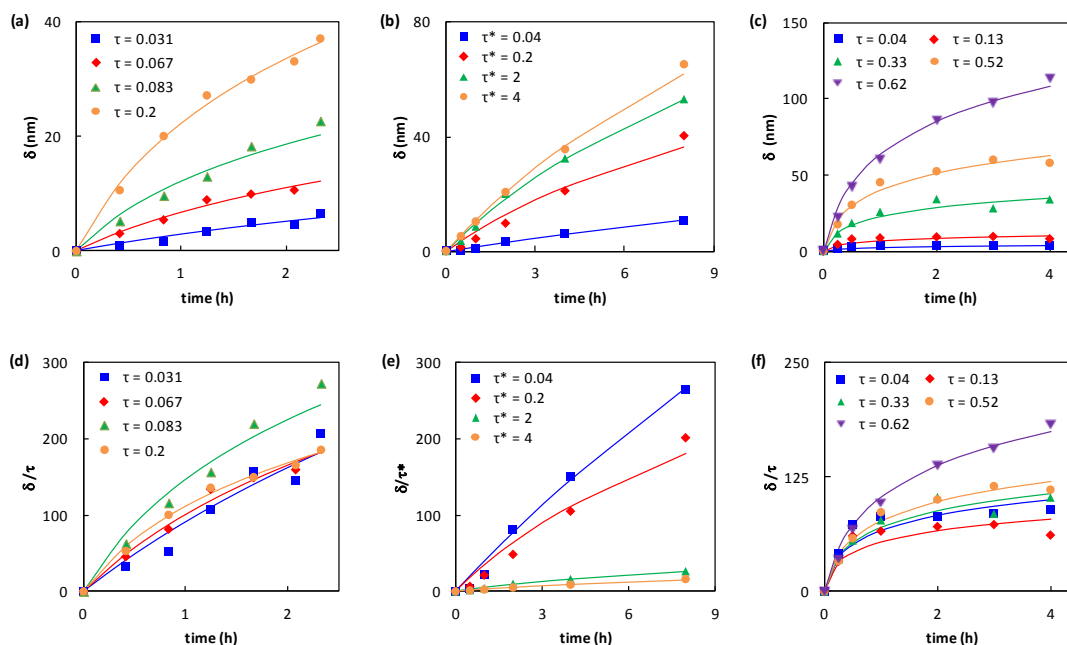


Figure 7-2. Growth profiles of the grafted polymer at various graft densities (or initiator densities, τ^*). Solid lines are guides to eyes. (a)–(c) dry thickness profile, (d)–(f) normalized dry thickness profile. (a),(b),(d),(e) SI-ATRP of poly(methyl methacrylate) (PMMA) on gold-coated surfaces.^[26,27] (c), (f) SI-ATRP of poly(N-isopropylacrylamide) (PNIPAM) on silicon wafers^[29]

In experiment, the grafting density is varied by controlling surface concentration of immobilized initiator using inert initiator spacers. ^[26,27,29] From experiment results, grafted layers grow faster for the systems with higher grafting densities (or initiator densities, τ^*), as shown in Figure 7-2 (a)–(c).^[26,27,29] This finding is as expected because dry thickness is proportional to the total mass of polymer formed (*i.e.*, $\delta \propto r_N \times \tau$), when density of the grafted polymer layer, ρ is assumed to be constant. Moreover,

Figure 7-3 illustrates the prediction results from *living-solution*, *propagation*, and *termination* models, which qualitatively agree with the experiment data. Unless otherwise stated, all the model predictions are simulated using parameters listed in Table 7-3. It should be noted that similar observations could be made from the explicit expressions, making the predicted trend discussed in this work independent of the parameters used.

Table 7-3. Simulation parameters used for the model prediction in Figure 7-3, Figure 7-4, and Figure 7-6

Model parameters	Value	Model parameters	Value
All models		Propagation model	
k_p (L/mol·s)	500	c_1 (dm)	3×10^{-8}
k_a (L/mol·s)	1	c_2 (dm/(chain/nm ²) ^{1/3})	6×10^{-9}
k_d (L/mol·s)	10^6	c_3 (dm/(chain/nm ²) ^{1/2})	3×10^{-9}
m (g/mol)	100	Termination model	
ρ (g/L)	1000	ω (nm ² /chain)	3.5
$[M]_b$ (mol/L)	ρ/m	A	6×10^{15}
$[C]:[XC]$	0.1		

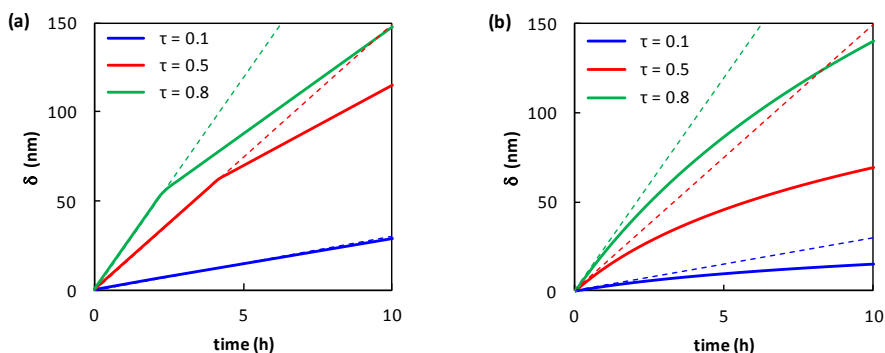


Figure 7-3. Dry thickness profiles of the grafted polymers grown via SI-ATRP for various grafting densities predicted with $[M]:[C] = 100$ using (a) propagation model (b) termination model. Dashed lines represent simulation results using living-solution model

In order to elucidate the effect of grafting density separately from the number of chains present, the thickness data are normalized by the corresponding grafting density (δ/τ), termed as the normalized thickness. The normalized thickness is proportional to the average chain length of the grafted chains. Unlike in the case of dry thickness, no clear trend is observed in kinetic growth of the normalized thickness from the experiment data, as illustrated in Figure 7-2 (d)–(f). The normalized thickness profiles calculated from the published data in Figure 7-2 (a) by Jones et al.^[27] are shown in Figure 7-2 (d). Increasing the grafting density first decreases and then increases the growth rate (the slopes of the curves). Moreover, in this set of data, the systems with the two lowest grafting densities do not exhibit any significant difference from one another. In a similar study by Bao et al.,^[26] the systems with higher grafting densities result in slower normalized thickness growth rates as shown in Figure 7-2 (e). In other words, polymer chains in the systems with higher grafting density grow slower. On the other hand, from the data reported by Wang et al.,^[29] the rates are similar to one another except for the system with the highest grafting density, which exhibits a higher growth rate, as can be seen in Figure 7-2 (f).

The prediction of normalized thickness growth from the *living-solution*, *propagation*, and *termination* models for the systems with various grafting densities are shown in Figure 7-4. From Equation (2), it is clear that the *living-solution* model predicts normalized thickness to be independent from the grafting density (or equivalently, dormant concentration). This generates a single master line for all the predicted

normalized thickness profiles by *living-solution* model, regardless of the grafting density values, as can be seen in Figure 7-4.

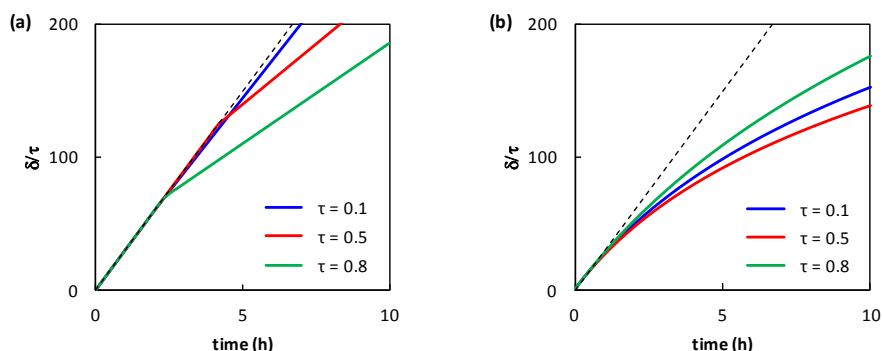


Figure 7-4. Normalized thickness profile of the grafted polymers grown via SI-ATRP for various grafting densities predicted with $[M]:[C] = 100$ using (a) propagation model (b) termination model. Dashed lines represent the simulation results obtained using living-solution model

From the *propagation* model's perspective, it can be expected that higher grafting density results in more severe crowding effect (lower γ), which causes the polymer to grow at lower rate. This could be observed from Equation (4) and Figure 7-4 (a). The *propagation* model predicts the trend of lower normalized thickness growth rate with higher grafting density (Figure 7-2 (e)). It cannot describe the opposite trend where higher growth rate with higher grafting density, as observed in some parts of the experiment data in Figure 7-2 (d) and (f). This may be due to over-simplification made in deriving the model. However, a careful re-examination of the assumptions listed in Table 7-1 for possible explanations revealed that (1) accounting for the spatial distribution of reactants would not have significant effect on the trend because the

distribution applies to all grafting densities, (2) taking diffusion into consideration should enhance the opposite trend because mass transfer limitation is more severe in a more crowded system, and (3) including the transition stage would not alter the trend, but make the predicted curve smoother. It becomes clear that the simple *propagation* model cannot explain all the observed trends of normalized thickness versus grafting density.

In the *termination* model, the effect of grafting density is not as straightforward. An increase in grafting density implies higher concentration of radicals, which results in higher termination rate. This in turn should reduce the normalized growth rate. However, from a previous simulation study, the termination rate constant was found to decrease with increasing grafting density, as expressed by Equation (6).^[18] Therefore, at $\tau < \omega^{-1}$ (refer to Equation (6)), the growth rate of normalized thickness decreases with increasing grafting density. As grafting density increases above ω^{-1} , the trend reverses. In other words, the *termination* model predicts that at low grafting density, the chain growth is slowed down by increasing grafting density, but at high grafting density, the chain growth is accelerated by the increased grafting density, as observed in Figure 7-2 (f)), but not as in Figure 7-2 (d). Clearly, neither *termination* model nor *propagation* model could fully explain the experiment data, reported in the literatures, regarding the dependence of normalized thickness growth rate (δ/τ) on grafting density (τ).

7.4.3 Effect of catalyst concentration (at constant $[C]/[XC]$)

Experiment data reported in the literatures have shown varying trends from one study to another, as shown in Figure 7-5.^[16,24,25] In a study by Kim et al., the growth rate of poly(methyl acrylate) thickness from gold-coated silicon wafer via SI-ATRP at room temperature decreased more rapidly with higher catalyst concentration, shown in Figure 7-5 (a).^[16] The same trend was also reported by Feng et al. for a similar SI-ATRP system but different monomer.^[25] However, as shown in Figure 7-5 (b), Jeyaprakash et al. observed the opposite trend for SI-ATRP of polystyrene on silicon wafer at 90°C, with lower catalyst concentration exhibiting slower growth rates.^[24]

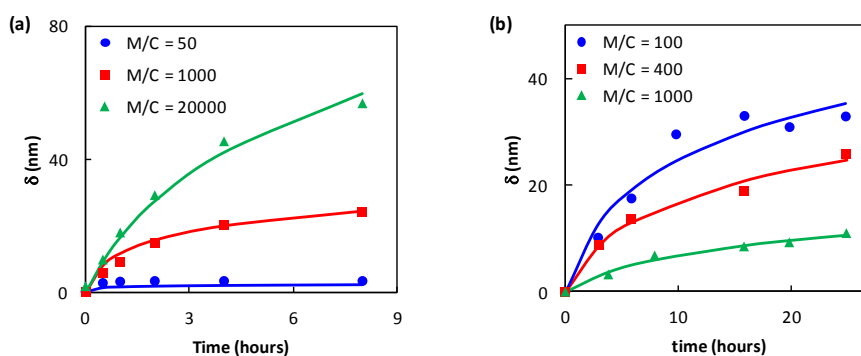


Figure 7-5. Dry thickness profiles for SI-ATRP at various catalyst levels with $\tau = 0.5$ chains/nm². Solid lines are guides to eyes. (a) $[M] = 2 \text{ mol/L}$, $[XC] = 0.3[C]$, and $[M]/[C]$ of 50, 1000, and 20,000.^[16] (b) $[M] = 8.7 \text{ mol/L}$, $[XC] = 0.1[C]$, and $[M]/[C]$ of 100, 400, and 1000^[24]

For *living-solution* model, the growth profile (Equation (2)) depends only on the ratio of catalyst and deactivator, but not on their absolute concentrations. The same observation could be made for the *propagation* model, shown by Equation (4). This is

illustrated in Figure 7-6, with both models each predicting a single line for different monomer to catalyst ratios. Therefore, the catalyst concentration dependence observed in the experiments, seen in Figure 7-5, cannot be explained by either *living-solution* model or *propagation* model.

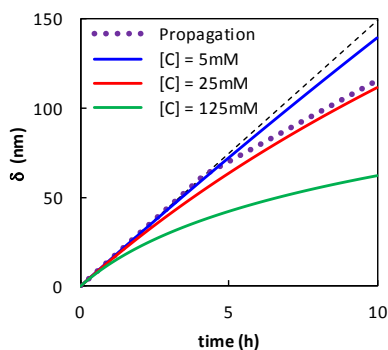


Figure 7-6. Dry thickness growth profiles predicted using various models at different catalyst concentrations. Solid lines denote predicted growth profiles using termination model

In contrast, the experiment trend observed in Figure 7-5 (a) has been explained by Zhou et al using the *termination* model by using the concept of “migration-assisted termination”, as described in Model Formulation section.^[18] In short, higher catalyst concentration results in a higher frequency of activation-deactivation cycle, which leads to a more frequent change in the location of active centre among the surface chains. This in turn increases the probability of a chain with radical centre to find another radical nearby to terminate with. Therefore, the migration rate and, by extension, the termination rate are higher with higher catalyst concentration, resulting in reduced growth rate. The predicted growth profiles for the *termination*

model are shown in Figure 7-6 for different catalyst concentrations, which agree with the trend observed in Figure 7-5 (a).

An opposite trend that is observed in Figure 7-5 (b) for SI-ATRP of styrene could not be explained by any of the models discussed in this study. A possible explanation for this discrepancy is the effect of catalyst concentration on grafting density. In simulation studies of SI-ATRP, the grafting density is often considered as a known parameter, which is unaffected by the initial concentrations of reactants. However, at lower catalyst concentration, the polymerization is less controlled due to lower frequency of activation-deactivation, resulting in more monomeric units added in one activation-deactivation cycle (forming long chains at the start). The presence of long chains at vicinity could shield the other initiator sites from being activated, resulting in a lower grafting density. This offers a possible explanation for Figure 7-5 (b), with lower catalyst concentration yielding lower grafting density, thereby yielding lower thickness. The initiator efficiency is an important remaining issue in SI-ATRP. Typically, silicon water surface contains >5 –OH groups per square nanometer. About 3~5 of the groups can be functionalized with ATRP initiator moieties. However, <1 of the initiators is activated and grown into polymer.

In summary, the effects of variables on the grafting kinetics of SI-ATRP on flat substrates are summarized in Table 7-4. It is evident that the *living-solution* model is completely inadequate in explaining the experiment trends. This implies that there is

significant crowding, termination, or other factors affecting the polymerization kinetics. The *propagation* model accounts for crowding of polymer chains and thus reduction in available monomer molecules inside the surface layer. The *termination* model considers migration-assisted radical termination and thus reduction in the number of active chains in the layer. From Table 7-4, it is clear that when considered separately, neither *propagation* model nor *termination* model could fully explain the reported experimental trends of thickness versus grafting density. It is also clear that the effect of catalyst concentration is still not fully understood. This implies that there could be other major factors, which are not accounted for in the existing model efforts. To fully understand the effects of various factors on the kinetics of SI-ATRP, further experiment and modeling studies are required, preferably in conjunction with each other.

Table 7-4. Comparison of experiment trends to the predicted results from various models

Variable	Experiment trend	Living-solution	Propagation	Termination
time ↑	$d\delta/dt \downarrow$	$d\delta/dt \sim \text{const}$	$d\delta/dt \downarrow$	$d\delta/dt \downarrow$
$\tau \uparrow$	$d\delta/dt \uparrow$	$d\delta/dt \uparrow$	$d\delta/dt \uparrow$	$d\delta/dt \uparrow$
	$dr_N/dt \uparrow \text{ or } \downarrow$	$dr_N/dt \sim \text{const}$	$dr_N/dt \downarrow$	$dr_N/dt \uparrow \text{ or } \downarrow$
$[C] \uparrow$	$d\delta/dt \uparrow \text{ or } \downarrow$	$d\delta/dt \sim \text{const}$	$d\delta/dt \sim \text{const}$	$d\delta/dt \downarrow$

§ 7.5 Conclusion

Despite the extreme importance of the area and numerous works published, there are still many fundamental questions remaining to be answered in the surface-initiated

atom transfer radical polymerization (SI-ATRP). One of the questions is: what limits the growth of chains on the surface? In most experiments, though frustrated with scarcity of the systematic data, the increase of polymer thickness slows down with time and finally stops. In many applications, we would like to have polymer layers as thick as possible. What is the maximum thickness of a polymer layer can grow to? In this study, we examined two theoretical models (namely, *propagation* model and *termination* model), trying to provide some explanation for the experimental observations. The *propagation* model attributes decrease in the growth rate over time to reduced monomer concentration in the surface layer, caused by crowding of grafted chains. Meanwhile, the *termination* model proposes the same phenomenon to be caused by decrease in the concentration of active chain ends due to radical termination reactions. The *propagation* model, used in this work as a first-approximation, was derived based on several simplifying assumptions. The *termination* model was adopted from the previous work.

Predictions of the two models were qualitatively compared to the experiment trends collected from the literatures. Particular attentions were paid to investigate the effects of grafting density and catalyst concentration (while ratio of catalyst to deactivator kept constant) on the growth rate of the grafted layer. From this comparison, we found that when considered separately, the two models could not sufficiently explain the experimentally observed trends. By increasing grafting density, experiment data collected show that the chain length growth rate could either

increase or decrease. The *propagation* model predicts a monotonous decrease in the chain length growth rate when grafting density is increased, due to the increased crowding. On the other hand, the *termination* model predicts that both trends are possible. The trends observed by varying the initial catalyst concentration shows that understanding on the mechanism of SI-ATRP is still lacking. Both the *propagation* and *termination* models could not predict the increase in thickness growth rate when catalyst concentration is increased as reported in the literature. Finally, it should be pointed out that while this work focused on ATRP, the conclusions of the study are generally applicable to other types of surface-initiated controlled radical polymerization such as reversible addition-fragmentation chain transfer radical polymerization (RAFT) and stable free radical polymerization (SRFP).

§ 7.6 References

- [1] Y. Tsujii, K. Ohno, S. Yamamoto, A. Goto, T. Fukuda, "Structure and Properties of High-Density Polymer Brushes Prepared by Surface-Initiated Living Radical Polymerization", in *Surface-Initiated Polymerization I*, R. Jordan, Ed., Springer Berlin Heidelberg, Berlin, Heidelberg, 2006, p. 1-45.
- [2] R. Barbey, L. Lavanant, D. Paripovic, N. Schüwer, C. Sugnaux, S. Tugulu, H.-A. Klok, *Chemical Reviews* **2009**, *109*, 5437-5527.
- [3] F. J. Xu, K. G. Neoh, E. T. Kang, *Prog Polym Sci* **2009**, *34*, 719-761.
- [4] A. Olivier, F. Meyer, J.-M. Raquez, P. Damman, P. Dubois, *Prog Polym Sci* **2012**, *37*, 157-181.
- [5] D. J. Siegwart, J. K. Oh, K. Matyjaszewski, *Prog Polym Sci* **2012**, *37*, 18-37.
- [6] O. Azzaroni, *J Polym Sci, Part A: Polym Chem* **2012**, *50*, 3225-3258.
- [7] C. M. Hui, J. Pietrasik, M. Schmitt, C. Mahoney, J. Choi, M. R. Bockstaller, K. Matyjaszewski, *Chem Mater* **2014**, *26*, 745-762.

- [8] S. Turgman-Cohen, J. Genzer, *Macromolecules* **2010**, *43*, 9567-9577.
- [9] S. Turgman-Cohen, J. Genzer, *J Am Chem Soc* **2011**, *133*, 17567-17569.
- [10] S. Turgman-Cohen, J. Genzer, *Macromolecules* **2012**, *45*, 2128-2137.
- [11] S. Eisenhaber, G. Zifferer, *Macromol Theory Simul* **2014**, *23*, 198-206.
- [12] H. Liu, M. Li, Z.-Y. Lu, Z.-G. Zhang, C.-C. Sun, *Macromolecules* **2009**, *42*, 2863-2872.
- [13] H. Liu, Y.-L. Zhu, J. Zhang, Z.-Y. Lu, Z.-Y. Sun, *ACS Macro Letters* **2012**, *1*, 1249-1253.
- [14] Y. Tsujii, M. Ejaz, K. Sato, A. Goto, T. Fukuda, *Macromolecules* **2001**, *34*, 8872-8878.
- [15] D. Xiao, M. J. Wirth, *Macromolecules* **2002**, *35*, 2919-2925.
- [16] J.-B. Kim, W. Huang, M. D. Miller, G. L. Baker, M. L. Bruening, *J Polym Sci, Part A: Polym Chem* **2003**, *41*, 386-394.
- [17] X. Gao, W. Feng, S. Zhu, H. Sheardown, J. L. Brash, *Macromol React Eng* **2010**, *4*, 235-250.
- [18] D. Zhou, X. Gao, W.-j. Wang, S. Zhu, *Macromolecules* **2012**, *45*, 1198-1207.
- [19] D. Zhou, E. Mastan, S. Zhu, *Macromol Theory Simul* **2012**, *21*, 602-614.
- [20] M. Husseman, E. E. Malmström, M. McNamara, M. Mate, D. Mecerreyes, D. G. Benoit, J. L. Hedrick, P. Mansky, E. Huang, T. P. Russell, C. J. Hawker, *Macromolecules* **1999**, *32*, 1424-1431.
- [21] K. Matyjaszewski, P. J. Miller, N. Shukla, B. Immaraporn, A. Gelman, B. B. Luokala, T. M. Siclovan, G. Kickelbick, T. Vallant, H. Hoffmann, T. Pakula, *Macromolecules* **1999**, *32*, 8716-8724.
- [22] D. Koylu, K. R. Carter, *Macromolecules* **2009**, *42*, 8655-8660.
- [23] R. Chen, W. Feng, S. Zhu, G. Botton, B. Ong, Y. Wu, *Polymer* **2006**, *47*, 1119-1123.
- [24] J. D. Jeyaprakash, S. Samuel, R. Dhamodharan, J. Rühle, *Macromol Rapid Commun* **2002**, *23*, 277-281.
- [25] W. Feng, J. Brash, S. Zhu, *J Polym Sci, Part A: Polym Chem* **2004**, *42*, 2931-2942.
- [26] Z. Bao, M. L. Bruening, G. L. Baker, *Macromolecules* **2006**, *39*, 5251-5258.
- [27] D. M. Jones, A. A. Brown, W. T. S. Huck, *Langmuir* **2002**, *18*, 1265-1269.
- [28] S. Edmondson, N. T. Nguyen, A. L. Lewis, S. P. Armes, *Langmuir* **2010**, *26*, 7216-7226.
- [29] S. Wang, Y. Zhu, *Langmuir* **2009**, *25*, 13448-13455.

- [30] A. Milchev, J. P. Wittmer, D. P. Landau, *The Journal of Chemical Physics* **2000**, *112*, 1606.
- [31] R. E. Behling, B. A. Williams, B. L. Staade, L. M. Wolf, E. W. Cochran, *Macromolecules* **2009**, *42*, 1867-1872.
- [32] A. Halperin, M. Kröger, E. B. Zhulina, *Macromolecules* **2011**, *44*, 3622-3638.
- [33] L. C. H. Moh, M. D. Losego, P. V. Braun, *Langmuir* **2011**, *27*, 3698-3702.

§ 7.7 Appendix

Derivation for “propagation model”

The grafted polymer chains are assumed to follow two different conformations depending on their chain lengths and grafting density. At the beginning of the polymerization, the grafted chains assume mushroom conformation, regardless of the grafting density. The grafted chains then transitioned to either semi-dilute brush or concentrated brush conformation as the polymer chains grow longer, depending on the grafting density. If grafting density is lower than a critical grafting density, *i.e.*, $\tau < \tau_c$, the mushroom conformation is transformed into semi-dilute brush, else it becomes concentrated brush. The dependence of wet thickness (δ_{wet}) on the average chain length (r_N) and grafting density (τ) for the mushroom and brush conformations are obtained from the literature, as tabulated in Table A7-1, for chains in good solvents.^[32,33] The value of τ_c is taken to be 0.4 chains/nm² in this study as an approximation. This value is reported by Moh et al. for poly(methyl methacrylate) in a good solvent (acetone).^[33]

Table A7-1. Relation between wet thickness to grafting density and average chain length for various grafted polymer conformation in good solvent

Conformation (<i>i</i> -value)*	$\delta_{\text{wet}} = c \times (r_N)^a \times (\tau)^b$		
	a_i	b_i	c_i
1 – Mushroom	3/5	0	c_1
2 – Semi-dilute, $\tau < \tau_c$	1	0.33	c_2
3 – Concentrated, $\tau > \tau_c$	1	0.5 – 0.6	c_3

* Subscript for the coefficient. τ_c is taken to be 0.4 chains/nm²

The transition stage between mushroom to brush conformation is not modeled in this study, replaced by an immediate change in conformation. The point of transition is assumed to occur at critical average chain length, r_N^* , which could be determined by Equation (A-1). This translates to transition time, t^* , and critical dry thickness, δ^* , as shown in Equation (A-2) and (A-3), respectively.

$$\delta_{\text{wet}}^* = c_1 (r_N^*)^{3/5} = c_i (r_N^*) \tau^{b_i} \quad (\text{A-1})$$

$$t^* = \left(\frac{c_i \tau^{b_i}}{c_1} \right)^{-5/2} \left(\frac{k_d [XC]}{k_a [C]} \right) \frac{1}{k_p [M]_b} \quad (\text{A-2})$$

$$\delta^* = \left(\frac{c_i \tau^{b_i}}{c_1} \right)^{-5/2} \frac{m}{\rho} [PX]_g \quad (\text{A-3})$$

where $i = 2$ for $\tau < \tau_c$ and $i = 3$ for $\tau > \tau_c$

Assuming negligible volume change, the mass balance of monomer (reacted and unreacted) inside the grafted layer at any time during the brush regime can be written as Equation (A-4). The resulting partition coefficient, γ , can be shown to follow Equation (A-5).

$$[M]_b \delta_{wet} A = [M]_b \gamma \delta_{wet} A + r_N [PX]_g A \quad (A-4)$$

$$\gamma = 1 - \frac{r_N [PX]_g}{\delta_{wet} [M]_b} = 1 - \frac{1}{N_{Av}} \left(\frac{\tau^{1-b_i}}{c_i [M]_b} \right) \quad (A-5)$$

where $i = 2$ for $\tau < \tau_c$ and $i = 3$ for $\tau > \tau_c$

It is clear that using this simplification, regardless of the brush conformation (semi-dilute or concentrated brush), the partition coefficient is found to be constant with time.

8 FACTORS AFFECTING GRAFTING DENSITY IN SI-ATRP

In this chapter, the effects of various reaction conditions on grafting density is investigated via simulation. This chapter is a manuscript draft that will be submitted for publication in a peer-reviewed journal in the near future.

Author contributions

Erlita Mastan conducted the simulations and prepared the first draft of the manuscript under the guidance of Dr. Li Xi and Dr. Shiping Zhu. The draft of manuscript included in this chapter was revised by Dr. Shiping Zhu.

§ 8.1 Abstract

In surface-initiated ATRP, knowledge of grafting density is of significant interest because it is one of the determining properties of grafted polymer. It is well known that not all of the immobilized initiators can grow into polymer chains. However little is known about why this happens and what affects the grafting efficiency. The lack of information is partly due to the difficulty in experimental determination of grafting density on flat substrates. To circumvent the problem, Monte Carlo simulation is used in this study to investigate the effects of various atom transfer radical polymerization (ATRP) conditions on the grafting density. The simulation results show lower grafting density with less deactivator present. In systems with lower deactivator concentration, the number of monomer added per activation cycle is higher. Coupling this with close proximity of immobilized initiators results in chains initiated at earlier time to shield their neighboring initiator moieties from adding monomers, thus lowering the grafting density in such a system. These simulation results also provide an explanation to the seemingly conflicting trend reported in the literatures.

§ 8.2 Introduction

Grafting polymers from surface via atom transfer radical polymerization (ATRP) is a versatile method to modify surface properties.^[1-4] Owing to the advantages offered by ATRP, the surface properties of a material can be tailored as desired by modifying the properties of polymer layer introduced (*e.g.*, thickness, surface grafting density,

chemical composition). Surface-initiated ATRP (SI-ATRP) also allows formation of polymers with complex architecture, which further expands possible surface properties.^[1-4]

When polymerization occurs strictly on surface (i.e., no initiator is present in solution), there is an abundance of monomer in the solution phase thus a constant rate of polymerization is expected. However, many experimental studies reported deceleration in the growth rate of polymer chains as polymerization progressed.^[5,6] There are two schools of theories that could explain this experimental phenomenon, *propagation* and *termination* theories. The propagation theory explains this trend through reduction of available monomers in the grafted layer due to crowding. On the other hand, the termination theory justifies the deceleration through decreased active chain ends due to surface radical termination, which is assisted by radical migration through the reversible activation-deactivation reactions involved in ATRP. These two theories have also been used to offer explanation under which conditions the solution and surface chains possess similar or different properties in a simultaneous solution and surface polymerization.^[7,8] This helps to evaluate whether the properties of free polymer chains formed in solution can be used as an estimate for those of the grafted polymer brush on surface for calculation of grafting density, as often assumed in experimental studies.

The dry thickness of polymer brush (δ) and its grafting density (τ) are two important parameters of grafted polymer layer. For flat substrates, the dry thickness of polymer brush can be related to the total number of monomer units grafted based on its mass balance, as shown in Equation (1). The surface grafting density also determines the polymer brush conformation. Therefore, variation in grafting density may significantly affect surface properties of the modified materials.^[4,9,10]

$$\delta = \frac{M_n \tau}{N_{Av} \rho} \quad (1)$$

where: δ is the dry thickness of polymer layer, τ is the grafting density, M_n is the number-average molecular weight of the polymer, and N_{Av} is the Avogadro's constant, and ρ is the density of polymer

Grafting density is usually varied by modifying the initiator density through various means, such as controlling the initiator immobilization time,^[5] partial removal of the immobilized initiator,^[9] or by introducing inert spacers during initiator immobilization.^[11] However there is still a fairly limited knowledge on how grafting density is affected by the experiment conditions, albeit the major role it plays in determining the surface properties. This is in part due to the difficulty in accurate determination of polymer grafting density on flat surfaces, arising from the limited amount of grafted polymer available for characterization. Several studies have harvested the grafted chains from large or multiple surfaces to collect enough polymer samples for molecular weight measurement, thus allowing grafting density

estimation by Equation (1).^[11-14] Others have used properties of free chains in solution as estimates for those of surface chains at surface.

Using molecular dynamics simulations, Liu et al. investigated the effect of initiator density and polymerization rate on the resulting grafting density for a perfectly living surface-initiated polymerization system.^[15] They reported that a faster rate of polymerization yields a lower grafting density. However, activation and deactivation reactions are not included in this study. The effects of activator and deactivator concentrations on grafting density could not be examined. Turgman-Cohen and Genzer used Monte Carlo simulation to investigate the effect of initiator density and solvent quality on the initiator efficiency in perfectly living surface polymerization systems.^[16] Systems with initiator density less than 50% of the maximum coverage were simulated under good and poor solvent conditions. They found that the efficiency decreased as the initiator density increased and the solvent quality worsened.

Kinetic models have also been used as a simple and straightforward approach to investigate the polymer growth in surface-initiated CRP systems.^[8,17-21] However, a prior knowledge of grafting density must be assumed when using such an approach. Moreover, it is often assumed that grafting density is unaffected by changes in the reaction conditions. Our group recently investigated the difference in growth kinetics of surface polymers predicted by the two schools of theories, *propagation* vs.

termination, using simplified kinetic models.^[21] The predicted kinetics based on these models are compared with the experimental trends from literatures. The comparison showed that neither of the two models could fully predict the reported trends. Some experimental studies reported increasing catalyst concentration in SI-ATRP resulted in a decrease of grafting rate,^[18,22] while another reported the opposite trend.^[6] These conflicting experiment trends on the effect of catalyst concentration on grafting could not be explained through either simplified *propagation* model or *termination* model.^[21]

While it is well-known that not all of the immobilized initiators can propagate with monomers and become polymer chains, it is still unclear how the experiment conditions affect this initiation efficiency. In this study, we attempt to shed lights on what causes the grafting efficiency to be lower than 100% in SI-ATRP. The effect of various experiment factors on the final grafting density in SI-ATRP systems are investigated using Monte Carlo simulation. Factors that are investigated in this study are the initial initiator surface density, catalyst concentration, and the catalyst-to-deactivator ratio. The variation in grafting density with these experimental conditions offers an explanation to the seemingly conflicting trend reported in the literatures.

§ 8.3 Simulation details

The lattice Monte Carlo algorithm used to simulate the growth of surface polymers in this study is shown in Figure 8-1. Similar to the previous Monte Carlo studies for SI-ATRP,^[7,16] we employ 3-dimensional bond fluctuation model (BFM) to simulate the motion and to dictate the allowed bonds between repeating units in a polymer chain. Following the BFM originally proposed by Carmesin and Kremer,^[23] each bead in this simulation occupies 8 lattice sites with no double occupancy allowed in the lattice. A total of 108 bond vectors are considered as allowed bonds in this algorithm to ensure there is no bond crossing, chosen as $P(\pm 2, 0, 0) \cup P(\pm 2, \pm 1, 0) \cup P(\pm 2, \pm 1, \pm 1) \cup P(\pm 2, \pm 2, \pm 1) \cup P(\pm 3, 0, 0) \cup P(\pm 3, \pm 1, 0)$ for 3D lattice systems.^[24,25] Therefore, the possible bond lengths allowed in these simulations are 2, $\sqrt{5}$, $\sqrt{6}$, 3, $\sqrt{10}$. Periodic boundaries are employed on the x and y -axes, while solid walls are introduced on the edges of z -coordinates.

There are four types of beads considered in this simulation, namely unreacted monomer, radical chain-end, dormant chain-end, and non-reactive species (consisting of reacted monomer and dead chain-end). The initiator moieties are represented by beads of dormant chain-end that are anchored to the xy -plane at $z = 1$. Catalyst and deactivator are assumed to be homogeneously distributed in the system, hence not present as beads in the lattice. The effects of their concentrations are accounted for directly in their reaction probabilities by considering ratios of their

concentrations to a reference concentration value. The reference concentration represents the concentration at which a chain-end will always find a neighboring catalyst/deactivator to react with (chosen as the bulk monomer concentration in this work).

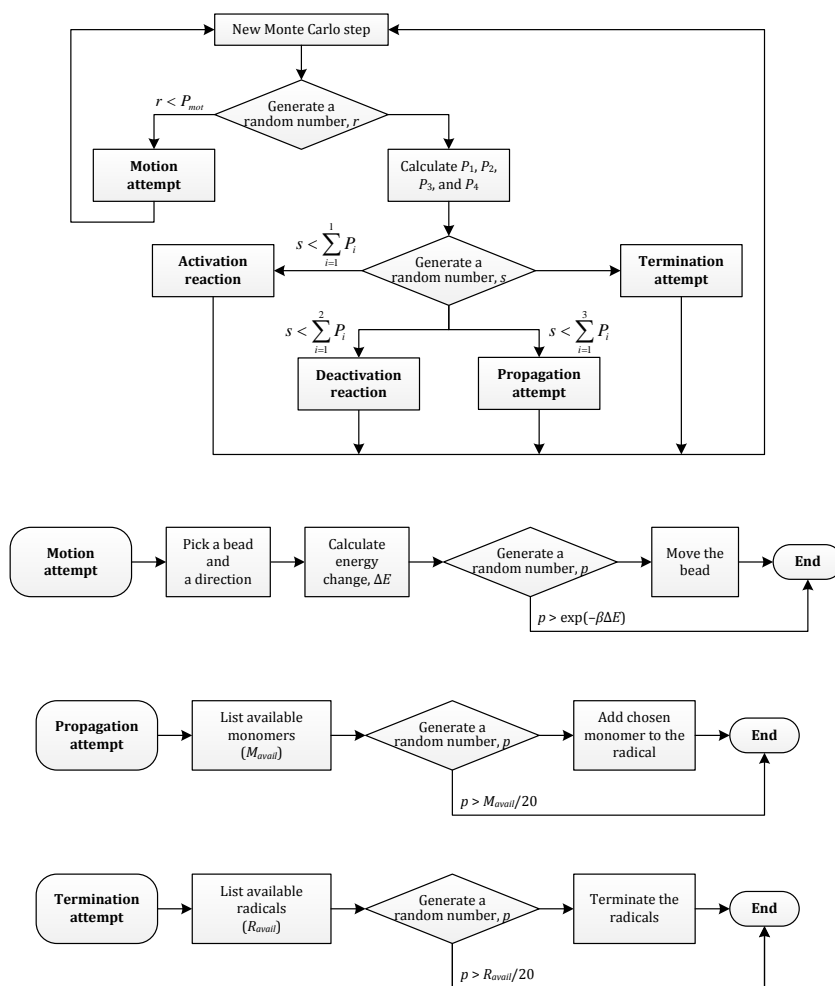


Figure 8-1. Monte Carlo algorithm used to simulate SI-ATRP process

In one Monte Carlo step, a random number r is first generated to determine whether a motion or a reaction is attempted based on a pre-specified motion probability, P_{mot}

(the value of this parameter is discussed later with the other simulation parameters). A motion attempt involves randomly choosing a bead and a direction ($\pm x, y$, or z). The movement is accepted if it passes Metropolis criterion, *i.e.*, if a random number generated is greater than the transitional probability, $W = \exp(-\beta\Delta E)$, which is calculated based on the energy change due to this movement. The energy change is calculated based on Equation (2) to account for the change in bond lengths, where the equilibrium chain length, L_0 , is chosen as 3.^[26] The value of β chosen in this study is 0.25 in order to obtain approximately 50% acceptance rate of the movement attempted for the reference condition chosen.

$$\Delta E = \begin{cases} \infty & \text{if chosen unit is anchored, new site is occupied, or} \\ & \text{the new bond is not one of the allowed bond vectors} \\ \varepsilon_0((L_{new,1} - L_0)^2 - (L_{old,1} - L_0)^2 + (L_{new,2} - L_0)^2 - (L_{old,2} - L_0)^2) & \end{cases} \quad (2)$$

where $L_{new,1}$ and $L_{new,2}$ are the lengths of the new bonds formed after the movement

$L_{old,1}$ and $L_{old,2}$ are the lengths of the bonds prior to the attempted move

L_0 is the equilibrium bond length, at which the energy is minimum

$\varepsilon_0 = 1/(2 - L_0)^2$ is introduced to normalize the energy change

If a reaction is attempted instead of motion (*i.e.*, $r > P_{mot}$) the probabilities P_1, P_2, P_3 , and P_4 are calculated for activation, deactivation, propagation, and termination, based on Equation (3). The variables n_{PX} and n_{Rad} are the number of dormant and radical chain-ends at that instant. These probabilities account for the concentration of chain-ends (dormant or radical) and the reaction rate constants. For activation and

deactivation reactions, the catalyst and deactivator concentrations are accounted directly in their reaction probabilities.

$$P_i = Rxn_i / \sum_{j=1}^4 Rxn_j \quad (3)$$

where	$Rxn_1 = k_a n_{pX} [C] / [M]_{bulk}$	for activation reaction
	$Rxn_2 = k_d n_{Rad} [XC] / [M]_{bulk}$	for deactivation reaction
	$Rxn_3 = k_p n_{Rad}$	for propagation attempt
	$Rxn_4 = k_t n_{Rad}$	for termination attempt

Another random number, s , is then generated to determine the reaction attempted and the chain-end undergoing that reaction. The reaction i is chosen based on the relation shown in Equation (4) (with possible i value of 1, 2, 3, or 4 representing activation, deactivation, propagation, or termination, respectively). From the same random number, the k^{th} chain-end is chosen to undergo reaction i based on the relation shown in Equation (5).

$$\sum_{j=1}^{i-1} P_j < s < \sum_{j=1}^i P_j \quad (4)$$

$$k = \text{ceil} \left(\frac{n_{chain}}{P_i} \left(s - \sum_{j=1}^{i-1} P_j \right) \right) \quad (5)$$

where $n_{chain} = n_{pX}$ for $i = 1$ and $n_{chain} = n_{Rad}$ for $i = 2, 3, \text{ or } 4$
 ceil is the ceiling function to round up the value to the nearest integer

Since the effect of catalyst and deactivator concentrations are already accounted for in the probabilities of activation and deactivation, these reactions will definitely occur once chosen. However, propagation and termination may fail once chosen in order to

account for the effect of local concentrations of monomer and radical surrounding the chosen chain-end. Based on the list of allowed bonds in BFM, there is a maximum of 20 neighboring beads that can react with one chain end at a time. Therefore, the number of monomer available is divided by 20 as a probability for the reaction to successfully occur. Another random number (p) is thus needed to determine whether the reaction attempt succeeds or fails. If p is greater than $M_{avail}/20$, then the propagation is assumed to fail (or $R_{avail}/20$ for termination). If the reaction occurs, this random number also determines which of the neighboring beads will undergo the reaction with the chosen chain-end, shown by Equation (6) for the k^{th} neighboring unit. This ensures that the radical with more neighboring beads has higher chance to successfully propagate than radical with less monomers around it (similarly for termination reaction).

$$k = \text{ceil}(20 \times p) \quad (6)$$

where *ceil* is the ceiling function to round up the value to the nearest integer

Using the formulation described above, no difference is expected for runs with different ratio of monomer to initiator bead, as long as the monomer concentration and initiator surface density are kept the same between runs (*i.e.*, the simulations are independent of the L_z/L_x ratio). This is consistent with what is expected in experiment settings, *i.e.*, changing the ratio of reaction volume to the surface area of material is not expected to affect the polymerization.

Full occupancy of lattice is assumed to correspond with the bulk monomer concentration. The variation in monomer concentration is then controlled by fraction of the occupancy. The reference run condition chosen as a benchmark is simulation with lattice size of $60 \times 60 \times 60$ ($L_x \times L_y \times L_z$), 3 mol/L monomer concentration (corresponding to 9000 beads, *i.e.*, a third of the full occupancy), and with the maximum initiator grafting density ($\tau_i/\tau^* = 1$, corresponding to 900 beads). Table 8-1 summarizes the variation in parameters used in our simulations.

Table 8-1. Reaction parameters used in the simulations

Parameter	Value
$[M]_{bulk}$ (mol/L) ^a	9
$[M]$ (mol/L)	1 or 3
$[M]:[C]$	25, 100, 500, or 1000
$[C]:[XC]$	5, 10, 20, or 50
τ_i/τ^*	0.1, 0.25, 0.5, 0.75, 0.9 or 1
k_p (L/mol s) ^a	1600
k_a (L/mol s) ^b	1
k_d (L/mol s) ^b	10^6
k_t (L/mol s) ^a	10^8

^a Based on typical polymerization of methyl methacrylate

^b Typical value of activation and deactivation constants in ATRP

A fixed number of 20 movement attempts per bead per second is chosen as a reference point. The effect of this simulation parameter is also briefly investigated. A more concentrated system has lower successful movement attempts due to Equation (2). Therefore, the number of movement attempts per second can be expressed as

Equation (7), where n_T represents the total number of beads in the simulation (monomer and initiator). The number of reaction attempts per second can be expressed as Equation (8), by assuming constant number of activation reactions per second. Here, $n_{PX,0}$ represents the total number of initiators. The number of reaction attempts may vary as polymerization progresses (due to termination), requiring recalculation of the motion probability, P_{mot} . However, since we are only interested in the final grafting density, which is obtained early in the polymerization, we assumed this change is insignificant and used a single value of P_{mot} per simulation run. The motion probability, P_{mot} , can then be simply calculated using Equation (9). The relation between time and the number of MC steps can be obtained by dividing the number of movement attempts made to the number of movement attempts per second (Equation (7)), as shown in Equation (10).

$$move_{attempt} / s = 20n_T \quad (7)$$

$$rxn_{attempt} / s = k_a [C] n_{PX,0} / P_1 \approx \left(k_a \frac{[C]}{[M]_{bulk}} + \left(k_d \frac{[XC]}{[M]_{bulk}} + k_p + k_t \right) \left(\frac{k_a [C]}{k_d [XC]} \right) \right) [M]_{bulk} n_{PX,0} \quad (8)$$

$$P_{mot} = \frac{move_{attempt} / s}{move_{attempt} / s + rxn_{attempt} / s} \quad (9)$$

$$t = \frac{P_{mot} MC}{20n_T} \quad (10)$$

Initially, the monomer beads are shuffled for at least 1000 MC steps/bead (*i.e.*, more than 9×10^6 MC steps for the reference simulation). For cases with $\tau_i / \tau^* < 1$, the initiator are also initially moved around the xy -plane at $z = 1$. The originally chosen

L_z/L_x ratio of 1 was found to be insufficient for some cases since the polymer brush grew too close to the top wall, which is not actually present in experiments. For such cases, larger L_z was used (100 instead of 60) with L_x and L_y kept at 60, while keeping the monomer concentration and initiator surface density constant. For cases where the polymer chains did not grow too close to the top wall, the results from runs with different L_z/L_x are comparable. This also serves as a proof that the monomer-to-initiator bead ratio does not affect the simulation results.

In order to obtain the final grafting density, the evolution of grafting density with time from each simulation run is fitted to a biexponential rise to a maximum function, with general form shown in Equation (11). Good fits were found for all simulation runs when fitted with this type of function. The grafting density reported is the average of final grafting density ($\tau/\tau^* = a + c$) from 5 identical runs, with error bars representing the standard deviation between these runs. As a clarification, the grafting density in this study only quantifies the initiator moieties that have added at least one monomer unit. Initiators that have undergone activation to form radicals but does not propagate (instead undergo termination or deactivation) are not considered as a part of the polymer population. The number of monomers reacted per area is used as an indicator of the thickness of polymer layer.

$$\tau / \tau^* \approx a(1 - e^{-bt}) + c(1 - e^{-dt}) \quad (11)$$

While termination reactions are observed in these simulations, the amount of dead chains predicted is expected to be lower than those from experiments. This underestimation is due to the low number of radicals compared to the dormant chains (typical radical to dormant ratio in ATRP is 10^{-4} to 10^{-6}). This multiple order of magnitude difference in concentration makes it difficult to accurately simulate termination reactions using statistical method, unless a large sample volume is chosen. However, a large sample volume comes at the cost of long simulation time. Therefore, in this study, we opted to sacrifice the accuracy in measuring the amount of terminated chains, since it is not expected to significantly affect the final grafting density, which is the very parameter under investigation.

§ 8.4 Results and discussions

The experiment factors that are examined in this study are the initiator surface density, the catalyst (activator) and deactivator concentrations (at a constant ratio of catalyst to deactivator), and the deactivator concentration (at a constant catalyst concentration). The number of movements per bead per second is also varied to investigate the effect of the chosen simulation parameter in this study on the grafting density.

8.4.1 The effect of initiator density

The effect of initiator density on the final grafting density had been experimentally and theoretically investigated in other studies.^[11,15] Based on the algorithm described in the previous section, we simulated this effect at the monomer concentration of 3 mol/L, $[M]/[C]$ of 25, and $[C]/[XC]$ of 10. Figure 8-2 (a) shows the grafting density evolution with time at various initiator densities for sample runs, while Figure 8-2 (b) shows the average results of final grafting density from 5 simulation runs per initiator density.

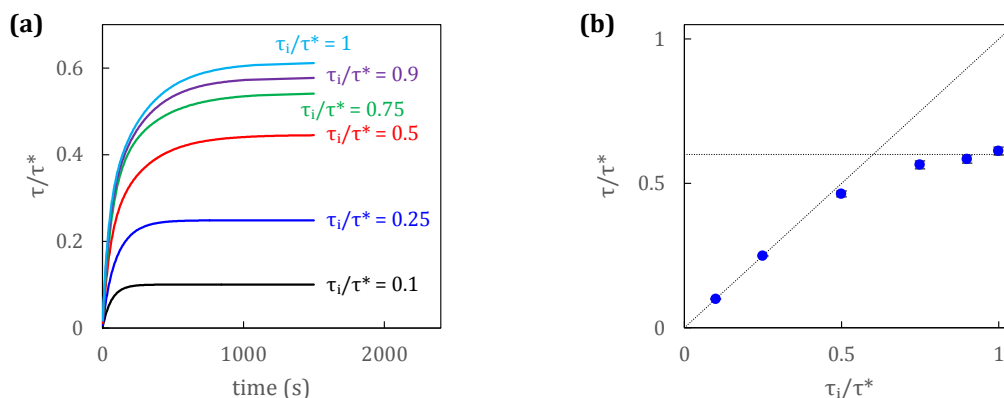


Figure 8-2. The effect of initiator density on the evolution of grafting density ($[M] = 3$ mol/L, $[M]/[C] = 25$, and $[C]/[XC] = 10$)

Our simulation results show a similar trend with findings from the previous studies, with grafting density increasing almost linearly with initiator density at low initiator density, but showing a weakening dependence at high initiator density. Moreover, the final grafting density found at the maximum initiator density (0.61 ± 0.13) is close to

the simulated average surface density of randomly adsorbing monolayer spheres on a flat surface reported by Tsujii et al (0.6).^[3]

8.4.2 The effect of catalyst concentration ($[C]$ at a constant $[C]/[XC]$)

Some experimental studies have reported increasing catalyst concentration in SI-ATRP result in a decrease of grafting rate,^[18,22] while another reported the opposite trend.^[6] Based on a previous study, these trends on the effect of catalyst concentration could not be explained through either simplified *propagation* model or *termination* model.^[21] These kinetic models assumed a known grafting density unaffected by the reaction conditions, which we believed could explain these opposite trends. Therefore, SI-ATRP at various catalyst concentrations was simulated to investigate the effect of catalyst concentration on the final grafting density, as shown in Figure 8-3.

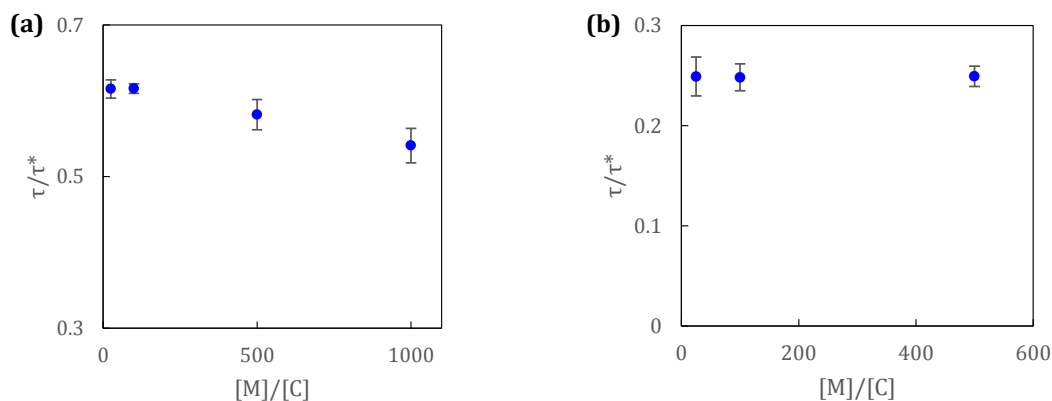


Figure 8-3. The effect of catalyst concentration on grafting density, simulated for systems with $[M] = 3$ mol/L, $[C]/[XC] = 10$, and (a) $\tau_i/\tau^* = 1$, (b) $\tau_i/\tau^* = 0.25$

Figure 8-3 (a) shows how the decrease of catalyst concentration results in a decrease of the final grafting density. This may be explained by comparing the number of monomers added per activation cycle in ATRP, where more monomer units are added per cycle in systems with lower catalyst (and deactivator) concentrations (*i.e.*, a less uniform growth).^[27] In bulk/solution systems, this variable does not significantly affect the initiation efficiency. On the other hand, this variable may cause a shielding effect in graft polymerization, where the initiators are anchored close to one another. When an initiator adds many monomers in one activation cycle, the resulting chain may shield its neighbors from reacting with free monomers, thus lowering the final grafting density. As seen from Figure 8-3 (b), the shielding effect is not observed in a system with lower initiator density since the initiator moieties are well separated and far apart from one another to shield the others from growing.

This shielding effect could also be observed by looking at the change in the number of monomers added per activation cycle. To elucidate this effect, systems with monomer to catalyst ratio of 25 and 500 are compared in Figure 8-4 for two initiator densities. The plotted value is the fractional change in the number of monomers added per cycle, calculated based on the maximum value for that system at the beginning of polymerization.

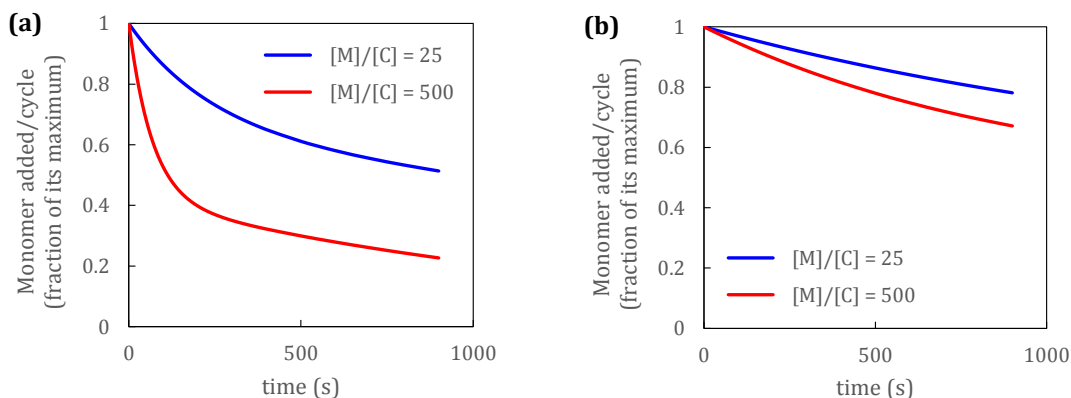


Figure 8-4. The number of monomers added per activation cycle with varying catalyst and deactivator concentrations. The value is calculated based on the maximum value exhibited by that system at the beginning of polymerization for $[M] = 3 \text{ mol/L}$, $[C]/[XC] = 10$, and (a) $\tau_i/\tau^* = 1$, (b) $\tau_i/\tau^* = 0.25$

From these plots, it can be seen that there is more shielding of initiator from reacting with monomer in system with lower catalyst concentration and higher initiator density. The larger decrease observed in this system could be mainly attributed to the failed attempt of initiator to add monomer and not due to the difference between the environments surrounding the polymer chains (since the grafting density is lower in this system). As a consequence of the lower grafting density exhibited by system with lower catalyst concentration, the polymerization rate for this system may also be slower, as depicted in Figure 8-5. The total number of monomers reacted per area of the surface is used as the equivalent of dry thickness in experiments.

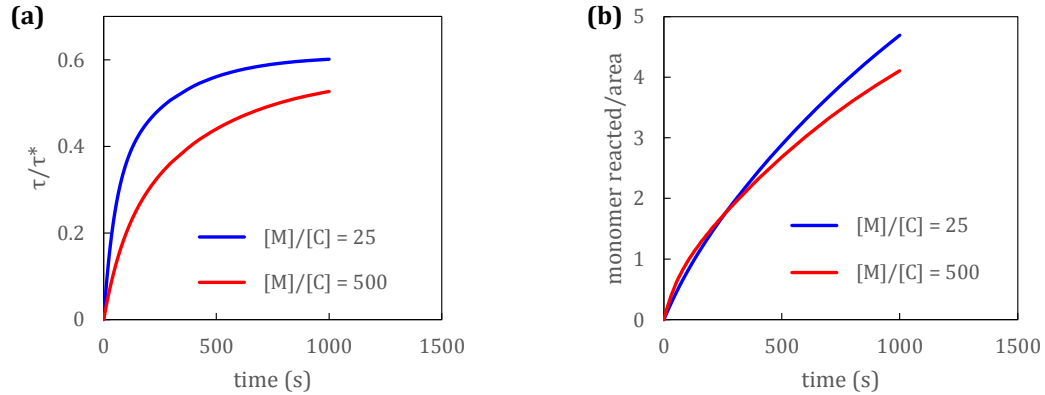


Figure 8-5. The evolution of grafting density and thickness with time for different catalyst and deactivator concentrations ($[M] = 3 \text{ mol/L}$, $\tau_i/\tau^* = 1$, and $[C]/[XC] = 10$)

This knowledge of how catalyst concentration affects grafting density can be applied to the previously derived *termination* model for dry thickness, shown in Equation (12).^[20] It becomes clear how the change in catalyst concentration may result in either an increase or a decrease of the thickness growth rate, as observed in experiments. Increasing catalyst concentration increases the termination via radical migration-assisted termination (termed as “hopping” mechanism), while at the same time it increases the resulting grafting density.

$$\delta = \alpha \ln(1 + \beta t) \quad (12)$$

$$\text{where } \alpha = \frac{m k_p [M]_b k_d [XC]_b}{\rho k_t k_a [C]_b} \quad \text{and} \quad \beta = k_t [PX]_g \left(\frac{k_a [C]_b}{k_d [XC]_b} \right)^2$$

$$k_t = A [C] \exp(-\omega \tau) \quad \text{and} \quad A = \frac{k_t^o}{[C]^o \exp(-\omega \tau^o)}$$

k_t^o is termination rate constant for the system at $[C] = [C]^o$ and $\tau = \tau^o$

8.4.3 The effect of catalyst/deactivator ratio

The effect of deactivator concentration on the grafting density is also investigated through MC simulation. Figure 8-6 shows the simulation results depicting the effect of decreasing deactivator on the final grafting density of surface polymerization. In ATRP systems, the polymerization rate depends on the ratio between catalyst and deactivator. Therefore, this factor can be compared with the effect of polymerization rate on grafting density studied by Liu et al. using molecular dynamics simulations.^[15]

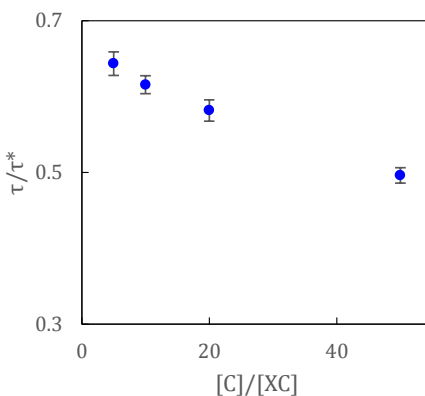


Figure 8-6. The effect of deactivator concentration on the grafting density ([M] = 3 mol/L, [M]/[C] = 25, and $\tau_i/\tau^* = 1$)

From Figure 8-6, increasing the ratio of catalyst to deactivator (by decreasing the deactivator concentration) results in a decrease of grafting density. A higher catalyst/deactivator ratio (*i.e.*, low deactivator concentration) in surface grafting results in more monomers added per activation cycle. This leads to a less uniform growth of polymer chains, which again results in lower grafting density (similar effect

as lowering both catalyst and deactivator concentrations described above). The trend observed here is in agreement with the simulation result of Liu et al., where the system with faster polymerization rate exhibits lower grafting efficiency.^[15] In addition, this result is also consistent with the recent experimental trend reported by Patil et al. for SI-ATRP of poly(methyl methacrylate),^[14] where a lower grafting density was reported for the system with less deactivator.

8.4.4 The effect of movement per second

One of the simulation parameters in this study is the number of movement attempts per second for each bead. We investigated the effect of this parameter on the grafting density, as shown on Figure 8-7 for two initiator densities (τ_i/τ^* of 0.25 and 1.0).

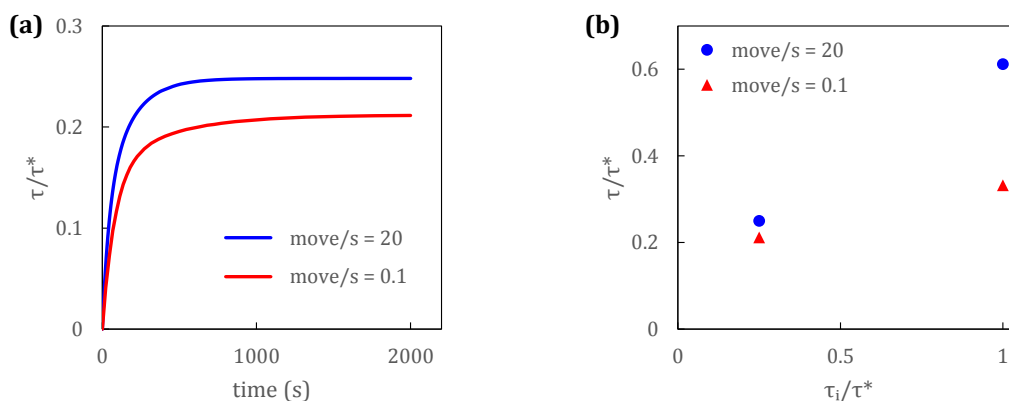


Figure 8-7. The effect of movement attempts per second on the final grafting density, simulated at $[M] = 3 \text{ mol/L}$, $[M]/[C] = 25$, and $[C]/[XC] = 10$. (a) $\tau_i/\tau^* = 0.25$, (b) $\tau_i/\tau^* = 0.25$ and 1.0

Figure 8-7 depicts the effect of movement attempts per second on the grafting density. The final grafting density predicted is drastically reduced when it is simulated with less movement attempts per second, especially at higher initiator surface density. This could be explained due to the more likely un-shielding of neighboring initiator moieties when more movement per second is attempted.

§ 8.5 Conclusion

Through Monte Carlo simulations, we have shown that the grafting density of SI-ATRP systems depends not only on the initiator surface density, but also on the polymerization conditions. The number of initiator moieties that will successfully become polymer chains (*i.e.*, the grafting efficiency) depends on the number of monomers added per activation cycle. This parameter can be associated to the experimentally adjustable factors, such as the types of reactants and the polymerization recipes. Simulation results show that the final grafting density decreases with an increased number of monomers added per activation cycle (a less uniform growth condition). This is because the chains that are initiated earlier shield the neighboring initiators from propagating with monomer.

These simulation results provide an explanation on the seemingly conflicting trends reported in experiments on the effect of catalyst concentrations (at a constant catalyst-to-deactivator ratio). Increasing catalyst concentration results in an increase

of termination due to radical migration-assisted termination (“hopping” mechanism), while at the same time it increases the resulting grafting density. The increase in termination results in a slower polymerization rate, whereas the increase in grafting density promotes faster polymerization. Therefore, depending on which factor is dominant, the growth of polymer layer may be faster or slower when the catalyst concentration is increased. Since grafting density is an important parameter that affects many of the surface properties, this study provides mechanistic insight and practical guidance which could be beneficial for designing further and systematic experimental studies to investigate how various reaction conditions affect SI-ATRP behaviors.

§ 8.6 References

- [1] C. M. Hui, J. Pietrasik, M. Schmitt, C. Mahoney, J. Choi, M. R. Bockstaller, K. Matyjaszewski, *Chem Mater* **2014**, *26*, 745-762.
- [2] A. Olivier, F. Meyer, J.-M. Raquez, P. Damman, P. Dubois, *Prog Polym Sci* **2012**, *37*, 157-181.
- [3] Y. Tsujii, K. Ohno, S. Yamamoto, A. Goto, T. Fukuda, "Structure and Properties of High-Density Polymer Brushes Prepared by Surface-Initiated Living Radical Polymerization", in *Surface-Initiated Polymerization I*, R. Jordan, Ed., Springer Berlin Heidelberg, Berlin, Heidelberg, 2006, p. 1-45.
- [4] R. Barbey, L. Lavanant, D. Paripovic, N. Schüwer, C. Sugnaux, S. Tugulu, H.-A. Klok, *Chemical Reviews* **2009**, *109*, 5437-5527.
- [5] J. Iruthayaraj, S. Chernyy, M. Lillethorup, M. Ceccato, T. Røn, M. Hinge, P. Kingshott, F. Besenbacher, S. U. Pedersen, K. Daasbjerg, *Langmuir* **2011**, *27*, 1070-1078.
- [6] J. D. Jeyaprakash, S. Samuel, R. Dhamodharan, J. Rühle, *Macromol Rapid Commun* **2002**, *23*, 277-281.

- [7] S. Turgman-Cohen, J. Genzer, *Macromolecules* **2012**, *45*, 2128-2137.
- [8] D. Zhou, E. Mastan, S. Zhu, *Macromol Theory Simul* **2012**, *21*, 602-614.
- [9] S. Yamamoto, M. Ejaz, Y. Tsujii, T. Fukuda, *Macromolecules* **2000**, *33*, 5608-5612.
- [10] A. Khabibullin, E. Mastan, K. Matyjaszewski, S. Zhu, "Surface-Initiated Atom Transfer Radical Polymerization", Springer Berlin Heidelberg, 2015, p. 1-48.
- [11] D. M. Jones, A. A. Brown, W. T. S. Huck, *Langmuir* **2002**, *18*, 1265-1269.
- [12] J.-B. Kim, M. L. Bruening, G. L. Baker, *J Am Chem Soc* **2000**, *122*, 7616-7617.
- [13] C. Kang, R. M. Crockett, N. D. Spencer, *Macromolecules* **2014**, *47*, 269-275.
- [14] R. R. Patil, S. Turgman-Cohen, J. Šrogl, D. Kiserow, J. Genzer, *Langmuir* **2015**, *31*, 2372-2381.
- [15] H. Liu, M. Li, Z.-Y. Lu, Z.-G. Zhang, C.-C. Sun, *Macromolecules* **2009**, *42*, 2863-2872.
- [16] S. Turgman-Cohen, J. Genzer, *Macromolecules* **2010**, *43*, 9567-9577.
- [17] X. Gao, W. Feng, S. Zhu, H. Sheardown, J. L. Brash, *Macromol React Eng* **2010**, *4*, 235-250.
- [18] J.-B. Kim, W. Huang, M. D. Miller, G. L. Baker, M. L. Bruening, *J Polym Sci, Part A: Polym Chem* **2003**, *41*, 386-394.
- [19] D. Xiao, M. J. Wirth, *Macromolecules* **2002**, *35*, 2919-2925.
- [20] D. Zhou, X. Gao, W.-j. Wang, S. Zhu, *Macromolecules* **2012**, *45*, 1198-1207.
- [21] E. Mastan, L. Xi, S. Zhu, *Macromol Theory Simul* **2015**.
- [22] W. Feng, J. Brash, S. Zhu, *J Polym Sci, Part A: Polym Chem* **2004**, *42*, 2931-2942.
- [23] I. Carmesin, K. Kremer, *Macromolecules* **1988**, *21*, 2819-2823.
- [24] H. Deutsch, K. Binder, *The Journal of chemical physics* **1991**, *94*, 2294-2304.
- [25] D. P. Landau, K. Binder, "A guide to Monte Carlo simulations in statistical physics", 3rd edition, Cambridge university press, 2009.
- [26] H.-P. Wittmann, K. Kremer, *Comput Phys Commun* **1990**, *61*, 309-330.
- [27] E. Mastan, D. Zhou, S. Zhu, *J Polym Sci, Part A: Polym Chem* **2013**, *52*, 639-651.

9 MAJOR CONTRIBUTIONS AND RECOMMENDATIONS

In this chapter, the major contributions made in this study are first summarized. Several recommendations on possible future research directions are also offered in this chapter.

§ 9.1 Major contributions

The major contributions made by this study in gaining better fundamental understanding into the mechanisms of ATRP and SI-ATRP can be summarized as follow:

- Derived a new expression for the full molecular weight distribution (MWD) of polymers synthesized by ATRP at constant concentrations of reactants. This is the first equation to account for the contribution of radical termination reactions on the MWD of bulk/solution ATRP systems. A method was also

developed to broaden the applicability of this equation to systems with varying concentrations of reactants

- Derived an easy-to-use explicit expression for polydispersity of ATRP systems that takes into account the presence of terminated chains. This equation provides a more accurate polydispersity prediction than the existing equations
- Identified that neither of the two existing schools of theories in SI-ATRP alone is sufficient to explain the experimental trends reported in the literatures
- Qualitatively determined the effect of reaction conditions on the resulting grafting density in SI-ATRP systems. The simulated trends can explain the seemingly contradicting experimental data

§ 9.2 Recommendations for future work

In keeping with the rest of the thesis, recommendations on future research work are also divided into two parts, bulk/solution ATRP studies and surface-initiated ATRP studies.

9.2.1 Bulk/solution ATRP studies

The values of reaction rate constant are crucial in prediction of kinetics and properties of polymers synthesized by any polymerization systems. In ATRP, there are four rate constants of interest, namely propagation, termination, activation, and deactivation rate constants (k_p , k_t , k_a , and k_d , respectively). Due to the nature of the active chain end

in ATRP, the first two rate constants are the same as those estimated for conventional free radical polymerization, which are tabulated for many common monomers in polymer textbooks and handbooks.^[1] The other two rate constants are often expressed by their ratio, *i.e.*, the equilibrium constant ($K_{ATRP} \equiv k_a/k_d$). The estimation of equilibrium constant under polymerization condition has been reported in literatures.^[2] This approach involves using the polymerization kinetic data for simple regression of the kinetic equation, an example is shown in Equation (1) for the systems following first-order kinetics. However, the estimation of the individual rate constant (k_a or k_d) under polymerization condition still poses a challenge. The polydispersity equation proposed in this study can potentially be used in the estimation of k_d , which will give the activation rate constant when combined with K_{ATRP} .

$$\ln(1-x) = K_{ATRP} k_p \left(\frac{[C][PX]_0}{[XC]} \right) t \quad (1)$$

The activation rate constant of the initiator moieties (k_a) is commonly determined via radical trapping method, which involves no monomer.^[3] Therefore, the value estimated is only applicable to the initiator, but not for the dormant chains. The initiation stage in ATRP is often considered as instantaneous (*i.e.*, the activation rate constant for the initiator is high), thus the polymerization kinetics is largely governed by the activation rate constant of the dormant chains, not the initiator.

Similar method using radical trapping was applied to macroinitiators instead of regular ATRP initiator to estimate the activation rate constant for dormant chains in the absence of monomer.^[4] Other methods to determine the activation rate constants under polymerization conditions (*i.e.*, monomer is present) have also been proposed in the literatures, such as by direct GPC peak resolution,^[5,6] by regression of early stage polydispersity data,^[7] or by utilizing ICAR ATRP.^[8] The GPC peak resolution method works best for systems where a large number of monomers is added per activation cycle (*i.e.*, slow deactivation rate). The regression of the early stage polydispersity data method relies on low conversion data to avoid the effect of side reactions, such as termination. This method utilizes the polydispersity equation at a constant monomer concentration, which can be rewritten as Equation (2) to give a linear plot with a slope of $k_a/2$. The ICAR ATRP method involves more reactions (thus more reaction rate constants) that could affect the estimation accuracy.

$$\left(PDI - 1 - \frac{1}{r_n} \right)^{-1} = \frac{k_a t}{2} \quad (2)$$

The use of polydispersity equation at higher conversion for estimation of rate constants must account for the effect of terminations because the contribution of dead chains is cumulative and may not be neglected at higher conversion. Therefore, by combining the new polydispersity equation with the existing kinetic equation, both activation and deactivation rate constants for ATRP can be determined under polymerization conditions. The only experimental data needed would be the kinetics

data (x vs. t) and polydispersity profile (PDI vs. x), which are already the two most often measured quantities in experiments along with the average molecular weight. Therefore, this estimation method does not require additional time-consuming measurements. The plot of average molecular weight as a function of conversion can be used to ensure the validity of some of the assumptions (*i.e.*, to ensure the termination occurs mainly by disproportionation and the initiation stage is sufficiently fast).

In addition, similar derivation approach can be used to obtain a polydispersity expression for ATRP systems exhibiting power-law kinetic behavior, or for ATRP of monomers that terminate mainly via combination instead of disproportionation. This derivation can also be extended for the other ATRP variants (*e.g.*, ICAR ATRP and ARGET ATRP). It is also possible to apply this approach to the other controlled radical polymerization systems, such as nitroxide-mediated radical polymerization (NMP) and reversible addition-fragmentation chain transfer (RAFT) polymerization.

9.2.2 Surface-initiated ATRP studies

Albeit rare, studies involving direct characterization of grafted polymers on flat substrates can be found in the literatures.^[9,10] These studies used relatively large wafers in order to collect enough polymer chains for characterization (~ 10 cm² or ~ 18 cm² wafer in comparison to the common wafer size used in SI-ATRP of ~ 1 cm²). A relatively thick polymer brush must also be obtained before the cleaved polymer is

enough for molecular weight determination (the minimum thickness required depends on the wafer size used, with the lowest reported as 48 nm for 18 cm² wafer). Since the characterization requires polymer brushes of certain thickness, it may not be possible to study the evolution of grafting density. However, this technique may be used to investigate the effect of various reaction conditions on the final grafting density for comparison with the trends predicted by simulations. It may help to gain insight on the validity of mechanisms assumed in the simulation. This direct characterization may also be used to confirm the surface termination reactions. By utilizing monomers that undergoes termination mainly via combination, the presence of terminated chains may be evident from the GPC curve, where the terminated chains would have twice the average-chain length of the dormant chains.

Due to the lack of understanding on SI-ATRP kinetics, polymerization on surface and in solution are often conducted simultaneously. The properties of solution chains are then used as estimates for those of surface chains. However, the validity of this estimation is often questioned. By getting a clear understanding of the surface polymerization mechanism, a general guideline as to when this estimation is valid can be proposed. Instead of doing numerous experiments to characterize the two polymer populations, modeling can be used to guide the experiment design to confirm the mechanisms of SI-ATRP. For this study, it should be noted that the grafted polymer layer in simultaneous polymerization is usually not as thick as that generated in

surface-only polymerization. Therefore, larger wafer may be necessary in such experiments in order to collect enough polymers for characterization.

While it is relatively easier to conduct characterization of SI-ATRP on particles than that on flat substrates, the opposite is true for theoretical investigations. The effect of curvature complicates the modeling of particle systems,^[11] thus more theoretical works are focusing on the flat substrates. This creates a gap between the experimental studies and the theoretical efforts. For example, the experimental data for grafting density of particle systems are abundant, but that is not the case for systems involving flat substrates. It would be interesting to conduct simulation work on particle systems to investigate if the reaction conditions have the same effect on the grafting density as observed for flat substrates. This would also provide easier comparison between the modeling and experimental work to validate the mechanism proposed based on the simulation results.

§ 9.3 References

- [1] J. Brandrup, E. H. Immergut, E. A. Grulke, A. Abe, D. R. Bloch, "*Polymer handbook*", Wiley New York, 1999.
- [2] Y. Wang, Y. Kwak, J. Buback, M. Buback, K. Matyjaszewski, *ACS Macro Letters* **2012**, *1*, 1367-1370.
- [3] A. Goto, T. Fukuda, *Macromol Rapid Commun* **1999**, *20*, 633-636.
- [4] G. Chambard, B. Klumperman, A. L. German, *Macromolecules* **2000**, *33*, 4417-4421.

- [5] A. Goto, T. Terauchi, T. Fukuda, T. Miyamoto, *Macromol Rapid Commun* **1997**, *18*, 673-681.
- [6] K. Ohno, A. Goto, T. Fukuda, J. Xia, K. Matyjaszewski, *Macromolecules* **1998**, *31*, 2699-2701.
- [7] T. Fukuda, A. Goto, *Macromol Rapid Commun* **1997**, *18*, 683-688.
- [8] C. Toloza Porras, D. R. D'hooge, P. H. Van Steenberge, M.-F. o. Reyniers, G. B. Marin, *Ind Eng Chem Res* **2014**, *53*, 9674-9685.
- [9] C. Kang, R. M. Crockett, N. D. Spencer, *Macromolecules* **2014**, *47*, 269-275.
- [10] R. R. Patil, S. Turgman-Cohen, J. Šrogl, D. Kiserow, J. Genzer, *Langmuir* **2015**, *31*, 2372-2381.
- [11] H. Liu, Y.-L. Zhu, J. Zhang, Z.-Y. Lu, Z.-Y. Sun, *ACS Macro Letters* **2012**, *1*, 1249-1253.